New Insights into Biobased epoxy resins: synthesis and characterization

Cheng Ding

PhD

University of York

Chemistry

July 2015

Abstract

The synthesis and characterization of a variety of novel biobased epoxy thermosets comprising plant oil-derived epoxy prepolymers and dicarboxylic acids (DCAs) and/or glutaric anhydride, in the presence of amine curing agents, in order to develop new insights on structure-property relationships, are reported.

The effect of:

i. different epoxy prepolymers: epoxidized linseed oil (ELO); epoxidized soybean oil (ESBO), and; their corresponding epoxidized methyl esters EML and EMS;
ii. systematically increasing carbon-carbon chain length of a series of α,ω-dicarboxylic acids (DCAs);
iii. different curing conditions based on type and concentration of accelerant: *N*,*N*-4-dimethylaminopyridine (DMAP); 1-methylimidazole (1-MI); 2-methylimidazole (2-MI); vinylimidazole (VI), and; trimethylamine (TEA), cure temperature and time.
iv. mixtures glutaric anhydride-adipic acid, and;
v. inclusion of native and modified starch to ELO-adipic acid resins,

on thermal and mechanical properties are discussed in detail.

Resins derived from DCAs gave soft and flexible materials. ELO-derived samples possessed higher T_g and better mechanical properties due to their higher oxirane content and functionality. Systematically increasing the carbon-carbon chain length improves thermal stability but reduces T_g, tensile strength, Young’s modulus, elongation at break and toughness. Among the various accelerants trialed, DMAP gave samples with best properties while TEA gave samples with poorest properties. Increasing DMAP concentration resulted in improved T_g, tensile strength and Young’s modulus but reduced thermal stability.

Resins derived from glutaric anhydride gave hard and rigid materials. By changing the ratio of glutaric anhydride to adipic acid, resins with various properties ranging from soft flexible to hard tough materials were attained.

Biobased thermoset composites comprising ELO-adipic acid and starch (native and modified) accelerated by DMAP, showed increased Young’s modulus while decreased tensile strength and elongation at break.

Table of Contents

Abstract 1

Table of Contents 3

List of Figures 9

List of Tables 17

Acknowledgements 19

Declaration 21

Chapter 1 Aims and Introduction 23

1.1 Overview and aims of this thesis 25

1.2 Sustainable development and green chemistry 27

1.3 Biobased polymers and epoxy thermosets 29

1.4 Production of DGEBA using biobased epichlorohydrin 32

1.5 Biobased epoxy monomers/prepolymers 33

1.5.1 Epoxy monomers from plant oils 33

1.5.2 Epoxy monomers from other renewable materials 37

1.6 Biobased curing agents 38

1.6.1 Modified plant oils 39

1.6.2 Biobased carboxylic acids and anhydrides 45

1.6.3 Biobased amines and their derivatives 50

1.6.4 Biobased phenols 53

1.6.5 Rosin- and terpene-based curing agents 57

1.6.6 Lignin-based curing agents 61

1.6.7 Miscellaneous 62

Chapter 2 Biobased epoxy resins of epoxidized plant oils cured with DCAs 65

2.1 Summary 67

2.2 Introduction 67

2.3 Effect of different epoxy precursors 69

2.3.1 DSC analysis 70

2.3.2 FT-IR analysis 73

2.4 Effect of different dicarboxylic acids ... 75

  2.4.1 DSC analysis ... 75

  2.4.2 Polymer extraction study ... 78

  2.4.3 Mechanical properties ... 81

  2.4.4 DMA analysis ... 83

  2.4.5 Thermal stability ... 86

2.5 Effect of different accelerators ... 88

  2.5.1 DSC analysis ... 89

  2.5.2 Polymer extraction study ... 92

  2.5.3 FT-IR analysis ... 93

  2.5.4 Mechanical properties ... 96

  2.5.5 Thermal stability ... 97

2.6 Effect of concentration of accelerator ... 97

  2.6.1 DSC analysis ... 98

  2.6.2 Polymer extraction analysis ... 100

  2.6.3 FT-IR analysis ... 101

  2.6.4 Mechanical properties ... 102

  2.6.5 Thermal stability ... 103

  2.6.6 SEM analysis ... 104

2.7 Effect of different T and t ... 106

  2.7.1 DSC analysis ... 107

  2.7.2 Mechanical properties ... 109

  2.7.3 Thermal stability ... 111

2.8 Conclusions ... 112

Chapter 3 Biobased epoxy resins of epoxidized plant oils cured with glutaric anhydride ... 115

3.1 Summary ... 117

3.2 Effect of temperature and time ... 117

  3.2.1 DSC analysis ... 118

  3.2.2 Mechanical properties ... 119

  3.2.3 Thermal stability ... 121

3.3 Effect of different epoxy prepolymers ... 122

3.3.1 DSC analysis ... 123
3.3.2 FT-IR analysis ... 125
3.3.3 Mechanical properties ... 126
3.3.4 Thermal stability ... 126
3.4 Effect of composition of curing agents (glutaric anhydride and adipic acid) ... 127
3.4.1 DSC analysis ... 128
3.4.2 FT-IR analysis ... 130
3.4.3 Mechanical properties ... 131
3.4.4 Thermal stability ... 133
3.4.5 SEM analysis ... 135
3.5 Conclusions ... 136
Chapter 4 Biobased epoxy resin and starch composites ... 137
4.1 Summary ... 139
4.2 Introduction ... 139
4.2.1 Starch composition and structure ... 139
4.2.2 Starch in composites ... 140
4.2.3 Starch modification ... 141
4.3 Effect of curing temperature ... 142
4.3.1 Mechanical properties ... 143
4.4 Effect of starch composition ... 144
4.4.1 Mechanical properties ... 144
4.4.2 Thermal stability ... 145
4.4.3 SEM analysis ... 147
4.5 Effect of starch concentration ... 148
4.5.1 Mechanical properties ... 149
4.5.2 Thermal stability ... 149
4.5.3 SEM analysis ... 150
4.6 Effect of starch modification ... 151
4.6.1 Characterization of starch esters ... 153
4.6.2 Characterization of composites ... 157
4.7 Conclusions ... 162

Chapter 5 Materials and Experimental 163
5.1 Materials and chemicals 165
5.2 Experimental details and instrumentation for Chapter 2 165
5.2.1 Film preparation 165
5.2.2 DSC analysis 166
5.2.3 Polymer extraction study 166
5.2.4 ATR-FTIR analysis 167
5.2.5 NMR analysis 167
5.2.6 GPC analysis 167
5.2.7 DMA analysis 168
5.2.8 Mechanical properties 168
5.2.9 CHN analysis 168
5.2.10 Thermal stability 168
5.2.11 SEM analysis 169
5.3 Experimental details and instrumentation for Chapter 3 169
5.3.1 Film preparation 169
5.3.2 Thermal stability 170
5.4 Experimental details and instrumentation for Chapter 4 170
5.4.1 Preparation of expanded starch 170
5.4.2 Preparation of starch esters 170
5.4.3 BET surface area measurement 171
5.4.4 Determination of degree of substitution by titration 171
5.4.5 Preparation of composites 171
5.4.6 Solid state NMR analysis 171
5.4.7 Thermal stability 172
5.4.8 Thermogravimetric-Fourier transform infrared spectroscopy (TG-FTIR) .. 172
Chapter 6 Concluding remarks and future insight 173
Appendix A 179
Glossary 183
References 189

List of Figures

Figure 1.1 Four groups of basic components used in this study. 26

Figure 1.2 The three spheres of sustainability (originally in colour). 27

Figure 1.3 Citation trends of publications on biobased polymers in recent years up to June 2015. 30

Figure 1.4 Global epoxy resin demand by sector (originally in colour). 30

Figure 1.5 Synthesis of DGEBA. 31

Figure 1.6 Types of curing agents (originally in colour). 31

Figure 1.7 Conventional synthesis of epichlorohydrin. 32

Figure 1.8 Synthesis of epichlorohydrin from glycerol. 33

Figure 1.9 Major vegetable oil world production since 2010 (originally in colour). 34

Figure 1.10 Fatty compounds as starting materials for synthesis: oleic acid (**1**), linoleic acid (**2**), linolenic acid (**3**), erucic acid (**4**), ricinoleic acid (**5**), petroselinic acid (**6**), 5-eicosenoic acid (**7**), calendic acid (**8**), a-eleostearic acid (**9**), punicic acid (**10**), santalbic acid (**11**), vernolic acid (**12**), 10-undecenoic acid (**13**), 9-decenoic (**14**), 13-tetradecenoic acid (**15**), and 5-hexenoic acid (**16**). NB: although not shown, their respective methyl esters are referred to as **1a–16a**.[27] 35

Figure 1.11 Reactive positions in triglycerides: ester groups (a), C=C double bonds (b), allylic positions (c), and α-positions of ester groups (d). 36

Figure 1.12 Conventional epoxidation of linseed oil. 36

Figure 1.13 Structure of BPH and G-POSS. 37

Figure 1.14 Structure of GPE, PGPE and SPE. 38

Figure 1.15 Structure of cardanol epoxy derivatives commercialized by Cardolite®. 38

Figure 1.16 Possible addition of MA to nonconjugated double bonds. (A) Diels-Alder adduct, (B) radical addition, and (C) cross-linking. 39

Figure 1.17 Chemical structures of thiols used in the transformation of oleochemicals into monomers and polymers. 41

Figure 1.18 Functionalization of soybean oil with thioglycolic acid. 42

Figure 1.19 Amination of GSO using CAHC by UV-initiated thiol-ene coupling. 42

Figure 1.20 Synthetic scheme of TPG. 43

Figure 1.21 Amine hardener by vegetable oil amidification. 43

Figure 1.22 Hydroxylation of epoxidized oils. 44

Figure 1.23 Structure of phosphorylated castor oil. 45

Figure 1.24 Oxidative scission of oleic acid (**1**) with ozone to give azelaic acid and pelargonic acid. Erucic acid (**4**) gives brassylic acid and pelargonic acid. Petroselinic acid (**6**) gives adipic acid and lauric acid. 46

Figure 1.25 Production of sebacic acid and capryl alcohol from castor oil 47

Figure 1.26 Schematic synthesis of maleic monoester used to cross-link ELO. 49

Figure 1.27 Route to renewable PA from biomass-derived furan and MA. 49

Figure 1.28 Chemical structures of (a) lysine and (b) tryptophan. 50

Figure 1.29 Synthesis and structure of polylysine (PL). 51

Figure 1.30 Synthesis of phenalkamine from cardanol. 52

Figure 1.31 Synthesis of the cardanol-based novolacs. 54

Figure 1.32 Structures of (a) catechin; (b) hydroxycinnamates; (c) procyanidins; (d) phloretin; (e) quercetin and its resonance structure. 54

Figure 1.33 Structure of tannic acid (TA). 55

Figure 1.34 Synthetic scheme of PGVNC. 56

Figure 1.35 Four common polymerizable terpenes (from left to right: β-pinene, α-pinene, limonene, and 3-carene) and abietic acid. 57

Figure 1.36 Chemical transitions of rosin acid to biobased amino and carboxyl curing agents.. 58

Figure 1.37 Synthesis of terpene-based acid anhydride (TPA) 60

Figure 1.38 Formula of (a) menthane diamines and (b) terpene diphenol (TPD). 60

Figure 1.39 Schematic model of lignin structure 61

Figure 1.40 Synthesis of Carboxylic Acid from Lignin. 62

Figure 1.41 Structure of Chitosan 62

Figure 2.1 Global adipic acid market volume share by application, 2012.[170] (Originally in colour) 67

Figure 2.2 Simplified reaction scheme of the current industrial process for AA production by catalytic oxidation of KA oil with nitric acid.[171] 68

Figure 2.3 Mechanisms proposed for ELO, DCA and DMAP. (1) esterification; (2) etherification. 69

Figure 2.4 Different epoxy prepolymers cured with adipic acid at 160 °C for 1 h. (Originally in colour) 70

Figure 2.5 EML and EMS samples cured at 160 °C for different times. (Originally in colour) 70

Figure 2.6 Thermograms of mixtures of different epoxy prepolymers with adipic acid. (Originally in colour) 71

Figure 2.7 Second heat thermograms of reaction mixtures of different epoxy prepolymers with adipic acid. (Originally in colour) 72

Figure 2.8 FT-IR spectra of EML sample cured at 160 °C for different time. (Originally in colour) 73

Figure 2.9 FT-IR spectra of EMS sample cured at 160 °C for different time. (Originally in colour) 74

Figure 2.10 Samples of ELO cured with different DCAs at 160 °C for 1h. (Originally in colour) 75

Figure 2.11 DSC thermograms of ELO with different DCAs at a heating rate of 10 °C/min. (Originally in colour) 76

Figure 2.12 Kissinger plot to determine activation energy (E_α). (Originally in colour) 77

Figure 2.13 DSC thermograms of cured ELO-DCAs films at 160 °C for 1 h. (Originally in colour) 78

Figure 2.14 FT-IR spectra of ELO, extracted soluble and insoluble residue after extraction from cured C_6 film. (Originally in colour) 79

Figure 2.15 ^{1}H NMR spectra of (a) ELO and (b) soluble. (Originally in colour) 81

Figure 2.16 ^{13}C NMR spectra of (a) ELO, (b) soluble and (c) solid state CP-MAS ^{13}C NMR spectrum of the residue. (Originally in colour) 81

Figure 2.17 Strain-stress curves of cured films with different DCAs. (Originally in colour) .. 82

Figure 2.18 Mechanical properties of films with different DCAs, (a) tensile strength; (b) elongation at break; (c) Young’s modulus; and (d) toughness. (Originally in colour) 83

Figure 2.19 Storage modulus (a) and tan δ (b) versus temperature for cured samples tested at 1 Hz. (Originally in colour) 84

Figure 2.20 Arrhenius plot for the β transition. (Originally in colour) 85

Figure 2.21 TGA and DTG of ELO-DCAs films in (a) N_2 and (b) air at 10 °C min^{-1} heating rate. (Originally in colour) 87

Figure 2.22 Chemical structures of accelerators..88

Figure 2.23 Samples with different accelerators (1 mol%) cured at 160 ^oC for 1 h. (Originally in colour)..88

Figure 2.24 Thermograms of mixtures in the presence of different accelerators (1 ^oC/min). (Originally in colour)..89

Figure 2.25 Kissinger plot to determine activation energy ($E\alpha$). (Originally in colour) 91

Figure 2.26 DSC thermograms of the cured epoxy systems with different accelerators. (Originally in colour)..92

Figure 2.27 Weight percentage of soluble substances and their corresponding M_w. (Originally in colour)..93

Figure 2.28 FT-IR spectra of reaction mixtures cured at 160 ^oC for 0 min and 60 min. (Originally in colour) 94

Figure 2.29 FT-IR of soluble substances for samples containing different accelerators. (Originally in colour)..95

Figure 2.30 Mechanical properties of ELO-C_6 samples with different accelerators. (Originally in colour)..96

Figure 2.31 Thermal stability of samples with different accelerators in N_2. (a) TG; (b) DTG. (Originally in colour)..97

Figure 2.32 Samples with different amount of DMAP cured at 160 ^oC for 1 h. (Originally in colour)..98

Figure 2.33 DSC thermograms of premixed samples containing different amount of DMAP (1 ^oC/min). (Originally in colour) 98

Figure 2.34 Thermograms of cured resins containing different amounts of DMAP. (Originally in colour)..100

Figure 2.35 Weight percent of soluble substances and their $M_{w.}$ (Originally in colour).........100

Figure 2.36 FT-IR spectra of cured films containing different amount of DMAP. (Originally in colour)..101

Figure 2.37 FT-IR analysis of extracted soluble samples containing different amounts of DMAP. (Originally in colour)..102

Figure 2.38 Mechanical properties of films containing different amount of DMAP. (Originally in colour)..103

Figure 2.39 Thermal stability of cured resins containing different amounts of DMAP. (Originally in colour).. 104

Figure 2.40 Fracture surface of samples with different amount of DMAP after tensile test. (a, b) 0%; (c, d) 1.0%; (e, f) 2.0%; (g, h) 3.0%; (i, j) 4.0%; (k, l) 5.0%.. 105

Figure 2.41 Fracture surface of samples with different amount of DMAP after immersing in DCM for 1 d. (a, b) 0%; (c, d) 1.0%; (e, f) 2.0%; (g, h) 3.0%; (i, j) 4.0%; (k, l) 5.0%...................... 106

Figure 2.42 Samples of ELO-C_6 with 1 mol% DMAP cured at different T for 1 h. (Originally in colour).. 107

Figure 2.43 Samples of ELO-C_6 with 1 mol% DMAP cured at 140, 160 and 180 °C for different t. (Originally in colour) 107

Figure 2.44 Thermograms of ELO-C_6 sample with 1 mol% DMAP cured at different temperature for 1 h. (Originally in colour)... 108

Figure 2.45 Mechanical properties of ELO-C_6 samples cured at different T. (Originally in colour) 109

Figure 2.46 Mechanical properties of ELO-C_6 samples cured at 140, 160 and 180 °C for different time. (Originally in colour) 110

Figure 2.47 TGA and DTG in N_2 of samples cured at different T for 1 h. (a) TG; (b) DTG. (Originally in colour) 112

Figure 3.1 Samples of ELO cured with glutaric anhydride at different temperatures for 1 h. (Originally in colour)...117

Figure 3.2 Samples of ELO cured with glutaric anhydride at 140, 160 and 180 °C for different times. (Originally in colour) 118

Figure 3.3 Thermograms of ELO-GA samples cured at different temperatures for 1 h. (Originally in colour)..118

Figure 3.4 Mechanical properties of ELO-GA samples cured at different temperatures for 1h. (Originally in colour).. 120

Figure 3.5 Mechanical properties of ELO-GA samples cured at 140, 160 and 180 °C for different time. (Originally in colour)... 121

Figure 3.6 Thermal stability of ELO-GA cured at different temperatures for 1 h. (Originally in colour)... 122

Figure 3.7 Samples of different epoxy prepolymers cured with glutaric anhydride in the presence

of 1 mol% DMAP. (Originally in colour)......123
Figure 3.8 Thermograms of different epoxy prepolymer with glutaric anhydride mixtures in the presence of 1 mol% DMAP. (Originally in colour)......123
Figure 3.9 Thermograms of cured resins of different epoxy prepolymers cured with glutaric anhydride. (Originally in colour)......124
Figure 3.10 FT-IR spectra of cured resins of different epoxy prepolymers cured with glutaric anhydride in the presence of 1 mol% DMAP. (Originally in colour)......125
Figure 3.11 Mechanical properties of different epoxy cured with glutaric anhydride. (Originally in colour)......126
Figure 3.12 Thermal stability of different epoxy cured with glutaric anhydride. (Originally in colour)......127
Figure 3.13 Samples of ELO cured with different compositions of glutaric anhydride and adipic acid. (Originally in colour)......128
Figure 3.14 Thermograms of premixed mixtures of ELO with different compositions of GA:AA. (Originally in colour)......128
Figure 3.15 Thermograms of cured resins of ELO with different compositions of GA:AA. (Originally in colour)......130
Figure 3.16 FT-IR spectra of ELO cured with different composition of GA and AA. (Originally in colour)......131
Figure 3.17 Stress-strain curves of ELO cured resins with different compositions of GA:AA. (Originally in colour)......132
Figure 3.18 Mechanical properties of ELO cured with different compositions of GA: AA. (a) elongation at break, (b) tensile strength, (c) Young's modulus and (d) toughness. (Originally in colour)......133
Figure 3.19 Thermal stability of ELO cured with different compositions of GA and AA. (Originally in colour)......134
Figure 3.20 SEM of fracture surface after tensile tests of ELO cured with different composition of GA and AA. (a, b) 100%GA, (c, d) 50%GA and (e, f) 0%GA......135
Figure 4.1 Structure of amylose and amylopectin......139
Figure 4.2 Starch multiscale structure. (a) starch granules from normal maize (30 μm), (b) amorphous and semicrystalline growth rings (120-500 nm), (c) amorphous and crystalline

lamellae (9 nm), magnified details of the semicrystalline growth ring, (d) blocklets (20-50 nm) constituting a unit of the growth rings, (e) amylopectin double helixes forming the crystalline lamellae of the blocklets, (f) nanocrystals: other representation of the crystalline lamellae called starch nanocrystals when separated by acid hydrolysis, (g) amylopectin's molecular structure, and (h) amylose's molecular structure (0.1-1 nm).[211, 212] 140

Figure 4.3 Mechanism of esterification of starch using glutaric anhydride and DMAP. 142

Figure 4.4 Samples (blank and with 10 wt% Hylon VII) cured at different temperatures for 8h. (Originally in colour) 143

Figure 4.5 Mechanical properties of samples (blank and with 10 wt% Hylon VII) cured at different temperatures for 8h. (Originally in colour) 143

Figure 4.6 Samples containing 10 wt% different starches cured at 140 °C for 8 h. (Originally in colour) 144

Figure 4.7 Mechanical properties of samples containing 10 wt% of different starches. (Originally in colour) 145

Figure 4.8 Thermal stability of different starches. (Originally in colour) 146

Figure 4.9 Thermal stability of cured composites containing 10 wt% of different starches. (Originally in colour) 147

Figure 4.10 Fracture surface of samples containing 10 wt% different kinds of starch. (a, b, c) amylose; (d, e, f) corn starch; (g, h, i) Hylon VII; (j, k, l) amylopectin. 148

Figure 4.11 Samples containing different amount of Hylon VII cured at 140 °C for 8h. (Originally in colour) 148

Figure 4.12 Mechanical properties of samples containing different amount of starch. (Originally in colour) 149

Figure 4.13 Thermal stability of composites containing different amount of starch. (Originally in colour) 150

Figure 4.14 Fracture surface of samples containing different amount of Hylon VII. (a, b, c) 0%; (d, e, f) 10 wt%; (g, h, i) 20 wt%; (j, k, l) 30 wt%. 151

Figure 4.15 Relationship between DS and amount of glutaric anhydride used. 152

Figure 4.16 Blank sample and its composites containing 10 wt% starches with different DS. (Originally in colour) 152

Figure 4.17 FT-IR spectra of starches with different DS. (Originally in colour) 153

Figure 4.18 Solid state ^{13}C CPMAS NMR of (a) expanded starch; (b) starch esters with DS0.8. 154

Figure 4.19 Thermal stability of starches with different DS. (Originally in colour) 155

Figure 4.20 IR spectra of evolved gases from TG-IR analysis taken at the maximum rate of decomposition. (Originally in colour) 156

Figure 4.21 DSC thermograms of premixed mixtures of epoxy resin and its composites with different DS. (Originally in colour) 157

Figure 4.22 DSC thermograms of cured composites containing starches with different DS. (Originally in colour) 158

Figure 4.23 Mechanical properties of epoxy resin and their composites with starches (different DS). (Originally in colour) 159

Figure 4.24 Thermal stability of epoxy resin and its composites with starches (different DS). (Originally in colour) 160

Figure 4.25 Fracture surface of composites containing 10 wt% starches with different DS. (a, b, c) blank; (d, e, f) ES; (g, h, i) DS0.2; (j, k, l) DS0.5; (m, n, o) DS0.8. 161

List of Tables

Table 1.1 Properties and fatty acid compositions of the most common vegetable oils.............. 34

Table 1.2 Top Sugar-Derived Building Blocks 45

Table 1.3 Unsaturated fatty acids and esters as substrate for synthesis of linear fatty diacids. .. 46

Table 1.4 Thermal and mechanical properties of SPE based epoxy networks........................... 56

Table 2.1 DSC results of different epoxy prepolymer systems... 72

Table 2.2 ΔH_T and T_P of ELO-DCAs systems with different heating rates (5, 10, 15, 20 °C/min) 76

Table 2.3 Thermal properties of ELO-DCAs systems and data related to the extracted soluble substances. 77

Table 2.4 Storage modulus (MPa) of samples tested under 1 Hz. 84

Table 2.5 Temperature of the β-relaxation (T_β) taken from the maxima of the Tan δ of the different ELO-DCAs samples tested using a DMA under different frequencies and calculated activation energy E_β and T_g at 1 Hz. 85

Table 2.6 Thermal stability of the cured epoxy resins in N_2 and air (italics)............................. 87

Table 2.7 Thermal properties for premixing mixtures in the presence of different accelerators. 90

Table 2.8 Thermal properties of cured resins in the presence of different accelerators............. 92

Table 2.9 Thermal properties of mixtures containing different amount of DMAP. 99

Table 2.10 Thermal properties of cured resins containing different amount of DMAP............. 99

Table 2.11 Thermal properties of ELO-C6 samples cured at different temperature for 1 h...... 108

Table 2.12 T_g and degree of cure of ELO-C6 samples cured at 140, 160 and 180 °C for different time. 109

Table 2.13 T_5 of samples ELO-C_6 samples cured at 140 °C for different time..........................111

Table 3.1 Thermal properties of ELO cured with glutaric anhydride at different T for 1 h.......119

Table 3.2 Thermal properties of ELO-GA cured resins at 140, 160 and 180 °C for different time. 119

Table 3.3 Thermal stability of samples cured at 140, 160 and 180 °C for 1, 2 and 24h............ 122

Table 3.4 Thermal properties of premixed mixtures of different epoxy prepolymer with glutaric anhydride 124

Table 3.5 Thermal properties of different epoxy cured with glutaric anhydride. 125

Table 3.6 Thermal properties of premixed mixtures and cured resins of ELO cured with different compositions of GA and AA. 129

Table 4.1 Thermal stability of different starches/their composites. 145

Table 4.2 Thermal stability of composites containing different amount of starch. 150

Table 4.3 Thermal stability of expanded starch and its esters with different DS. 155

Table 4.4 Thermal properties of composites (mixtures and cured films) with different DS. 157

Table 5.1 Sample compositions and curing conditions 166

Table 5.2 Sample compositions and curing conditions 169

Acknowledgements

First of all, I would like to express the most sincere appreciation to my supervisor, Dr. Avtar Matharu, for his excellent supervision and continuous support and encouragement during my PhD study. I am grateful to Avtar for providing me lots of chances to attend training courses and conferences and valuable experiences in collaboration with companies and industry. Especially, I would like to thank Professor James Clark for his guidance and advices on my projects.

I would like to thank Paul Elliott and Dr Hannah Briers for their professional and prompt technical support in the lab, Dr. Helen Parker for her help with porosity analysis, Dr. Meg Stark for her assistance with SEM, Dr. Pedro Aguiar for his help with solid state ^{13}C NMR analysis and Dr. Peter Shuttleworth for his help with DMA analysis and suggestions for the published papers. Huge thanks to all the members of the group past and present for their help and suggestions with my projects. I also like to thank Akcros Chemicals and Croda International Plc for their kindly supply of epoxidized plant oils and Pripol 1009F, respectively.

Special thanks to my friends and colleges including Yuan Yuan, Guangmao Tian, Tengyao Jiang, Abdul Alweihaibi and Dr Rob McElroy and all my flat mates past and present. Without your listening, understanding and encouragement all the time, I would not have been able to suffer from the stresses and finish writing my thesis.

For financial assistance, I would like to thank the Department of Chemistry at the University of York for providing me a Wild Fund scholarship for my PhD study. I also would like to thank the Great Britain-China Educational Trust (GBCET) for the Chinese Student Awards in 2014.

Finally and most importantly, I would like to thank my parents, sister and brother for their unconditional love and consideration. Thanks for believing me and always being there for me.

Declaration

Some of the results presented in this thesis were obtained by, or in collaboration with other workers. Their contributions are fully acknowledged in the text. All the other results are the work of the author.

Cheng Ding

July 2015

Chapter 1

Aims and Introduction

Parts of the work described in this chapter has been published in:

"Recent Developments on Biobased Curing Agents: A Review of Their Preparation and Use."

C. Ding and A. S. Matharu, *ACS Sustainable Chemistry & Engineering*, 2014, **2**, 2217-2236.

DOI: 10.1021/sc500478f

(Impact factor 2015, 4.642)

1.1 Overview and aims of this thesis

This thesis aims to develop a range of biobased thermosetting epoxy resins, derived from epoxidized plant oils (EPOs), α,ω-diacids and/or anhydrides, and where appropriate starch, in the presence of amine accelerators (4-dimethylaminopyridine (DMAP), 1-methylimidazole (1-MI), 2-methylimidazole (2MI), vinylimidazole (VI) and trimethylamine (TEA)) as potential replacements for current petroleum derived materials, e.g., polyvinyl chloride (PVC), used in a range of applications from flooring (non-food grade) to gaskets for enclosures (food grade). The raw materials reported in this study are categorized into four groups: epoxy prepolymers; curing agents/cross-linkers; accelerators, and; additives, as shown in Figure 1.1.

In Chapter 2, the effect of epoxy prepolymers, variation in chain length of a series of α,ω-dicarboxylic acids (DCAs), accelerant type and concentration, cure temperature and time on the thermal and mechanical properties of the obtained resins is described in detail. This is the first comprehensive study of the effect on systematically extending the chain length of a series of α, ω-DCAs (even carbon number DCAs from C_6 to C_{18} and a bio-derived C_{36} diacid Pripol 1009F) on the physical and mechanical properties of the resultant biobased ELO crosslinked systems.

In order to improve the stiffness (Young's modulus) and strength of the obtained resins, two methods are exploited, *i.e.*, using anhydride as curing agents or adding fillers. In Chapter 3, glutaric anhydride was firstly reported to be used as curing agents for plant oil-derived epoxies. Effects of epoxy prepolymers, curing temperature and time on the thermal and mechanical properties of the obtained resins cured by glutaric anhydride were studied. Then various compositions of adipic acid and glutaric anhydride were used as curing agents and their effects on the thermal and mechanical properties of the obtained resins were also studied. Due to the different structure of glutaric anhydride and adipic acid, resins with various properties changing gradually from soft and flexible polymers to hard and rigid polymers.

In Chapter 4, starch was chosen as the renewable filler to improve the stiffness and strength. Firstly, native Hylon VII starch and starches with various compositions were added as additives to the epoxy resin matrix to make biobased composites. Then in order to improve the compatibility between starch and the epoxy resin, starch was expanded and modified with glutaric anhydride to introduce acid groups onto starch molecules. Their effects on the thermal and mechanical properties of the obtained composites were studied.

Chapter 5 summarizes all the experimental procedures used in the study and the thesis ends with Chapter 6 that concludes the work and proposes insights into future work.

(a) Epoxy prepolymers, for example

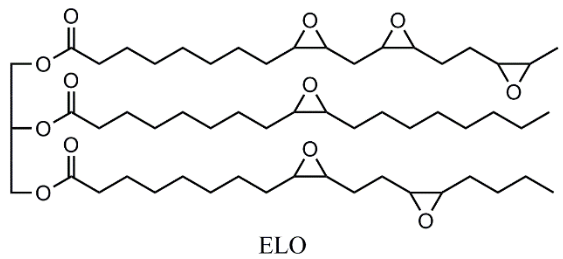

(b) Curing agents / Cross-linkers

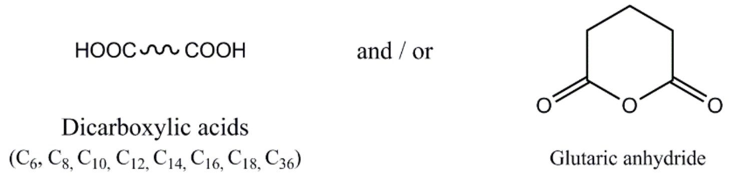
HOOC∿∿COOH
and / or
Dicarboxylic acids
(C6, C8, C10, C12, C14, C16, C18, C36)
Glutaric anhydride

(c) Accelerators

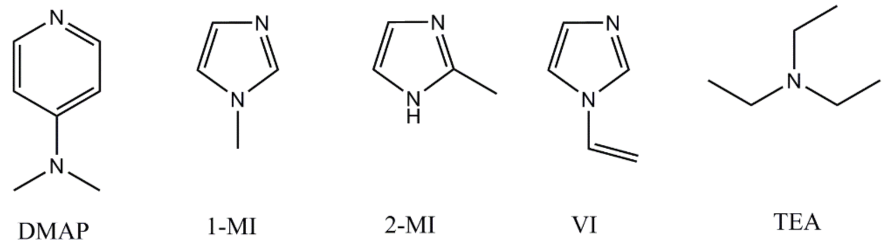
DMAP
1-MI
2-MI
VI
TEA

(d) Additives (starch)

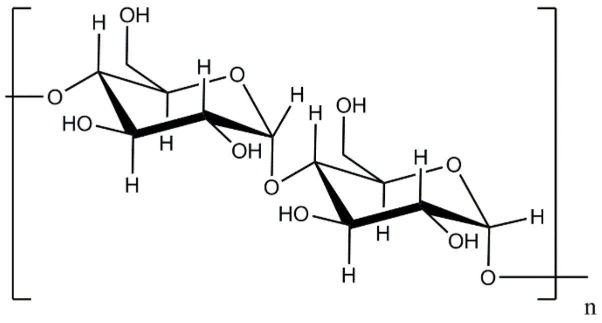

Figure 1.1 Four groups of basic components used in this study.

1.2 Sustainable development and green chemistry

In an era of declining petroleum resources and increasing environmental concerns associated with manufacture of petroleum-derived products 21st Century society must continue to adopt and practice the principles of sustainable development set out in the Bruntland Report, "Our Common Future".[1] Sustainable development is defined as "the development that meets the needs of the present without compromising the ability of future generations to meet their own needs." The three basic components of sustainable development are environment, society and economy (Figure 1.2). Only these three components develop simultaneously that the goals of sustainable development can be achieved.

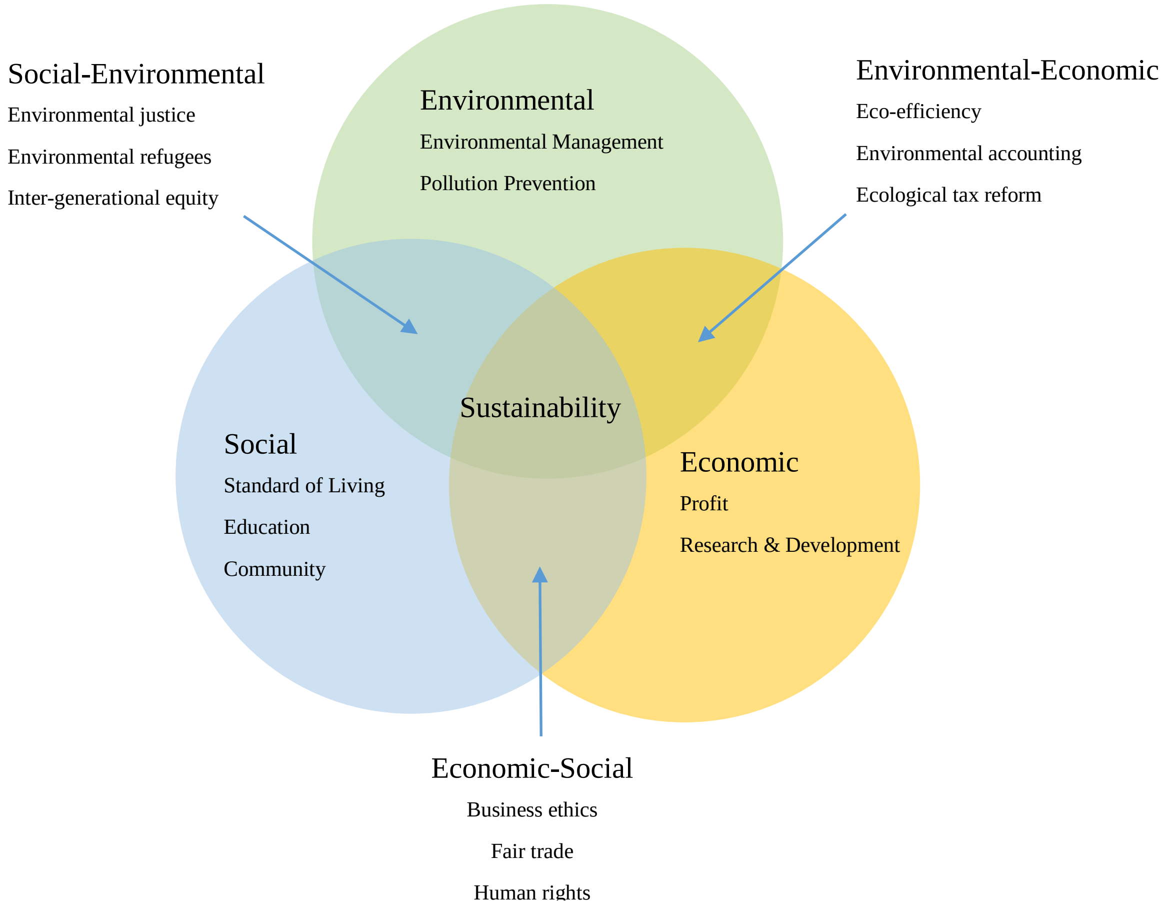
Social-Environmental
Environmental justice
Environmental refugees
Inter-generational equity
Environmental
Environmental Management
Pollution Prevention
Environmental-Economic
Eco-efficiency
Environmental accounting
Ecological tax reform
Sustainability
Social
Standard of Living
Education
Community
Economic
Profit
Research & Development
Economic-Social
Business ethics
Fair trade
Human rights

Figure 1.2 The three spheres of sustainability (originally in colour).

Furthermore, we cannot continue to use fossil fuels as our source of energy, chemicals and materials without comprising climate change targets; McGlade and Ekins reported that globally, 33% of oil reserves, 50% of gas reserves and more than 80% of current coal reserves should remain unused from 2010 to 2050 in order to meet the Intergovernmental Panel for Climate

Change target of 2 °C.[2] Utilization of biomass as an alternative feedstock to fossil fuels for our future energy, chemicals and materials requirements coupled with the development of global biobased economies is an attractive proposition for sustainable development. Unlike fossil fuels, biomass is carbon neutral and can provide complex molecules with inherent structure and functionality that would otherwise have to be chemically engineered. In addition, where chemical manipulations are needed we need to ensure they are carried out in sustainable manner.

In the 1990's, the concept of green chemistry, also known as sustainable chemistry, "the invention, design and application of chemical products and processes to reduce or to eliminate the use and generation of hazardous substances", was coined by Anastas and Warner along with the 12 principles of green chemistry (stated below).[3] With the utilization of these 12 principles, chemists and scientists are able to design and synthesize safer and more environmentally friendly chemicals and products.

1. *Prevention*

It is better to prevent waste than to treat or clean up waste after it has been created.

2. *Atom Economy*

Synthetic methods should be designed to maximize the incorporation of all materials used in the process into the final product.

3. *Less Hazardous Chemical Syntheses*

Wherever practicable, synthetic methods should be designed to use and generate substances that possess little or no toxicity to human health and the environment.

4. *Designing Safer Chemicals*

Chemical products should be designed to affect their desired function while minimizing their toxicity.

5. *Safer Solvents and Auxiliaries*

The use of auxiliary substances (e.g., solvents, separation agents, etc.) should be made unnecessary wherever possible and innocuous when used.

6. *Design for Energy Efficiency*

Energy requirements of chemical processes should be recognized for their environmental and economic impacts and should be minimized. If possible, synthetic methods should be conducted at ambient temperature and pressure.

7. Use of Renewable Feedstocks

A raw material or feedstock should be renewable rather than depleting whenever technically and economically practicable.

8. Reduce Derivatives

Unnecessary derivatization (use of blocking groups, protection/ deprotection, temporary modification of physical/chemical processes) should be minimized or avoided if possible, because such steps require additional reagents and can generate waste.

9. Catalysis

Catalytic reagents (as selective as possible) are superior to stoichiometric reagents.

10. Design for Degradation

Chemical products should be designed so that at the end of their function they break down into innocuous degradation products and do not persist in the environment.

11. Real-time analysis for Pollution Prevention

Analytical methodologies need to be further developed to allow for real-time, in-process monitoring and control prior to the formation of hazardous substances.

12. Inherently Safer Chemistry for Accident Prevention

Substances and the form of a substance used in a chemical process should be chosen to minimize the potential for chemical accidents, including releases, explosions, and fires.

1.3 Biobased polymers and epoxy thermosets

As the bioeconomy grows, new developments in biobased products are gaining significant or renewed interest, which are in line with the 7th principle of green chemistry, *i.e.*, use of renewable feedstocks.[4-6]

Biobased- or bioderived-polymers represent a significant opportunity for development as there are less than 1% of such polymers available on the market globally.[7] Importantly, as policy and legislative initiatives come to the fore, such as *Lead Market Initiative* (European Union)[8] and *BioPreferred* (USA),[9] the demand for biobased polymers will increase tremendously. As indicated by Web of Science™, the number of publication citations on biobased polymers in recent years increases dramatically, as shown in Figure 1.3.

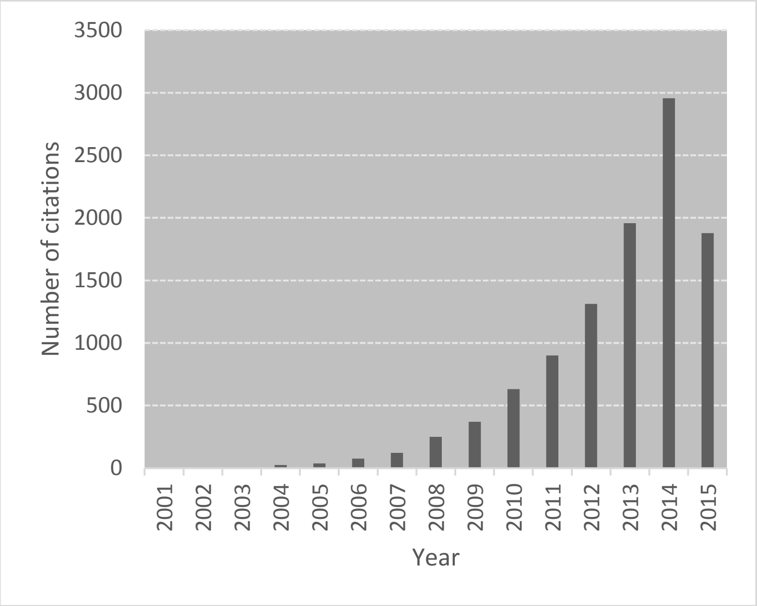

Figure 1.3 Citation trends of publications on biobased polymers in recent years up to June 2015.

Extensive literature exists on the use of renewable materials to make thermoplastic polymers and materials focusing mainly on starch, cellulose, polylactic acid (PLA) and polyhydroxyalkanoates (PHA).[10-12] Compared to the rapid development of thermoplastic polymers from renewable resources which have a market share of over 80%, research on biobased thermosetting materials has received much less recent attention.[13]

Epoxy resins (containing at least one epoxide or oxirane functional group) find a broad range of applications as depicted in Figure 1.4 due to their excellent dimensional, thermal, and environmental stabilities and ease of processability.[14]

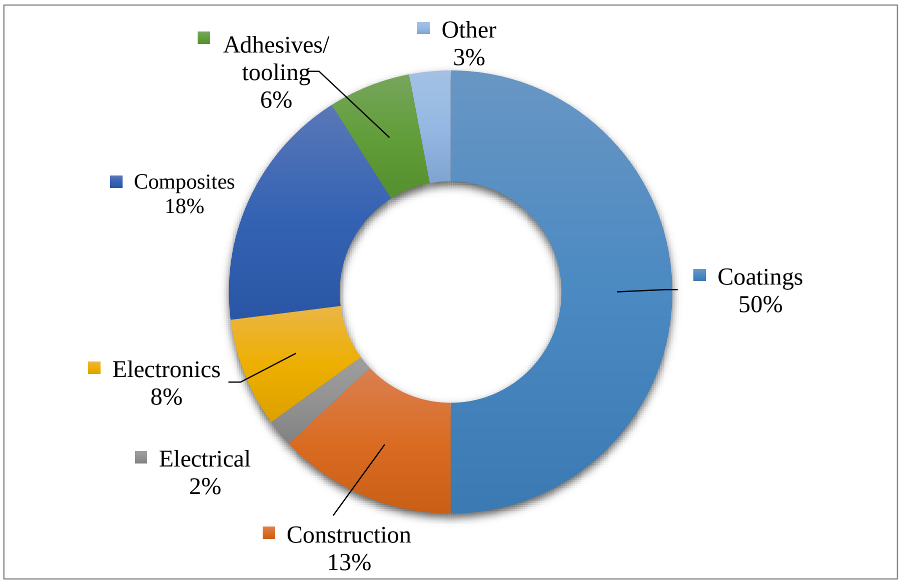

Figure 1.4 Global epoxy resin demand by sector (originally in colour).

Amongst the various epoxy monomers, diglycidyl ether of bisphenol A (DGEBA) is the commonest accounting for almost 75% of the global epoxy prepolymers market.[13] DGEBA is traditionally synthesized from Bisphenol A (BPA) and epichlorohydrin in the presence of NaOH as shown in Figure 1.5.

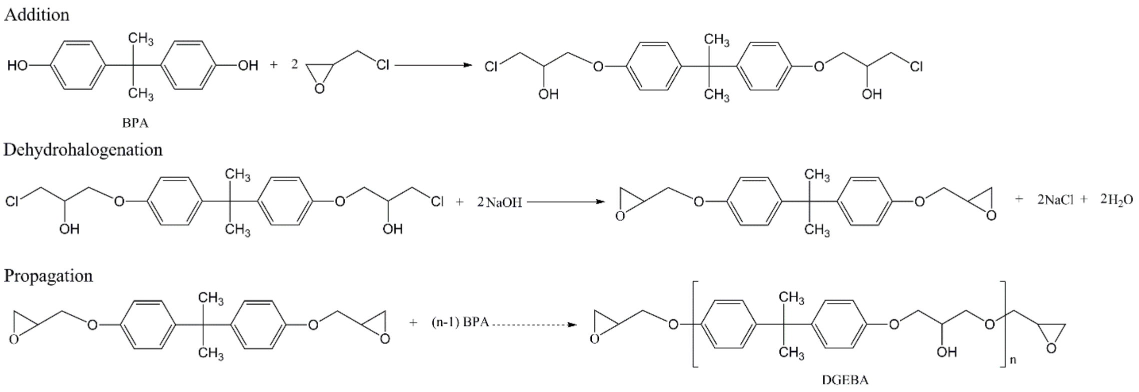

Figure 1.5 Synthesis of DGEBA.

In order to achieve the desired properties, curing agents (also sometimes known as hardeners, accelerants and catalysts) are used to cross-link epoxy prepolymers and either act as catalysts or react with the epoxide group via polyaddition/copolymerization reactions to generate hard, infusible, thermoset networks.[15,16] Mika and Bauer[17] categorized epoxy curing agents into three broad types (Figure 1.6).

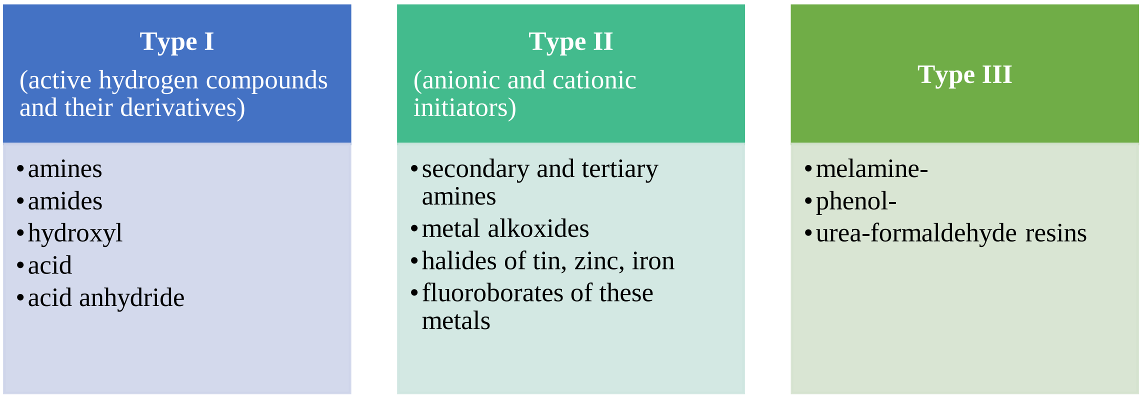

Type I (active hydrogen compounds and their derivatives)	**Type II** (anionic and cationic initiators)	**Type III**
• amines • amides • hydroxyl • acid • acid anhydride	• secondary and tertiary amines • metal alkoxides • halides of tin, zinc, iron • fluoroborates of these metals	• melamine- • phenol- • urea-formaldehyde resins

Figure 1.6 Types of curing agents (originally in colour).

Xiao and Wong[18] highlighted the toxicity of some amine curing agents, which is of growing concern because certain aliphatic- (diethylenetriamine, DETA, and triethylentetramine TETA), cycloaliphatic- (isophoronediamine, IPDA), and aromatic-amines (methylenedianiline, MDA) are well-known skin sensitizers. The latter are carcinogenic in animals and possibly human beings.[19] The Health Council of The Netherlands reports acid anhydrides, for example, hexahydrophthalic anhydride (HHPA), maleic anhydride (MA), methyl tetrahydrophthalic anhydride (MTHPA), phthalic anhydride (PA), tetrachlorophthalic anhydride (TCPA), tetrahydrophthalic anhydride (THPA), and trimellitic anhydride (TMA), cause sensitization and, PA and MTHPA cause asthma additionally.[20] Furthermore, toxicity may still exist in products in the form of residual curing agents and uncured monomers due to incomplete cure.

Thus, it is of great importance to develop biobased chemicals from renewable materials rather than petroleum-derived materials for producing next generation biobased epoxy networks. In general, there are three ways to improve the biobased content in epoxy resins:

1) Production of DGEBA using biobased epichlorohydrin;
2) Utilization of biobased epoxy monomers/prepolymers, and;
3) Utilization of biobased curing agents.

1.4 Production of DGEBA using biobased epichlorohydrin

As mentioned earlier, DGEBA is produced from BPA and epichlorohydrin. Conventionally, epichlorohydrin is synthesized by the chlorohydrination of allyl chloride, which in turn is made by chlorination of propylene (Figure 1.7).[21] Disadvantages involved in this process include the particularly low chlorine atom efficiency and hypochlorination steps which produce lots of unwanted chlorinated organics.

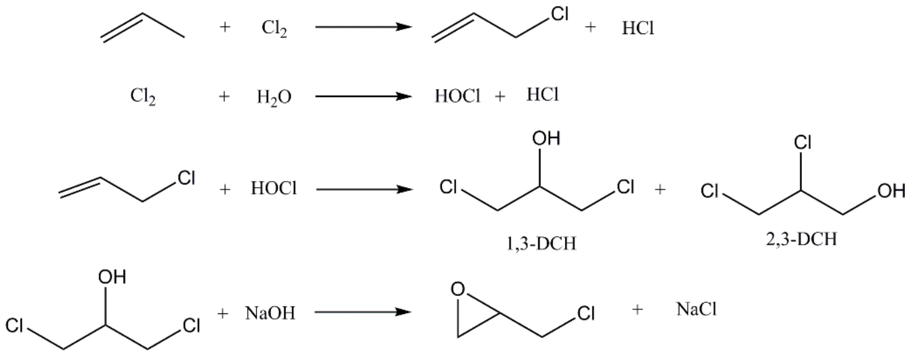

Figure 1.7 Conventional synthesis of epichlorohydrin.

In recent years, the process of producing biobased epichlorohydrin from glycerol via 1,3-dichloropropanol was developed making it possible to produce partially biobased DGEBA (Figure 1.8).[21, 22] Compared to the traditional process (Figure 1.7), the selectivity on

1,3-dichlorohydrin (1,3-DCH) is much higher (up to 93% under optimum conditions) and with reduced chlorinated residues and water to a greater extent.[23] The utilization of glycerol as a byproduct from biodiesel production will make the process more sustainable.

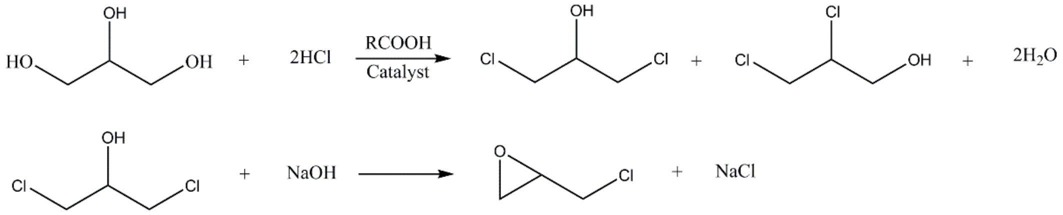

Figure 1.8 Synthesis of epichlorohydrin from glycerol.

Biobased DGEBA is chemically identical with petroleum-based DGEBA hence biobased DGEBA can fully substitute petro-based DGEBA. However, BPA, accounting for more than 67% of the molar mass of DGEBA, is still from fossil fuels. More importantly, BPA is classified as a reprotoxic R2 substance and is toxic to human health and the environment.[24]

1.5 Biobased epoxy monomers/prepolymers

Recently, Auvergne *et al.*[25] have reviewed biobased epoxy prepolymers derived from various renewable materials including vegetable oils, woody biomass and lignin, starch and sugar, polyphenols, terpenes, terpenoids and resin acids. Thus, in this part, attention will be focused on epoxidized plant oils (EPOs) whilst others will be mentioned briefly.

1.5.1 Epoxy monomers from plant oils

Plant oils represent a significant renewable resource for applications such as paints, coatings, cosmetics, detergents, lubricants, biodiesel and composites due to their wide availability, inherent biodegradability, and low toxicity.[26] As depicted in Figure 1.9, total global production of vegetable oils reached 175 million metric tons (mMT) in 2014 compared to 90 mMT in 2000, representing a 95% increase. The four major oilseed crops are palm, soybean, rapeseed and sunflower.

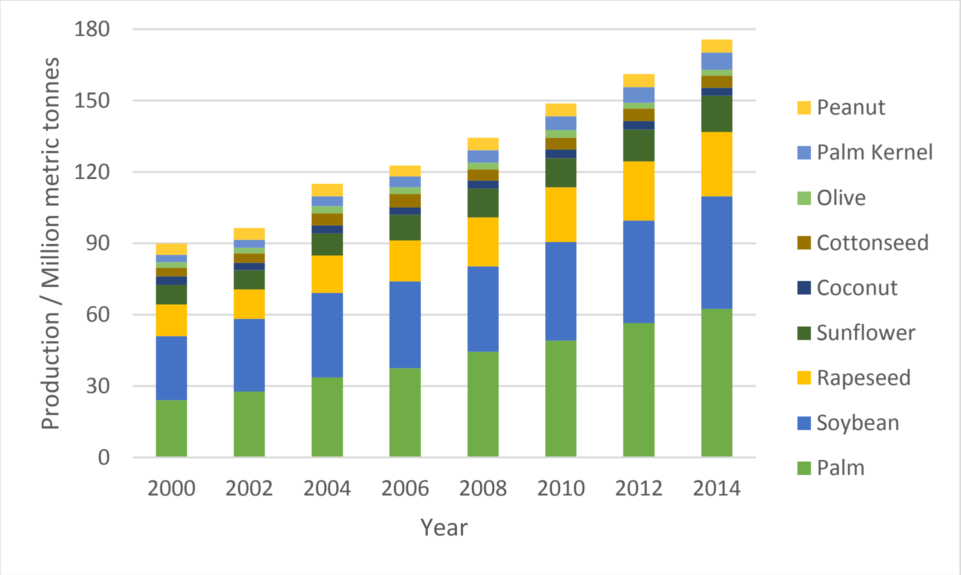

Figure 1.9 Major vegetable oil world production since 2010 (originally in colour).

Plant oils predominantly comprise triglyceride molecules, i.e., esters derived from glycerol and fatty acids. Most common plant oils contain fatty acid groups varying in carbon chain length from 14 to 22 and comprising 0 to 3 double bonds (C=C) per chain (Figure 1.10).[27] Thus, plant oils are a mixture of various triglycerides with differing degrees of (un)saturation. The properties and fatty acid compositions of the most common vegetable oils are shown in Table 1.1.[28]

Table 1.1 Properties and fatty acid compositions of the most common vegetable oils.

Vegetable oil	Double bonds[a]	Iodine value[b] / mg per 100 g	Fatty acids (%)				
			Palmitic	Stearic	Oleic	Linoleic	Linolenic
Palm	1.7	44-58	42.8	4.2	40.5	10.1	-
Olive	2.8	75-94	13.7	2.5	71.1	10.0	0.6
Groundnut	3.4	80-106	11.4	2.4	48.3	31.9	-
Rapeseed	3.8	94-120	4.0	2.0	56.0	26.0	10.0
Sesame	3.9	103-116	9.0	6.0	41.0	43.0	1.0
Cottonseed	3.9	90-119	21.6	2.6	18.6	54.4	0.7
Corn	4.5	102-130	10.9	2.0	25.4	59.6	1.2
Soybean	4.6	117-143	11.0	4.0	23.4	53.3	7.8
Sunflower	4.7	110-143	5.2	2.7	37.2	53.8	1.0
Linseed	6.6	168-204	5.5	3.5	19.1	15.3	56.6

[a] Average number of double bonds per triglyceride.

[b] The amount of iodine (mg) that reacts with the double bonds in 100 g of vegetable oil.

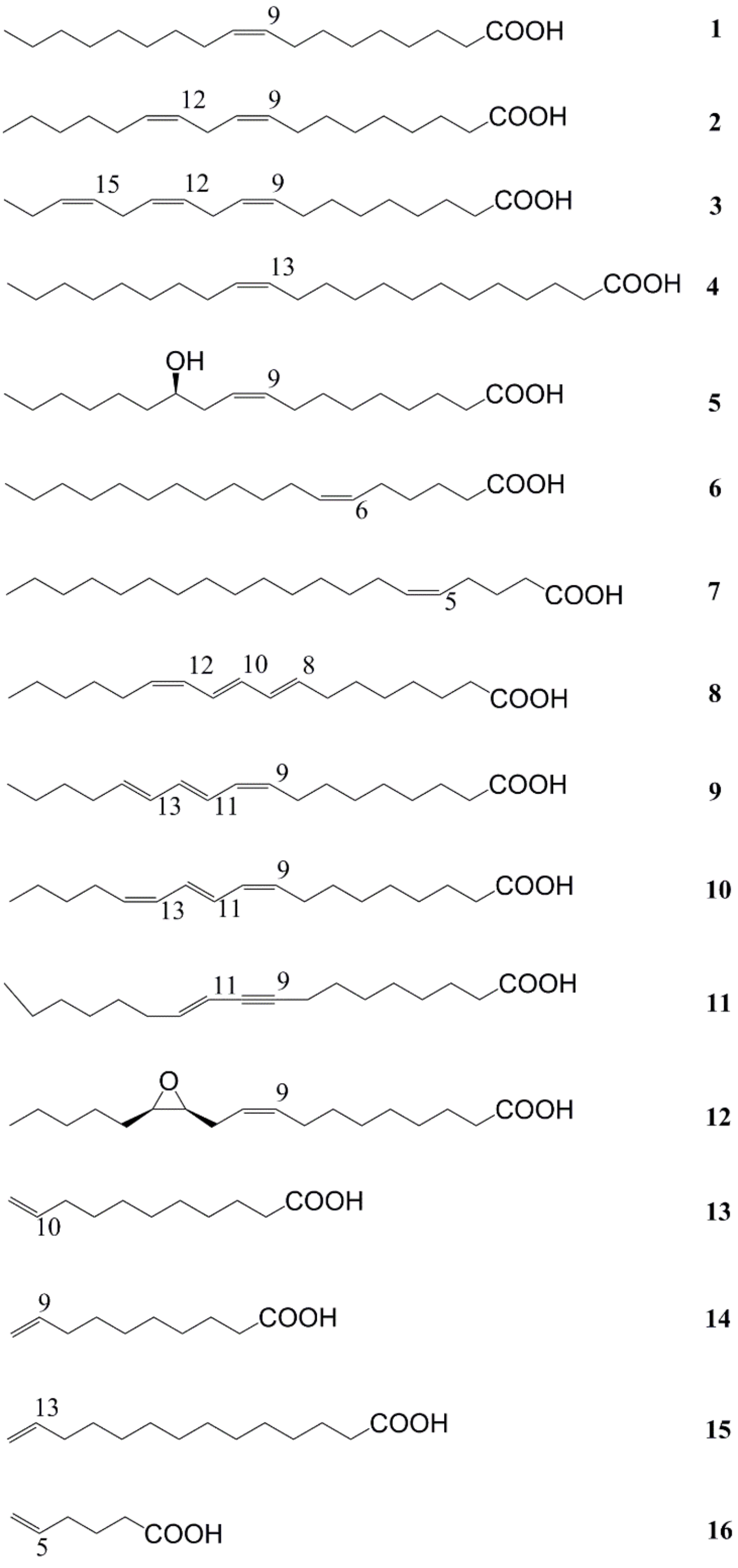

Figure 1.10 Fatty compounds as starting materials for synthesis: oleic acid (**1**), linoleic acid (**2**), linolenic acid (**3**), erucic acid (**4**), ricinoleic acid (**5**), petroselinic acid (**6**), 5-eicosenoic acid (**7**), calendic acid (**8**), a-eleostearic acid (**9**), punicic acid (**10**), santalbic acid (**11**), vernolic acid (**12**), 10-undecenoic acid (**13**), 9-decenoic (**14**), 13-tetradecenoic acid (**15**), and 5-hexenoic acid (**16**). NB: although not shown, their respective methyl esters are referred to as **1a–16a**.[27]

The double bonds act as reactive sites for coatings and paints, but usually, additional functionalization methods need to be used for preparation of polymeric materials.[29] Figure 1.11 shows possible reactive sites within a triglyceride: ester groups, C=C double bonds, allylic positions, and; α-positions of ester groups.[30]

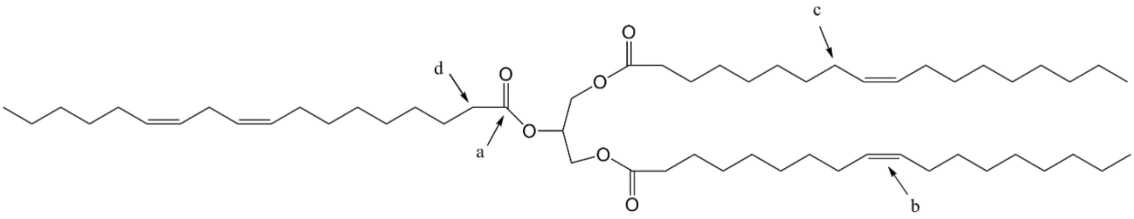

Figure 1.11 Reactive positions in triglycerides: ester groups (a), C=C double bonds (b), allylic positions (c), and α-positions of ester groups (d).

Vernonia oil is a naturally occurring EPO comprising vernolic acid (**12)** which accounts for 80% of the total fatty acid contents.[31] Epoxidized soybean oil (ESBO) and epoxidized linseed oil (ELO) are two popular EPOs currently due to their commercial availability. For example, Lankroflex E2307 (ESBO) and Lankroflex L (ELO) produced by Ackros Chemicals. The oxirane contents of ESBO and ELO are about 7% and 9%, respectively.

Generally, commercial EPOs are produced via the Prileshajev-epoxidation process with peracetic or performic acid generated *in situ* from hydrogen peroxide in the presence of an acid catalyst (Figure 1.12). In order to improve epoxide selectivity, minimize side reactions and better safety, other methods like acidic ion exchange resin, chemo-enzymatic epoxidation and metal-catalyzed systems are exploited for the epoxidation process.[32] More double bonds per triglyceride result in higher functionality and higher iodine value results in higher oxirane content, both of which are responsible for the higher cross-link density.

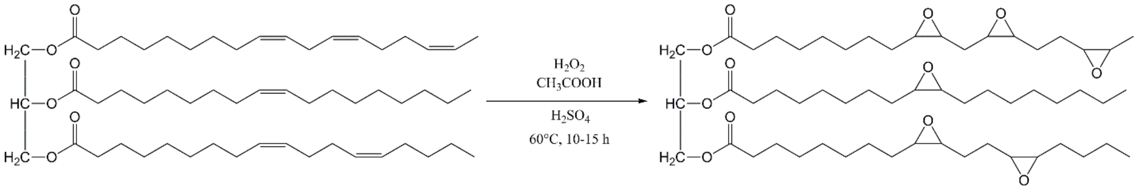

Figure 1.12 Conventional epoxidation of linseed oil.

EPOs are generally used as plasticizers or stabilizers for PVC synthesis,[33] toughening agents for petroleum-based epoxy systems, or as epoxy prepolymers for the production of thermosetting resins.[32, 34]

Park *et al.*[35] studied the cationic polymerization of ESBO and epoxidized castor oil (ECO) with a latent thermal initiator *N*-benzylpyrazinium hexafluoroantimonate (BPH, Figure 1.13). The glass transition temperature, T_g, for ECO/BPH and ESBO/BPH systems were 38 ^{o}C and 24 ^{o}C, respectively. The higher T_g for ECO/BPH system was attributed to the higher intermolecular interactions caused by the presence of –OH groups. EPOs can also be cured with conventional amine or anhydride curing agents.[36-38] Their studies showed that the structure and concentration of the curing agents played an important role on the properties of the cured resins.[36-38]

In order to improve the properties of EPO-based epoxy systems, petroleum-based epoxy compounds like DGEBA are used to blend with EPOs.[39-41] Park *et al.* investigated the effect of different ECO[39] and ESBO[41] contents on the properties of DGEBA systems cured by BPH. They found that with the addition of ESBO or ECO the impact strength of the DGEBA based resin improved significantly.

EPO-based composites have also been studied with various reinforcing agents such as fibres[42] and inorganic materials.[43, 44] Lligada *et al.*[43] prepared bio-nanocomposites from ELO and 3-glycidylpropylheptaisobutyl-T8-polyhedral oligomeric silsesquioxane (G-POSS, Figure 1.13). Higher T_g and storage modulus in both the glassy state and rubber plateau were observed for the nanocomposites due to the reinforcement effect of the G-POSS cages.

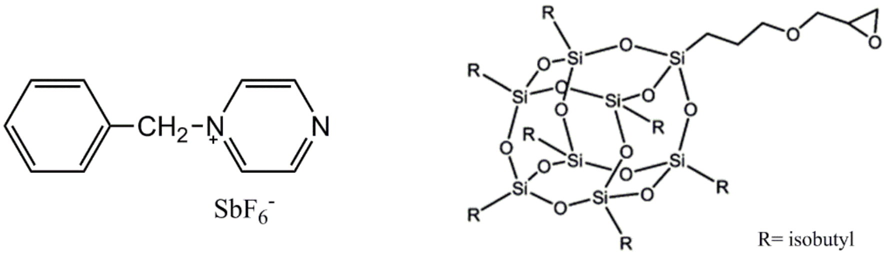

BPH

G-POSS

Figure 1.13 Structure of BPH and G-POSS.

1.5.2 Epoxy monomers from other renewable materials

As mentioned before, epoxy precursors from various renewable materials are already summarized in a recent review,[25] herein only some commercial epoxy products will be discussed briefly.

Glycerol-derived epoxy precursors such as polyglycidyl ether (GPE) and polyglycerol polyglycidyl ether (PGPE), and sorbitol-derived epoxy precursors such as sorbitol polyglycidyl ether (SPE) are commercially available, known as the Denacol™ aliphatic epoxies (Figure 1.14).

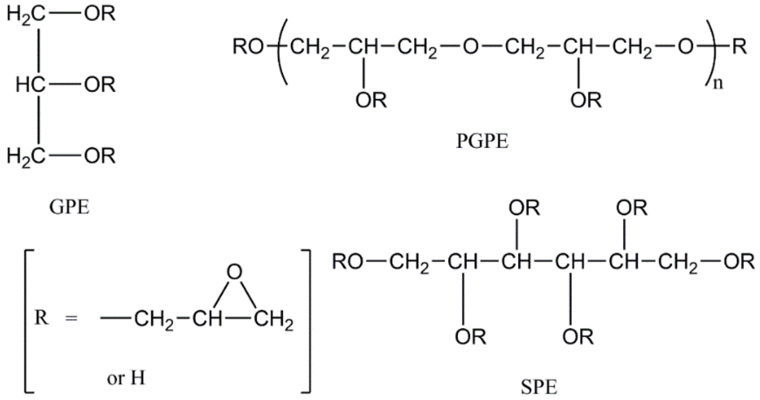

Figure 1.14 Structure of GPE, PGPE and SPE.

Cashew nutshell liquid (CNSL) based di-functional and tri-functional reactive epoxy resins Cardolite® NC-514 and NC-547 (Figure 1.15) are also commercially available with main application as coatings for maritime industries.

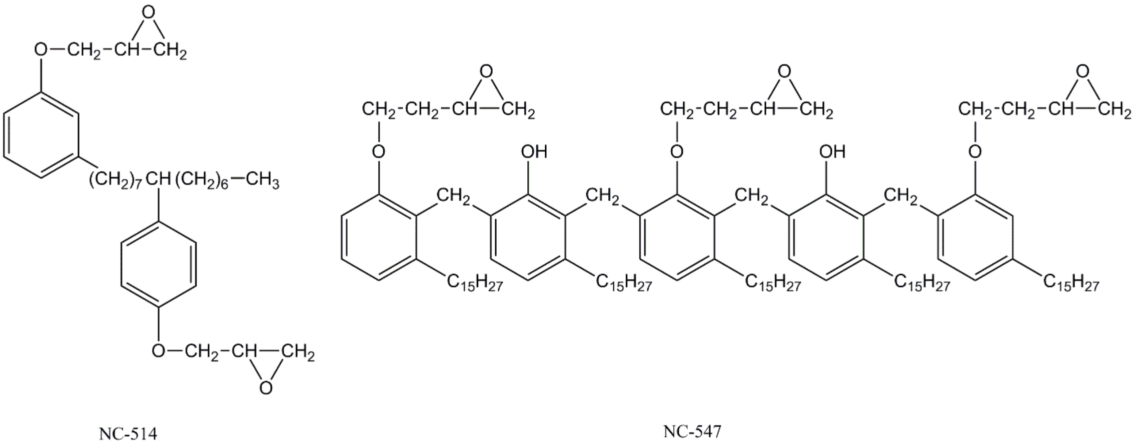

Figure 1.15 Structure of cardanol epoxy derivatives commercialized by Cardolite®.

1.6 Biobased curing agents

Herein, recent developments in Type I and Type III curing agents derived from potentially renewable, biobased resources are reviewed because they contribute significantly (by wt%) to the total weight of an epoxy resin system. Attention is given to modified plant oils, biobased acids, and anhydrides, amines, biobased phenols, rosin acids, terpenes, and lignin as biobased curing agents for primarily epoxy resin or biobased epoxy resin systems.

1.6.1 Modified plant oils

1.6.1.1 Reaction at double bonds: maleinization

Maleinization, the reaction of maleic anhydride (MA) with a double bond, is a common method to introduce an anhydride group into a triglyceride. For example, Warth *et al*.[45] prepared maleated plant oil (MPO) by directly reacting a triglyceride with MA in an inert atmosphere (nitrogen) at 200 °C for 7 h. Although this review will not focus on peroxides, it is noteworthy to mention that the use of peroxide catalysts, such as benzoyl peroxide,[46] 2,5-bis(*tert*butylperoxy)-2,5-dimethylhexane peroxide, and di-*tert*-butyl peroxide,[47] allows maleinization to proceed faster and at lower temperatures.

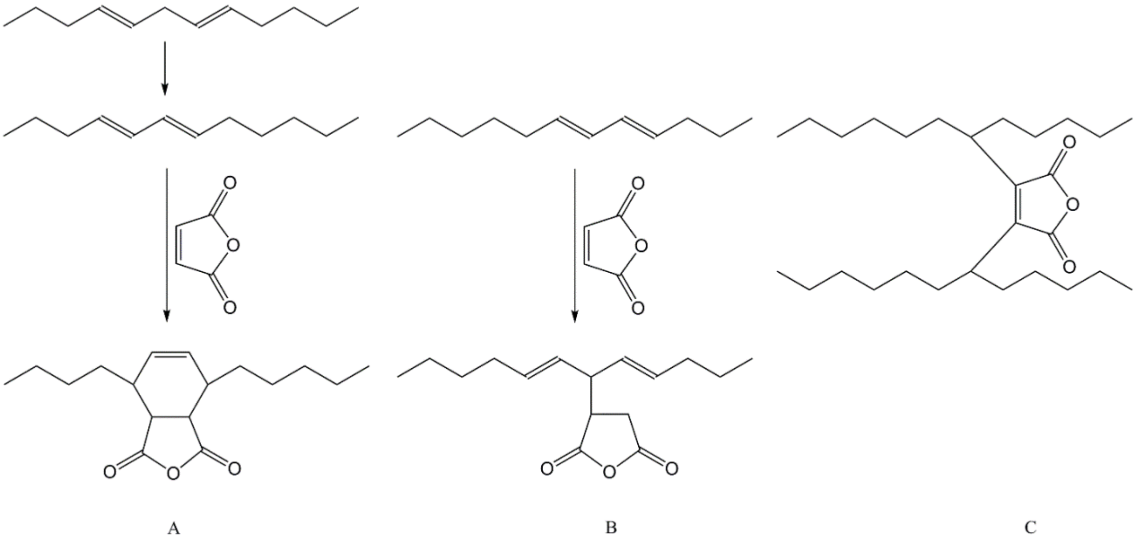

Figure 1.16 Possible addition of MA to nonconjugated double bonds. (A) Diels-Alder adduct, (B) radical addition, and (C) cross-linking.

As shown in Figure 1.16, Tran *et al*.[47] summarized three possible product pathways for maleinization yielding either a Diels-Alder adduct (A), radical addition product (B), or cross-linking, whereby the MA links two triglyceride chains (C).

The long-chain carbon backbone confers flexibility, and many MPOs have been used as flexible anhydride curing agents for epoxy resins.[45, 48, 49] Warth *et al*.[45] reported the use of maleated soybean oil (MSO) and maleated linseed oil (MLO) as flexible hardeners for diglycidyl ether of bisphenol A (DGEBA) and epoxidized natural oils, in the presence of aluminum acetylacetonate as catalyst, to yield highly cross-linked amorphous polyesters. The thermal and mechanical properties of the resultant polyesters depended on the type and concentration of anhydride employed and in particular the epoxy to anhydride molar ratio. MLO, which has higher anhydride content than MSO, afforded better thermal and mechanical properties.

Besides reacting with triglycerides directly, modified plant oils, such as methyl soyate,[48] acrylated epoxidized soybean oil (AESO),[50] and soybean oil monoglycerides (SOMGs),[51] have been maleinized to further improve their reactivity. Tran *et al.*[48] compared the curing properties of maleated methyl soyate (MMS) and MSO with epoxidized soybean oil (ESBO) in the presence of hexamethylenediamine (HMD) and 4-dimethylaminopyridine (DMAP), showing that MSO provided higher gel content (almost no weight loss) after Soxhlet extraction compared with MMS. Interestingly, to the best of our knowledge, maleated AESO and SOMGs have not been explored as curing agents for epoxy resins but have been reported as blends with styrene to produce thermoset copolymers.[50, 51]

Biermann *et al.* reported that the Diels–Alder addition of MA to methyl α-eleostearate occurred both regio- and stereoselectively at positions C-11 and C-14 of the ester.[52] The latter is derived from α-eleostearic acid (9-*cis*,11,13-*trans*-octadecatrienoic acid, **9**), a conjugated triene acid found in the oil from the nuts of the tung oil tree and, hence, is also known as tung oil.[53] Xu *et al.*[54] prepared nanocomposites composed of epoxy resin, tung oil anhydride (TOA), and montmorillonite (MMT). The resultant nanocomposites were exfoliated to good effect such that the individual silicate layers were dispersed in the polymer matrix, and the glass transition temperature (T_g) decreased with increasing MMT content.

1.6.1.2 Reaction at double bonds: thiolation

Thioethers are of great importance in changing the functionality of double bonds and have been synthesized traditionally via the thiol-ene reaction, which is the addition of a thiol to an alkene forming a thioether.

A thiol-ene reaction is high yielding, regio- and stereospecific, and able to introduce various functional groups.[55] Gerald *et al.*[56] summarized a wide variety of sulfur-based monomers (Figure 1.17) and their subsequent polymers that may be realized by the thiol-ene reactions.

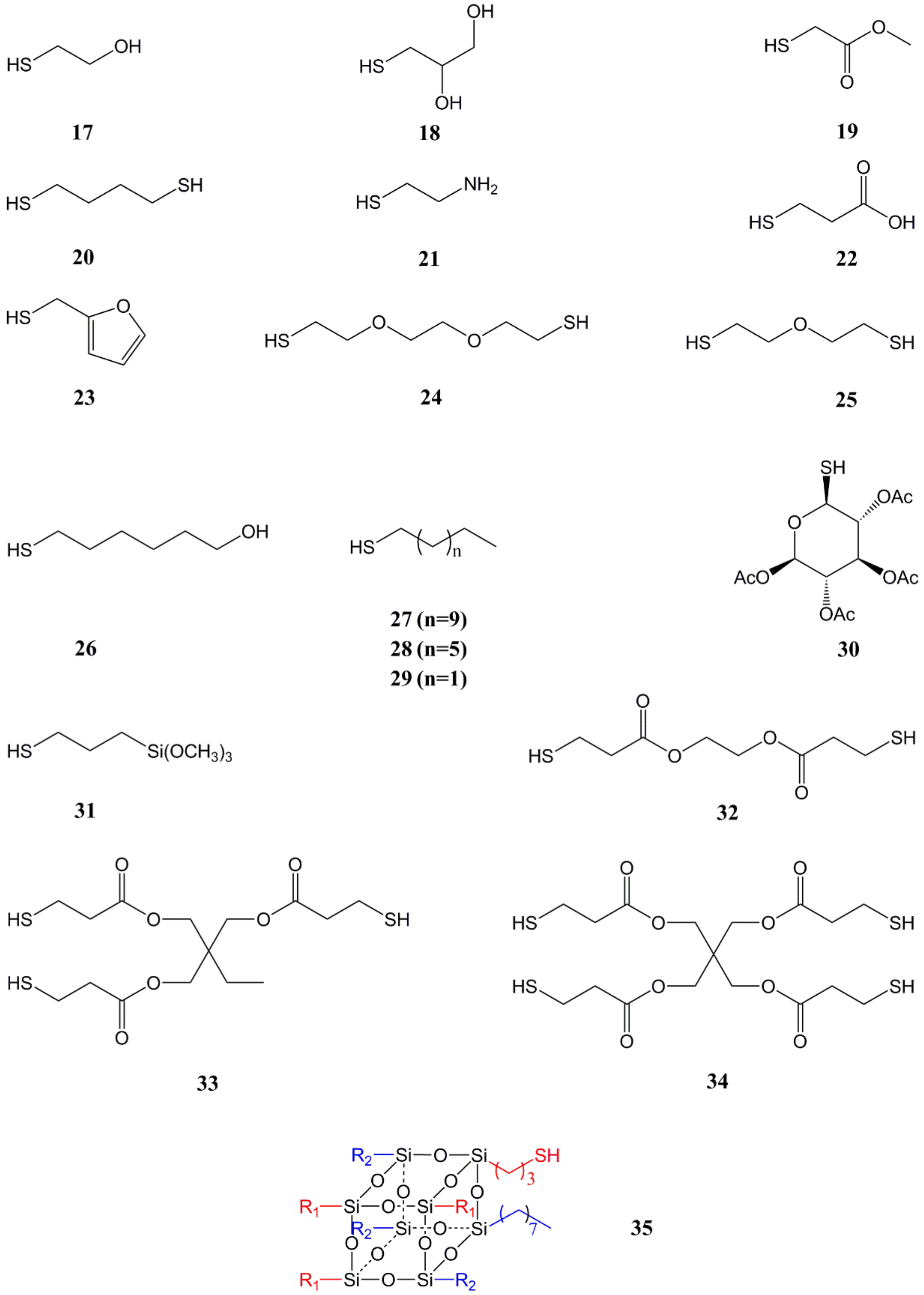

17 **18** **19**

20 **21** **22**

23 **24** **25**

26 **27 (n=9)** **28 (n=5)** **29 (n=1)** **30**

31 **32**

33 **34**

35

Figure 1.17 Chemical structures of thiols used in the transformation of oleochemicals into monomers and polymers.

Jaillet *et al.*[57] reported a novel biobased polyacid hardener derived from soybean oil by thiol-ene coupling with thioglycolic acid (Figure 1.18). ^{1}H NMR analysis revealed an acid funtionality of 3.3 per triglyceride molecule and with only 15% of thioester as byproduct. The latter and further side reactions have been investiagted by Desroches *et al*.[58] using NMR, FT-IR, LC-MS, and iodine titration based on oleic acid as a model compound. The performance of the sulfur-containing polyacid hardener when studied with DGEBA showed increased reactivity compared to conventional amine hardeners.

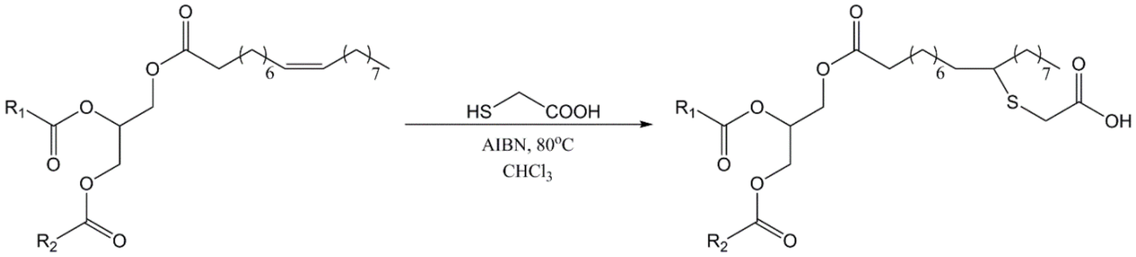

Figure 1.18 Functionalization of soybean oil with thioglycolic acid.

Stemmelen *et al*.[59] used the thiolene reaction to good effect by reacting grape seed oil (GSO) with cysteamine chloride (**21)** (Figure 1.17) to yield aminated grape seed oil (AGSO). In their study, GSO with 4.75 double bonds per triglyceride was modified to AGSO with 4.13 amine units per triglyceride for 87% of conversion.

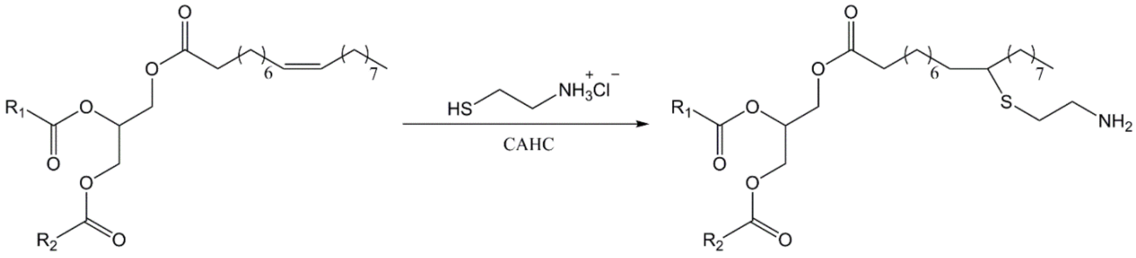

Figure 1.19 Amination of GSO using CAHC by UV-initiated thiol-ene coupling.

1.6.1.3 Reaction at double bonds: allylic reaction

The allylic position (Figure 1.11, position c) has been modified to good effect by several researchers. For example, Shibata *et al*.[60] introduced pyrogallol (PG) moieties into tung oil triglycerides to afford tung oil-pyrogallol resin (TPG) catalyzed by *p*-toluenesulfonic acid (Figure 1.20). Unlike soybean and linseed oils, which give oligomerized materials on reaction with pyrogallol, the presence of a conjugated triene moiety in tung oil triglycerides furnishes a cleaner and less troublesome reaction in acidic conditions with a degree of addition of PG to the C=C double bonds of 2.3 per triglyceride. Furthermore, Shibata *et al*.[60] produced biocomposites comprising sorbitol polyglycidyl ether (SPE, Figure 1.14) as epoxy resin, TPG as hardener, and wood flour, which showed much higher storage moduli than SPE-TPG resin alone. The tensile strength, modulus, elongation and T_g (measured by dynamic mechanical analysis, DMA) for the

SPE–TPG network cured under 190 °C for 3 h were 28.2 MPa, 1070 MPa, 7.4%, and 53.5 °C, respectively.

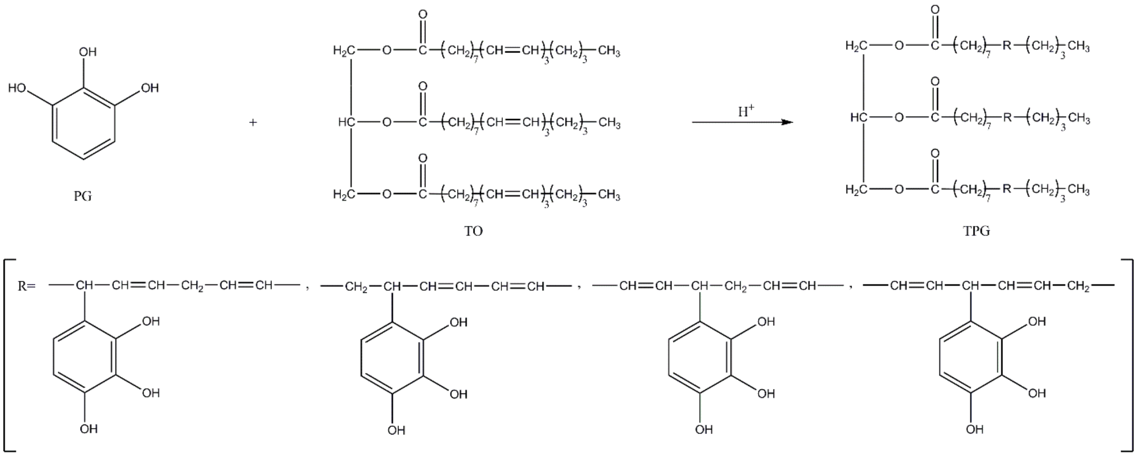

Figure 1.20 Synthetic scheme of TPG.

1.6.1.4 Reaction at the carbonyl group

Desroches *et al*.[61] successfully produced an amido-amine hardener in a one-step reaction between DETA and the carbonyl group within vegetable oils (Figure 1.21) with an average functionality of 3. The monoadduct was used as amine hardener with DGEBA epoxy precursors to yield a resin with T_g of 32 °C.

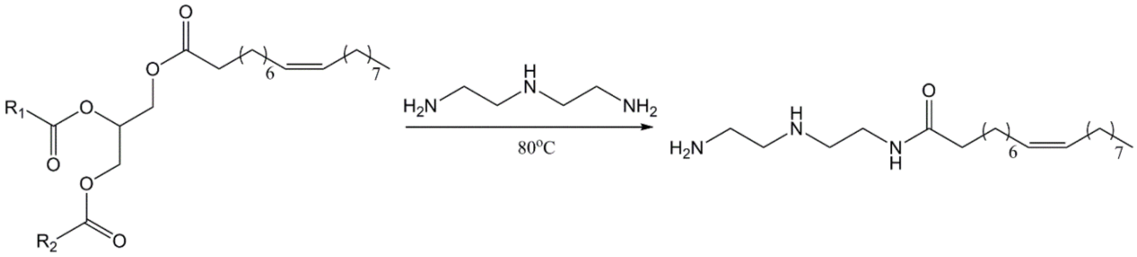

Figure 1.21 Amine hardener by vegetable oil amidification.

Although Zhao *et al.*[62] reported amine-functionalized triglycerides. In the context of biobased materials and sustainability that the reaction conditions used to obtain the corresponding triamine are very poor, *i.e.*, a couple series of reactions were undertaken including epoxidation, reduction, bromination, substitution and reduction.

1.6.1.5 Biobased polyols

Most biobased polyols are derived from plant oils and fatty acids via a variety of methods, for example, hydroxylation of double bonds, ring opening of epoxidized plant oils (EPOs), and dimerization of fatty acids.[63, 64] Polyols in the main are used to make polyurethane polymers, and relatively few papers report their use as curing agents for epoxy resins. However, Czub *et al*.[65] prepared hydroxylated soybean oil and rapeseed oil via ring opening of their respective epoxidized precursors, either monoethylene glycol (MEG) or diethylene glycol (DEG), in the presence of sulfuric acid as catalyst (Figure 1.22), which on subsequent reaction with DGEBA produced a high molecular weight epoxy resin. Ahn *et al*.[66] have made biobased pressure sensitive adhesive (PSA) tapes from the reaction between dihydroxyl soybean oil (DSO) and ESBO in the presence of phosphoric acid, which have comparable peel strengths to commercial nonbiobased PSA tapes. The PSA tapes were produced at 110 °C within 30 s through a simple air-drying process possessing good thermal and chemical stability and optical transparency.

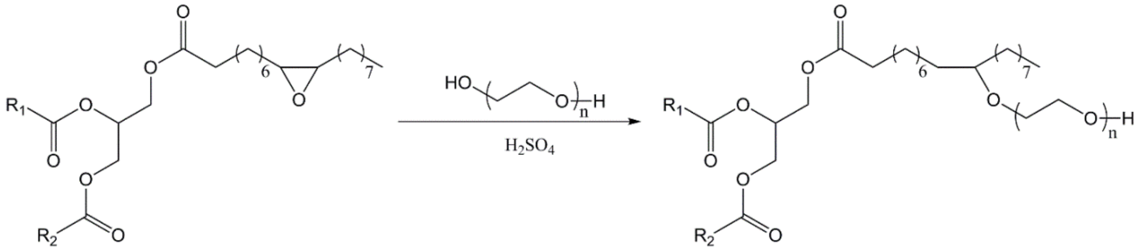

Figure 1.22 Hydroxylation of epoxidized oils.

Alternatively, certain plant oils inherently contain hydroxyl (alcohol) groups. For example, the hydroxyl group within castor oil can be further derivatized to yield hardeners. Liu *et al*.[67] reacted castor oil with phosphoryl chloride to produce phosphorylated castor oil (PCO, Figure 1.23) in high yield (80% conversion ratio for the hydroxyl phosphorylation) followed by a reaction with ESBO or ELO to give elastomers without the need for additives at 37 °C.

Plant oil-derived fatty acids, which can be easily obtained by either simple hydrolysis or alcoholysis of triglycerides, are potential biobased hardeners and will be discussed in next section.

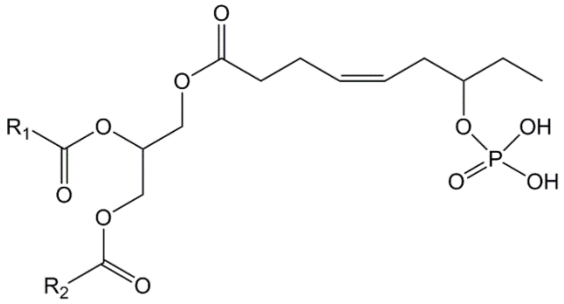

Figure 1.23 Structure of phosphorylated castor oil.

1.6.2 Biobased carboxylic acids and anhydrides

1.6.2.1 Biobased carboxylic acids

Traditionally, dicarboxylic acids (DCAs, $HOOC(CH_2)_nCOOH$) are mainly derived from petrochemical feedstocks. From the view of renewable starting materials, short-chain DCAs may be obtained either by fermentation or chemical transformation of carbohydrates, while long-chain DCAs could be obtained either by chemical or enzymatic modification of fatty acids. In 2004, the U.S. Department of Energy (DOE) identified 12 sugar-derived building blocks (Table 1.2), the so-called "platform molecules", eight of which are DCAs easily accessible from glucose.[69-72]

Table 1.2 Top Sugar-Derived Building Blocks

Building Blocks
1,4-diacids (succinic, fumaric and malic)
2,5-furan dicarboxylic acid
3-hydroxypropionic acid
aspartic acid
glucaric acid
glutamic acid
itaconic acid
levulinic acid
3-hydroxybutyrolactone
glycerol
sorbitol
xylitol/arabinitol

Fatty acids are easily available by either hydrolysis or alcoholysis of animal and vegetable oils and fats. The hydrolysis process of triglycerides was summarized by Corma *et al*.[70] A range of DCAs synthesized from fatty acids either by chemical or enzymatic transformations are shown in

Table 1.3. The structures of these substrates are shown in Figure 1.10.[27]

Table 1.3 Unsaturated fatty acids and esters as substrate for synthesis of linear fatty diacids.

Entry	Substrate	Synthesis	Diacid[a]	Co-product
1	**6**	Ozonolysis	6	Dodecanoic acid
2	**7a**	Cross-metathesis with methyl acrylate; hydrogenation	7[b]	Methyl heptadecanoate
3	**6a**	Cross-metathesis with methyl acrylate; hydrogenation	8[b]	Methyl heptadecanoate
4	**1**	Ozonolysis	9	Nonanoic acid
5	**5**	Splitting with caustic soda	10	2-Octanol
6	**1a**	Cross-metathesis with methyl acrylate; hydrogenation	11[b]	Methyl undecanoate
7	**13a**	Cross-metathesis with methyl acrylate; hydrogenation	12[b]	Ethene
8	**1a**	Cross-metathesis with 2-butene; methoxycarbonylation, hydrogenation	12[b]	Methyl dodecanoate
9	**4**	Ozonolysis	13[b]	Nonanoic acid
10	**13a**	Cross-metathesis with 2-butene; methoxycarbonylation	14[b]	-
11	**4a**	Cross-metathesis with methyl acrylate; hydrogenation	15[b]	Methyl undecanoate
12	**4a**	Cross-metathesis with 2-butene; methoxycarbonylation	16[b]	Dodecanoic acid
13	**15a**	Cross metathesis with 1-butene; methoxycarbonylation	17[b]	-
14	**1a**	Self-metathesis; hydrogenation	18[b]	Octadecane
15	**14a**	Self-metathesis; hydrogenation	18[b]	Ethene
16	**1**	Microbial oxidation	18	-
17	**1**	Methoxycarbonylation	19	-
18	**13a**	Self-metathesis; hydrogenation	20[b]	Ethene
19	**7a**	Methoxycarbonylation	21[b]	-
20	**4a**	Methoxycarbonylation	23[b]	-
21	**4a**	Self-metathesis; hydrogenation	26[b]	Octadecane
22	**15a**	Self-metathesis; hydrogenation	26[b]	Ethene

[a] Number of carbon atoms of diacids; [b] Dimethyl ester

For example, as outlined in Figure 1.24, ozonolysis is an efficient way of making DCAs. Ozonolysis of oleic acid (**1**, entry 4 in Table 1.3) furnishes pelargonic and azelaic acid. Ozonolysis of petroselenic acid (**6**, entry 1 in Table 1.3) affords adipic acid. Brassylic acid can be obtained from erucic acid (**4**, entry 9 in Table 1.3). Vasishtha *et al.*[73] used high temperature (250 °C) alkali hydrolysis of castor oil to produce sebacic acid via ricinoleic acid (Figure 1.25, entry 5 in Table 1.3).

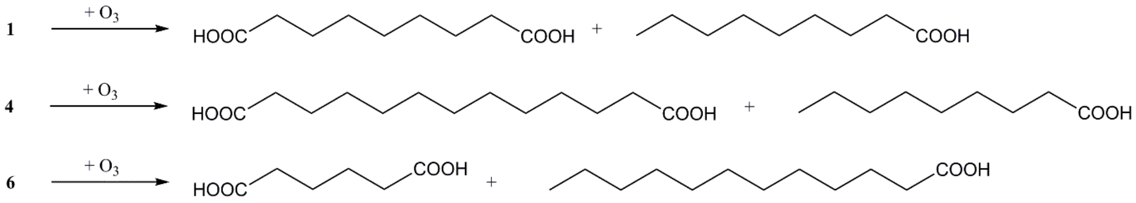

Figure 1.24 Oxidative scission of oleic acid (**1**) with ozone to give azelaic acid and pelargonic acid. Erucic acid (**4**) gives brassylic acid and pelargonic acid. Petroselinic acid (**6**) gives adipic acid and lauric acid.

Microbial methods of ω-oxidation of the terminal CH_3 group of long-chain fatty acids to produce diacids are gaining impetus. *Candida tropicalis* is widely used in the production of DCAs of different chain lengths to good effect with yields exceeding 100 g/L.[74,75]

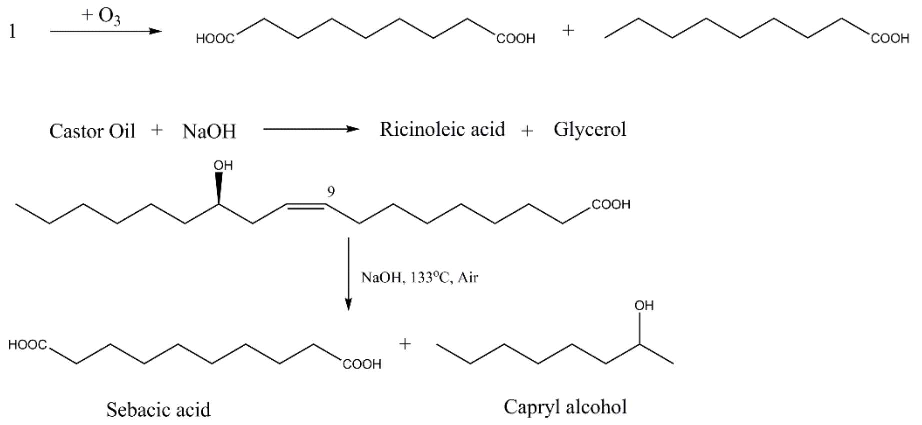

Figure 1.25 Production of sebacic acid and capryl alcohol from castor oil.

Ahn *et al*.[76] reported magnesium stearate (Mg stearate) as a biobased acid catalyst to ring open ESBO in a one-step process without using a solvent or purification process. Different products were obtained depending on the ratio of the epoxy group and Mg stearate, namely, a biogrease material for ratios of 1:1 to 1:2 and a thermoplastic-like material for a ratio of 1:4 with a T_g of -27 °C and T_m of 90 °C.

Shogren *et al*.[77] studied the biodegradation behavior of epoxy networks from ESBO cross-linked with different aliphatic carboxylic acids (citric acid, succinic acid, adipic acid, and sebacic acid) in the presence of either aluminum acetyl acetonate or tetrabutyl ammonium bromide as catalyst. The epoxy networks showed fairly rapid degradation in soil due to the inherent polyester structure formed between reactions of epoxy groups with acid groups. Although the full mechanism is yet to be elucidated, the main reaction is considered to be the addition esterification reaction between epoxy and carboxylic acid groups, accompanied by several side reactions.[78] The polymerized ESBO and citric acid combination was further used as coatings on Kraft paper to slow the degradation process.[79] Under certain conditions, for example, in the absence of catalysts, polyols were obtained from epoxidized vegetable oils with different biobased diacids (C_6-C_{12})[80] or mono fatty acids (acetic acid, lactic acid, and glycolic acid).[81]

Interesting applications of biobased diacids include vulcanizing epoxidized natural rubber (ENR) using dodecanedioic acid[82] and cross-linking with liquid crystalline (LC) epoxy monomers to form liquid crystalline elastomers (LCEs, C_6-C_{10}).[83] Compared with the sulfur vulcanization process, the reaction between ENR and dibasic acids lessened the detrimental effect of heat treatment and eliminated the use of some toxic additives like zinc oxide. As for the LCEs, their properties were largely dependent on the nature of epoxy monomers and curing agents.

DCAs may also be made by dimerization of fatty acids, for example, C_{18}. The products obtained through this process are a mixture of dimers, trimers, and isostearic acid due to the existence of many side reactions.[70] A range of different C_{36} dimer and trimer fatty acids, namely, Pripol™ and Unidyme™, are available from Croda and Arizona Chemical, respectively. Supanchaiyamat *et al*.[84] reported synthesis and properties of a fully biobased flexible and water-resistant network derived from ELO and Pripol 1009 in the presence of different catalysts, triethylamine (TEA), 1,8-diazabicyclo[5.4.0]undec-7-ene (DBU),1-methylimidazole (1-MI), 2-methyl- imidazole (2-MI), and DMAP.

Montarnal *et al*.[85] amidated Pripol 1040 (70 wt% trimer acids) with aminoethylimidazolidone (UDETA) and subsequently cross-linked it with DGEBA in the presence of 2-MI to generate cross-linked materials combining the supramolecular chemistry of urea with the chemistry of epoxies. The presence of H-bonding groups in the material improved matrix-filler interactions thus producing composites with better mechanical properties. Leibler *et al*.[86-88] reported a new concept of epoxy networks termed "vitrimers", which are strong organic glass covalent formers able to change their topology through thermoactivated bond exchange reactions. Vitrimers were obtained from the cross-linking reactions between DGEBA and Pripol 1040 or anhydrides in the presence of different transesterification catalysts. Different temperature welding experiments[87] and effects of catalyst types and concentrations[88] were also studied. The welding process was achieved in different time-temperature windows without any changes of the dimensions of the materials. Faster welds were achieved at higher temperatures: with higher catalyst concentration, a higher force at break was obtained. Zinc acetate ($Zn(OAc)_2$) and triazobicyclodecene (TBD) were found to be more efficient transesterification catalysts compared with triphenylphosphine (PPh_3).

On the basis of the concept of vitrimers, Pei *et al*.[89] developed liquid crystal elastomers with exchangeable links (xLCEs) from the reaction of DGEBA or diglycidyl ether of 4,4'-dihydroxybiphenol (DGE-DHBP) with sebacic acid in the presence of triazobicyclodecene as catalyst. The resultant LCEs were easily processable with monodomain alignment making them useful as actuators and artificial muscles.

Carter *et al.* [90] reported a carboxyl-terminated polyester (Figure 1.26) for potential use in heavy duty flooring applications synthesized from the reaction of dipropylene glycol and MA followed by cross-linking with ELO.

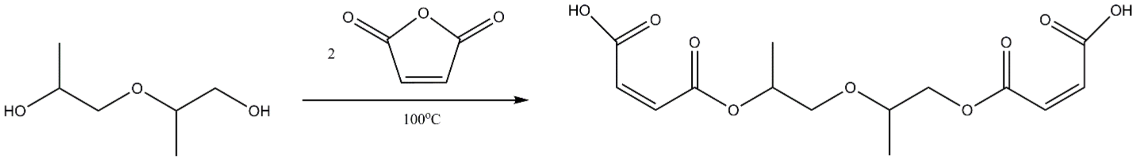

Figure 1.26 Schematic synthesis of maleic monoester used to cross-link ELO.

1.6.2.2 Biobased anhydrides

Hu *et al.* [91] reported an efficient and convenient method to synthesize DCAs from carboxylic acids with sulfated zirconia by phase transfer catalysis (PTC), which on heating give five- or six- membered cyclic anhydrides, succinic anhydride, and glutaric anhydride. MA can be obtained renewably, for example, by the dehydrogenation of succinic anhydride using iron phosphate based catalysts,[92] oxidation of furfural using a VO_x/Al_2O_3 catalyst,[93] oxidation of 5-hydroxymethylfurfural in the liquid phase,[94] and fermentation containing butanol using a catalyst based on oxides of vanadium and/or molybdenum.[95] Biobased PA (Figure 1.27) can be made via Diels-Alder addition between biobased furan and MA followed by dehydration of the resultant adduct. [96]

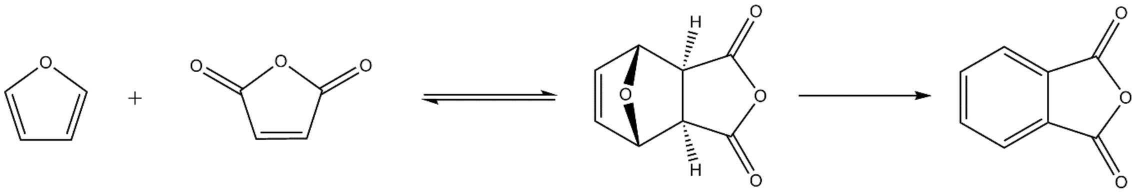

Figure 1.27 Route to renewable PA from biomass-derived furan and MA.

Vitrimers were also obtained from the cross-linking reaction between glutaric anhydride and DGEBA in the presence of zinc acetylacetonate dehydrate ($Zn(acac)_2$).[86] Compared with acid cured samples, harder networks with much higher stress and modulus were obtained. The effects of anhydride types (MA, succinic anhydride, PA, HHPA, and dodecenylsuccinic anhydride (DDS)) on dynamic mechanical and thermal behavior of epoxy resin based on ESBO were studied by Gerbase *et al.*[29], who showed that anhydrides with rigid structures like MA, PA, and HHPA gave higher T_g and cross-linking densities. Whereas, thermosets obtained from DDS produced lower thermal stability because that the side chain of the molecule started decomposition at lower temperature.

1.6.3 Biobased amines and their derivatives

1.6.3.1 Amino acids and their homopolymers

Amino acids and their homopolymers, e.g., polylysine, represent an important class of biobased amines and their derivatives. Currently, amino acids are mainly manufactured either by fermentation or enzymatic methods.[97]

Lysine[98] and tryptophan[18] (Figure 1.28) are two amino acids reported as ecofriendly cross-linking agents for epoxy resins in the electronics industry. Both the amino and carboxyl functional groups are able to ring open an epoxy moiety with the former being slightly less reactive than the latter due to absence of an active hydrogen. Li *et al.*[98] reported the T_g and thermal degradation temperatures for lysine comprising networks with a cycloaliphatic-type epoxy of 91.37 and 195.49 °C, respectively. In comparison, the network between the cycloaliphatic-type epoxy and methylhexahydrophthalic anhydride (MHHPA) gave temperatures of 127.36 °C (T_g) and 367.03 °C (degradation temperature), respectively. Tryptophan cross-linked with DGEBA in the presence of an imidazole catalyst yields networks with reasonably high T_g (107 °C) and thermal stability (284 °C).

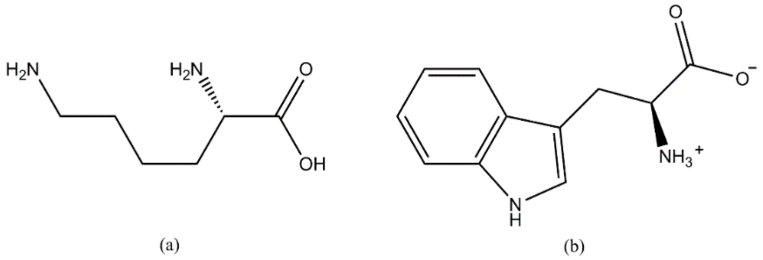

Figure 1.28 Chemical structures of (a) lysine and (b) tryptophan.

ε-Polylysine (PL) obtained by aerobic bacterial fermentation of a broth comprising *Streptomyces albulus*, glucose, citric acid, and ammonium sulfate has also been exploited as an example of an amino acid/homoploymer curing agent.[99, 100] Scholl and co-workers [101, 102] reported dendrimers of PL (Figure 1.29) obtained via homopolymerization of lysine chlorohydrate in the presence of KOH at 150 ºC. The existence of multiple pendant α-amino groups makes the resultant dendrimer potentially a very reactive cross-linking agent.

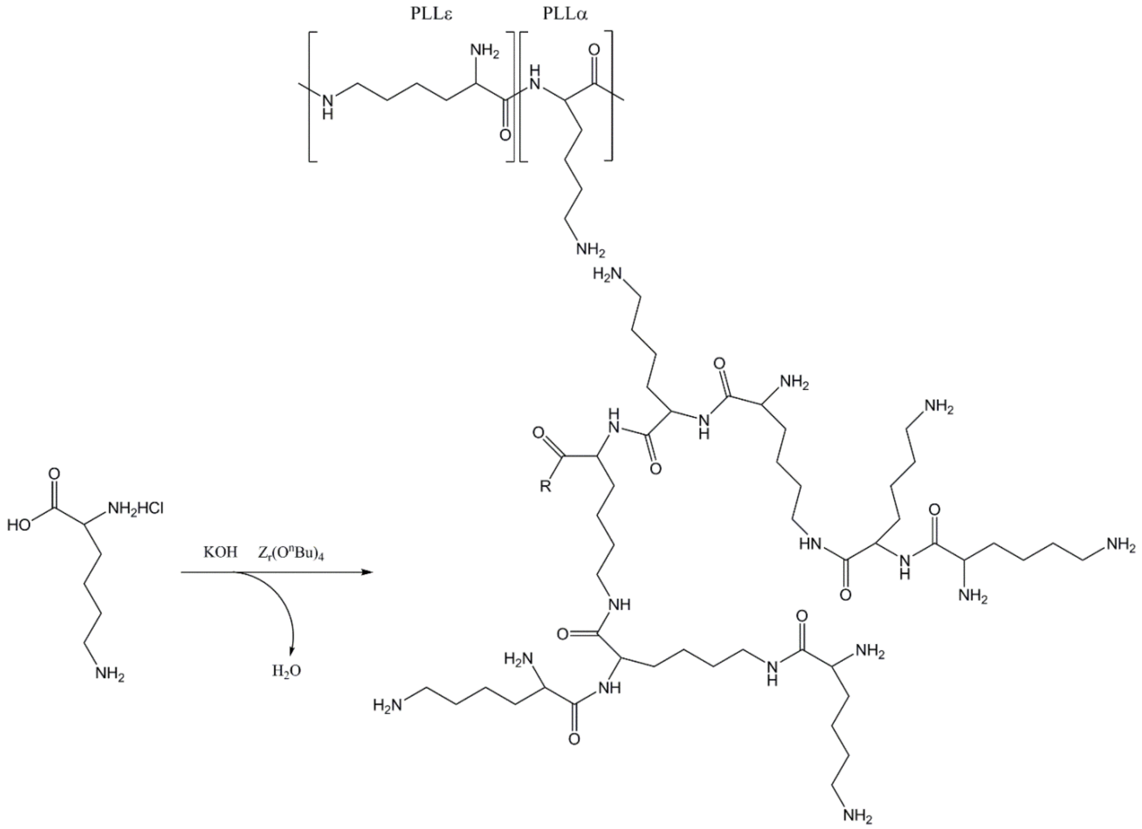

Figure 1.29 Synthesis and structure of polylysine (PL).

Takada *et al.*[103] employed PL as cross-linking agent with glycerol polyglycidyl ether (GPE) and polyglycidyl ether of polyglycerol (PGPE) epoxy prepolymers to form GPE-PL and PGPE-PL networks, respectively. The latter possessed a greater T_g compared with GPE-PL due to higher epoxy content. The incorporation of 15 wt% MMT in to the formulation significantly increased both tensile strength from 4 to 42 MPa and modulus from 6 MPa compared with its counterpart neat PGPE-PL network.

1.6.3.2 Biobased amines

Biobased amines can be made via either biotechnological or traditional chemical routes. For example, 1,5-diaminopentane, an important industrial platform chemical, may be bioengineered from *Corynebacterium glutamicum* or *Escherichia coli.*[104] Biobased amines can also be derived from isosorbides via conversion of isosorbide hydroxyl groups into cyano groups followed by hydrogenation.[105-108] Decamethylene diamine (DDA) can be obtained from castor oil-derived sebaconitrile under harsh conditions.[109] Wang *et al.*[110] made a new series of poly (epoxidized soybean oil-co-decamethylene diamine) (PESD) elastomers from the cross-linking reaction of ESBO and DDA. Further cross-linking with succinic anhydride produced materials of higher T_g and tunable tensile strength (0.8 to 8.5 MPa) compared its uncross-linked counterparts, which possessed low T_g (-30 to -17 °C). The crossed-linked elastomers showed good damping property, water resistance, and degradation resistance in phosphate buffer solution, making them potentially useful as biomaterials, e.g., actuators.

Phenalkamines are an interesting set of hardeners derived from cardanol, a component of cashew nut shell liquid (CNSL), which is a by-product from the cashew industry.[111-115] The main component of solvent-extracted CNSL is anacardic acid with a smaller amount of cardanol, cardol, and its methyl derivatives;[113] whereas, CNSL produced by roasting (high temperature) is rich in cardanol because the anacardic acid readily decarboxylates.[112]

Phenalkamines are prepared by the Mannich reaction occurring between cardanol, formaldehyde, and appropriate diamines (Figure 1.30).[116] The resultant Mannich base curing agents are advantageous because of speed, low temperature of cure, and excellent chemical and physical properties. Some phenalkamines are food contact approved and some are used in potable water coatings.

Furthermore, phenalkamines blended with polyamine salts[118] and phenalkamines comprising at least one aromatic- or alicyclic-ring in the diamine side chain[119] have also been developed to give coatings with reduced Gardner color index compared to phenalkamines.

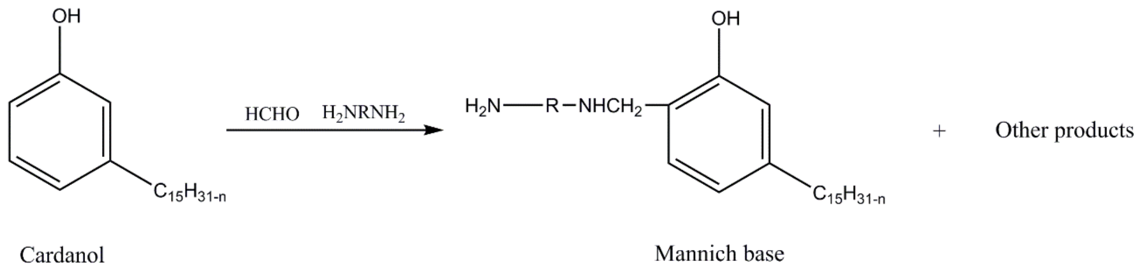

Figure 1.30 Synthesis of phenalkamine from cardanol.

1.6.3.3 Biobased polyamides

Polyamides may also be used as curing agents. Polyamides are condensation products of dimerized fatty acids and polyamines, and are commercially available from Arizona Chemical under the trade name Uni-Rez. Vijayalakshmi *et al.*[120] reported polyamides prepared from C_{21} cycloaliphatic dicarboxylic acid or C_{36} dimer acids with various amines, namely, DETA, TETA, and tetrathylenepentamine (TEPA), which subsequently were reacted with epoxy resins at different weight ratios. The cured product (binder) derived from an equivalent weight ratio of polyamide to epoxy showed better binding properties. Furthermore, C_{21} DCAs-derived binders were better than C_{36} DCAs-derived binders. Biobased amides can also be derived either from sugars such as isosorbide, isomannide, and isoidide or fatty acids as reported by Fenouillot *et al.*[121] and Fomina *et al.*[122]

Similar to phenalkamines discussed earlier, phenalkamides derived from the chemical combination of phenalkamines and polyamides can be used as curing agents for epoxy systems. The chemical and physical properties of phenalkamides are similar to phenalkamines, for example, excellent anticorrosion properties, good color stability, and extended overcoatability.

1.6.4 Biobased phenols

Phenolics are a group of epoxy curing agents that are cross-linked with epoxy groups via the phenolic hydroxyl group such as in phenol-, cresol-, and bisphenol A-terminated.

Campaner *et al.*[124] synthesized cardanol-based Novolac resins by the condensation reaction of cardanol and paraformaldehyde using oxalic acid as catalyst (Figure 1.31). By varying the ratio of cardanol to catalyst, two different types of novolacs (Nov-I and Nov-II) were obtained. The average number of cardanol units and the amount of unreacted cardanol in Nov-I and Nov-II were 3.8, 35% and 5.2, 20%, respectively. The curing properties of these two novolacs were studied with different ratios of DGEBA and the results showed that higher cross-linking density was obtained with higher amounts of epoxy resin. Compared with Nov-I, the cured resin using Nov-II had a higher T_g and better mechanical properties but similar thermal degradation properties due to the higher molecular weight and lower unreacted cardanol content.

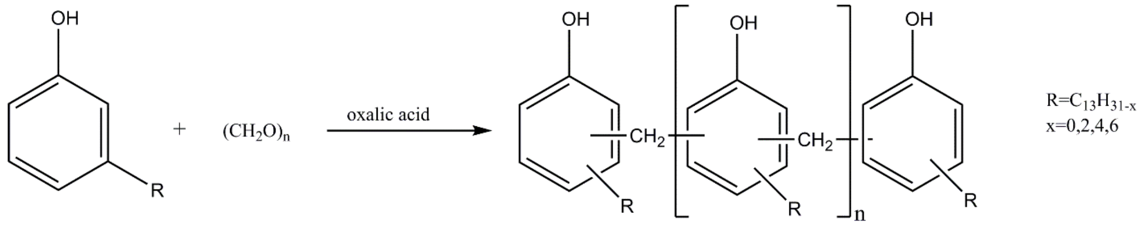

Figure 1.31 Synthesis of the cardanol-based novolacs.

Biobased polyphenols are abundant in nature albeit in low concentrations. Quideau *et al.*[125] summarized the chemical properties, biological activities and synthesis of a wide variety of plant polyphenols. Polyphenols may also be recovered or isolated from biproducts during food processing processes as reported by Schieber *et al.*[126] For example, apple pomace has potential to be exploited to produce polyphenols including catechins (Figure 1.32, a), hydroxycinnamates (Figure 1.32, b), procyanidins (Figure 1.32, c), phloretin glycosides (Figure 1.32, d) and quercetin glycosides (Figure 1.32, e).

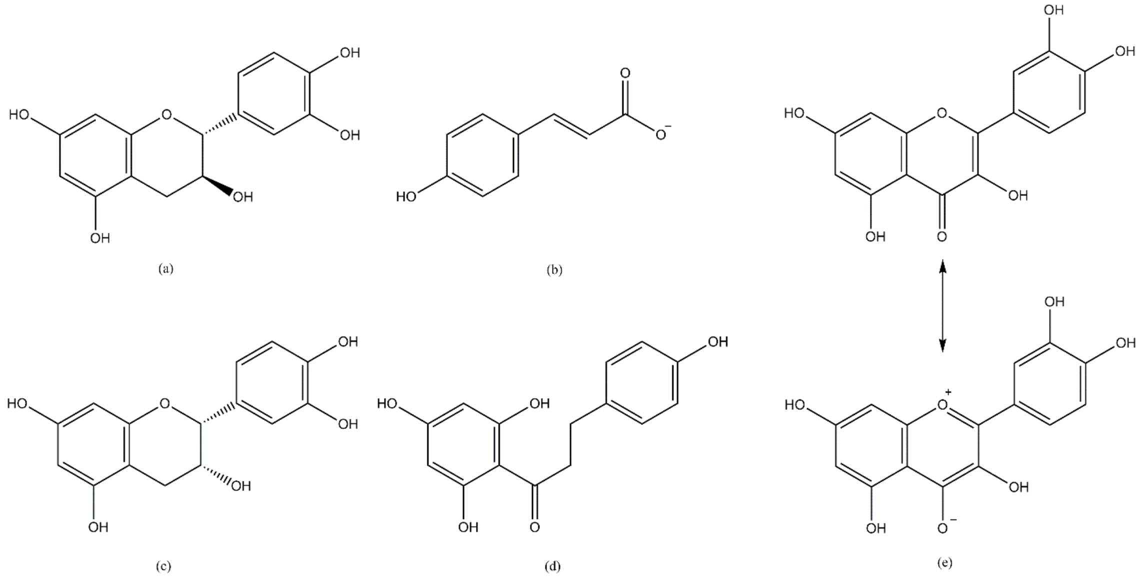

Figure 1.32 Structures of (a) catechin; (b) hydroxycinnamates; (c) procyanidins; (d) phloretin; (e) quercetin and its resonance structure.

Tannins are defined as chemicals mainly composed of phenolic structures, including condensed or polyflavonoid tannins and hydrolyzable tannins.[127] Commercial tannic acid (TA, $C_{76}H_{52}O_{46}$, Figure 1.33) is based mainly on glucose ester of gallic acid.

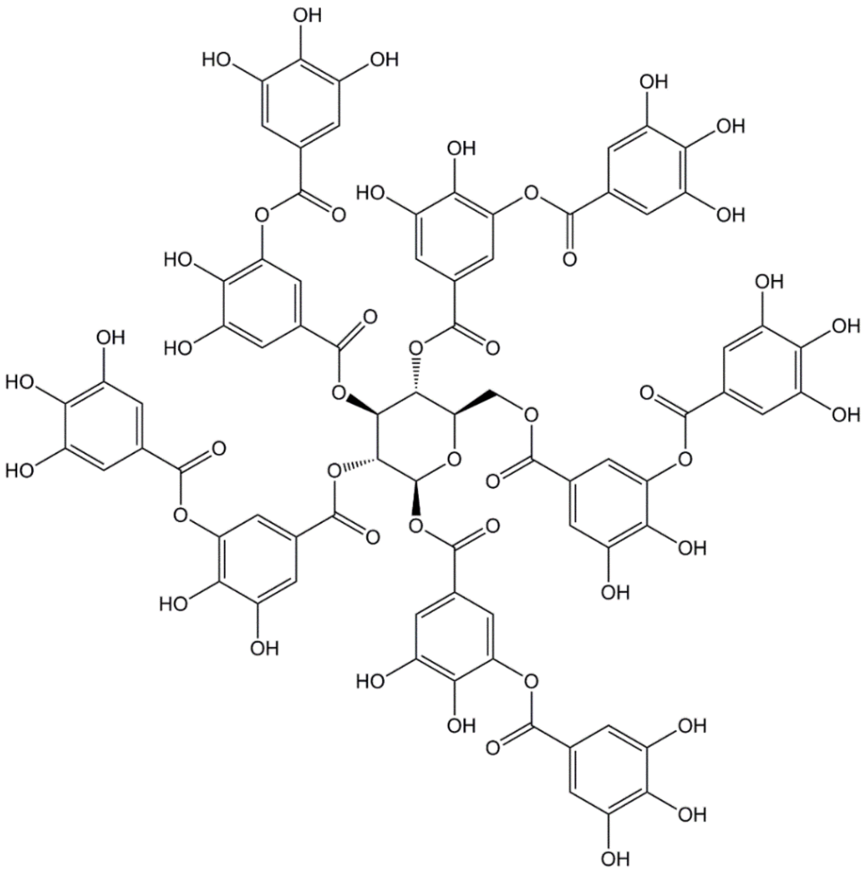

Figure 1.33 Structure of tannic acid (TA).

The Mitsuhiro group[60, 128-131] have explored several biobased polyphenols as curing agents. For example, they have used TA as a curing agent with GPE, SPE (Figure 1.14) and ESBO to form biobased resins.[128, 129] The most balanced thermal and mechanical properties were obtained for a 1:1 epoxy (either GPE or SPE) to hydroxyl (TA) ratio whereas a slightly higher ratio was needed for ESBO (1:1.4) because of the additional steric hindrance of the epoxy groups in ESBO. Consequently, T_g, tensile strength, and modulus of the ESBO epoxy resin system was lower than those of GPE and SPE. Shibata *et al.*[128, 129] also investigated the effect of adding microfibrillated cellulose (MFC) to the epoxy resins, which significantly enhanced both thermal and mechanical properties of the resultant network.

Shimasaki *et al.*[130] reported the synthesis of a pyrogallol–vanillin calixarene (PGVNC) via the reaction of PG and vanillin (VN) catalyzed by *p*-toluenesulfonic acid in moderate yield (51%) (Figure 1.34). PGVNC has a high biobased content because PG is prepared via decarboxylation of gallic acid, which is found in gallnuts, sumac, witch hazel, tea leaves, oak bark, and other plants; and VN exists in the essential oil of clove or vanilla or can be prepared from biobased eugenol or guaiacol. Spectral analyses revealed that PGVNC was mainly composed of guaiacyl pyrogallol arenes. In contrast to other calixarenes formed by PG, for example, with benzaldehyde, *p*-methylbenzaldehyde, and *p*-methoxybenzaldehyde, PGVNC is able to dissolve in common organic solvents for ease of processing.

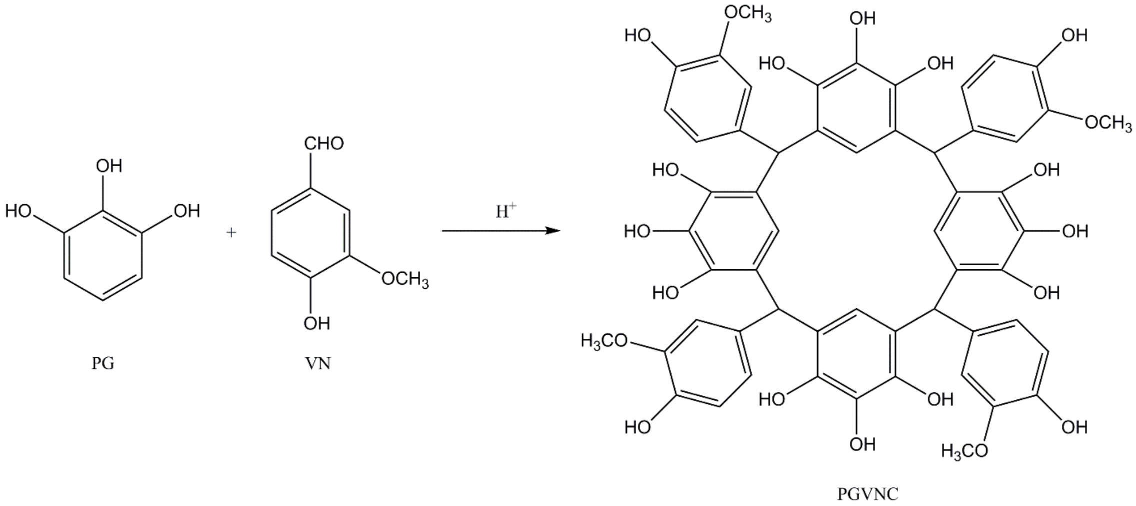

Figure 1.34 Synthetic scheme of PGVNC.

Compared with TA, QC and PGVNC have lower hydroxyl values but higher aromatic contents.[130, 131] When cured with SPE, higher T_g and thermal degradation temperatures were obtained as expecteds but tensile stress and modulus were decreased. When compared with petroleum-derived phenol Novolac (PN), the thermal and mechanical properties of the SPE-QC epoxy network had slightly higher T_g but comparable mechanical properties than that of SPE-PN, while the SPE-PGVNC epoxy network possessed much higher T_g and thermal degradation temperature but lower tensile strength and elongation than that of SPE-PN.

Table 1.4 Thermal and mechanical properties of SPE based epoxy networks.

Curing agent	R[a]	T_g[b] (°C)	T_5[c] (°C)	Tensile strength (MPa)	Tensile modulus (MPa)	Elongation at break (%)	Ref
TA	1	95	314.0	60	1700	-	128
QC	1.2	85.5	342.5	45	1380	4.3	131
PGVNC	2.65	148.1	319.2	15	1700	0.9	130
TPG	1	53.5	361.1	28.2	1070	7.4	60

[a]: hydroxyl group/epoxy group; [b]: glass transition temperature measured by DMA
[c]:5% weight loss temperature

Later, Shibata *et al.*[131] prepared SPE/QC biocomposites with wood flour that showed increased tensile strength and modulus due to additional hydrogen bonding interactions between the unsaturated carbonyl group of QC (Figure 1.32) with the lignocellulose component of wood flour.

The thermal and mechanical properties of some phenolic cross-linked SPE networks are summarized in Table 1.4, which all show high tensile modulus and good thermal stability.

1.6.5 Rosin- and terpene-based curing agents

Terpenes and rosin (a mixture of unsaturated polycyclic carboxylic acids, of which abietic acid is the major component) are a typical class of “natural resins” (Figure 1.35).[132]

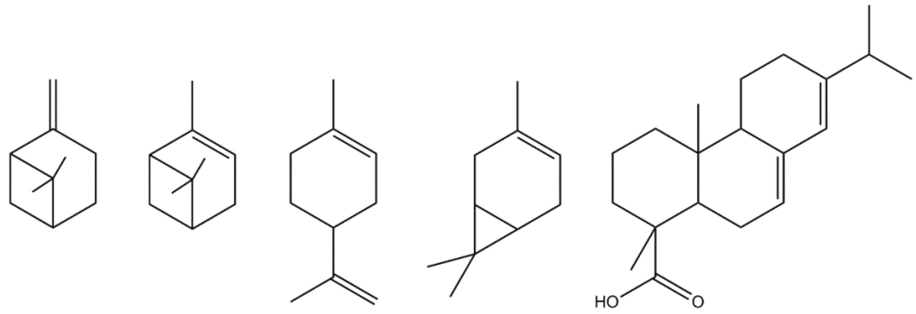

Figure 1.35 Four common polymerizable terpenes (from left to right: β-pinene, α-pinene, limonene, and 3-carene) and abietic acid.

1.6.5.1 Rosin-based curing agents

Rosin, obtained directly from pine and conifer exudates or as a byproduct from the pulping process, is an abundantly available natural product with annual production of 1-1.2 million tons.[133] Rosin is a complex mixture of naturally occurring high molecular weight organic acids (~90%, generally named rosin acids) and related neutral materials (~10%). Rosin acids are mainly composed of isomeric abietic-type acids and pimaric-type acids.[134] Rosin acids and their derivatives could become important biobased alternatives to current petroleum-derived cyclic aliphatic and aromatic monomers in polymers due to the presence of a hydrogenated phenanthrene ring structure.

Figure 1.36 summarizes rosin-derived acids, anhydrides, amines, and amides that were explored to be used as curing agents in epoxy resins. Maleopimaric acid (MPA), obtained via Diels-Alder reaction between levopimaric acid and MA, is probably one of the most important and abundantly available rosin derivatives. MPA itself can be used as curing agent or easily modified with acids and amines to form new types of curing agents.

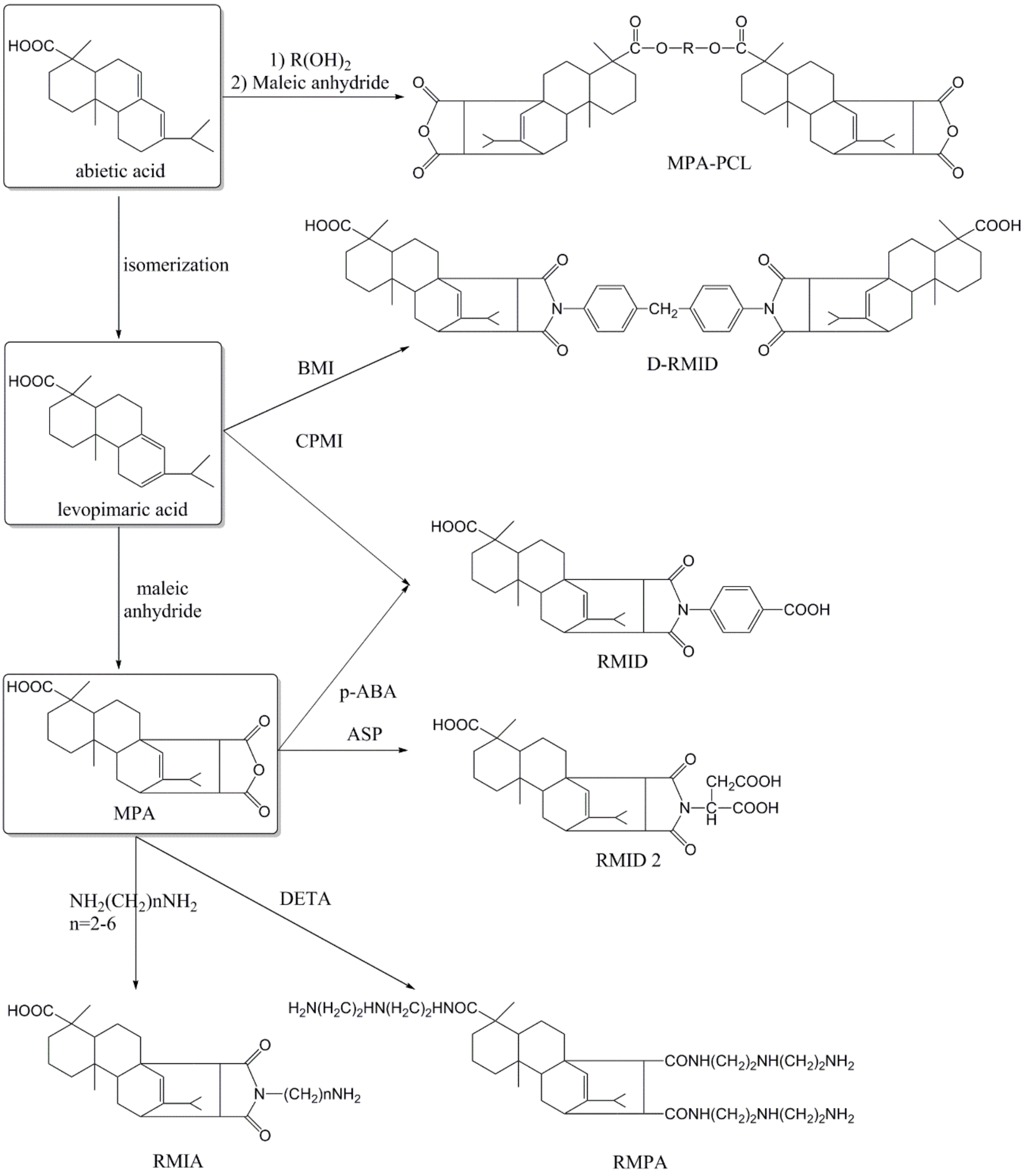
abietic acid
1) R(OH)2
2) Maleic anhydride
MPA-PCL
isomerization
D-RMID
levopimaric acid
BMI
CPMI
maleic anhydride
RMID
p-ABA
ASP
MPA
RMID 2
NH2(CH2)nNH2
n=2-6
DETA
RMIA
RMPA

Figure 1.36 Chemical transitions of rosin acid to biobased amino and carboxyl curing agents.

Zhang's group have synthesized several epoxy curing agents derived from rosin, namely, MPA, methyl maleopimarate (MMP), rosin maleic anhydride imidodicarboxylic acid (RMID), di-RMID (D-RMID), and MPA terminated polycaprolactones (MPA-PCL).[135-139] RMID was synthesized either by the reaction of levopimaric acid with carboxyphenylmaleimide (CPMI) or by the reaction of MPA with p-aminobenzoic acid (p-ABA).[139,140] D-RMID was synthesized by the reaction of levopimaric acid with 1,1'-(methylenedi-4,1-phenylene)bismaleimide (BMI)[139] and RMID 2 was synthesized by the reaction of MPA with aspartic acid (ASP).[140] The thermal mechanical properties and thermal stability of the epoxy systems cured by MPA and MMP were compared with their petrochemical analogues, i.e., 1,2-cyclohexanedicarboxylic anhydride (CHDB) and 1,2,4-benzenetricarboxylic anhydride (BTCA), respectively.[136] The existence of a hydrogenated phenanthrene ring into the molecule led to higher T_g and modulus but slightly lower thermal stability. In order to improve the flexibility of rosin-based anhydride curing agents, different chain lengths of PCLs were introduced between two terminal maleopimarate entities.[138] An increase in the chain length reduced the stress, modulus and thermal stability due to lower crosslink density. Furthermore, rosin-based imide-diacids (RMID, D-RMID) were synthesized and the cross-linked resins showed higher thermal stability compared with that of resins cured by MPA and MMP.[139]

Recently, Zhen *et al*.[141] reported the synthesis of a rosin-based polyamide (RMPA) from MPA with DETA as a potential curing agent for epoxy systems. The cured epoxy resin had comparable properties with petrochemical-cured epoxies: shear strength of 21.6 MPa, thermal decomposition temperature of 343.0 ^oC, and T_g of 146.6 ^oC. Wang *et al*.[142] compared the curing behavior of rosin-based imidoamine (RMIA), which was obtained by the reaction of MPA with diamines, with MPA and a commercial aromatic amine curing agent diaminodiphenylmethane (DDM) in order to investigate structure-property relationships. They found that epoxies cured with RMIA produced the highest T_g and higher moduli and thermal stability compared with MPA but slightly lower moduli and thermal stability compared with DDM, which revealed the importance of the structure of curing agents.

1.6.5.2 Terpene-based curing agent

Terpenes comprise repeat isoprene units (2-methyl-1,4-butadiene) and are secondary metabolites synthesized by many fauna and flora. For example, turpentine is a generic name given to the volatile fraction isolated from pine resin. The major components of turpentine are a few unsaturated hydrocarbon monoterpenes ($C_{10}H_{16}$) namely, α-pinene (45–97%) and β-pinene (0.5–28%), with smaller amounts of other monoterpenes.[143]

As shown in Figure 1.37, Milks and Lancaster[144] synthesized a terpene-based acid anhydride (TPA) via Diels-Alder reaction of MA and alloocimene (obtained by the isomerization of α-pinene). The resultant TPA network possessed higher T_g and tensile strength and modulus than those of networks formed between conventional anhydride HHPA and MLO.[145] Recently, Chang *et al.*[146] compared the curing properties of TPA with MPA and a petroleum-based curing agent methyl nadic anhydride (MNA) based on an isosorbide epoxy system. Their results showed that epoxy resin obtained with MPA had higher T_g and better thermal stability due to the high functionality of MPA. TPA derivatives with amine or hydroxyl groups were obtained by further modification of TPA with amines or amino alcohols.[147]

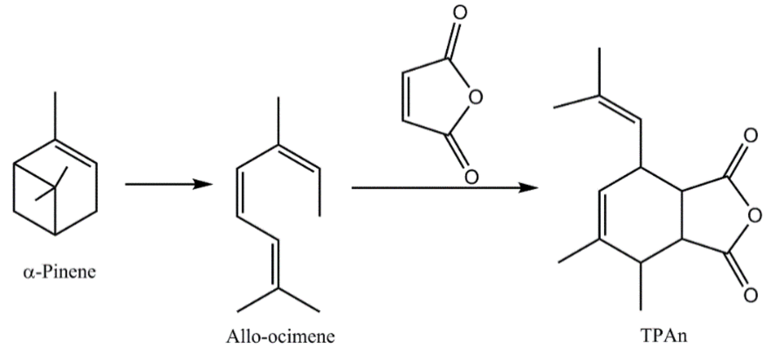

Figure 1.37 Synthesis of terpene-based acid anhydride (TPA).

Auvergne *et al.*[25] have recently summarized terpenes containing amine or phenol groups, which include menthane diamines (Figure 1.38, a) synthesized from limonene[148], terpene diphenol (TPD, Figure 1.38, b)[149] and polyphenol-based terpene synthesized from terpene, phenol and formaldehyde. [150]

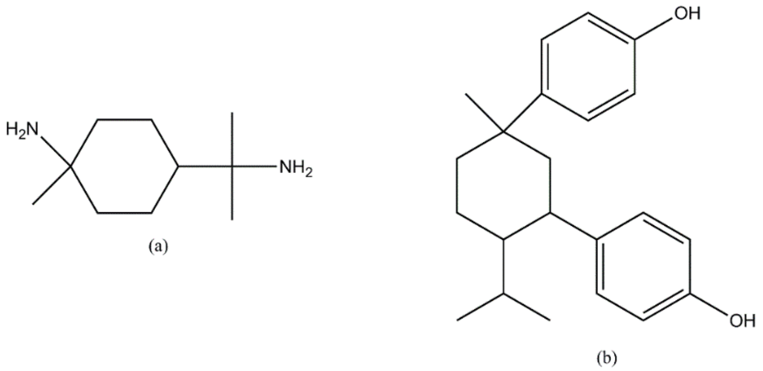

Figure 1.38 Formula of (a) menthane diamines and (b) terpene diphenol (TPD).

TPD was further reacted with formaldehyde and aniline to form terpenediphenol- based benzoxazine (TPDB) by Kimura *et al.*[151] Good heat stability, mechanical properties, electrical insulation, and especially low water absorption were obtained for DGEBA networks cured with TPDB.

1.6.6 Lignin-based curing agents

After cellulose, lignin is the second most abundant biopolymer from renewable materials viewpoint. The annual production of lignin on Earth ranges from 5–36 × 10^8 tons.[152] Lignin is very important because it is considered as a potential source of aromatic compounds and renewable feedstock. Lignin is a complex phenolic polymer (Figure 1.39) comprising three hydroxycinnamyl alcohols or monolignols: *p*-coumaryl alcohol (MH), coniferyl alcohol (MG) and sinapyl alcohol (MS) in the main.[153]

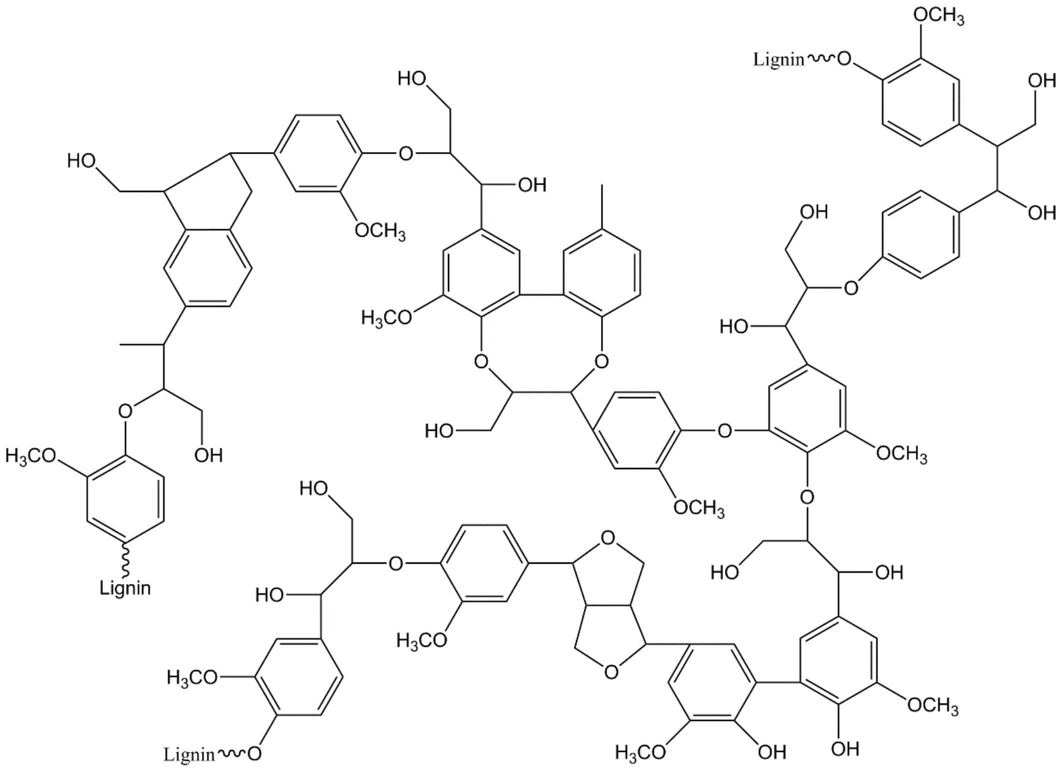

Figure 1.39 Schematic model of lignin structure.

Different methods used to synthesize lignin-based cross-linking agents for epoxy systems have been summarized.[25, 153, 154] On the whole, lignin-based curing agents are prepared by two different methods, either the reaction of lignin with ozone in the presence of NaOH to give lignin with unsaturated carboxyl groups[155-157] or via reaction of modified lignin (partially depolymerized lignin or polyol solutions of alcoholysis lignin) with anhydrides or trimellitic anhydride chloride (e.g., Figure 1.40).[158-163] Qin *et al.*[158] reported that epoxy resins cured by partially depolymerized lignin-based poly(carboxylic acid) (LPCA) (acid value of 229 g/mol) exhibited comparable T_g and storage modulus to that cured with a commercial anhydride curing agent.

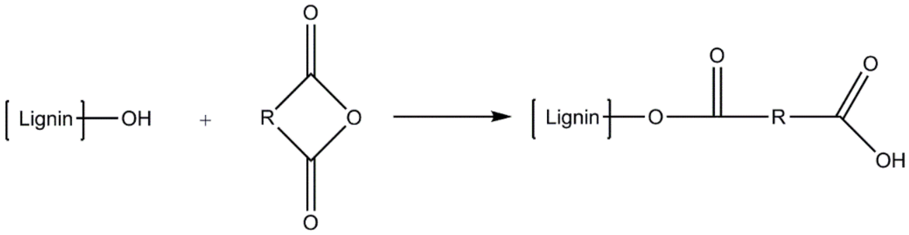

Figure 1.40 Synthesis of Carboxylic Acid from Lignin.

1.6.7 Miscellaneous

Chitosan (Figure 1.41), the partially deacetylated derivative of chitin, is mainly composed of two kinds of structural units: *N*-acetylglucosamine and *D*-glucosamine. Due to the presence of primary amine and acetamido groups in the structure, chitiosan has the potential to cross-link with epoxy prepolymers. Few studies used chitosan as an epoxy hardener to react with poly(ethylene glycol) diglycidyl ether (PEGDE),[164] ethylene glycol diglycidyl ether(EGDE),[165] or with DGEBA[166, 167] for different applications including hydrogels,[164] polymeric stents,[165] cement slurry,[166] and waterborne epoxy dispersions.[167]

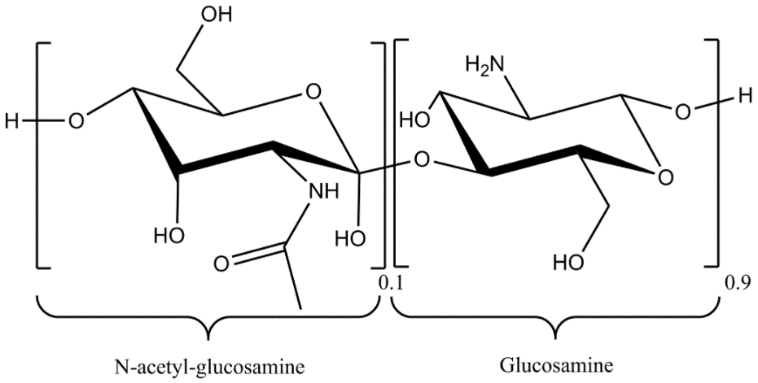

Figure 1.41 Structure of Chitosan.

Liu *et al.*[168] used dextrin, a hydrolyzate from starch, modified with TMA as the curing agent for waterborne epoxy systems used to bond wood. The adhesion properties were comparable with that of a phenol-formaldehyde resin reinforcing the use of starch, another large amount of renewable materials, as curing agents possible.

Interestingly, due to the high percentage of carboxylic acid and phenolic groups in graphene oxide (GO), Ahn *et al.*[169] have reacted GO with epoxidized methyl oleate (EMO) using a one-step process without catalyst or solvent to obtain oleo-functionalized GO (oleo-GO) dispersible in a wide range of solvents. Puig *et al.*[170] have prepared superparamagnetic nanocomposites by dispersing oleic acid (OA)-coated magnetite nanoparticles in an epoxy compound based on DGEBA modified with OA. By modification with OA, a large mass fraction (at least up to 8 wt%) of OA-stabilized magnetite nanoparticles was homogeneously dispersed in a DGEBA-based epoxy matrix. The obtained nanocomposites showed a shape memory effect.

Chapter 2

Biobased epoxy resins of epoxidized plant oils cured with DCAs

Parts of the work described in this chapter has been published in:
“New insights into the curing of epoxidized linseed oil with dicarboxylic acids.”
C. Ding, P. S. Shuttleworth, S. Makin, J. H. Clark and A. S. Matharu, *Green. Chem.*, 2015., **2**, 2217-2236.
DOI: 10.1039/C5GC00912J
(Impact factor 2015, 8.02)

2.1 Summary

The effect of epoxy prepolymers (ELO and ESBO and their corresponding epoxidized fatty acid methyl esters, FAMEs) on the thermal and mechanical properties of the resultant crosslinked systems is reported initially. Thereafter, a comprehensive study of the effect on systematically extending the chain length of a series of α, ω-DCAs (even carbon number DCAs from C_6 to C_{18} and a bio-derived C_{36} diacid Pripol 1009F) on the physical and mechanical properties of the resultant biobased ELO crosslinked systems is investigated. The effects of different accelerators and the amounts of DMAP on the physical and mechanical properties of the resultant biobased ELO crosslinked systems are studied. This chapter concludes with an investigation of the influence of an ELO-adipic acid-DMAP system on curing temperature and time with respect to physical and mechanical properties.

2.2 Introduction

Carboxylic acids or polyesters and anhydrides are the second most important class of epoxy curing agents after amines. Amongst the various biobased DCAs, succinic acid (C_4), adipic acid (C_6), sebacic acid (C_{10}) and dodecanedioic acid (C_{12}) are already commercially available from various companies such as Verdezyne, Rennovia, BioAmber, Celexion, Genomatica and Arkema.

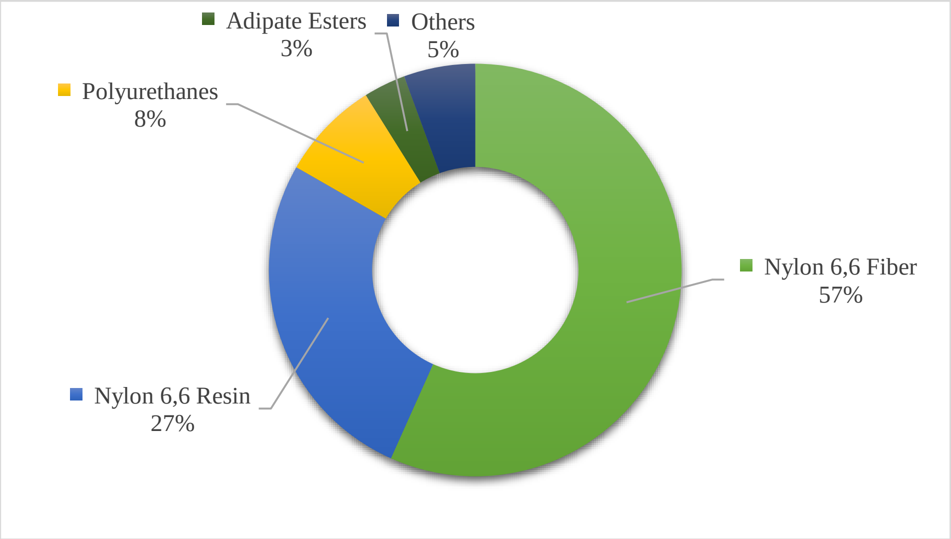

Figure 2.1 Global adipic acid market volume share by application, 2012.[171] (Originally in colour)

For example, adipic acid is one of the most important current platform molecule with global market volumes expected to increase to 3.747 kilo tons by 2020 from its current value of 2,610 kilo tons.[171] The main application of adipic acid is as a precursor for the synthesis of Nylon-6, 6 (Figure 2.1), polyesters and polyurethane resins. In addition, adipic acid is used as a plasticizer for PVC and polyvinyl butyral (PVB), and as an approved additive in cosmetics, gelatins, lubricants, fertilizers, adhesives, insecticides, paper and waxes.

Adipic acid is synthesized industrially from the oxidation of a mixture of cyclohexanol and cyclohexanone, the unrefined mixture is also known as KA oil, derived from benzene (Figure 2.2).[172] One serious concern involved in the current industry process is the generation of ozone-depleting greenhouse gas nitrous oxide (N_2O) generated by the reduction of nitric acid. The production of biobased adipic acid from renewable resources, either from glucose or from long-chain carbon substrates, has already been summarized by several authors.[173, 174] Compared to petroleum-derived adipic acid, biobased adipic acid is both environmentally friendly and cost competitive including lower capital, utilities cost and manufacturing cost.[171]

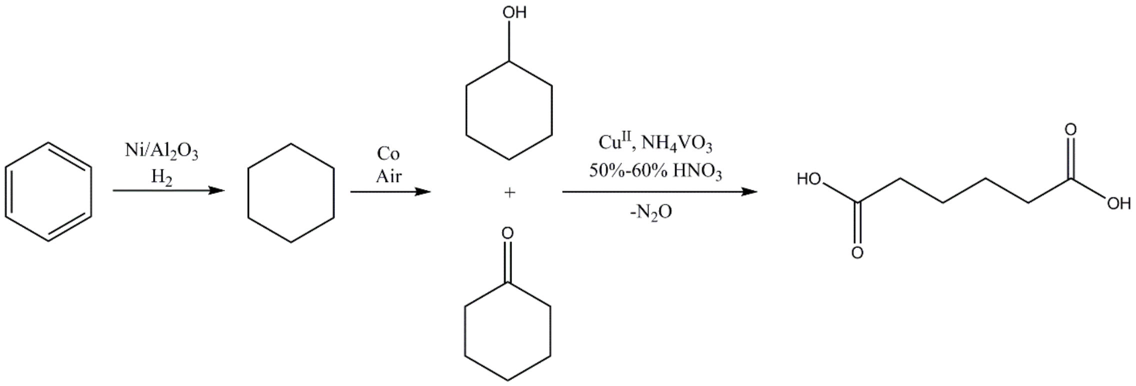

Figure 2.2 Simplified reaction scheme of the current industrial process for AA production by catalytic oxidation of KA oil with nitric acid.[172]

The reaction mechanism between an epoxide and a carboxyl group is rather complicated and as yet to be elucidated. However, the following four types of reactions, proposed by Shechter and Wunstra[78], are generally regarded as a common.

1) epoxide + acid → monoester (addition esterification)

2) epoxide + monoester → ether (etherification)

3) acid + monoester → diester + water (condensation esterification)

4) epoxide + water → glycol (hydrolysis)

Libor *et al*.[175] studied the base catalyzed reactions of a model system of phenylglycidyl ether and caproic acid. Their results showed that reactions (2) (3) and (4) did not happen or had no significant contribution depending on catalyst types and the molar ratio of acid/epoxy group. Based on previous studies,[176-179] the possible interactions between ELO, DCAs and base accelerators, for example, DMAP, are summarized in Figure 2.3.

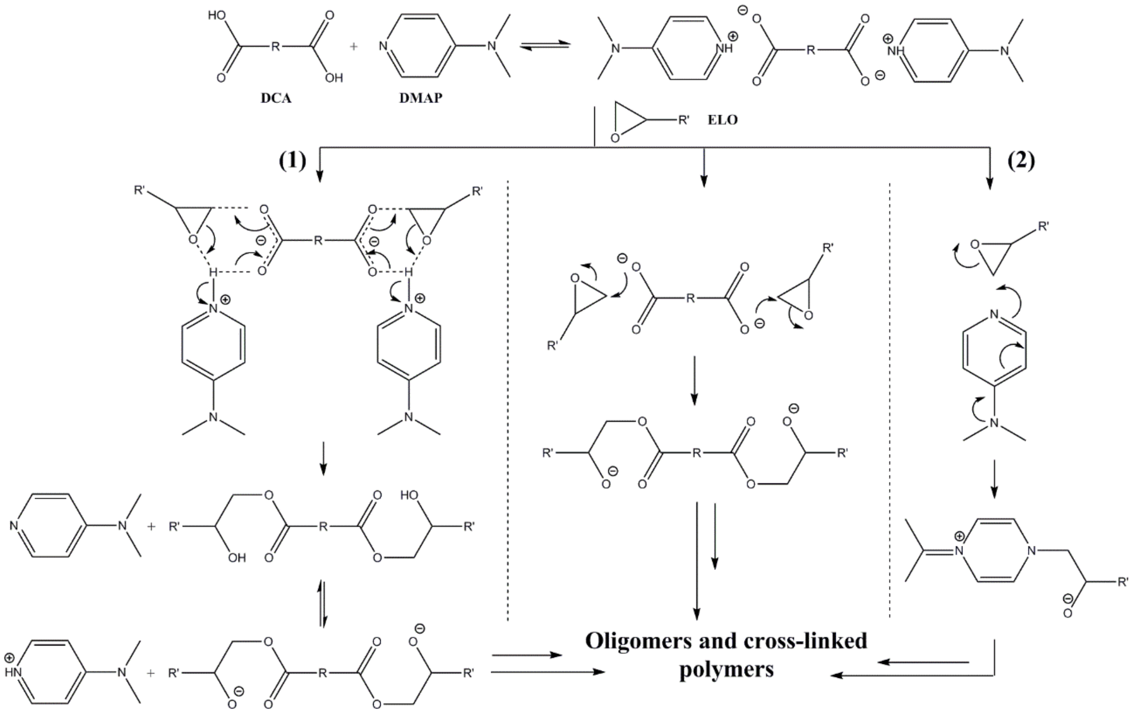

Figure 2.3 Mechanisms proposed for ELO, DCA and DMAP. (1) esterification; (2) etherification.

2.3 Effect of different epoxy precursors

In this study, four different epoxy precursors derived from plant oils ESBO, ELO, and their FAMEs, EMS and EML were used to crosslink with adipic acid in the presence of DMAP. The oxirane contents for ELO, ESBO, EML and EMS were 9%, 6.5%, 8.6% and 6.2%, respectively. If, we consider the molecular weights for ELO/ESBO and EML/EMS are approximately 1000 and 330, respectively, then the epoxy functionalities for ELO, ESBO, EML and EMS are 5.6, 4.1, 1.8 and 1.3, respectively.

- Oxirane content: the weight percentage of oxirane oxygen in a molecule (obtained from the product data sheet, for example, 9% for ELO);
- Epoxy functionality: number of epoxide groups per molecule (calculated from

definition, for example, 1000×9%/16=5.6 for ELO).

Figure 2.4 shows samples with different epoxy prepolymers (ELO, ESO and their methyl esters EML and EMS) cured with adipic acid in the presence of 1.0 mol% DMAP at 160 ^{o}C for 1 h. The ELO and ESBO samples cured successfully to afford soft flexible films whereas EML and EMS samples furnished a viscous liquid. The latter is consistent with the work of Reiznautt *et al.*[180] who studied the curing between epoxidized methyl ester of sunflower oil and *cis*-1,2-cyclohexane dicarboxylic anhydride in the presence of TEA as initiator. Viscous liquid samples described as oligoesters were obtained even after reacting at 160 ^{o}C for 4 h.

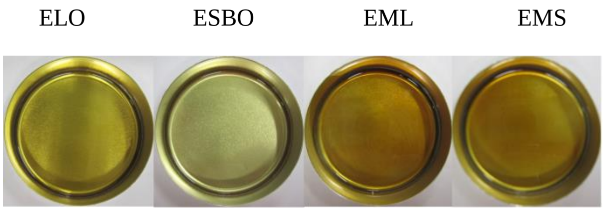

Figure 2.4 Different epoxy prepolymers cured with adipic acid at 160 ^{o}C for 1 h. (Originally in colour)

Thus extending the time period at fixed temperature (160 ^{o}C) as shown in Figure 2.5 in an attempt to cure EML and EMS samples was investigated which revealed significant darkening of samples only without subsequent film formation even after curing for 24 h.

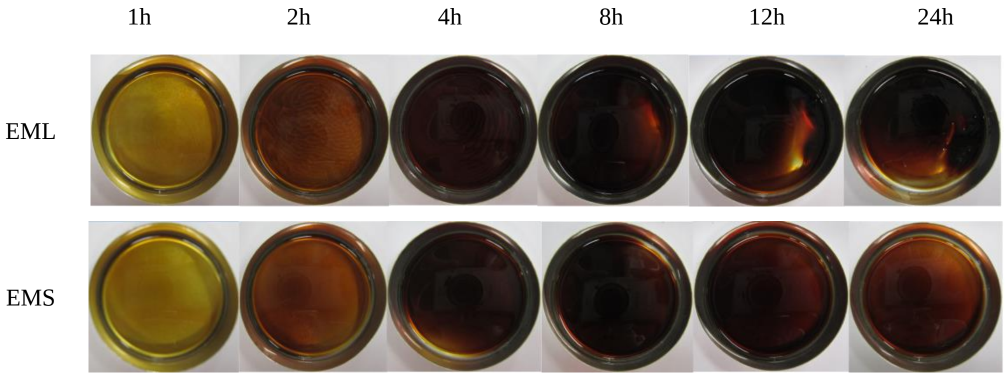

Figure 2.5 EML and EMS samples cured at 160 ^{o}C for different times. (Originally in colour)

2.3.1 DSC analysis

Modulated differential scanning calorimetry (MDSC) was used to study the curing reaction during heating (Figure 2.6, Table 2.1). An exothermic curing peak was observed for all samples.

Two overlapping exothermic curing transitions were observed in ESBO and EMS samples while one exothermic curing transition was observed in ELO and EML sample. The presence of two exothermic transitions implies the possibility of multiple cure reactions occurring simultaneously or sequentially. The first peak is attributed to the esterification reaction between epoxy groups and carboxyl groups; and the second peak to the etherification reaction of epoxy groups with hydroxyl groups formed during the reaction.[181-183]

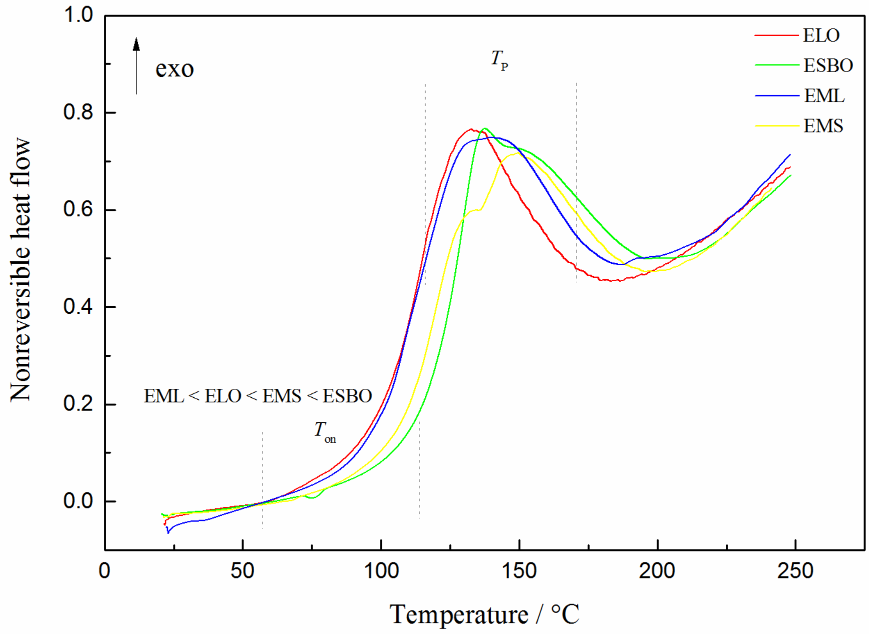

Figure 2.6 Thermograms of mixtures of different epoxy prepolymers with adipic acid. (Originally in colour)

T_{on} (onset initial curing temperature) for these four samples increases in the order: EML (99.2 ºC) < ELO (102.3 ºC) < EMS (109.2 ºC) < ESBO (118.9 ºC). Whilst T_P (peak curing temperature) changed in the order: EML (131.0 ºC) ≈ ELO (131.3 ºC) < EMS (133.0 ºC, 145.8 ºC) ≈ ESBO (135.9 ºC, 150.3 ºC). A possible reason for the lower T_{on} observed in FAMEs samples may due to less steric hindrance and thus higher reactivity compared to EPOs. ΔH_T (total heat of curing) for ELO and EML systems were about 190 $J.g^{-1}$, whilst for ESBO and EMS systems ΔH_T were in the region of 180 $J.g^{-1}$. These observations may be partly related to the oxirane content of the epoxy precursors: ELO (9.0 %); EML (8.6 %); ESBO (6.5 %) and; EMS (6.2 %), with the largest oxirane content giving highest ΔH_T. However, chain mobility, diffusion, accessibility to reactive groups and viscosity will also play an important role.[184]

Zhu *et al.*[185] added different soybean oil-based epoxy compounds, ESBO and EMS, into a conventional petroleum-based epoxy resin system. The dynamic DSC runs showed that samples containing the same amount of ESBO and EMS possessed similar T_P (134 ºC for both samples containing 30% ESBO and EMS) and ΔH_T (265 and 257 $J.g^{-1}$), in agreement with the findings in this study.

Table 2.1 DSC results of different epoxy prepolymer systems.

Epoxy prepolymers	ΔH_T (J.g^{-1})	T_{on} (°C)	T_{P1} (°C)	T_{P2} (°C)	T_g (°C)
ELO	188.2	102.5	131.3	-	-1.7
ESBO	180.5	119.0	135.9	150.3	-24.9
EML	190.1	99.2	131.0	-	-38.9
EMS	179.8	109.2	133.0	145.8	-56.9

Figure 2.7 shows the second heat thermograms of reaction mixtures of different epoxy prepolymers with adipic acid. All samples show clearly a step change in the heat flow signal which corresponds to the glass transition temperature T_g. The T_g for these four samples decreases in the order: ELO (- 1.7 °C) > ESBO (- 24.9 °C) > EML (- 38.9 °C) > EMS (- 56.9 °C), in accordance with their epoxy functionalities. ELO sample gave the highest T_g of - 1.7 °C, which was 23 °C higher than ESBO sample. In addition, the T_g is in agreement with their physical appearance, *i.e.*, ELO and ESBO samples formed films whereas EML and EMS samples formed viscous liquids.

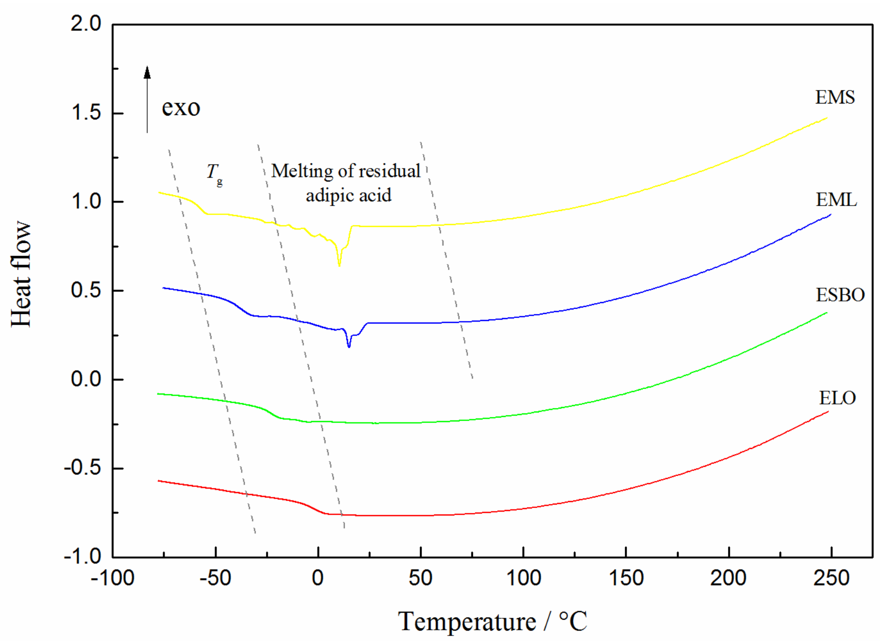

Figure 2.7 Second heat thermograms of reaction mixtures of different epoxy prepolymers with adipic acid.

(Originally in colour)

The endothermic transitions after T_g observed in EML and EMS samples were attributed to the melting of the residual adipic acid, which was also found in Reiznautt's study.[180] Due to the steric hindrance effect in ELO and ESBO triglyceride molecules, there will be some unreacted epoxy groups still present after the curing reaction. While for EML and EMS samples, due to their relative ease of accessibility, all epoxy groups were reacted and some adipic acid remained after the reaction. The higher T_g of ESBO sample than that of EML sample indicated that the functionality of the molecule played more important role in forming the crosslinked networks than the total epoxy groups in the composition.

2.3.2 FT-IR analysis

Figure 2.8 and Figure 2.9 shows the FT-IR spectra of EML and EMS cured with adipic acid at 160 °C for different times, respectively.

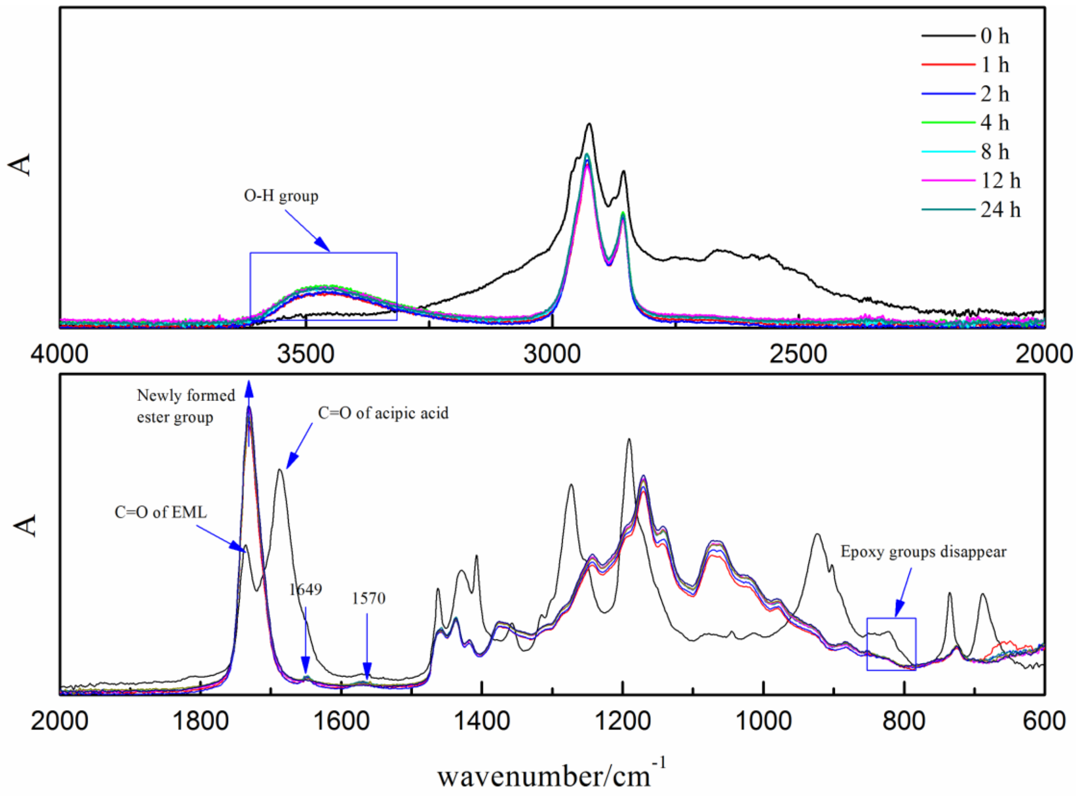

Figure 2.8 FT-IR spectra of EML sample cured at 160 °C for different time. (Originally in colour)

After curing for 1 h, newly formed hydroxyl groups were observed in the range of 3200 cm^{-1} to 3600 cm^{-1}. The carboxyl band of adipic acid at 1685 cm^{-1} disappeared while the ester carbonyl C=O band of EML and EMS at 1740 cm^{-1} shifted to 1732 cm^{-1}. Bands appeared at 1649 cm^{-1} and 1570 cm^{-1} were attributed to the signals of protonated DMAP which linked to the carboxylate anion of adipic acid.[84] The characteristic twin bands of epoxy groups at 823 cm^{-1}

and 842 cm^{-1} disappeared signifying that the epoxy groups were fully ring-opened in the curing reaction. With an increase of curing time, the intensity of the newly formed ester carbonyl C=O band (1732 cm^{-1}) with other C-O stretching bands, *e.g.*, 1158 cm^{-1} and 1099 cm^{-1}, increased indicating that the curing reaction was still ongoing.

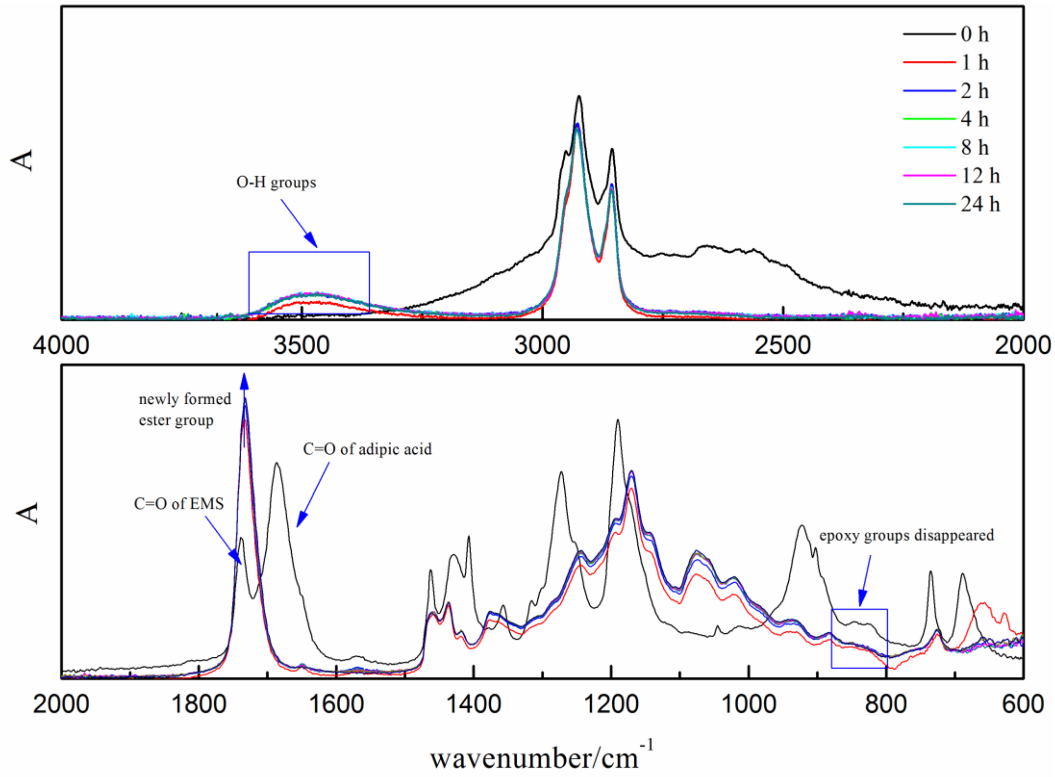

Figure 2.9 FT-IR spectra of EMS sample cured at 160 °C for different time. (Originally in colour)

As mentioned earlier, EML and EMS samples were still liquid even after curing for 24 h, which indicated either no significant reaction or that lowly cross-linked polymers were formed with EML and EMS samples. The main difference between EPOs (ELO and ESBO) and their epoxidized methyl esters (EML and EMS) is that EPOs have the basic triglyceride structure and in average there are four to five epoxy groups in one molecule while there are two to three epoxy groups in their esters. The much higher epoxy functionality in EPOs resulted higher cross-linked networks.

In conclusion, all four plant oil-based epoxy prepolymers were able to crosslink with adipic acid while only ELO and ESBO gave solid films with higher T_g. The molecular structure and oxirane contents of epoxy prepolymers are very important for the formation of crosslinked networks. In order to better understand the curing process, more analyses such as GPC, DMA and rheology need to be studied in the future.

2.4 Effect of different dicarboxylic acids

In this work, ELO was cured with different chain length of biobased DCAs (C_2, C_4, C_6, C_8, C_{10}, C_{12}, C_{14}, C1$_6$, C_{18} and C_{36} Pripol 1009F). Oxalic acid (C_2) and succinic acid (C_4) samples cross-linked immediately during the premixing stage (190 °C) and were not further investigated.

Figure 2.10 shows samples of ELO cured with different DCAs (C_6, C_8, C_{10}, C_{12}, C_{14}, C_{16}, C_{18} and C_{36}) at 160 °C for 1 h. Transparent and flexible films were formed for all the DCAs investigated. Although, the C_8, C_{14}, C_{16} samples gave deeper color followed by C_6, C_{10}, C_{12}, C_{18} and then Pripol 1009F it is important to note that there is no direct connection of the chain length of DCAs with respect to sample colour.

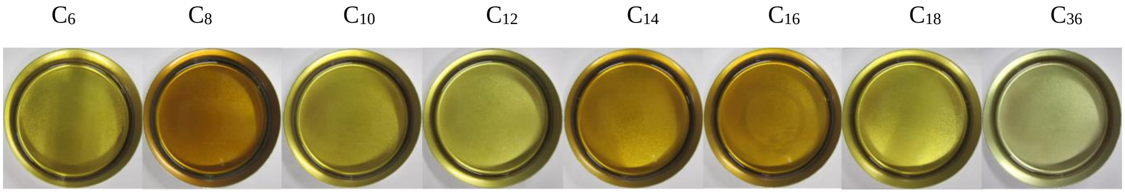

Figure 2.10 Samples of ELO cured with different DCAs at 160 °C for 1h. (Originally in colour)

2.4.1 DSC analysis

Dynamic DSC analysis was used to study the cure process and to determine the activation energy (E_α). Figure 2.11 shows the DSC thermograms of the epoxy mixtures (obtained after premixing) at heating rate of 10 °C min^{-1}. The first endotherm at around 100 to 125 °C is attributed to the melting of the DCAs before the exothermic transition which is associated with the curing process. This curing process in most cases starts immediately after the DCAs have melted. For the C_6 sample, the melting transition of adipic acid was not as obvious as the others probably due to its higher initial reactivity during the premixing stage.

The total enthalpy of curing ΔH_T and peak temperature of the exothermic curing peak T_P at different heating rates are listed in Table 2.2. It can be seen that T_P increases with heating rate and DCA chain length. The higher T_P with increased heating rate is attributed to the thermal lag caused by higher heating rate as reported by Haines.[186] The total enthalpy released during the curing reaction decreased with the increase of chain length.

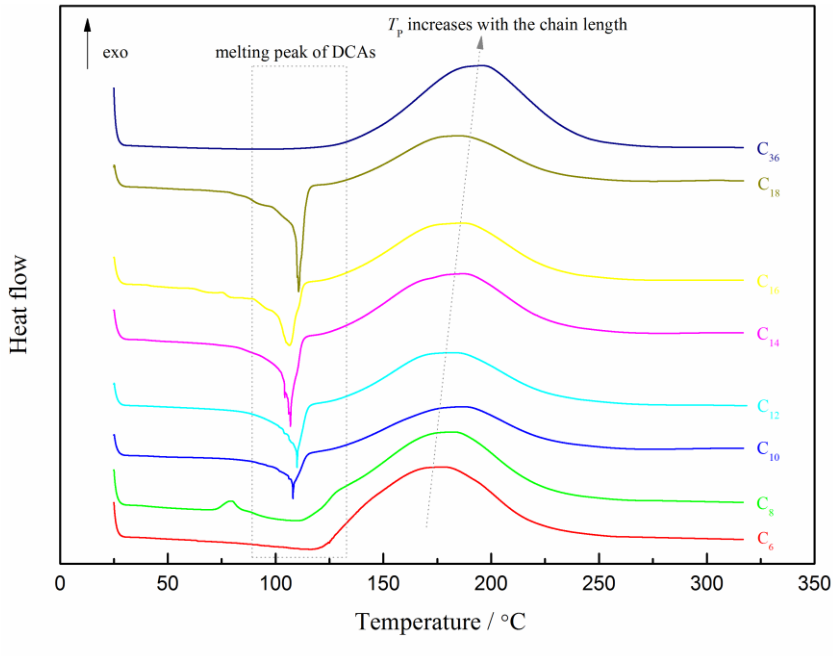

Figure 2.11 DSC thermograms of ELO with different DCAs at a heating rate of 10 ºC/min. (Originally in colour)

Chiu *et al.*[187] also showed a similar trend for the curing process of sulfone epoxy monomers with different amine curing agents, i.e., amine curing agents with longer chain lengths generated lower ΔH_T whilst T_P shifted to higher values. The increased T_P and decreased ΔH_T is probably due to a higher probability of entanglement of the polymeric or oligomeric chains with increasing chain length which would increase the steric hindrance of the curing reaction and thus decrease curing reactivity.

Table 2.2 ΔH_T and T_P of ELO-DCAs systems with different heating rates (5, 10, 15, 20 ºC/min)

DCAs	T_P (ºC)				ΔH_T (J/g)			
	5	10	15	20	5	10	15	20
C_6	162.5±0.4	177.8±1.1	185.7±1.3	192.4±0.2	253.2±7.8	254.3±13.4	261.7±16.5	250.3±8.4
C_8	168.8±0.1	181.6±0.9	190.5±0.8	196.2±0.6	235.6±6.7	244.2±6.5	232.0±1.0	230.4±7.5
C_{10}	169.5±1.2	184.8±1.8	191.1±2.4	196.1±0.1	250.8±5.4	248.9±5.0	247.9±4.1	258.5±3.0
C_{12}	169.9±0.5	183.1±2.0	191.9±2.4	197.0±0.7	239.6±8.5	265.7±5.1	270.6±9.0	267.8±8.8
C_{14}	172.8±0.1	186.8±0.2	194.5±0.6	200.2±0.2	213.8±6.4	234.5±10.2	246.0±10.3	249.4±9.1
C_{16}	171.8±1.0	185.5±1.7	194.0±1.9	199.8±0.9	222.7±7.2	239.5±5.9	234.2±8.5	233.3±4.2
C_{18}	170.8±0.6	185.5±1.1	193.6±1.2	200.1±2.2	217.7±3.5	241.3±2.9	237.4±1.0	245.1±8.5
C_{36}	180.9±0.7	196.2±0.4	204.5±1.3	210.3±0.7	170.8±4.9	173.6±2.9	176.3±2.1	170.9±0.5

The activation energy (E_a) of the curing process was determined using the Kissinger method (eq. (1))

$$\frac{d[ln(q/T_P^2)}{d(1/T_P)} = -\frac{E_a}{R} \qquad (1)$$

where R is the universal gas constant,

by plotting of $\ln(q/T_P^2)$ versus $1/T_P$ as shown in Figure 2.12 (Kissinger plot), whereby the gradient corresponds to E_α. The Kissinger plots show good linearity for all DCAs studied with E_α in the range 70 to 85 kJ mol^{-1}.

Table 2.3 Thermal properties of ELO-DCAs systems and data related to the extracted soluble substances.

Sample	ΔH_T [J g^{-1}]	E_α [kJ mol^{-1}]	T_g [°C]	ΔH_R [J g^{-1}]	Degree of cure ^{a} (%)	Soluble [wt%]	M_w
C_6	254.9±4.9	70.7±0.7	7.0	23.7	90.7	1.85±0.05	2935
C_8	235.6±6.2	78.9±1.8	3.7	30.4	87.1	1.96±0.05	2271
C_{10}	251.6±4.8	82.9±3.9	0.4	25.5	89.9	1.87±0.04	2288
C_{12}	260.9±14.4	79.2±1.0	-2.2	22.2	91.5	1.78±0.06	2396
C_{14}	235.9±16.1	81.3±0.5	-3.6	11.3	95.2	1.74±0.01	2460
C_{16}	232.4±7.0	78.6±7.7	-5.0	11.2	95.8	1.53±0.06	2436
C_{18}	235.3±12.2	75.3±4.3	-5.5	13.7	94.2	1.74±0.04	2638
C_{36}	172.9±2.6	78.9±4.4	-15.1	13.2	92.3	3.05±0.01	2487

^{a}: degree of cure = $(\Delta H_T - \Delta H_R) / \Delta H_T$

Adipic acid (C_6) gave the lowest E_α which further suggests its fast reactivity with ELO in the presence of DMAP as an accelerator. Ghodsieh *et al.*[188] reported the curing kinetics of epoxy resin mixtures based on DGEBA and ESBO with C_{10} sebacic acid which gave activation energies in the range 50-64 kJ mol^{-1}. Compared with our results, the lower activation energies may be due to the fact that glycidyl groups in DGEBA are disposed terminally rather than internally as is the case for our epoxidized vegetable oils, thus are more reactive due to the less steric hindrance.

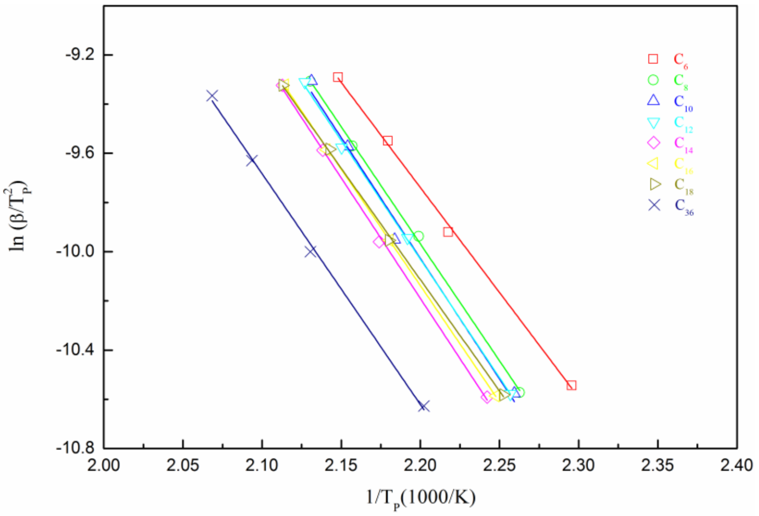

Figure 2.12 Kissinger plot to determine activation energy (E_α). (Originally in colour)

Figure 2.13 shows the T_g of films obtained by curing ELO with different DCAs at 160 ºC for 1 h. With increasing DCA chain length, T_g decreased from 7.0 ºC for C_6 to -15.1 ºC of C_{36} probably due to the decrease in crosslink density. Shorter crosslinkers lack flexibility and form tighter or closer crosslinked networks. With the increase of crosslink density, the free volume within the resin system decreased thus the motion of the network segments in samples with high crosslink density was restricted, which was responsible for the increase of T_g.

A similar trend was observed by Shimbo *et al.* [189] who studied properties of epoxy networks of DGEBA cured with different DCAs (C_4, C_6, C_{10}, C_{12})[190] and different aliphatic α, ω-diamines (C_2, C_4, C_6, C_{12}). Though, the reported T_g values were much higher and attributed to the 'hard' aromatic groups of DGEBA, ranging from 51 ºC (C_{12}) to 101 ºC (C_4) and from 89 ºC (C_{12}) to 96 ºC (C_2) for the diamines. However, all samples showed residual cure, which was also found by Xiao *et al*. in epoxidized sucrose esters-anhydride thermosets.[191] After 1 h of curing, all samples achieved 87-95% curing.

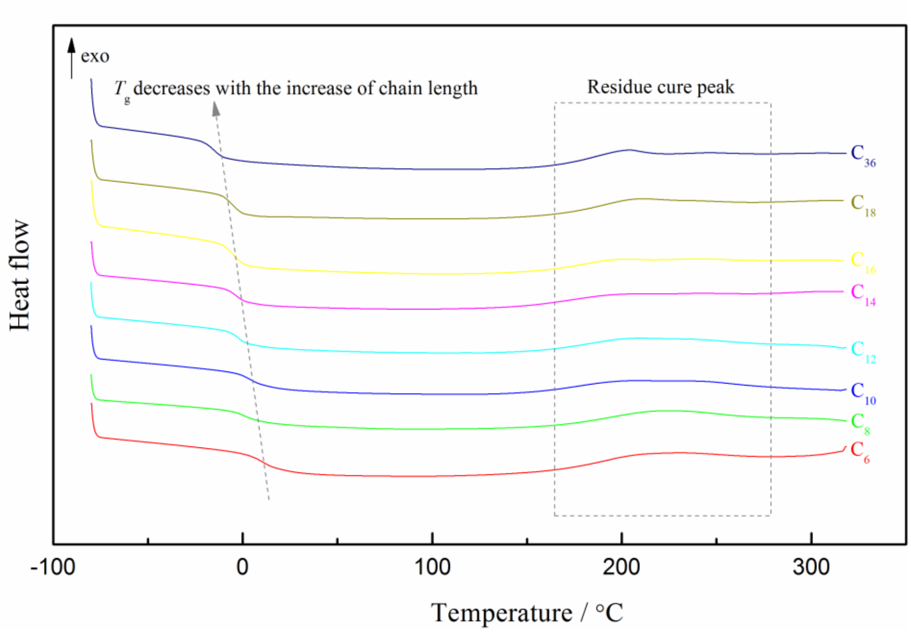

Figure 2.13 DSC thermograms of cured ELO-DCAs films at 160 ºC for 1 h. (Originally in colour)

2.4.2 Polymer extraction study

The weight percentage of the extracted soluble parts and their weight average molecular weight (M_w) from films subjected to dissolution in CH_2Cl_2 for 7 days are shown in Table 2.3. All the samples showed good solvent stability and the gel content was less than 2% for all the samples except C_{36} sample which was 3%. The molecular weight of the soluble substances was about 2500 which indicated that the soluble parts were small molecules of the ring-opening products of ELO.

2.4.2.1 FT-IR analysis

The infrared spectra of ELO, extracted soluble and insoluble part (residue) of C_6 film are shown in Figure 2.14. ELO clearly showed characteristic bands of the epoxy groups, oxirane C-O twin bands at 823 cm^{-1} and 842 cm^{-1}.[49, 192] The ester carbonyl C=O group stretching band was observed at 1742 cm^{-1}. The other bands observed were: 723 cm^{-1} (methylene in-phase rocking), 959 cm^{-1}, 1010 cm $^{-1}$, 1102 cm^{-1} (ether, antisymmetric stretch), 1155 cm^{-1}, 1240 cm^{-1} (ester carbonyl, antisymmetric stretch), 1379 cm^{-1} (methyl symmetric deformation), 1463 cm^{-1} (methyl antisymmetric deformation) and 2854 cm^{-1}, 2923 cm^{-1} (methylene symmetric and antisymmetric stretch).[192]

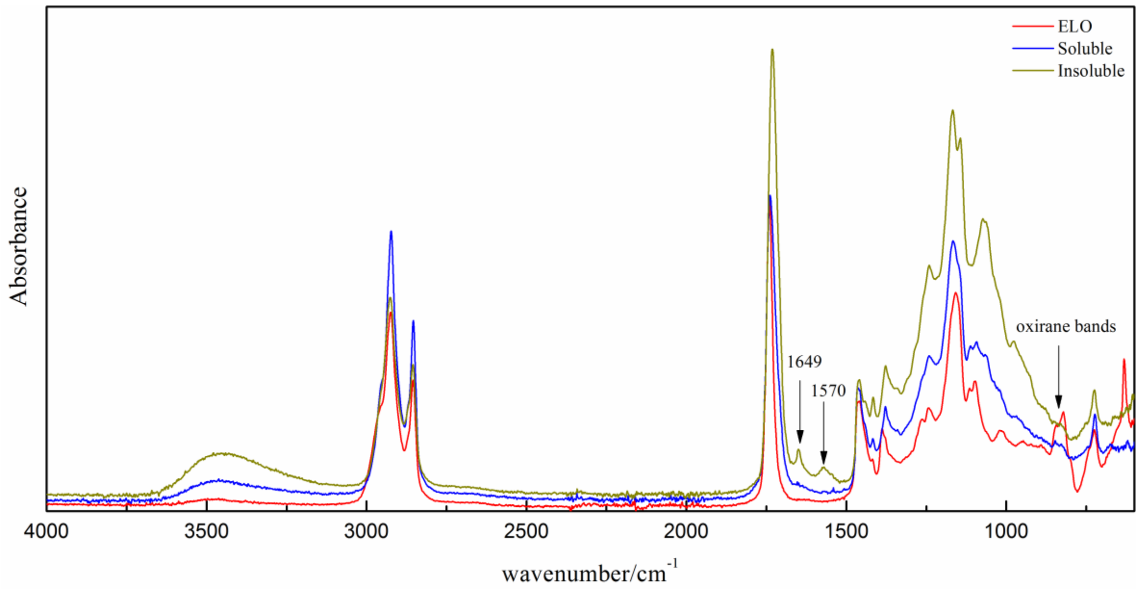

Figure 2.14 FT-IR spectra of ELO, extracted soluble and insoluble residue after extraction from cured C_6 film.

(Originally in colour)

Compared with ELO, the characteristic oxirane absorption bands at 823 cm^{-1} and 842 cm^{-1} were not present in both cured products soluble and insoluble fractions. The carbonyl stretching band shifted from 1742 cm^{-1} in ELO to 1738 cm^{-1} for the extracted soluble sample and further shifted to 1732 cm^{-1} in the insoluble substances. Instead of a single band at 1155 cm^{-1} in ELO, the ester C-O antisymmetric stretch band split into two bands (1168 cm^{-1}, 1145 cm^{-1}) in the insoluble samples and a band (1168 cm^{-1}) and a shoulder (1145 cm^{-1}) for the soluble samples. In addition, new ether group signals were found at 1073 and 979 cm^{-1} in both the soluble and insoluble samples. These findings indicated that new ester and ether groups were formed between the acid group of DCAs and the epoxy groups of ELO. The CH_2Cl_2 soluble substances are most likely low molecular weight ring-opening products of ELO, which have also been reported by Liu *et al.*[193] The two bands at 1649 and 1570 cm^{-1} in the insoluble product that remained after extraction have been attributed to the signals of protonated DMAP which, is linked to the carboxylate anion of these DCAs.[84] Interestingly, these two bands were not observed in the soluble, indicating that DMAP was not homogeneously dispersed in the resin system and therefore within these regions curing was not as effective and only smaller molecular DCM soluble clusters were formed.

2.4.2.2 NMR analysis

The ^1H and ^{13}C NMR spectra of ELO and the cured extracted soluble fraction are shown in Figure 2.15 and Figure 2.16, respectively.

^1H NMR measurement on ELO indicated that the epoxy group was present from the signal in the δ 3.0-3.2 ppm region. The ELO base sample also showed signals at δ 5.1-5.3 ppm and 4.0-4.4 ppm which correlate to the methine proton of $-CH_2-C\mathbf{H}-CH_2-$ and methylene proton of $-C\mathbf{H}_2-CH-C\mathbf{H}_2-$ of glycerol’s backbone, respectively. Other signals include $C\mathbf{H}_2$ proton adjacent to two epoxy group at δ 2.8-3.0 ppm, $\alpha-C\mathbf{H}_2$ to carbonyl group at δ 2.2-2.4 ppm, $\alpha-C\mathbf{H}_2$ to epoxy ring at δ1.7-1.9 ppm, $\beta-C\mathbf{H}_2$ to carbonyl group at δ 1.55-1.7 ppm, $\beta-C\mathbf{H}_2$ to epoxy ring at δ1.4-1.55 ppm, saturated methylene group at δ 1.1-1.4 ppm and terminal $-C\mathbf{H}_3$ groups at δ 0.8-1.0 ppm.[194] Compared with ELO, the characteristic epoxy signals at δ 3.0-3.2 were absent in the soluble sample suggesting no unreacted ELO was present post curing and verifying the findings from the FT-IR analysis. The peak at δ 2.8-3.0 ppm changed from a multiple peak to a single peak which further confirmed the ring-opening reaction. The disappearance of peak at δ 0.9-1.0 ppm was attributed to the $C\mathbf{H}_3$ of the linoleic acid.[195]

^{13}C NMR measurement on ELO indicated that the epoxy group is present in the δ 54-58 ppm region. The presence of ^{13}C NMR peak at 173.1 ppm was due to carbonyl carbon of triacylglycerol and peaks at 68.9 ppm and 62.1 ppm, respectively, assigned to methine carbon of

-CH_2-**C**H-CH_2- and methylene carbon of -**C**H_2-CH-**C**H_2- backbone. Again, compared with ELO the extracted soluble substances did not show the characteristic epoxy peaks in the δ 54-58 ppm region. Solid state ^{13}C-NMR of the insoluble substances clearly showed the existence of carbonyl/ester groups at 174 ppm, which was also complemented by presence of C=O stretch of an ester as shown in the FTIR spectrum in Figure 2.14.

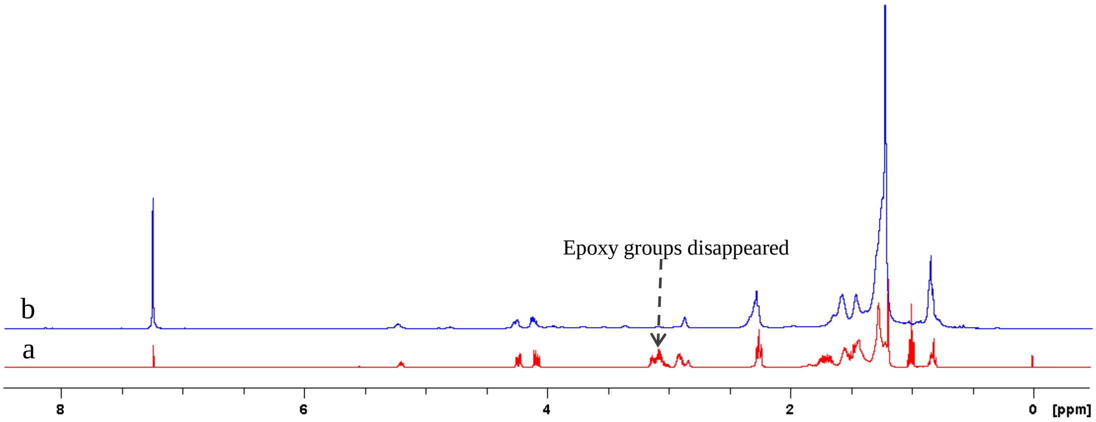

Figure 2.15 ^{1}H NMR spectra of (a) ELO and (b) soluble. (Originally in colour)

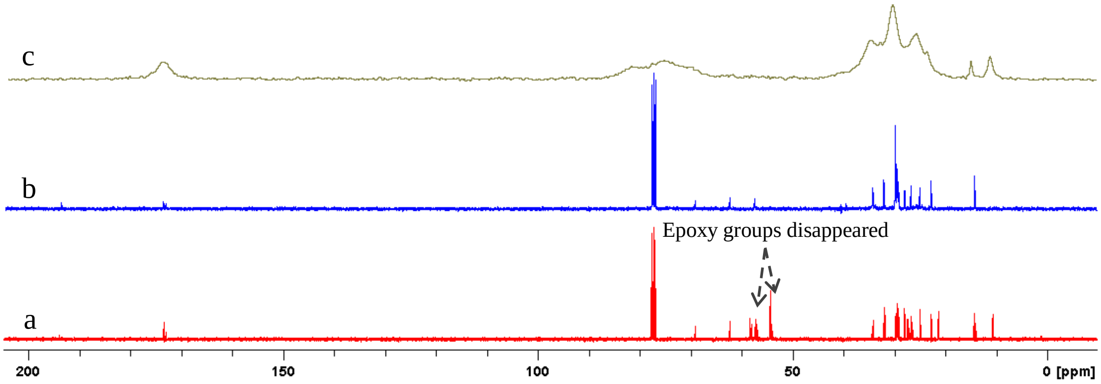

Figure 2.16 ^{13}C NMR spectra of (a) ELO, (b) soluble and (c) solid state CP-MAS ^{13}C NMR spectrum of the residue. (Originally in colour)

2.4.3 Mechanical properties

Figure 2.17 shows the relationship between stress and strain of the cured ELO-DCAs products. Except for the sample cured with adipic acid (C_6), all others show a linear relationship between stress and strain. In this case, strain hardening can be observed helping to account for its much higher mechanical properties. Strain hardening is possibly related to the orientation effects during tensile strain. For longer DCAs, chains could prevent this orientation effect and hence, explaining their marked decrease in mechanical properties. Strain hardening has also been observed in adipate polyurethane elastomers which was explained by the crystallization/orientation of the amorphous polyol chains during the applied strain.[196]

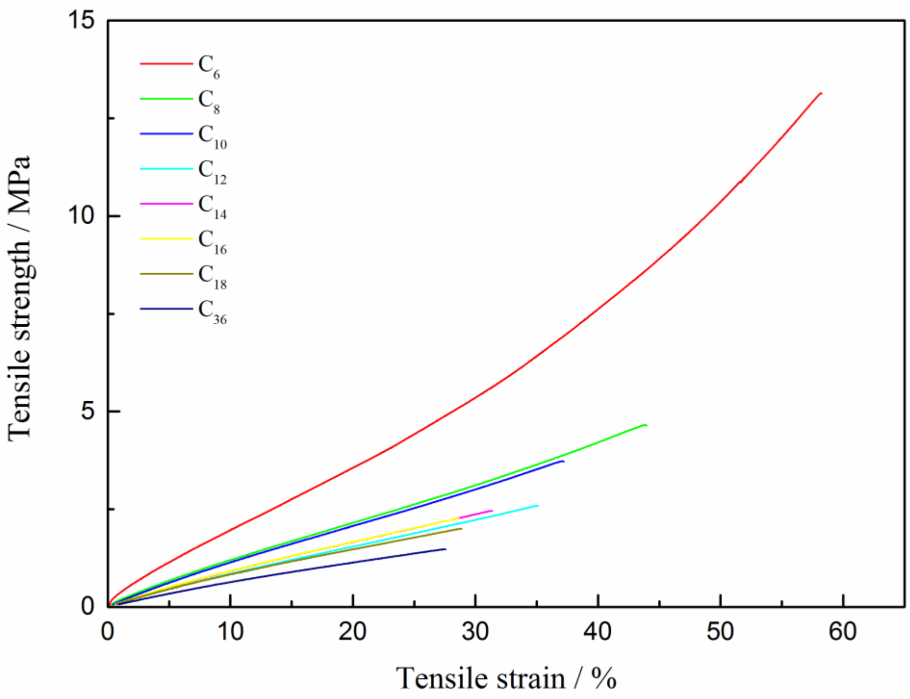

Figure 2.17 Strain-stress curves of cured films with different DCAs. (Originally in colour)

Figure 2.18 shows the effect of different DCAs on the mechanical properties of the obtained thermosetting resins. The film derived from adipic acid (C_6) gave the best mechanical properties with elongation at break of 55%, tensile strength of 8.8 MPa, Young's modulus of 22.0 MPa and toughness of 3.1 MJ m^{-3}. Toughness, which is defined as the amount of energy per volume that a material can absorb before rupturing, is a material's resistance to fracture when stressed. Brittle materials have low toughness, while ductile materials are very tough.[197] In a tensile test, both the tensile strength and the elongation at break contribute to the toughness of a material. The mechanical properties after C_6 as mentioned previously can be seen to dramatically decrease initially, and then gradually decrease with increasing chain length. The elongation properties of the materials however, after a DCA chain length of C_{10}, remained constant around 30%. Compared with the C_6 film that derived from Pripol 1009F (C_{36}) had the poorest tensile strength (1.1 MPa), Young's modulus (4.70 MPa) and toughness (0.2 MJ m^{-3}) due to longer chain of Pripol increasing the free volume of the polymer, plasticising the network.

Additional differences in the mechanical properties of these materials with DCA chain length could be related to the films cured with shorter DCAs having a T_g close to RT and still within the leathery material zone (T_g ± 10 ºC), and as such, will show better mechanical properties than those in the rubbery state.[198] Though, tensile strength and elongation of DGEBA cured with various DCAs in the absence of accelerators were reported by Shimbo *et al.*,[190] which showed that tensile strength and elongation decreased with increase of chain length except for C_6 adipic acid that gave the worst elongation. Yang *et al.*[199] reported that epoxy resins cured with shorter diamines (Jeffamine D-230) had better tensile strength and modulus but poorer elongation at break compared with longer diamines (Jeffamine D-400).

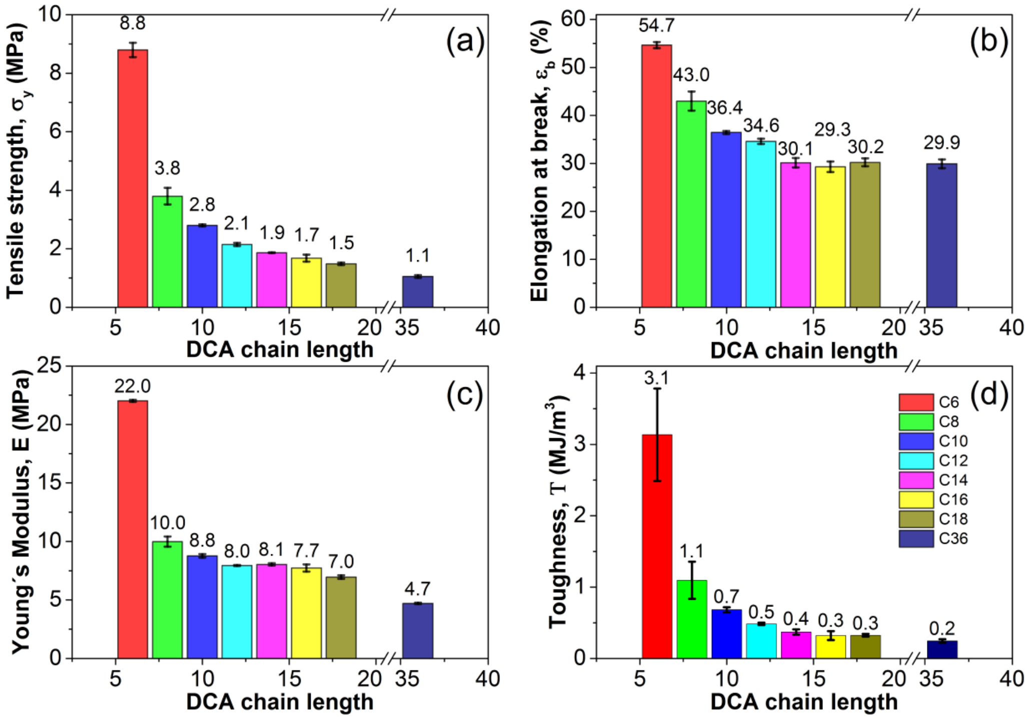

Figure 2.18 Mechanical properties of films with different DCAs, (a) tensile strength; (b) elongation at break; (c) Young’s modulus; and (d) toughness. (Originally in colour)

2.4.4 DMA analysis

DMA tests were undertaken at five different frequencies 1, 3, 7, 10 and 20 Hz. Data for the storage modulus and tan δ versus temperature at 1 Hz are shown in Figure 2.19. Table 2.4 and Table 2.5 compares the dependencies of storage modulus and loss modulus on temperature for the epoxy cured with different DCAs, and the T_g was defined as the peak temperature of loss modulus.

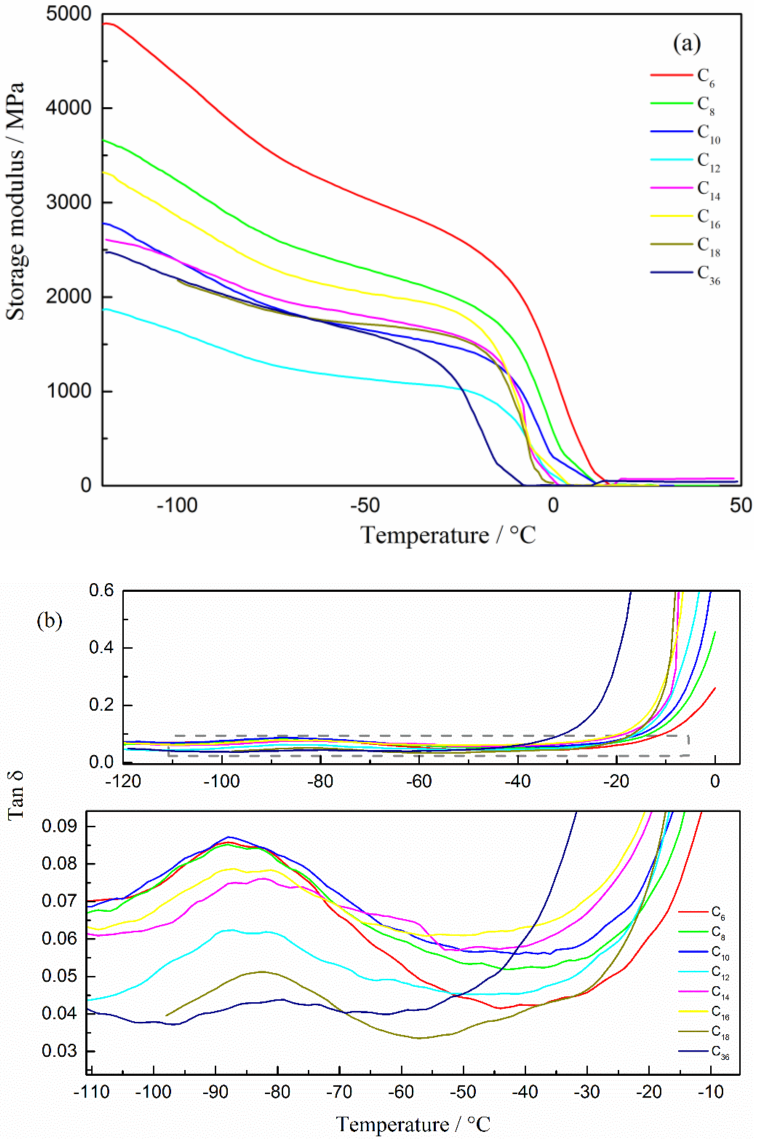

Figure 2.19 Storage modulus (a) and tan δ (b) versus temperature for cured samples tested at 1 Hz. (Originally in colour)

Table 2.4 Storage modulus (MPa) of samples tested under 1 Hz.

Sample	-100 ºC	-80 ºC	-60 ºC	-40 ºC	-20 ºC	0 ºC
C_6	4536	3958	3217	2888	2485	1231
C_8	3231	2732	2416	2182	1872	568
C_{10}	2387	1976	1735	1582	1390	302
C_{12}	1634	1339	1180	1090	969	115
C_{14}	2337	1893	1670	1514	1286	62
C_{16}	2856	2395	2128	1986	1686	173
C_{18}	2274	1864	1645	1551	1530	30
C_{36}	2195	1929	1722	1492	664	5

Due to the large change in the storage modulus after the T_g and the sample thickness limitations the values generated after this point were deemed invalid and beyond the test limit of the instrument. However, similar to the tests carried out at RT on the Instron the storage modulus below the T_g decreased with increasing DCA chain length due to decreased crosslink density, with the C_6 sample showing the highest storage modulus over the analysed range of -100 to 0 ºC.

Table 2.5 Temperature of the β-relaxation (T_β) taken from the maxima of the Tan δ of the different ELO-DCAs samples tested using a DMA under different frequencies and calculated activation energy E_β and T_g at 1 Hz.

Sample	T_β [ºC]					E_β [kJ·mol^{-1}]	T_g at 1 Hz [ºC]
	1 Hz	3 Hz	7 Hz	10 Hz	20 Hz		
C_6	-86.1	-81.0	-77.32	-75.2	-72.3	29.1	1.5
C_8	-87.3	-81.4	-78.4	-75.5	-69.6	23.7	-2.9
C_{10}	-86.9	-81.7	-76.5	-75.0	-69.0	23.2	-3.8
C_{12}	-87.5	-80.6	-76.1	-73.9	-67.8	21.5	-7.5
C_{14}	-85.5	-74.9	-72.4	-67.7	-63.0	19.0	-8.2
C_{16}	-87.9	-80.4	-74.3	-72.9	-68.5	20.9	-9.0
C_{18}	-85.3	-80.8	-75.4	-72.4	-69.5	24.9	-10.9
C_{36}	-81.7	-75.7	-72.1	-70.0	-64.7	26.0	-19.0

However, similar to the mechanical testing (Figure 2.18) there was a considerable decrease (33% ± 1) in the storage modulus changing from the C_6 sample to the C_8, though not as significant as the decline (132%) observed in tensile strength. This further supports that the C_6 sample was analyzed while partially in the leathery region and/ or additional orientation effects occurred during the RT (Instron) testing.

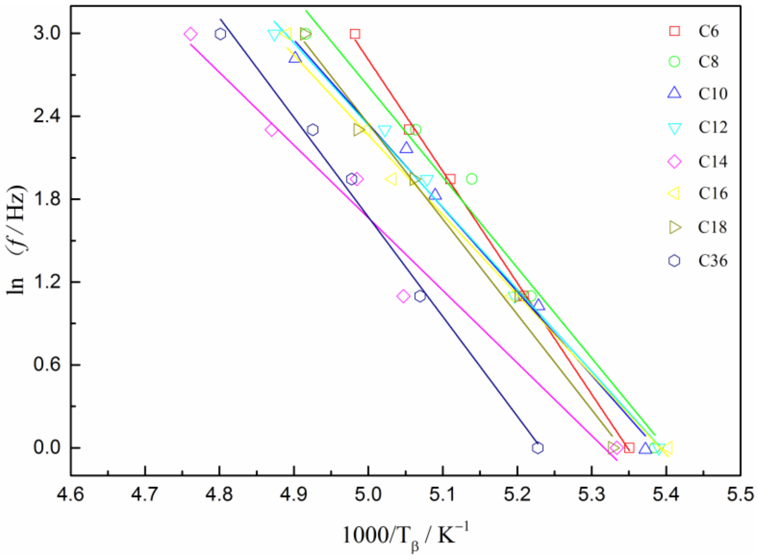

Figure 2.20 Arrhenius plot for the β transition. (Originally in colour)

T_g of these samples tested by DMA were in the same trend with DSC results and the shorter chain sample had the higher T_g. The activation energy of the beta transition, E_β, was obtained by applying the Arrhenius law (equation 2).[200]

$$E_\beta = -\mathrm{R}\left[\frac{\mathrm{d}(\ln f)}{\mathrm{d}(1/\mathrm{T}_\beta)}\right] \qquad (2)$$

by plotting of ln$f$ versus $1/T_\beta$ as shown in Figure 2.20 whereby the gradient corresponds to E_β.

Table 2.5 shows that the activation energy for the β transition, i.e., approximately 55 kJ mol^{-1} is similar to that reported by Boquilon *et al.*,[36] (63 kJ mol^{-1}) for a ELO-THPA (*cis*-1,2,3,6-tetrahydrophthalic anhydride) system. The presence of a β transition can be seen for all samples with those prepared with a shorter DCAs having a higher intensity than those prepared from the longer DCAs as can be seen in the Figure 2.19. For some materials it has been shown that there is an interrelationship with its proportion and to the general mechanical properties (toughness) of the materials tested, thus the higher intensity of β transition the better mechanical properties of the materials. In this case, there is a broad correlation with the shorter chain length DCAs having a higher tan δ intensity, and the longer DCAs a weaker intensity and poorer storage modulus. For these types of materials the β relaxation is reported to occur around -60 ºC and to be due to the motion of the diester segments formed between two crosslinks.[201]

2.4.5 Thermal stability

The thermal stability profiles as determined by thermogravimetric analysis (TGA) of the obtained epoxy resins are shown in Figure 2.21 and summarised in Table 2.6. All films showed similar degradation behaviour in both N_2 and air with good thermal stability, i.e., T_5 (5% weight loss temperature) ranging from 347 ºC to 369 ºC in N_2 and 337 ºC to 348 ºC in air.

A weight loss of 94%-99% was obtained at temperatures up to 600 ºC. From Table 2.6, it’s shown that the decomposition temperatures and residue at 450 ºC increased with the increase of chain length. Resins cured with longer chain length of DCAs had better thermal stability due to their being more bonds to absorb and dissipate energy for internal re-ordering. Vilela *et al.*[202] studied the thermal stability of polyesters prepared from C_{26} dicarboxylic acid with different chain length of diols (C_4, C_{12}, C_{26}) and their study confirmed that better thermal stability was obtained with higher chain length of polyesters.

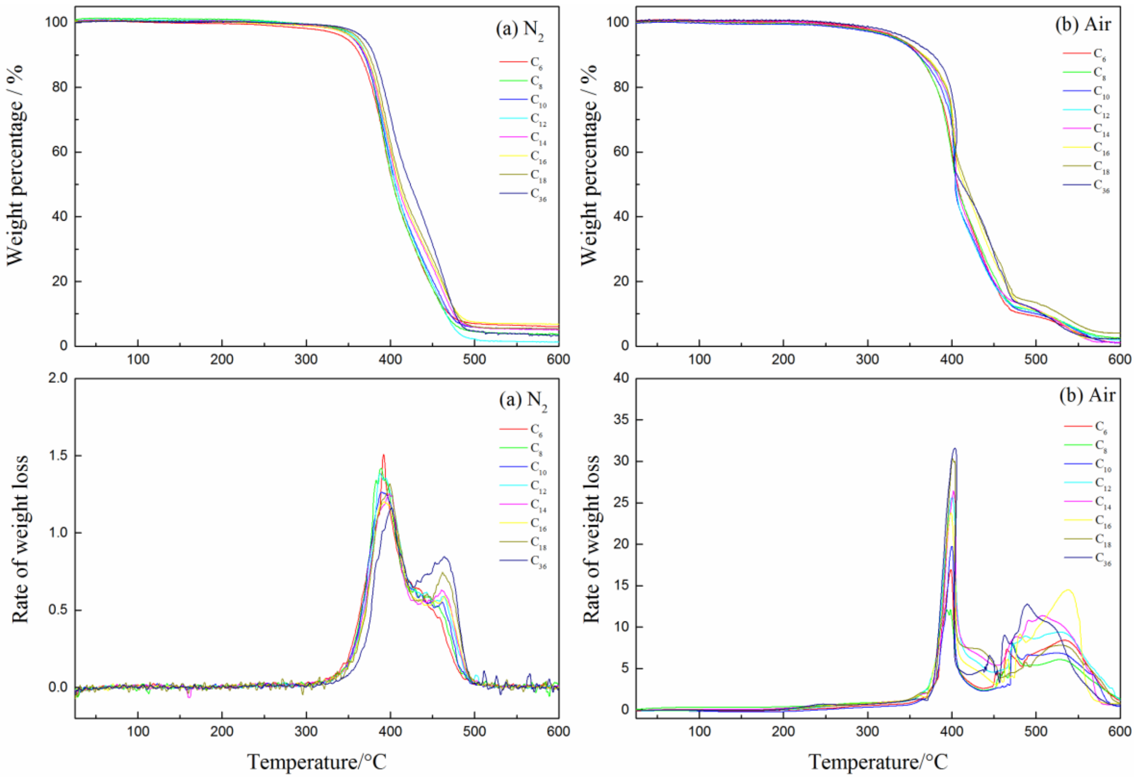

Figure 2.21 TGA and DTG of ELO-DCAs films in (a) N_2 and (b) air at 10 °C min^{-1} heating rate. (Originally in colour)

Figure 2.21 (a) clearly shows that the resins experienced a two-stage decomposition process in N_2. Since these two stages show the same decomposition profile in both N_2 and air, they were caused by the scission of ester linkages.[203]

Table 2.6 Thermal stability of the cured epoxy resins in N_2 and air (italics).

	T_5 [°C]	T_{10} [°C]	T_{50} [°C]	T_{max} [°C]	R_{300} [%]	R_{450} [%]	R_{600} [%]
C$_6$	347.4	363.7	403.2	391.8	98.5	17.8	6.0
	337.5	*360.1*	*406.3*	*400.4*	*98.1*	*19.8*	*1.0*
C$_8$	357.1	368.6	403.0	391.3	99.6	17.6	3.6
	334.9	*359.0*	*406.2*	*401.1*	*97.6*	*21.7*	*2.4*
C$_{10}$	356.1	368.5	405.6	391.7	99.0	20.4	5.1
	332.2	*360.1*	*404.3*	*401.4*	*97.1*	*19.6*	*1.0*
C$_{12}$	359.6	371.4	406.3	390.5	99.5	19.2	1.3
	337.0	*363.8*	*405.0*	*404.6*	*97.6*	*18.9*	*1.9*
C$_{14}$	357.1	370.6	408.8	401.8	99.0	24.7	5.1
	337.2	*363.8*	*406.1*	*404.8*	*98.0*	*20.0*	*1.1*
C$_{16}$	357.4	371.3	410.3	395.1	99.0	25.6	6.8
	337.4	*366.7*	*414.6*	*404.3*	*97.8*	*26.6*	*2.4*
C$_{18}$	362.7	374.9	412.5	397.4	99.6	27.1	5.3
	337.9	*365.0*	*417.3*	*400.5*	*97.7*	*29.4*	*3.9*
C$_{36}$	368.8	380.0	423.5	402.7	99.5	31.4	3.3
	348.4	*378.3*	*412.1*	*404.2*	*98.9*	*28.6*	*2.3*

The first stage from 350 ºC to 430 ºC resulted from chain scission in the linseed oil ester groups which was confirmed by the decomposition process of pure ELO.[176, 204] While the second stage beyond 430 ºC resulted from the ester groups formed by the ring-opening reactions between DCAs and epoxy groups. With the increase of chain length, the second stage became more apparent. Under oxidative conditions, the decomposition process is more complex with an additional higher temperature main stage of the decomposition occurring beyond 500 ºC, which corresponds to the further oxidation of the residual char.[205]

2.5 Effect of different accelerators

In this work, 1.0 mol% different accelerators (DMAP, 1-MI, 2-MI, VI, TEA and blank sample) were used in ELO-adipic acid epoxy systems to study the effects of accelerators on the properties of epoxy resins. The chemical structures of these accelerators are shown in Figure 2.22.

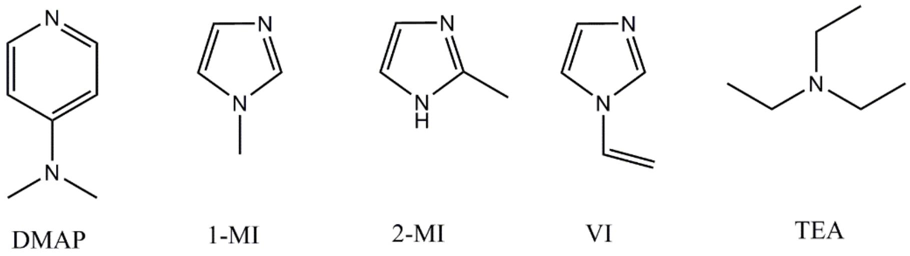

Figure 2.22 Chemical structures of accelerators.

Figure 2.23 shows samples of ELO cured with adipic acid in the presence of different accelerators. All samples formed solid films after curing at 160 ºC for 1 h including the blank sample without any accelerator. However, the blank sample gave the lightest color and was slightly sticky compared to the others.

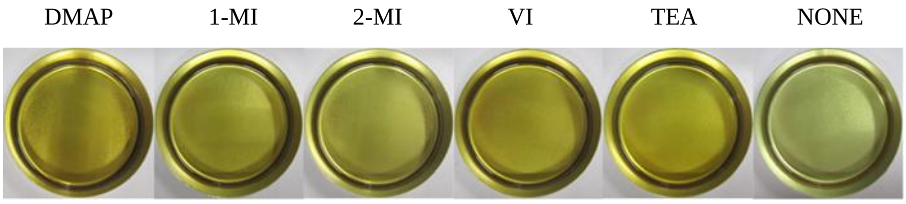

Figure 2.23 Samples with different accelerators (1 mol%) cured at 160 ºC for 1 h. (Originally in colour)

Supanchaiyamat *et al.*[84] carried out the study of ELO cured with Pripol 1009 in the presence of different accelerators. Their results showed that, in order to obtain a solid film, sample without accelerator and with TEA the curing process needed to be done at 140 °C for 6 and 3.5 h, respectively. Even though the temperature was 20 °C lower the time taken was much longer.

2.5.1 DSC analysis

Figure 2.24 shows the thermograms of ELO-C_6 systems in the presence of different accelerators and their corresponding thermal properties are summarized in Table 2.7. Two exothermic peaks were observed in the blank and TEA samples while there is only one exothermic peak was observed in other samples. The possible reason for the existence of one curing peak was due to the better selectivity of the esterification reaction for DMAP and imidazoles used as accelerators.

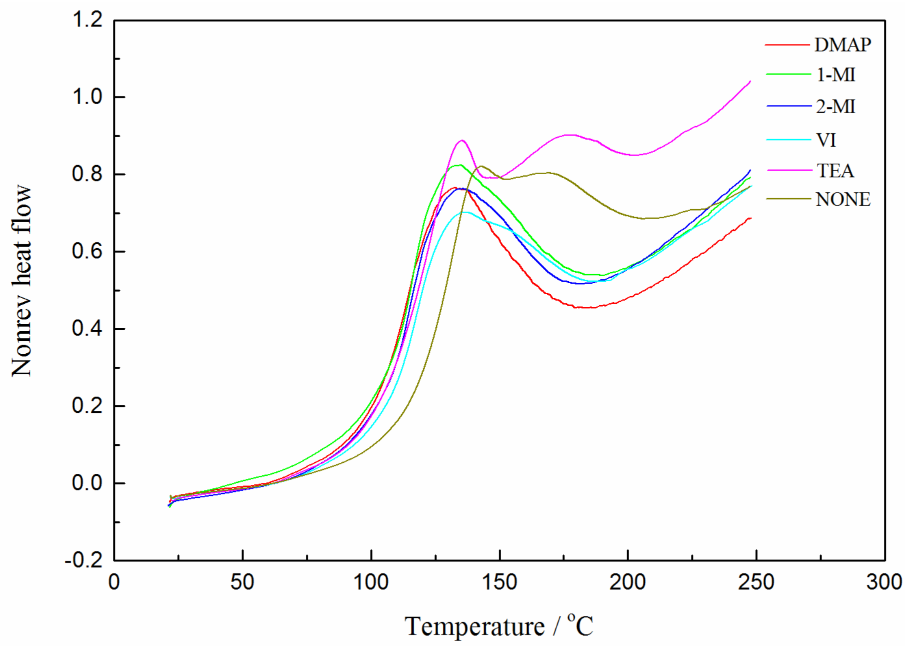

Figure 2.24 Thermograms of mixtures in the presence of different accelerators (1 °C/min). (Originally in colour)

When compared with the blank sample without any accelerators, the addition of different accelerators did decrease both T_{on} and T_P of the curing reaction. The decreased T_{on} and T_P indicated that the crosslinking reaction proceeded faster and the rate of the reaction was improved by the addition of accelerators. The peak temperature of curing decreases in the order: blank (141.8 °C) > TEA (134.1 °C) ≈ VI (133.5 °C) > 2-MI (132.4 °C) ≈ 1-MI (131.4 °C) ≈ DMAP (131.3 °C), which indicated that DMAP, 1-MI and 2-MI performed better than VI and TEA as accelerators. The reason for the poor performance of TEA may be due to the lone pair of electrons on the central nitrogen being blocked by the three ethyl chains.

The heat of reaction decreases in the order: blank (248.1 J g^{-1}) > DMAP (188.2 J g^{-1}) ≈ 1-MI (188.7 J g^{-1}) > TEA (183.6 J g^{-1}) > 2-MI (177.0 J g^{-1}) > VI (167.6 J g^{-1}). Interestingly, all samples with accelerators showed lower ΔH than the blank sample. The main reason could possibly relate to heat generated by the second etherification peak in Figure 2.24. Even though TEA was the poorest accelerator, ΔH was comparable to that of DMAP and imidazoles due to the existence of the second peak. These finding were quite different from those of Supanchaiyamat *et al.*,[84] who showed that ΔH decreased in the order: blank (161.9 J g^{-1}) > 2-MI (160.7 J g^{-1}) > DMAP (131.9 + 30 J g^{-1}) > TEA (79.1 J g^{-1}). The main reason for these differences was the much higher reactivity of adipic acid compared to Pripol 1009. Liu *et al.*[182] studied the curing of DGEBA with a poly(aryl ether ketone) bearing pendant carboxyl groups in the presence of DMP-30·HA and 2-ethyl-4-methylimidazole (2E4MI), respectively. Similarly, in the presence of accelerators, only one exothermic peak was observed instead of two exothermic peaks with the blank sample. However, their findings showed that higher ΔH was observed with DMP-30·HA sample while lower ΔH with 2E4MI sample. The lower ΔH indicated a much more incomplete reaction.

Table 2.7 Thermal properties for premixing mixtures in the presence of different accelerators.

Accelerators	ΔH/(J/g)	T_{on}/°C	T_{P1}/°C	T_{P2}/°C	E_α/(KJ/mol)
DMAP	188.2	102.5	131.3	-	70.8
2-methylimidazole	177.0	105.9	132.4	-	78.8
1-methylimidazole	188.7	106.6	131.4	-	72.3
Vinylimidazole	175.0	107.7	133.4	-	84.7
TEA	183..6	108.9	134.1	175.5	81.7
NONE	248.1	119.8	141.8	172.4	81.6

The activation energy (E_α) of the curing process was determined using the Kissinger method (eq. (1)) the Kissinger plot is shown in Figure 2.25. The Kissinger plots show good linearity for different accelerators studied with E_α in the range 70 to 85 kJ mol^{-1} (Table 2.7). Except that vinylimidazole sample showed higher E_α than that of the blank sample, all the other samples showed lower E_α than that of the blank sample. This finding suggested that, with the help of accelerators, the curing reaction proceeded more easily, which was consistent with the decreased T_{on} and T_P in the presence of accelerators.

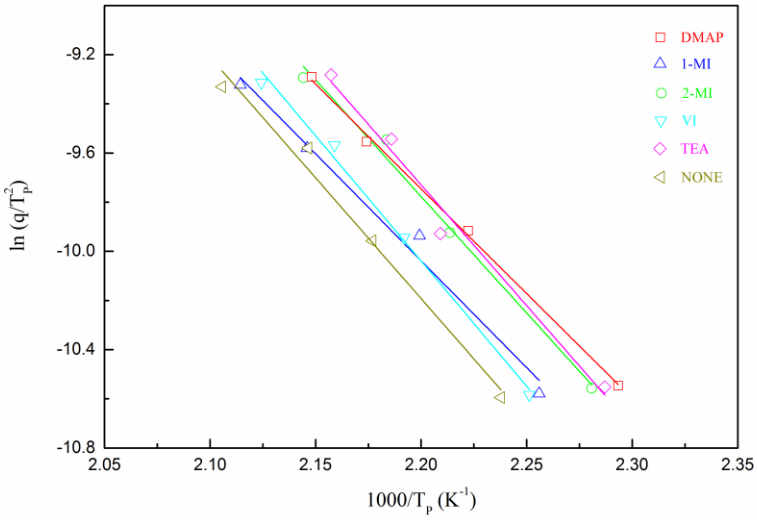

Figure 2.25 Kissinger plot to determine activation energy ($E\alpha$). (Originally in colour)

Figure 2.26 shows the DSC thermograms of the cured ELO-adipic acid films in the presence of different accelerators and are summarized in Table 2.8. The step changes in the baseline are assigned as the T_g of the films and the peaks occurring after 140 °C are assigned as the residual cure peak. The use of accelerators did increase the T_g of the film by 7 °C to 20 °C due to higher crosslink density for systems containing accelerators compared to the blank film. Without the addition of accelerators, the T_g of the film was -12.4 °C. Among different accelerators, film with DMAP as accelerator gave the highest T_g of 7.0 °C following by 1-methylimidazole and 2-methylimidazole with T_g of 4.8 and 4.4 °C, respectively; and then vinylimidazole and TEA with T_g of 0.1 and -5.8 °C, respectively. The changing trends for T_g and degree of cure are similar thus the higher the degree of conversion resulted higher T_g. With the increase of degree of conversion, the free volume within the cured polymers decreased which constrained the movement of network segments and thus increased T_g.

For the ELO-Pripol 1009 systems, Supanchaiyamat *et al.* also showed that DMAP and 2-methylimidazole samples had higher T_g than TEA and blank samples.[84] As expected, the T_g of all the ELO-C_6 samples were much higher than those of the ELO-Pripol 1009 samples due to the higher crosslink density obtained with C_6 samples. For samples curing in the presence of DMAP, T_g for ELO-C_6 and ELO-Pripol 1009 systems are 7.0 and -13.3 °C, respectively. While for blank samples, T_g for ELO-C_6 and ELO-Pripol 1009 systems were -12.4 and -17.6 °C, respectively.

Table 2.8 Thermal properties of cured resins in the presence of different accelerators.

Accelerators	T_g/°C	ΔH_R/(J/g)	Degree of cure/%	T_5 /°C	Soluble/%	M_w
DMAP	7.0	23.7	88.2	347.35	1.85	2935
2-methylimidazole	4.4	25.9	85.3	351.36	2.02	1840
1-methylimidazole	4.8	23.9	86.0	350.99	2.10	1735
Vinylimidazole	0.1	31.8	81.0	351.24	2.66	1480
TEA	-5.8	27.2	85.2	349.26	5.55	1651
NONE	-12.4	67.1	73.0	347.94	6.61	1643

The transition occurring after 140 °C was attributed to the residual curing reaction. Blank sample and TEA sample showed two peaks while the others showed only one residual curing peak, which were in agreement with their mixtures thermograms. The reason for the existence of the first peak was possibly due to some unreacted epoxy groups while the reason for the existence of the second peak was due to much higher peak temperature than the curing temperature. The residual curing peaks were also observed by other authors and they showed that with the increase of curing time, it’s possible to reduce or remove the residual cure.[181, 191]

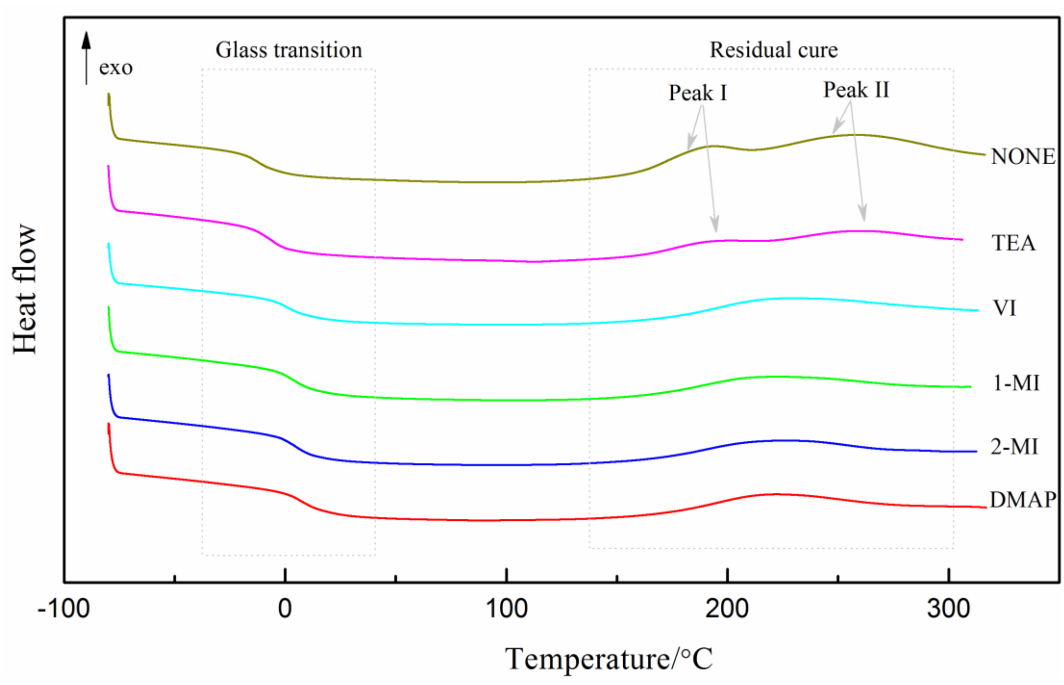

Figure 2.26 DSC thermograms of the cured epoxy systems with different accelerators. (Originally in colour)

2.5.2 Polymer extraction study

Figure 2.27 and Table 2.7 show the weight percentage of soluble substances and their corresponding M_w. Blank samples contained the most soluble substances (about 6.6%) followed by TEA samples (5.6%) and then vinylimidazole samples (2.6%). The soluble contents for other samples were about 2%. Interestingly, this trend was the same with respect to that for their mechanical properties. The higher the amount of soluble substances sample contained, the poorer the mechanical properties it possessed. As for the M_w, except DMAP sample formed the biggest soluble molecules with M_w about 2935, all the other samples had almost the same M_w around 1600. In the extraction study on ESBO polymerized by boron trifluoride diethyl etherate ($BF_3 \cdot OEt_2$) carried out by Liu e*t al.*, the M_w of the soluble substances were around 1600 to 3800 depending on the catalyst concentration and curing conditions.[193]

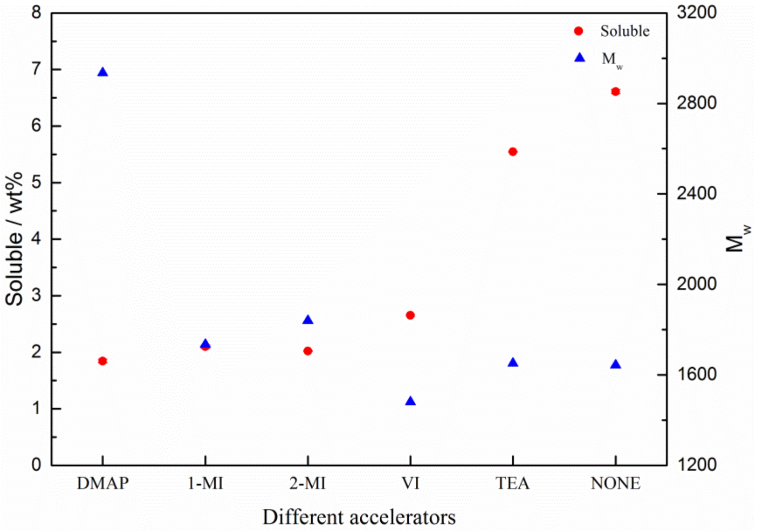

Figure 2.27 Weight percentage of soluble substances and their corresponding M_w. (Originally in colour)

2.5.3 FT-IR analysis

Figure 2.28 shows FT-IR spectra of reaction mixtures in the presence of different accelerators cured at 160 °C for 0 min and 60 min, respectively.

After premixing at 150 °C for 5 min, the shoulders observed in DMAP and imidazoles samples or the bands observed in TEA and blank samples at 1688 cm^{-1} were attributed to the carbonyl group of adipic acid, which further confirmed that DMAP and imidazoles performed better than TEA as accelerators. After curing for 1 h at 160 °C, all samples with different accelerators showed characteristic changes for the epoxy-acid reactions including newly formed O-H groups and ester carbonyl groups and the disappearance of epoxy groups and acid group.

For the ELO-Pripol system, Supanchaiyamat *et al.*[84] observed characteristic bands of accelerators near 1568 cm^{-1} was observed for imidazoles and TEA samples, while the band was not observed or negligible in ELO-C_6 systems.

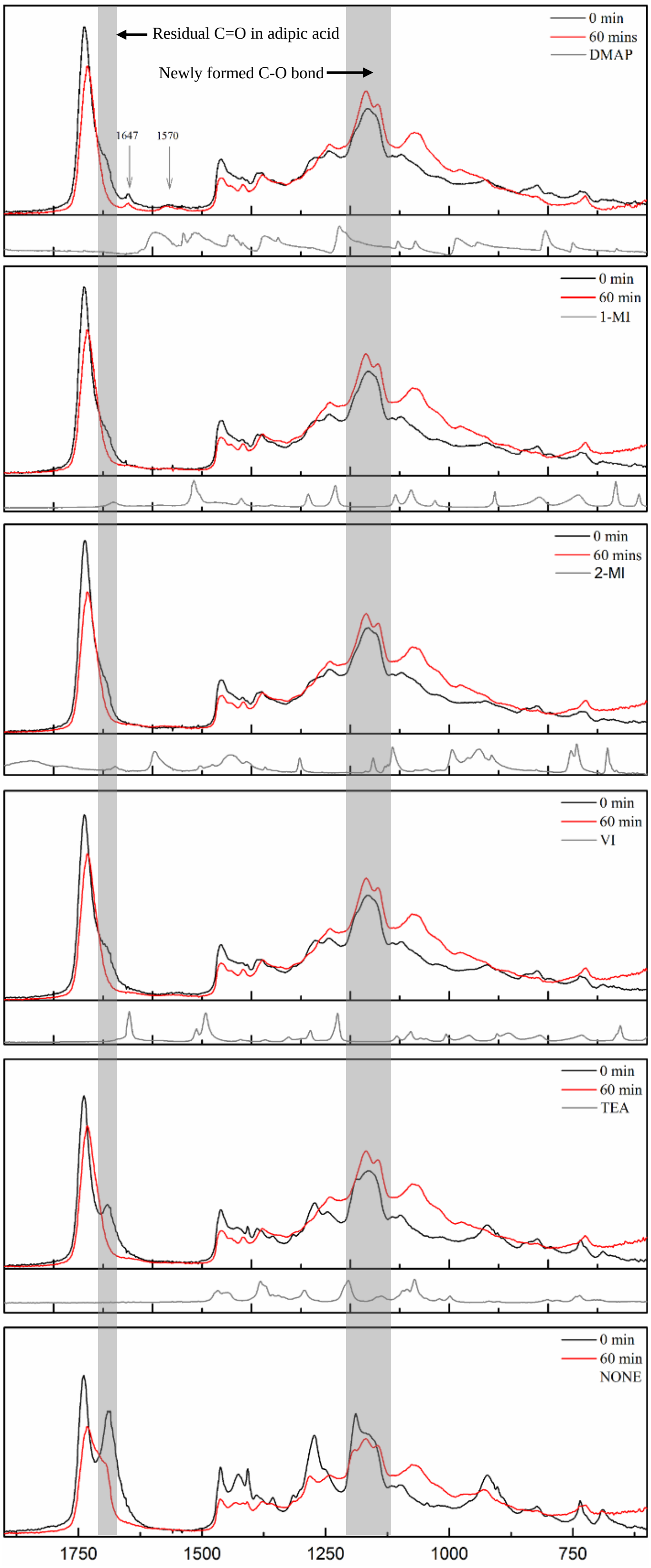

Figure 2.28 FT-IR spectra of reaction mixtures cured at 160 ºC for 0 min and 60 min. (Originally in colour)

A possible reason for this is that, compared to 1 wt% amount of accelerators used in their study, 1 mol% amount of accelerators were used in this study, which were less than 0.5 wt% if converted to weight ratio. In addition, only one ester C-O antisymmetric stretch band at 1155 cm^{-1} were observed by Supanchaiyamat *et al.*[84] whilst three bands at 1192, 1168 and 1144 cm^{-1} were observed in blank sample and two bands at 1168 and 1144 cm^{-1} were observed in other samples, which possibly suggested more complex reactions happened in the blank sample.

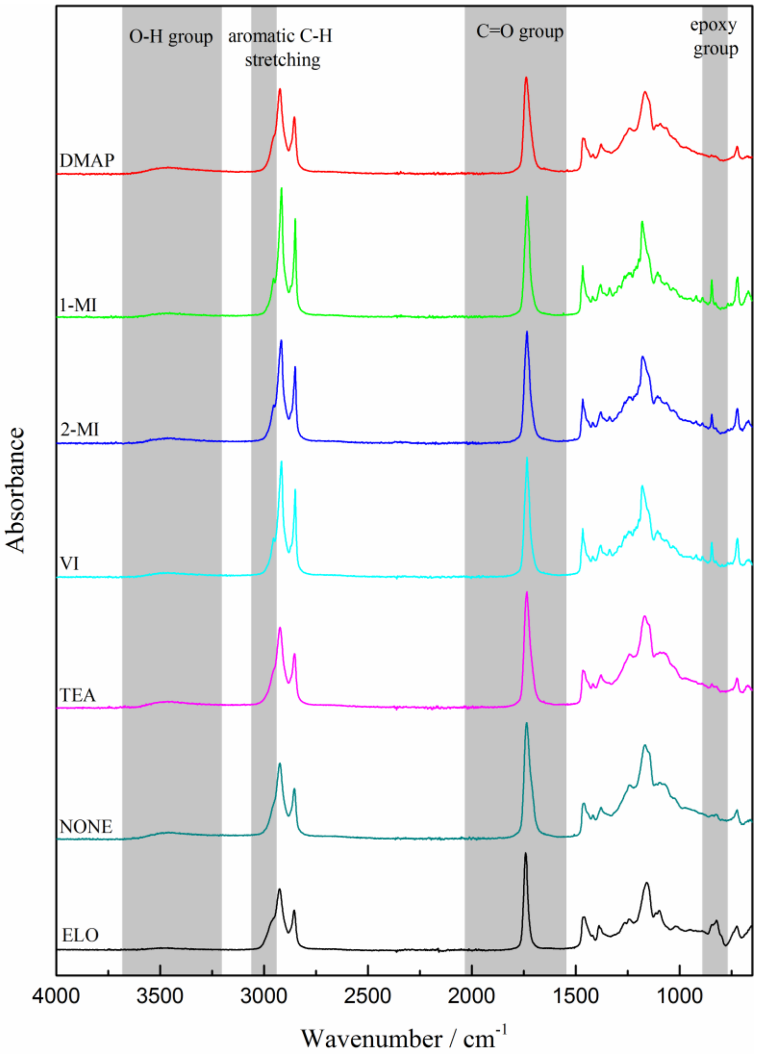

Figure 2.29 FT-IR of soluble substances for samples containing different accelerators. (Originally in colour)

Figure 2.29 shows the FT-IR spectra of ELO and soluble substances for samples containing different accelerators. In all soluble samples, a new broad O-H band at 3450 cm^{-1} was appeared, the ester carbonyl C=O band shifted from 1740 cm^{-1} in ELO to 1738 cm^{-1} and the characteristic bands of epoxy groups were not observed or negligible.

All these findings combined with their M_w suggested that the soluble substances were small molecules of the ring-opening products of ELO, which was also found by Liu *et al.*.[193] A small or shoulder band at 2954 cm^{-1} was assigned as the C-H stretching vibrations in imidazole ring and the sharp band at 845 cm^{-1} was assigned as the C-H deformation of the imidazole ring, which indicated the existence of accelerators in the soluble part.

2.5.4 Mechanical properties

Figure 2.30 shows the mechanical properties of ELO-C_6 samples in the presence of different accelerators. Compared to the blank sample without accelerators, the addition of accelerators increased all the mechanical properties including tensile strength, Young's modulus and elongation at break. The blank sample had the poorest mechanical properties with tensile strength of 0.9 MPa, Young's modulus of 4.1 MPa and elongation at break of 25.9%. Amongst the various accelerators, DMAP sample gave the best mechanical properties with tensile strength of 8.8 MPa, Young's modulus of 22.0 MPa and elongation at break of 55%, respectively. TEA sample gave the poorest mechanical properties with tensile strength of 1.2 MPa, Young's modulus of 5.2 MPa and elongation at break of 31.1%. In general, the trend of mechanical properties was the same with that of T_g and degree of cure. Samples with lower degree of cure had more free volume in the crosslinked network which impaired the mechanical properties.

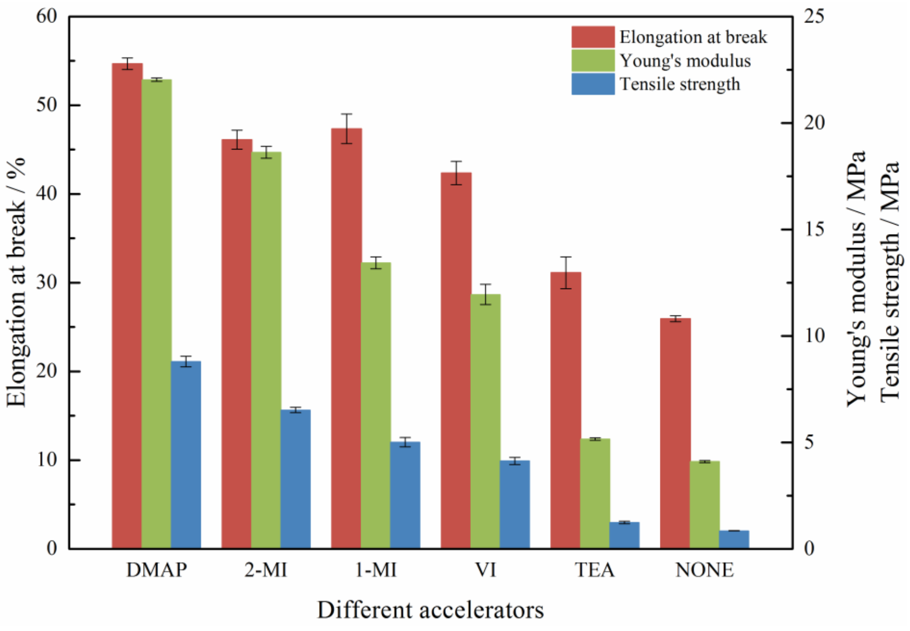

Figure 2.30 Mechanical properties of ELO-C_6 samples with different accelerators. (Originally in colour)

Compared to the ELO-Pripol 1009 system, the best mechanical properties was also found in DMAP sample with tensile strength of 1.2 MPa, Young's modulus of 6 MPa and elongation at break of 25%.[84] The big improvement on all the mechanical properties in this study is due to the shorter chain length of adipic acid resulting in higher crosslink density and more compacted networks.

2.5.5 Thermal stability

Figure 2.31 and Table 2.7 show the thermal stability of samples in the presence of different accelerators in N_2 atmosphere. As expected, the type of accelerators has negligible effect on the thermal stability of the cured resins.[84]

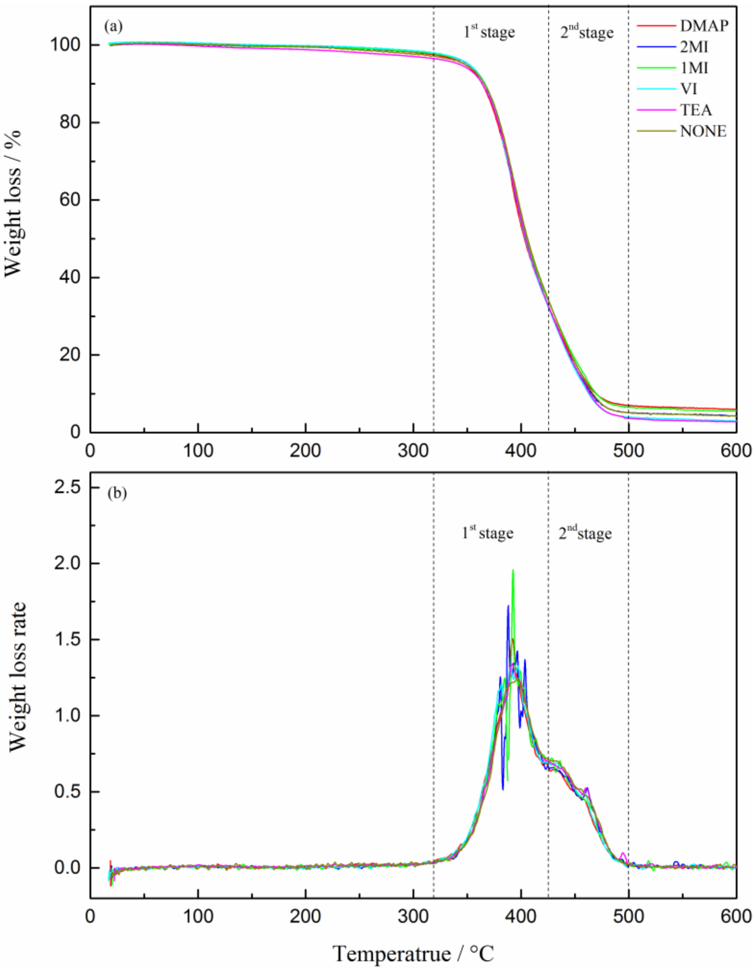

Figure 2.31 Thermal stability of samples with different accelerators in N_2. (a) TG; (b) DTG. (Originally in colour)

2.6 Effect of concentration of accelerator

In this study, the effect of the amount (concentration) of DMAP (0 mol% to 5.0 mol%) on the thermal and mechanical properties of the samples were studied.

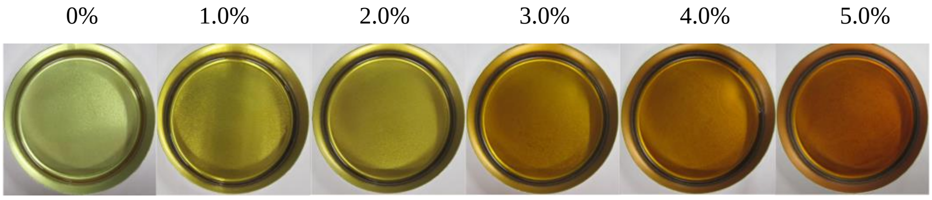

Figure 2.32 Samples with different amount of DMAP cured at 160 °C for 1 h. (Originally in colour)

Figure 2.32 shows samples with different amount of DMAP (0 mol%, 1 mol%, 2 mol%, 3 mol %, 4 mol% and 5 mol% based on the total mole amount of epoxy groups) cured at 160 °C for 1 h. The more DMAP was used, a deeper color was obtained. Some heterogeneity was observed in samples with high loading of DMAP.

2.6.1 DSC analysis

Figure 2.33 shows the thermograms of premixed mixtures containing different amounts of DMAP and their thermal properties are summarized in Table 2.9.

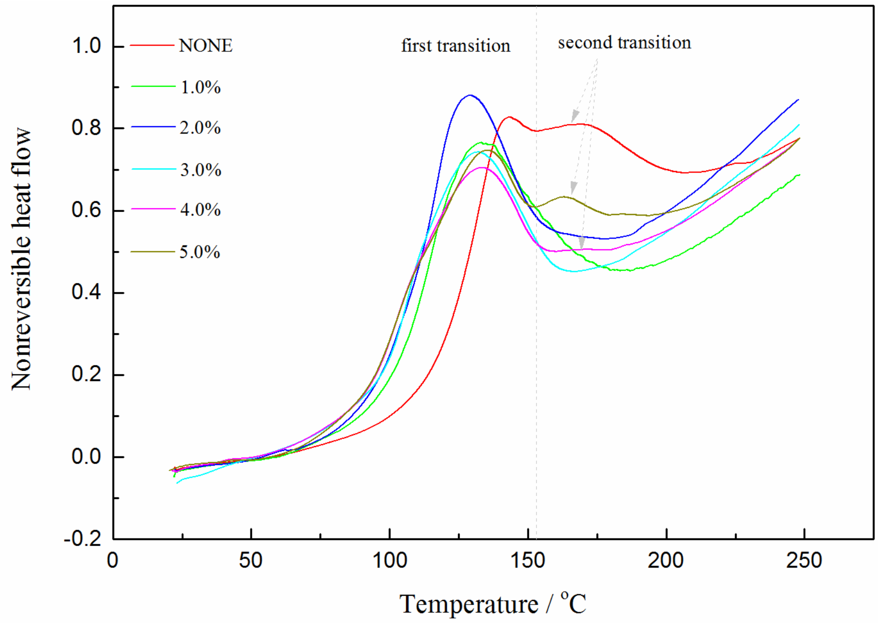

Figure 2.33 DSC thermograms of premixed samples containing different amount of DMAP (1 °C/min). (Originally in colour)

As can be seen from Figure 2.33, two exothermic curing peaks with T_P at 141.8 and 172.4 °C were observed in the blank sample corresponding to the esterification reaction and etherification reaction (see earlier in Figure 2.3). Increasing the DMAP concentration from 1 mol% to 5 mol% shows a change in the reaction mechanism. The esterification reaction (first transition) is dominant at low concentrations of DMAP (1 mol% to 3 mol%) and thereafter, the etherification reaction (second transition) begins to emerge (4 mol% and 5 mol%). The thermograms of the blank sample and that for the 5 mol% DMAP sample are similar.

When the concentration of DMAP increased from 0% to 5.0%, T_{on} decreased about 30 ^{o}C from 119.8 ^{o}C to 91.4 ^{o}C due to the higher reaction rate associated with the higher accelerator concentration. The decreased trend was also observed in ΔH_T until 4.0% DMAP was used, which was also observed in ELO-THPA using 2-ethyl-4-methylimidazole (2E4MI) as accelerator.[36]

Table 2.9 Thermal properties of mixtures containing different amount of DMAP.

Concentration of DMAP / mol%	T_{on}/^{o}C	T_{P1}/^{o}C	T_{P2}/^{o}C	ΔH_T/(J/g)
0	119.8	141.8	172.4	248.1
1.0	102.5	131.3	-	188.2
2.0	103.3	127.5	-	178.6
3.0	97.6	129.5	-	161.6
4.0	93.1	130.5	169.7	151.8
5.0	91.4	132.7	162.8	163.8

When the concentration of DMAP increased up to 5.0%, ΔH_T increased slightly possibly due to a higher extent of the etherification reaction as can be seen from Figure 2.33 (the bigger peak in 5.0% sample than that in 4.0% sample).

Table 2.10 Thermal properties of cured resins containing different amount of DMAP.

Concentration of DMAP / mol%	T_g/^{o}C	ΔH_R/(J/g)	Degree of cure/%	T_5 /^{o}C	Soluble/%	M_w	N/%[a]
0	-12.4	67.1	73.0	347.9	6.61	1643	0.00 (0.00)
1.0	7.00	23.7	88.2	347.8	1.85	2935	0.00 (0.12)
2.0	11.4	21.1	88.2	354.4	1.29	2641	0.16 (0.24)
3.0	12.0	23.6	85.4	346.3	1.46	2300	0.28 (0.36)
4.0	14.4	25.7	83.4	336.9	1.70	2049	0.73 (0.48)
5.0	14.86	16.11	90.2	329.2	1.96	1884	0.88 (0.60)

[a] nitrogen content in soluble part tested by CHN analysis (theoretical nitrogen content in cured resin assuming all the accelerators remained after the curing reaction).

Figure 2.34 shows the thermograms of cured resins with different concentrations of DMAP after curing at 160 ^{o}C for 1 h. The blank sample showed the lowest T_g of -12.4 ^{o}C and, with the increase of concentration of DMAP, T_g improved to reach a constant around 14.0 ^{o}C. However, all samples showed residual cure peak, two peaks for the blank sample and one for the others. The use of accelerators increased the reaction rate thus the degree of cure was improved within the same time. The degree of cure for the blank sample was 73% while 85-90% for other samples.

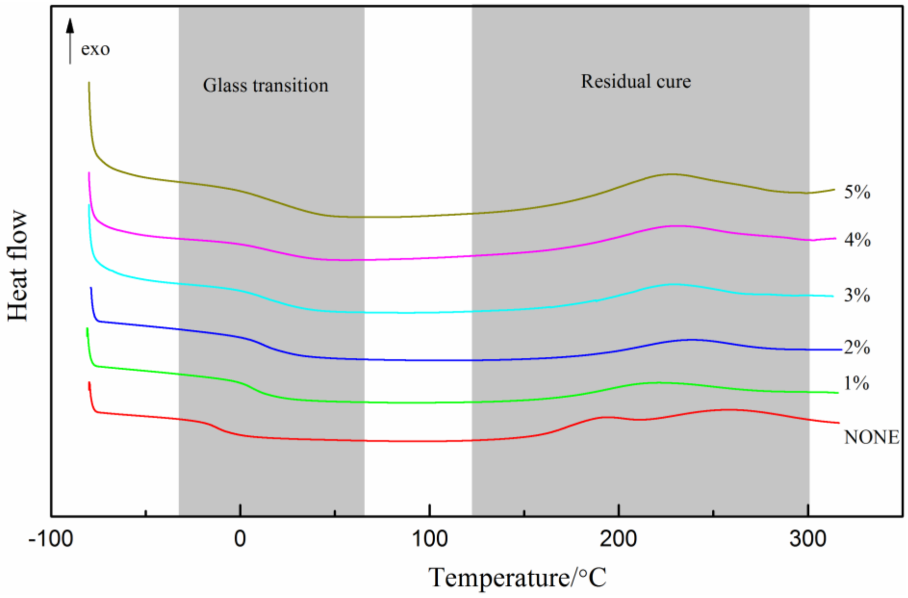

Figure 2.34 Thermograms of cured resins containing different amounts of DMAP. (Originally in colour)

2.6.2 Polymer extraction analysis

Figure 2.35 shows the weight percentage of soluble substances and their corresponding M_w for samples in the presence of different amount of DMAP.

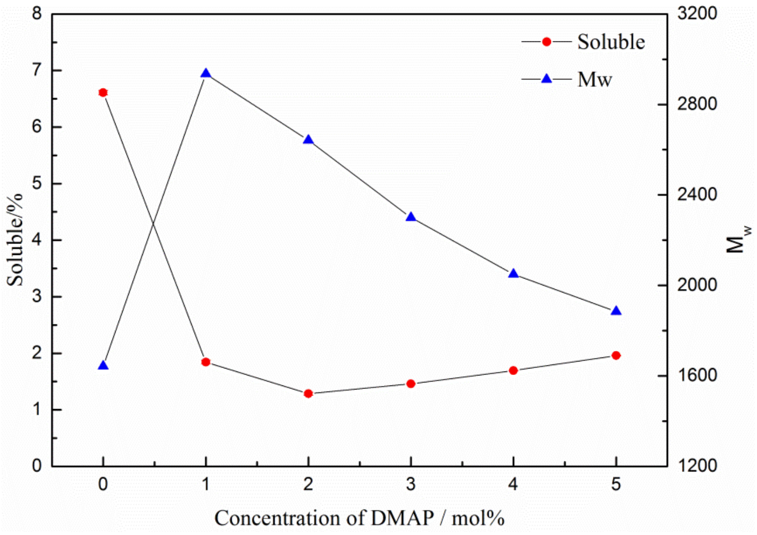

Figure 2.35 Weight percent of soluble substances and their $M_{w.}$ (Originally in colour)

The blank sample (without DMAP) had the highest amount of soluble content (ca. 6.5%) and all the other samples contained about 1.7%. The blank sample (without DMAP) gave soluble molecules with lowest M_w of 1643 and sample containing 1 mol% DMAP gave soluble molecules with largest M_w of 2935. After the concentration of DMAP was over 1 mol%, the M_w of the soluble substances decreased with the increase of DMAP concentration. With the increase of the amount of DMAP, the crosslink density increased thus the M_c, the molecular weight between crosslinks decreased, lower M_w substances extracted out in CH_2Cl_2 were obtained. Liu *et al.*[193] also found a decreasing trend in M_w with the increase of concentration of $BF_3 \cdot OEt_2$ for polymerized ESBO.

When looking at the nitrogen content in these soluble substances, as expected, the nitrogen content increased with the increase of DMAP concentration. Interestingly, when the concentration of DMAP increased up to 4.0% and 5.0%, the nitrogen content in the soluble substances were higher than the theoretical content in cured resins.

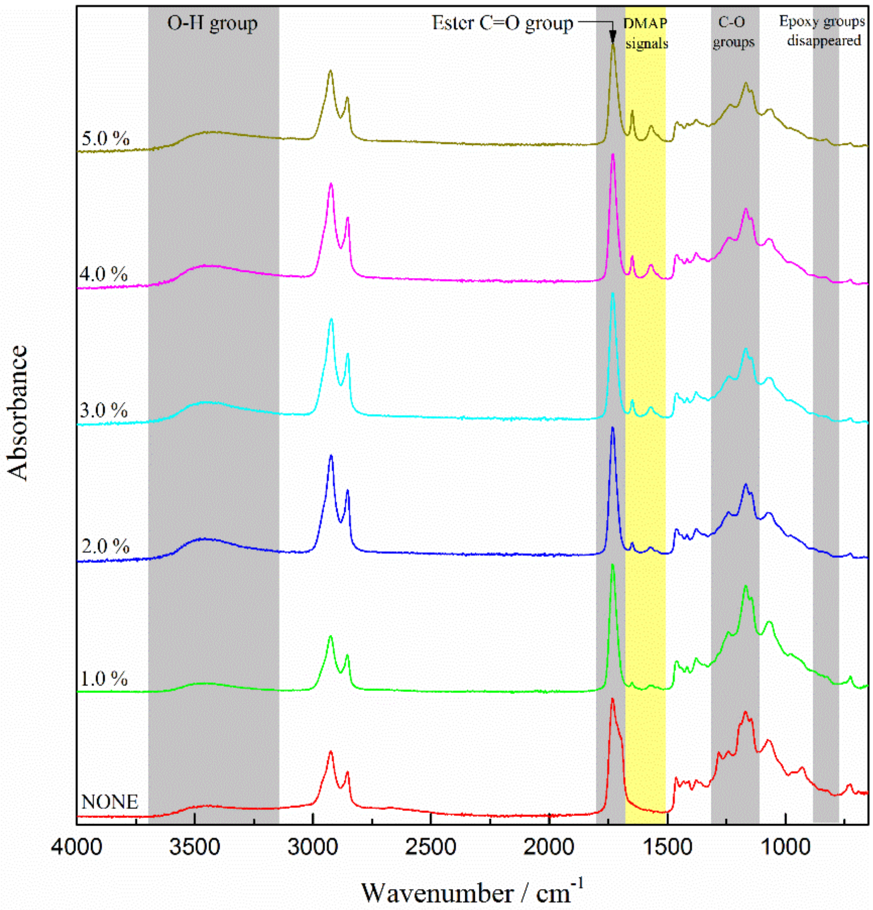

Figure 2.36 FT-IR spectra of cured films containing different amount of DMAP. (Originally in colour)

2.6.3 FT-IR analysis

Figure 2.36 shows the FT-IR spectra of cured resins containing different amount of DMAP. With the increase of concentration of DMAP, the intensities of these two signals (1649 and 1570 cm^{-1}) associated with DMAP also increased.

Figure 2.37 shows the FT-IR spectra of soluble substances for samples containing different amount of DMAP. The soluble substances were ring-opening products of ELO. With the increase of concentration of DMAP, aromatic C-H stretch band at 2954 cm^{-1} and bands related to the pyridine ring of DMAP at 1649, 1607 and 1567 cm^{-1} were observed and their intensities also increased. Also in the region from 820 to 850 cm^{-1}, the epoxy groups disappeared and more DMAP signals relating to aromatic C-H deformation appeared.

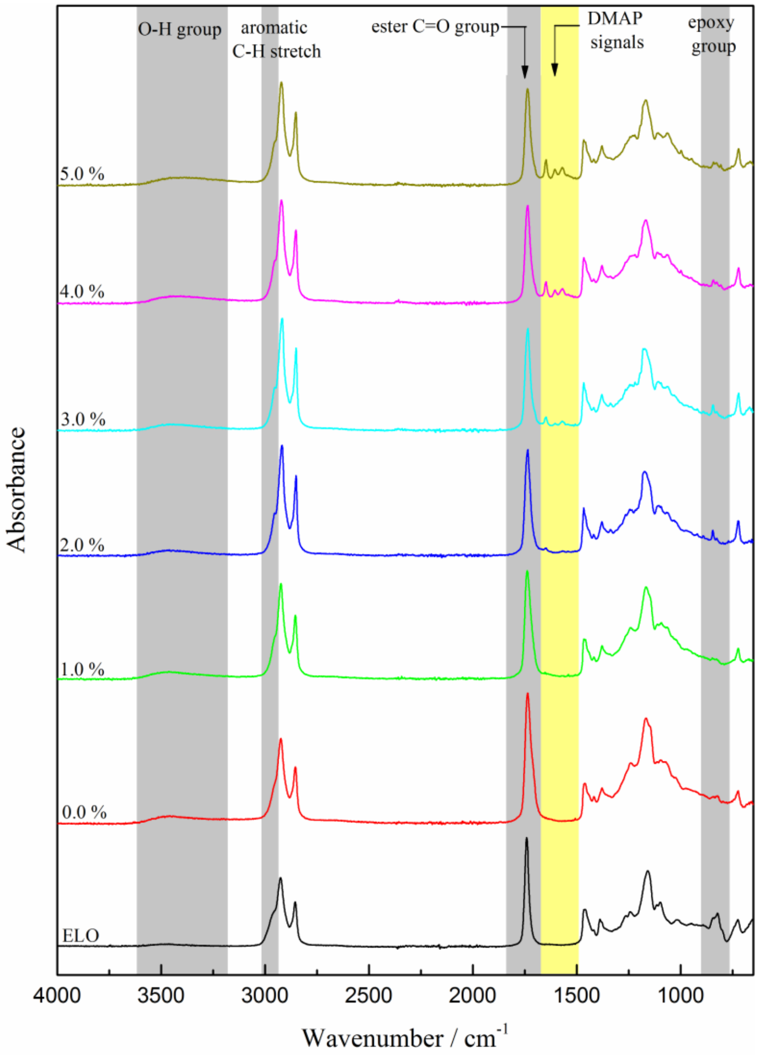

Figure 2.37 FT-IR analysis of extracted soluble samples containing different amounts of DMAP. (Originally in colour)

2.6.4 Mechanical properties

Figure 2.38 shows the mechanical properties of ELO-C$_6$ systems in the presence of different amounts of DMAP. The addition of DMAP improved all the mechanical properties. The blank sample had the poorest mechanical properties with elongation at break of 25.9%, tensile strength of 0.9 MPa and Young's modulus of 4.1 MPa. With an increase in DMAP concentration, tensile strength and Young's modulus increased rapidly while the elongation at break decreased from 55% to 30%. Compared to the blank sample, when the concentration of DMAP reached 5%, tensile strength increased by 2000% (17.7 MPa) and Young's modulus increased by 3100% (133.7 MPa). While elongation at break increased first and reached its maximum about 55% with 1.0% of accelerators and then started to decrease back to 30% with 5.0% of accelerators. Compared to the blank sample, all the other samples had higher degree of cure and thus potentially less free volume. The sample became stiffer as detected by a rapid increase in tensile strength and Young's modulus. With the increase of M_c, sample became more difficult to extend with the applied force which explained the decreased elongation at break.

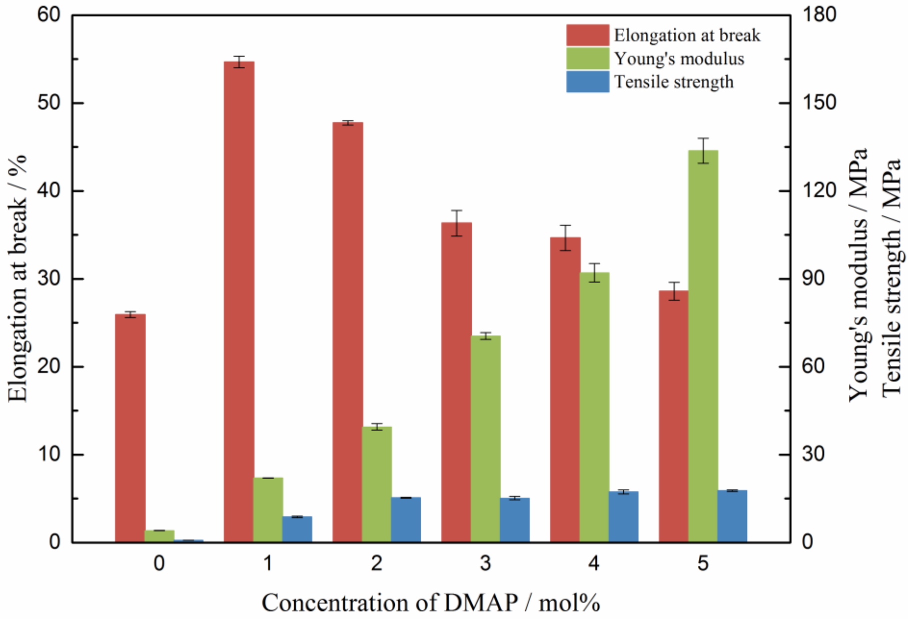

Figure 2.38 Mechanical properties of films containing different amount of DMAP. (Originally in colour)

2.6.5 Thermal stability

Figure 2.39 and Table 2.10 show the thermal stability of cured resins with different concentration of DMAP in N_2 with heating rate of 10 °C/min. With the increase of amount of accelerators, the decomposition temperature dropped about 20 °C from 350 °C to 330 °C. The finding was consistent with the M_w of their soluble substances. Samples containing smaller M_w of soluble substances decomposed at lower temperatures.

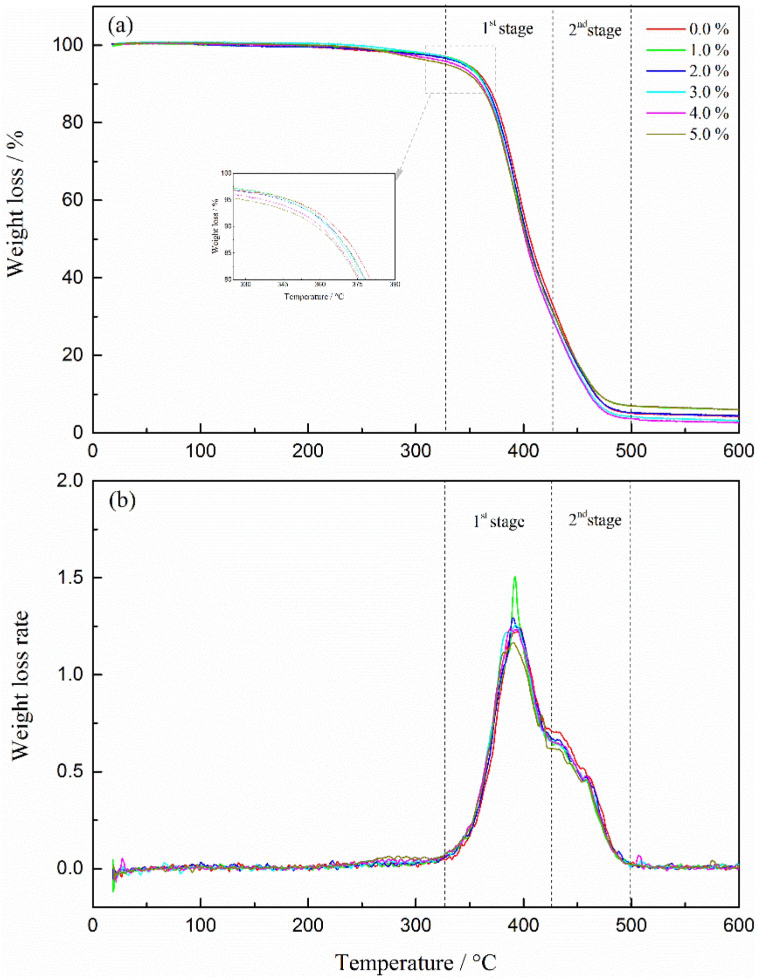

Figure 2.39 Thermal stability of cured resins containing different amounts of DMAP. (Originally in colour)

2.6.6 SEM analysis

Post tensile tests, the resultant fracture dumbbell was analyzed by SEM to study the effects of the amount of DMAP on the morphology (Figure 2.40).

Samples with lower concentration of DMAP showed smooth fracture surface after tensile test while the fracture surfaces of samples with higher concentration of DMAP (3%, 4% and 5%) were rougher with cracks in the sample. The higher concentration of DMAP, more cracks were observed within the sample. Crystallites were found on the fracture surface of the blank sample probably associated with some unreacted adipic acid. Samples containing 1.0% and 2.0% DMAP showed fairly smooth surface while samples containing 3.0%, 4.0% and 5.0% showed a rough surface with lots of nodules in the size range of 10-100 nm. These nodules were suggested to be sites of higher crosslink density resulting from intramolecular crosslinking and cyclization reactions.[206]

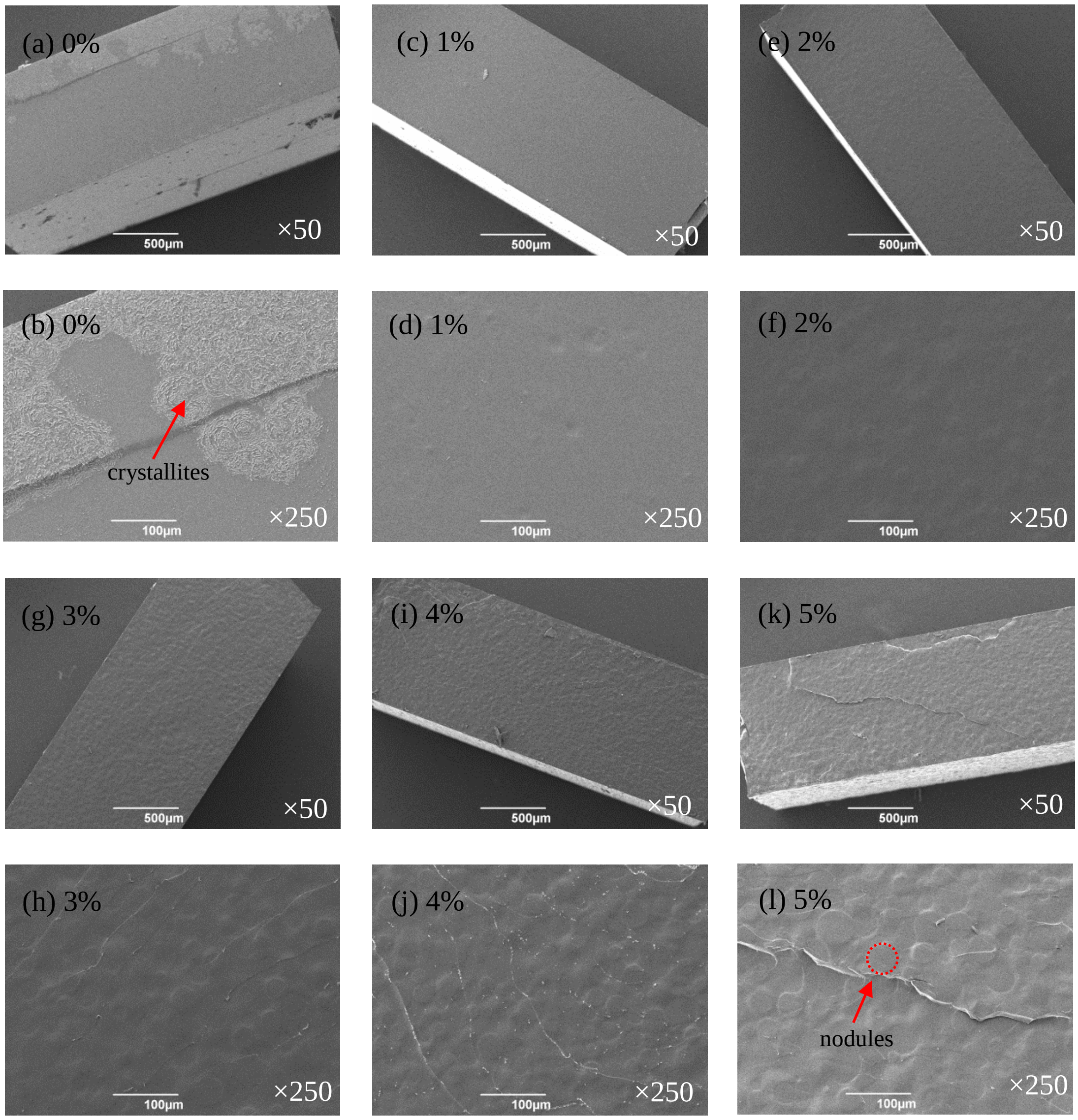
(a) 0%
500μm
×50
(c) 1%
500μm
×50
(e) 2%
500μm
×50
(b) 0%
crystallites
100μm
×250
(d) 1%
100μm
×250
(f) 2%
100μm
×250
(g) 3%
500μm
×50
(i) 4%
500μm
×50
(k) 5%
500μm
×50
(h) 3%
100μm
×250
(j) 4%
100μm
×250
(l) 5%
nodules
100μm
×250

Figure 2.40 Fracture surface of samples with different amount of DMAP after tensile test. (a, b) 0%; (c, d) 1.0%; (e, f) 2.0%; (g, h) 3.0%; (i, j) 4.0%; (k, l) 5.0%.

Also the number of these nodules increased with the increase of DMAP concentration. In other words, with the increase of contention of DMAP, the extent of inhomogeneity was bigger. One possible reason for the generation of inhomogeneity is the competition reaction between esterification and etherification reactions.

By re-examing the fracture surface after immersing in CH_2Cl_2 for 1 d (Figure 2.41), all samples were destroyed greatly. It was found that the white crystalline particles on the fracture surface of the blank sample disappeared to leave a smooth surface. The sample containing 2.0 mol% DMAP showed the smoothest surface which is possibly related to the fact it had the lowest content of soluble substances. With the increase of amount of DMAP, the surface became rougher.

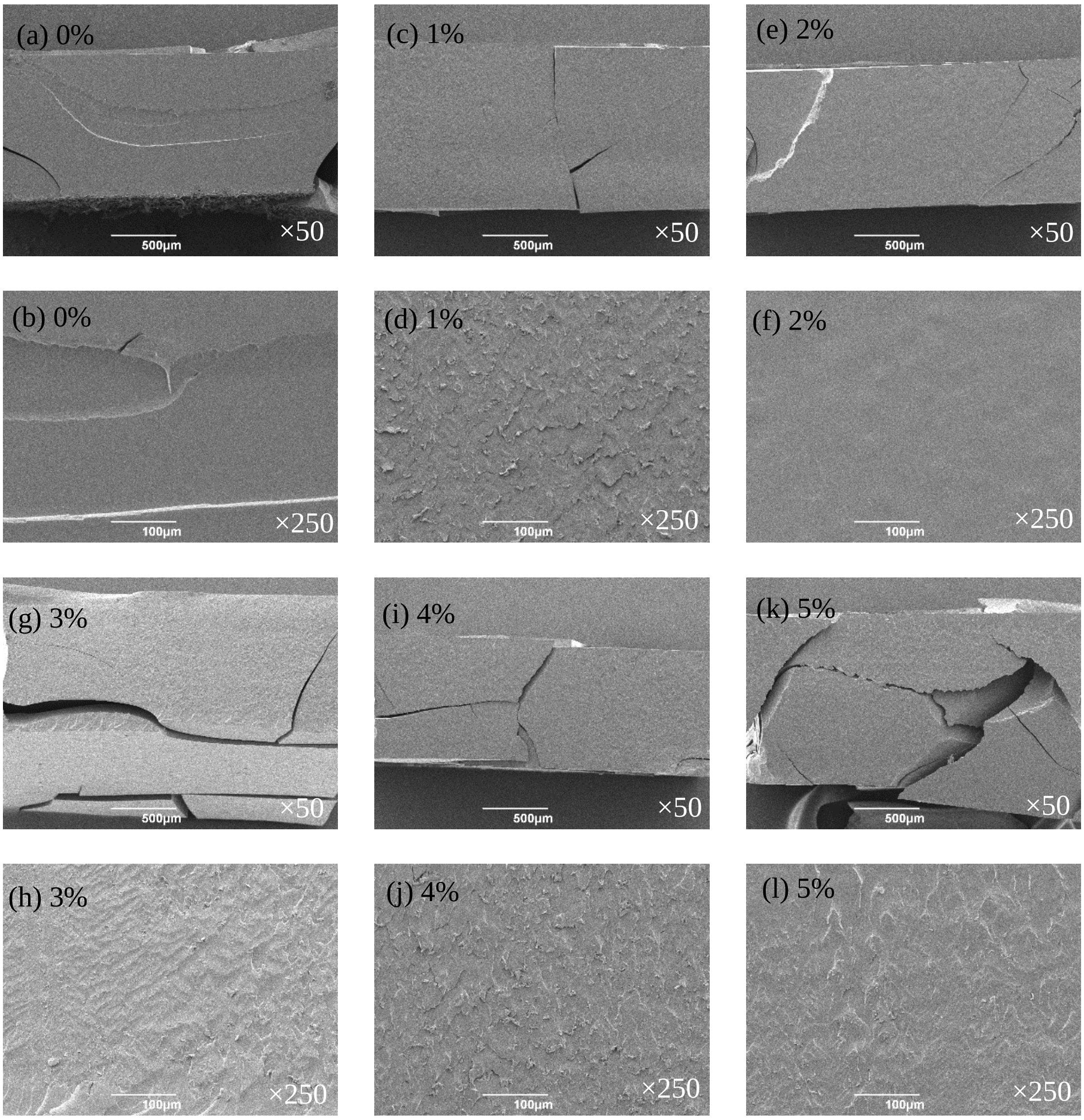
(a) 0%
×50
500μm
(c) 1%
×50
500μm
(e) 2%
×50
500μm
(b) 0%
×250
100μm
(d) 1%
×250
100μm
(f) 2%
×250
100μm
(g) 3%
×50
500μm
(i) 4%
×50
500μm
(k) 5%
×50
500μm
(h) 3%
×250
100μm
(j) 4%
×250
100μm
(l) 5%
×250
100μm

Figure 2.41 Fracture surface of samples with different amount of DMAP after immersing in DCM for 1 d. (a, b) 0%; (c, d) 1.0%; (e, f) 2.0%; (g, h) 3.0%; (i, j) 4.0%; (k, l) 5.0%.

2.7 Effect of different T and t

In this study, the effects of curing temperature (T) and time (t) on the properties of samples were studied. Five different temperatures (140, 160, 180, 200 and 220 ºC) and nine different curing times (1, 2, 4, 6, 8, 12, 16, 20 and 24 h) were chosen. Figure 2.42 shows ELO-C_6 sample with 1 mol% DMAP cured at different temperatures for 1 h. With the increase of temperature, the color of the samples became deeper from pale yellow to light brown.

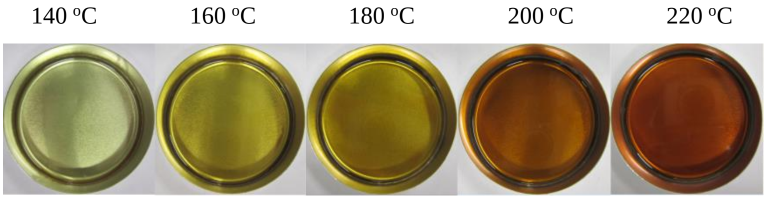

Figure 2.42 Samples of ELO-C_6 with 1 mol% DMAP cured at different T for 1 h. (Originally in colour)

Figure 2.43 shows ELO-C_6 sample with 1 mol% DMAP cured at 140, 160 and 180 °C for different times. With the increase of time, the color of the samples became deeper. Curing temperature and time are important to the appearance of the samples. To some extent, samples with the same properties may be obtained either by curing at lower temperatures for longer time or by curing at higher temperatures for shorter time. The thermal and mechanical properties of this effect will be described in the following part. It's possible to cure samples at 200 and 220 °C for short times (less than one hour), however, evidence suggested that samples cured at such high temperatures gave poorer properties due to partial decomposition process happened within the sample.

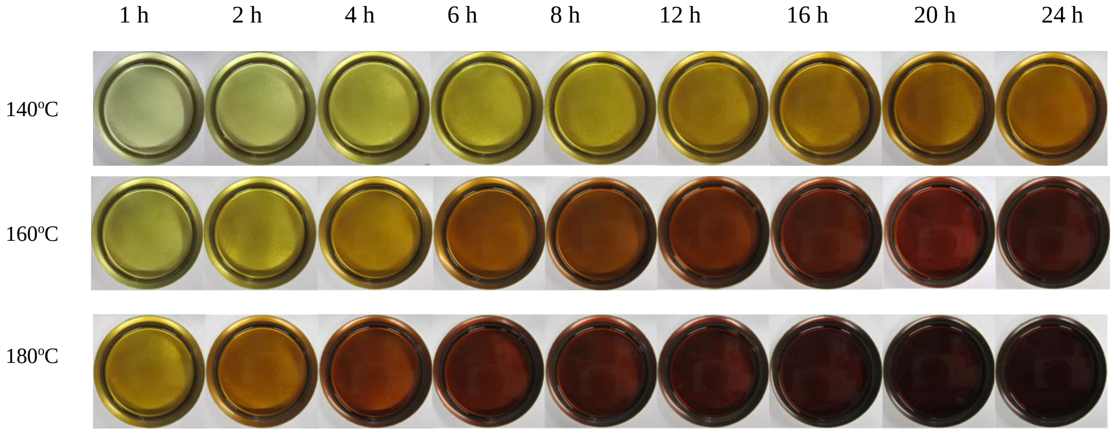

Figure 2.43 Samples of ELO-C_6 with 1 mol% DMAP cured at 140, 160 and 180 °C for different t. (Originally in colour)

2.7.1 DSC analysis

Figure 2.44 shows ELO-C_6 sample with 1 mol% DMAP cured at different temperatures for 1 h. With the increase of curing temperature, T_g shifted to higher temperatures due to the higher degree of cure (Table 2.11). Sample cured at 140 °C showed the lowest T_g of -5.0 °C. The highest T_g of 12.5 °C was observed in sample cured at 200 °C. While when temperature increased up to 220 °C, T_g started to drop even though the degree of cure was the highest.

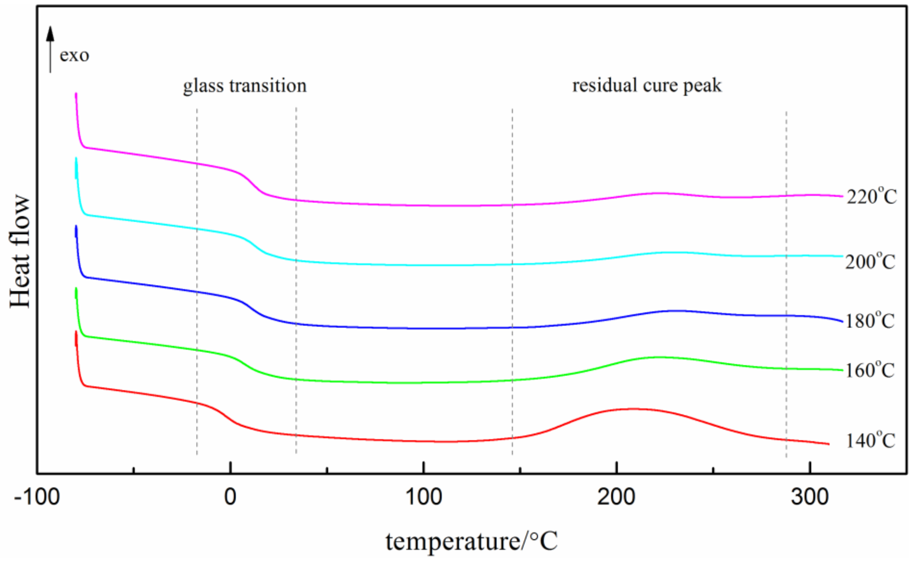

Figure 2.44 Thermograms of ELO-C6 sample with 1 mol% DMAP cured at different temperature for 1 h. (Originally in colour)

The sample cured at 140 °C was the least cured with a degree of cure of only 76% which was responsible for it having a lowest T_g. The lower of the degree of cure, the lower level of crosslinking reached and thus the lower T_g. When the curing temperature increased by 20 °C, the degree of cure increased up to 91% and kept constant at around 96% after 180 °C.

Table 2.11 Thermal properties of ELO-C6 samples cured at different temperature for 1 h.

Curing temperature / °C	T_g / °C	$\triangle H_R$ / J.g^{-1}	Degree of cure / %	$T_{5\%}$ / °C	T_{max} / °C
140	-5.00	60.5	76.2	345.1	390.5
160	7.0	23.7	90.7	347.4	391.8
180	10.6	10.7	95.8	351.4	390.4
200	12.5	7.0	97.2	353.0	393.0
220	10.9	5.7	97.8	352.3	390.6

Table 2.12 shows T_g and degree of cure of ELO-C6 samples cured at 140, 160 and 180 °C for different curing times. At 140 °C, with the increase of curing time, T_g increased rapidly in the first 4 h from –5.0 °C to 8.9 °C accompanied by the decrease of residual cure and then kept constant at about 12.0 °C. At 160 °C, T_g increased by 3 °C from 7.0 °C to 9.8 °C by increasing the curing time from 1 h to 2 h. After that T_g was quite constant around 13.0 °C. At 180 °C, T_g was fairly constant during the increasing curing time and the degree of cure kept at 96%. The trend of the change of T_g was the same for that of mechanical properties for samples cured at 140 °C and 160 °C. Whilst it was different for samples cured at 180 °C which indicated that the increase of curing time at higher temperatures had greater influence on mechanical properties

that that on T_g.

Table 2.12 T_g and degree of cure of ELO-C6 samples cured at 140, 160 and 180 °C for different time.

	140 °C			160 °C			180 °C		
Time/h	T_g/ °C	△H_R / J.g^{-1}	Degree of cure/%	T_g/ °C	△H_R / J.g^{-1}	Degree of cure/%	T_g/ °C	△H_R / J.g^{-1}	Degree of cure/%
1	-5.0	60.5	76.2	7.0	23.7	90.7	10.6	10.7	95.8
2	1.0	32.8	87.1	9.8	16.5	93.5	11.7	12.0	95.3
4	8.9	24.8	90.2	11.5	16.1	93.7	11.4	11.9	95.3
6	10.2	22.7	91.1	11.9	15.1	94.1	12.6	12.1	95.2
8	10.4	12.0	95.3	12.0	10.7	95.8	12.5	9.8	96.1
12	10.5	11.1	95.6	12.4	8.3	96.7	11.4	7.3	97.1
16	10.6	9.9	96.1	12.8	7.3	97.1	11.1	8.0	96.9
20	12.5	10.8	95.8	13.8	7.0	97.2	10.9	9.9	96.1
24	12.1	9.7	96.2	13.1	7.2	97.2	10.9	9.8	96.1

2.7.2 Mechanical properties

Figure 2.45 shows mechanical properties of ELO-C_6 samples with 1 mol% DMAP cured at different temperatures for 1 h. Sample cured at 140 °C for 1 h had the poorest mechanical properties with elongation at break of 42.3%, tensile strength of 2.4 MPa and Young's modulus of 7.5 MPa.

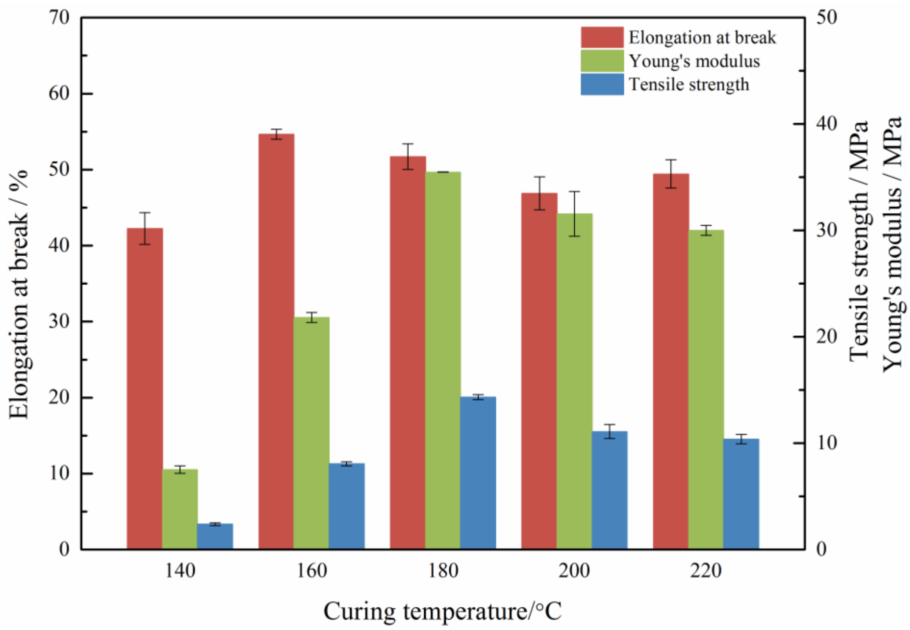

Figure 2.45 Mechanical properties of ELO-C_6 samples cured at different T. (Originally in colour)

By increasing curing temperature by 20 °C, all the mechanical properties were improved especially tensile strength and Young's modulus. Elongation at break was improved by 24%, tensile strength was improved by 236% and Young's modulus was improved by 190%, respectively. Sample cured at 180 °C had the best mechanical properties that elongation at break kept almost the same while tensile strength increased up to 14.3 MPa and Young's modulus increased up to 35.5 MPa. After the temperature increased over 180 °C, all the mechanical properties started to drop, especially with curing times greater than 8 h.

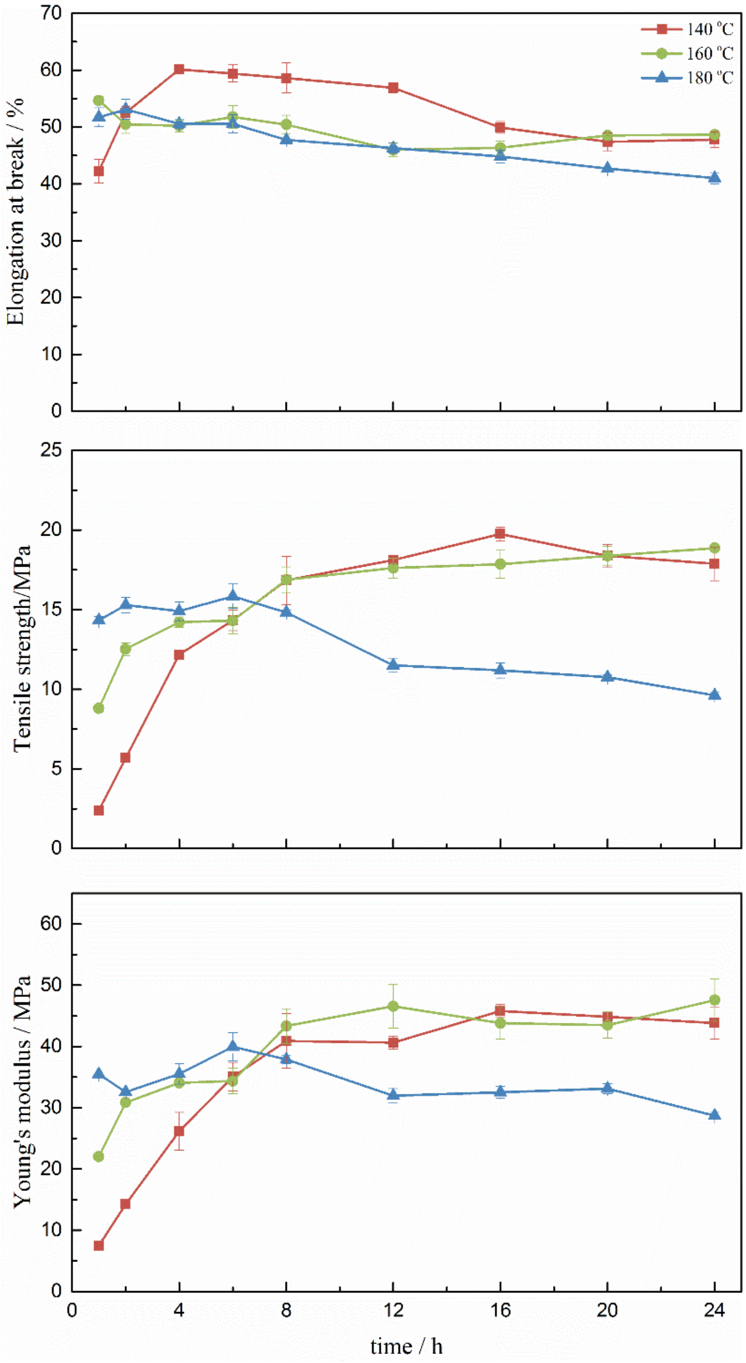

Figure 2.46 Mechanical properties of ELO-C_6 samples cured at 140, 160 and 180 °C for different time. (Originally in colour)

Figure 2.46 shows mechanical properties of ELO-C_6 samples with 1 mol% DMAP cured at 140, 160 and 180 ºC for different times. At 140 ºC, with the increase of curing time, elongation increased up to 60% after 4 h and then started to drop back to 50% after 16 h and kept at 50% until 24 h; tensile strength increased apparently up to 16.8 MPa after 8 h and then reached a plateau; and Young's modulus also improved a lot and reached to 41 MPa and then kept constant. At 160 ºC, with the increase of curing time, elongation at break remained constant about 50%; tensile strength increased up to 17 MPa after 8 h and then remained stable; and Young's modulus increased up to 43 MPa after 8 h and then plateaued. At 180 ºC, with the increase of curing time, elongation at break kept decreasing to 41% after 24 h; tensile strength kept at 14 MPa up to 8 h and then decreased to 9.6 MPa after 24 h; and Young's modulus was fairly constant around 33 MPa.

In general, at lower temperatures (140 and 160 ºC), with the increase of curing time, all mechanical properties increased and went to constant after a certain time. At higher temperature 180 ºC, elongation at break kept decreasing while tensile strength and Young's modulus increased at the beginning and then decreased with the increase of curing time. The decreased mechanical properties were attributed to some partial decomposition processes generated within the system. Vallo *et al.*[207] also suggested avoiding postcuring for long times at high temperatures due to the possibility of depolyetherification reactions.

2.7.3 Thermal stability

Figure 2.47 and Table 2.11 show the thermal stability in N_2 of samples cured at different temperatures (140, 160, 180, 200 and 220 ºC) for 1 h. All samples showed good thermal stability with decomposition temperature T_5 (5% weight loss temperature) around 350 ºC. With the increase of curing temperature, the decomposition temperature was improved a bit, which means that the increase of curing temperature had negligible improvement on thermal stability.

Table 2.13 T_5 of samples ELO-C_6 samples cured at 140 ºC for different time.

Curing time / h	1	2	4	6	8	12	16	20	24
T_5 / ºC	345.1	354.0	354.3	351.6	350.8	354.6	351.9	350.5	354.3

Table 2.13 shows the T_5 for samples cured at 140 ºC for different time. All samples showed similar T_5 around 350 ºC, which means that the effect of curing time on the thermal stability of these samples was negligible. Cheng *et al.*[208] also studied the effect of curing time (1 to 6 h) and temperature (140 to 220 ºC) on the thermal decomposition temperature of a trifunctional epoxy resin cured by 4, 4'-diaminodiphenyl sulfone (DDS). The thermal decomposition temperature increased slightly due to a higher crosslink density associated with longer cure time and higher cure temperature.

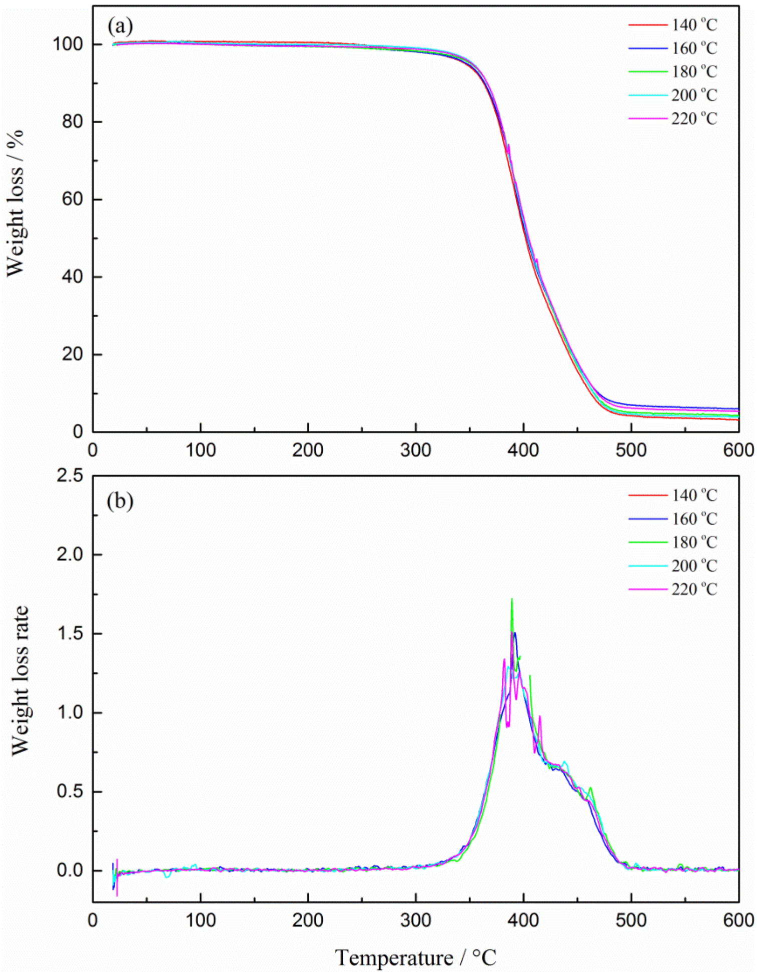

Figure 2.47 TGA and DTG in N_2 of samples cured at different T for 1 h. (a) TG; (b) DTG. (Originally in colour)

2.8 Conclusions

The properties of the cured epoxy resins depend on the structure and functionality of epoxy prepolymers and curing agents, the type and amount of accelerators and also curing conditions (temperature and time).

Among different plant oil-derived epoxy prepolymers including ELO, ESBO and their epoxidized FAMES EML and EMS, only ELO and ESBO gave cured solid resins while EML and EMS gave viscous oligoesters. ELO preformed best due to its triglyceride molecule structure and higher epoxy functionality.

With the increase of chain length of DCAs, T_g and mechanical properties decreased while thermal stabilities increased. Strain hardening effect was only observed in adipic acid samples which accounted for its much higher mechanical properties.

The addition of accelerators increased the reaction rate of the curing process and T_g and mechanical properties. Among various accelerators, DMAP performed best while TEA performed poorest.

With the increase of amount of DMAP, T_g and mechanical properties (tensile strength and Young's modulus) were increased while thermal stabilities were decreased. All samples showed inhomogeneity with nodule morphology in the size range of 10-100 nm were observed in samples with high DAMP concentration.

With the increase of temperature, T_g and mechanical properties increased first and then started to decrease due to partial decomposition processes. With the increase of time, at lower temperatures (140 and 160 ^{o}C), T_g and mechanical properties increased and then kept to be constant; at higher temperature (180 ^{o}C), T_g and mechanical properties started to decrease after curing for 8 h.

Chapter 3

Biobased epoxy resins of epoxidized plant oils cured with glutaric anhydride

3.1 Summary

Carboxylic acids and their derivatives, in particular (poly)esters and anhydrides, are the second most important class of epoxy curing agents just after amines. Herein, a study on the effect of curing temperature and time based on ELO-glutaric anhydride systems is presented. Then the synthesis, characterization and properties of a variety of plant oil-derived epoxy prepolymers (ELO, ESBO, EML, and EMS) cured with glutaric anhydride in the presence of DMAP are investigated to study the effect of structure and functionality of epoxy prepolymers on the properties of cured resins. At last, the effect of different combinations of glutaric anhydride and adipic acid was studied. Due to the different structures of glutaric anhydride and adipic acid, samples with various properties from soft flexible rubbery plastics to hard rigid plastics are expected to be made.

3.2 Effect of temperature and time

In this study, the effects of curing temperatures and curing times on the properties of ELO-GA (in the presence of DMAP as accelerator) resins are studied. Figure 3.1 shows ELO cured with glutaric anhydride in the presence of 1 mol% DMAP cured at different temperatures but at fixed time, 1h. The samples darkened, changing from pale yellow to dark brown, on increasing the temperature from 140 °C to 220 °C. In fact, for samples cured at 200 °C and 220 °C the resultant resins broke into several pieces due to the existence of residual stress after heating.

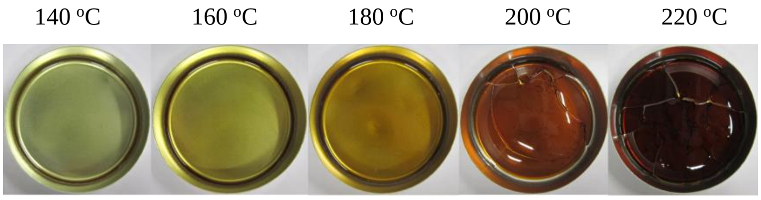

Figure 3.1 Samples of ELO cured with glutaric anhydride at different temperatures for 1 h. (Originally in colour)

Figure 3.2 shows ELO cured with glutaric anhydride in the presence of DMAP cured at 140, 160 and 180 °C for different times (1, 2, 4, 6, 8, 12, 16, 20, 24h). The color of samples became deeper with an increase of curing temperature and curing time. For samples cured at 180 °C over 8 h, cracks were generated in the samples.

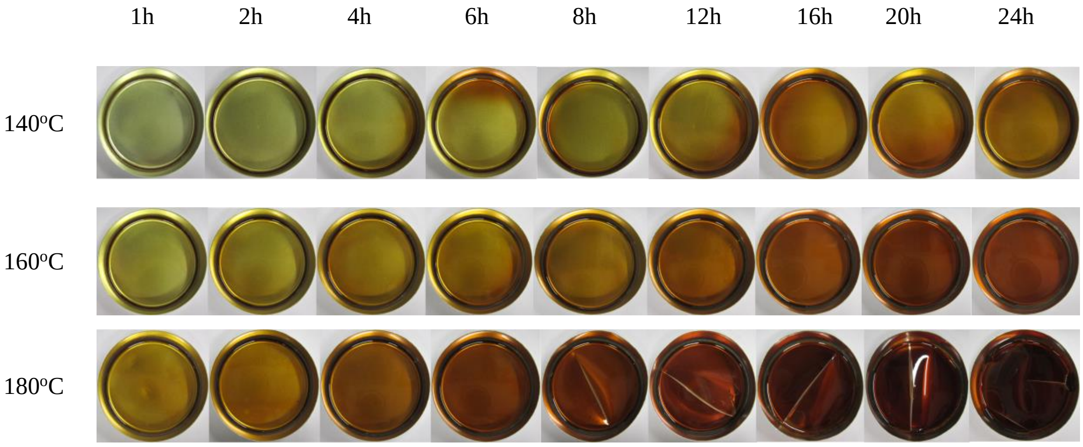

Figure 3.2 Samples of ELO cured with glutaric anhydride at 140, 160 and 180 °C for different times. (Originally in colour)

3.2.1 DSC analysis

Figure 3.3 shows the thermograms of ELO-GA resins cured at different temperatures for 1 h.

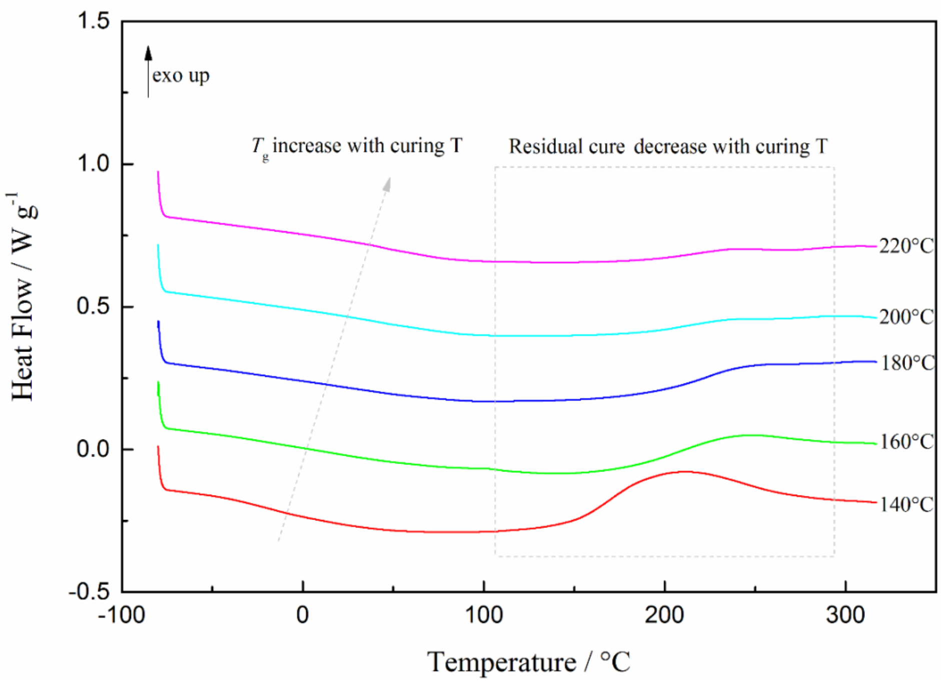

Figure 3.3 Thermograms of ELO-GA samples cured at different temperatures for 1 h. (Originally in colour)

With the increase of curing temperature, T_g shifted to higher temperatures and the residual cure ΔH_R decreased. Sample cured at 140 °C had the poorest T_g of -17.6 °C and the degree of cure was only about 82%. By increasing the curing temperature 20 °C, T_g was improved by 33 °C from -17.6 °C to 16.0 °C and the degree of cure was improved to 94%. When the temperature was over 200 °C, T_g increased to 43 °C.

Table 3.1 Thermal properties of ELO cured with glutaric anhydride at different T for 1 h.

Curing temperature (^{o}C)	T_g (^{o}C)	ΔH_R (J.g^{-1})	Degree of cure (%)	T_d (^{o}C)	T_{max1} (^{o}C)	T_{max2} (^{o}C)
140	-17.6	75.1	81.7	349.2	367.2	432.0
160	16.0	26.2	93.6	346.4	367.5	423.0
180	18.2	8.2	98.0	343.9	362.3	450.0
200	42.1	2.6	99.4	344.0	362.0	449.0
220	43.9	3.7	99.1	343.9	362.8	440.7

Table 3.2 summarizes T_g, residual cure ΔH_R and degree of cure for samples cured at 140, 160 and 180 ^{o}C for different times. Generally, increasing the curing time increased T_g and degree of cure but decreased ΔH_R.

Table 3.2 Thermal properties of ELO-GA cured resins at 140, 160 and 180 ^{o}C for different time.

Curing time/h	140 ^{o}C			160 ^{o}C			180 ^{o}C		
	T_g/ ^{o}C	$\triangle H_R$ / J.g^{-1}	Degree of cure/%	T_g/ ^{o}C	$\triangle H_R$ / J.g^{-1}	Degree of cure/%	T_g/ ^{o}C	$\triangle H_R$ / J.g^{-1}	Degree of cure/%
1	-17.6	75.1	81.7	16.02	26.2	93.6	18.2	8.2	98.0
2	13.7	39.7	90.3	17.7	20.2	95.1	41.6	8.0	98.1
4	15.8	22.6	94.5	43.0	12.2	97.0	41.6	2.4	99.4
6	16.4	23.3	94.3	42.6	12.9	96.9	42.1	3.6	99.1
8	16.1	15.9	96.1	41.5	9.5	97.7	43.2	3.0	99.3
12	16.2	16.6	96.0	42.6	9.3	97.7	42.6	5.2	98.7
16	17.2	16.3	96.0	42.0	7.2	98.2	44.2	6.5	98.4
20	41.1	11.3	97.2	42.2	7.8	98.1	42.9	6.3	98.5
24	41.4	12.7	97.0	42.3	9.6	97.7	43.4	6.3	98.5

3.2.2 Mechanical properties

Figure 3.4 shows the mechanical properties of ELO-GA samples cured at different temperatures for 1 h. For samples cured at 200 ^{o}C and 220 ^{o}C, tensile samples were not able to be made due to cracks in the film.

With an increase in curing temperature, elongation at break decreased while tensile strength and Young's modulus increased. Sample cured at 140 ^{o}C had elongation at break of 12%, tensile strength of 6.2 MPa and Young's modulus of 99 MPa. By increasing the curing temperature 20 ^{o}C, elongation at break decreased greatly by 70% while tensile strength increased by 147% and Young's modulus increased greatly by 780%. By further increasing the curing temperature to 180 ^{o}C, elongation at break decreased to 2.3% while tensile strength increased to 18.3 MPa and Young's modulus increased to 1243 MPa.

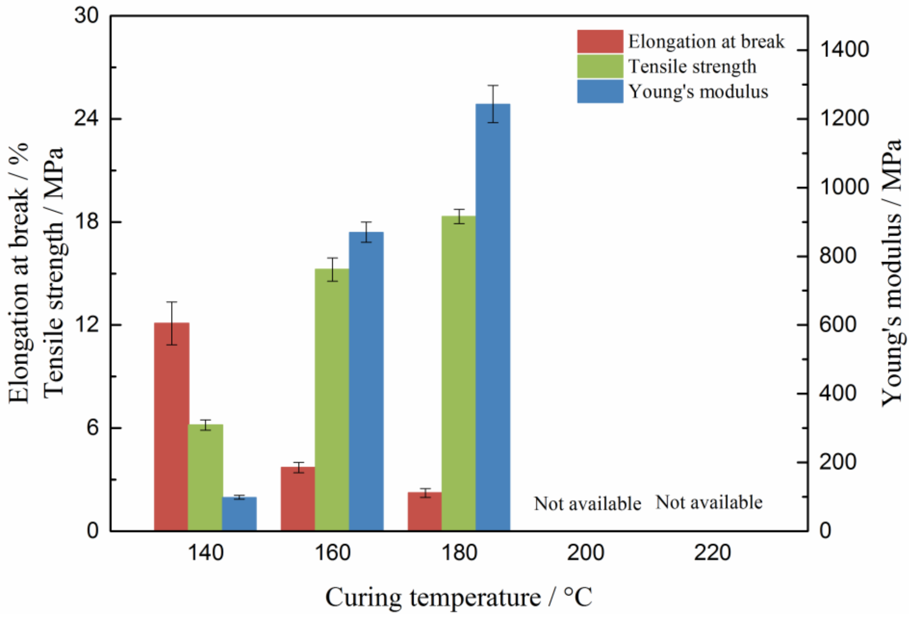

Figure 3.4 Mechanical properties of ELO-GA samples cured at different temperatures for 1h. (Originally in colour)

Figure 3.5 shows the mechanical properties of ELO-GA samples cured at 140, 160 and 180 ^{o}C for different time. Generally, with an increase of curing time, elongation at break decreased while tensile strength and Young’s modulus increased.

At 140 ^{o}C, by increasing the curing time from 1 h to 2 h, elongation at break decreased by 60% from 12.1% to 5.0% and kept decreasing to 3.2% after 6 h; tensile strength increased twice from 6.2 MPa to 13.0 MPa and kept increasing to 20 MPa after 6 h; Young’s modulus increased six times from 99 MPa to 625 MPa and kept increasing to 1250 MPa after 6 h. When the curing time kept increasing the mechanical properties kept quite constant with slight changes.

At 160 ^{o}C and 180 ^{o}C, the effects of curing time on the mechanical properties were not obvious. Elongation at break, tensile strength and Young’s modulus were about 2.0%, 20 MPa and 1400 MPa, respectively.

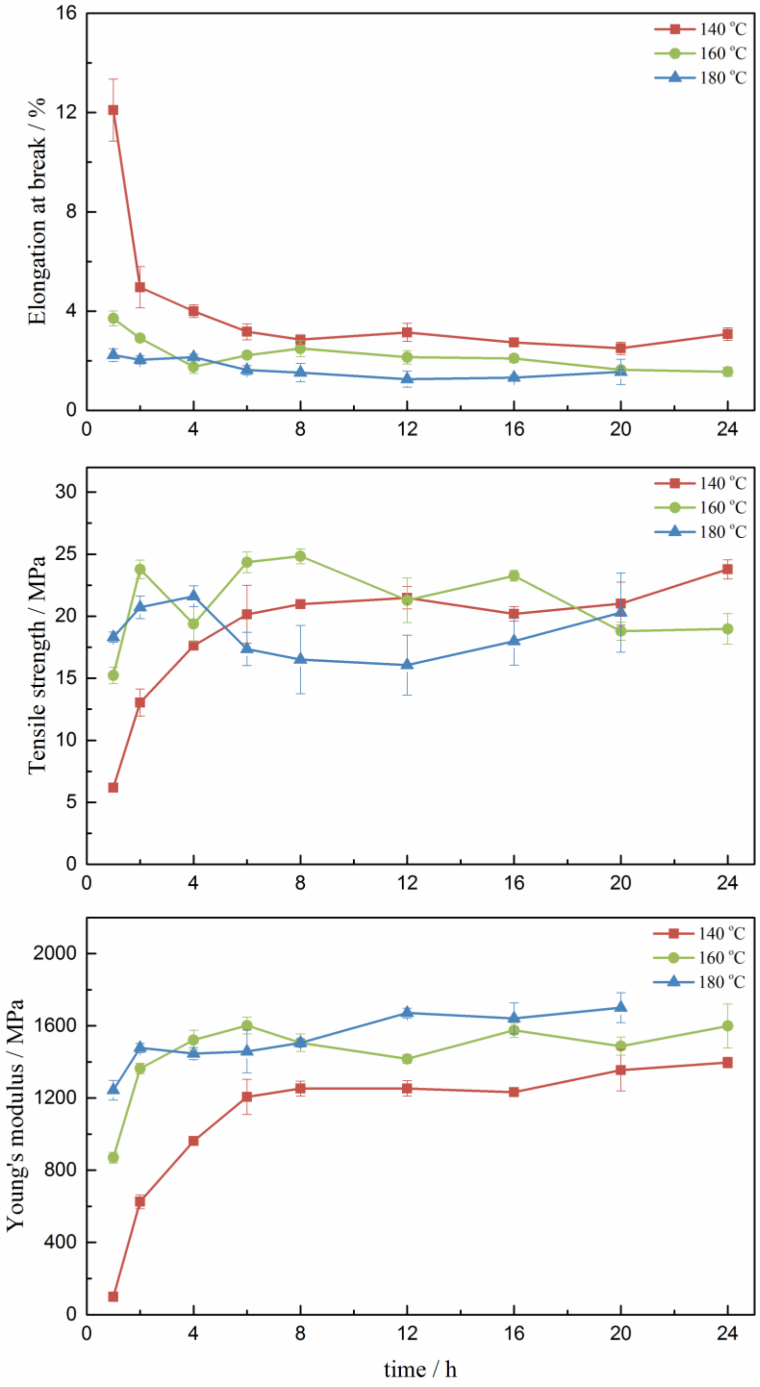

Figure 3.5 Mechanical properties of ELO-GA samples cured at 140, 160 and 180 °C for different time. (Originally in colour)

3.2.3 Thermal stability

Figure 3.6 shows the thermal stability of ELO-GA samples cured at different temperatures for 1 h. All samples show good thermal stability with T_d about 350 °C. As shown in Table 3.1, with the increase of curing temperature, the decomposition temperature T_d decreased gradually from 349.2 °C cured at 140 °C to 343.9 °C cured at 220 °C.

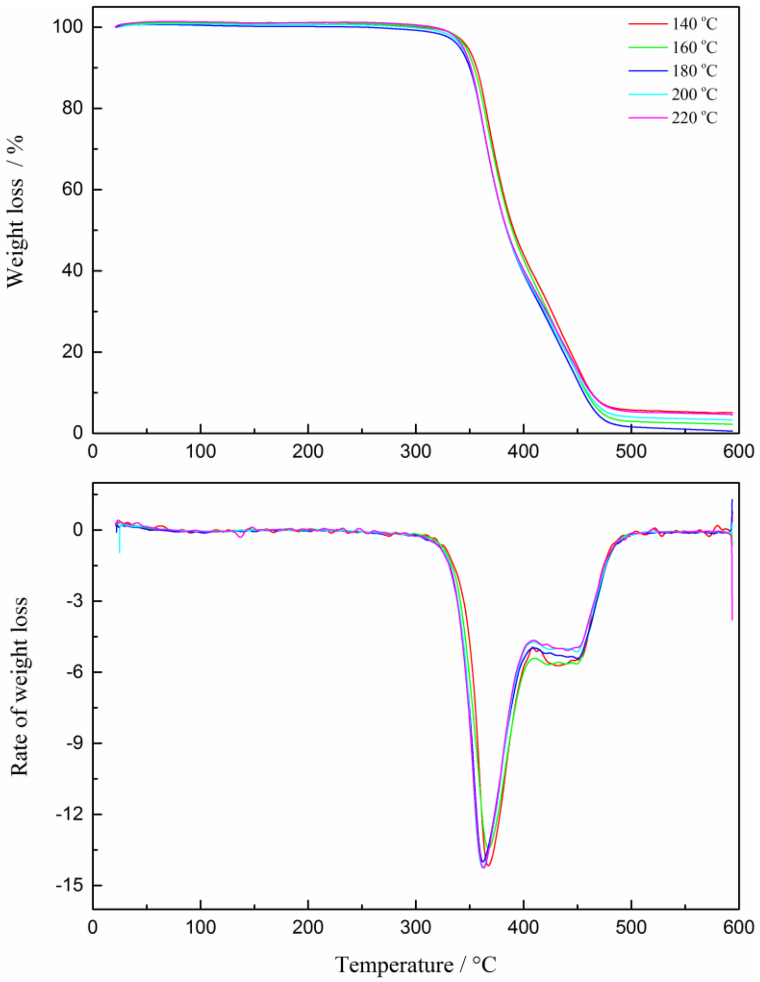

Figure 3.6 Thermal stability of ELO-GA cured at different temperatures for 1 h. (Originally in colour)

Table 3.3 summarizes the thermal stability of samples cured at 140, 160 and 180 °C for 1 h, 2 h and 24 h, respectively. For samples cured at 140 °C, T_{d} declined slightly with the increasing of curing time. While for samples cured at 160 and 180 °C, T_{d} kept quite constant and the effect of curing time on thermal stability of samples cured at such high temperatures was negligible.

Table 3.3 Thermal stability of samples cured at 140, 160 and 180 °C for 1, 2 and 24h.

	140 °C			160 °C			180 °C		
	1h	2h	24h	1h	2h	24h	1h	2h	24h
T_{on}	349.2	348.3	343.0	346.4	344.0	344.8	343.9	345.6	345.4
T_{max1}	367.2	368.0	367.1	367.5	362.8	364.2	362.3	364.1	363.6
T_{max2}	432.0	450.6	439.0	423.0	364.1	363.6	450.0	450.8	434.1

3.3 Effect of different epoxy prepolymers

In this study, different plant oil-derived epoxy prepolymers ELO, ESBO and their FAMEs EML and EMS were used to cure with glutaric anhydride. Figure 3.7 shows the appearance of ELO, ESBO, EML and EMS cured with glutaric anhydride in the presence of DMAP at 180 °C for 2 h, which gave stable properties in two hours (Figure 3.5). After curing at 180 °C for 2 h, all samples were able to form soft solid resins but ESBO and EMS samples stuck to the aluminum plate making them difficult to remove for further testing.

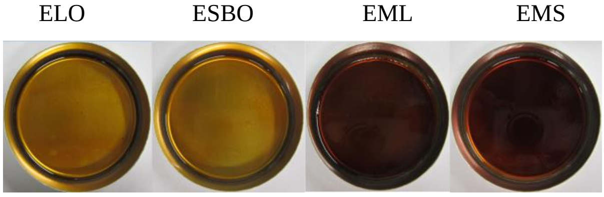

Figure 3.7 Samples of different epoxy prepolymers cured with glutaric anhydride in the presence of 1 mol% DMAP. (Originally in colour)

3.3.1 DSC analysis

Figure 3.8 shows the DSC thermograms of different plant oil-derived epoxy prepolymers with glutaric anhydride premixed mixtures in the presence of 1 mol% DMAP as accelerator and their interpolated thermal properties are summarized in Table 3.4. All samples exhibited an endothermic peak at approximately 50 °C corresponding to the melting of glutaric anhydride, followed by the main curing exothermic peak around 200 °C (Figure 3.8).

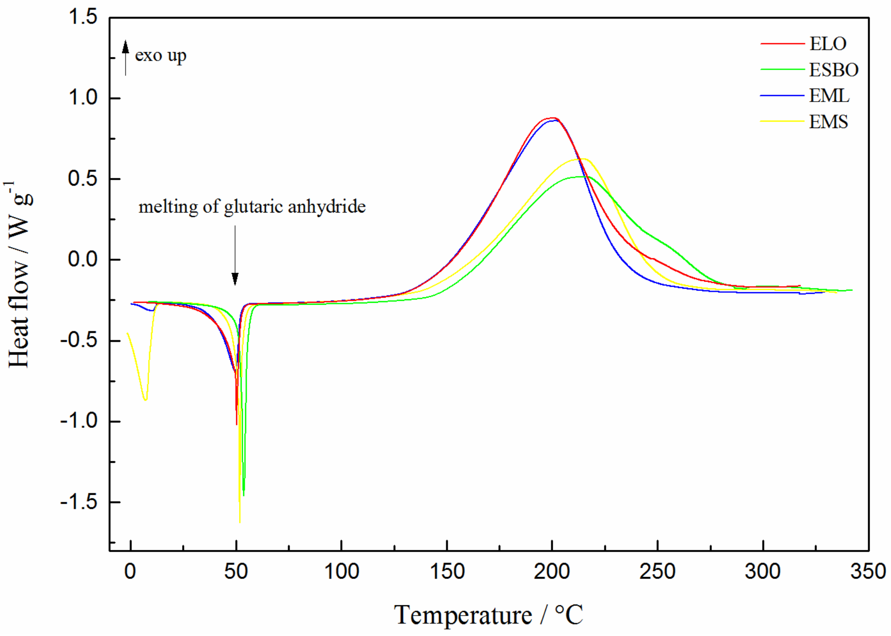

Figure 3.8 Thermograms of different epoxy prepolymer with glutaric anhydride mixtures in the presence of 1 mol% DMAP. (Originally in colour)

On closer inspection both T_{on} and T_{P} of ELO and EML samples are lower than those of ESBO and EML samples due to the higher oxirane content of the former. The curing heat ΔH_{T} decreases in the order: ELO (405.2 J g^{-1}) > EML (365.3 J g^{-1}) > ESBO (336.7 J g^{-1}) > EMS (317.5 J g^{-1}). The decreasing trend of ΔH_{T} is the same with their oxirane content, the higher the oxirane content the higher ΔH_{T}.

Table 3.4 Thermal properties of premixed mixtures of different epoxy prepolymer with glutaric anhydride

Epoxy prepolymer	ΔH_{T} (J.g^{-1})	T_{on} (°C)	T_{P} (°C)
ELO	405.2	148.3	200.3
ESBO	336.7	151.6	215.7
EML	377.8	144.9	202.3
EMS	317.5	150.6	214.7

Figure 3.9 and Table 3.5 show the thermal properties of cured resins of different epoxy prepolymers with glutaric anhydride in the presence of 1 mol% DMAP after curing at 180 °C for 2 h.

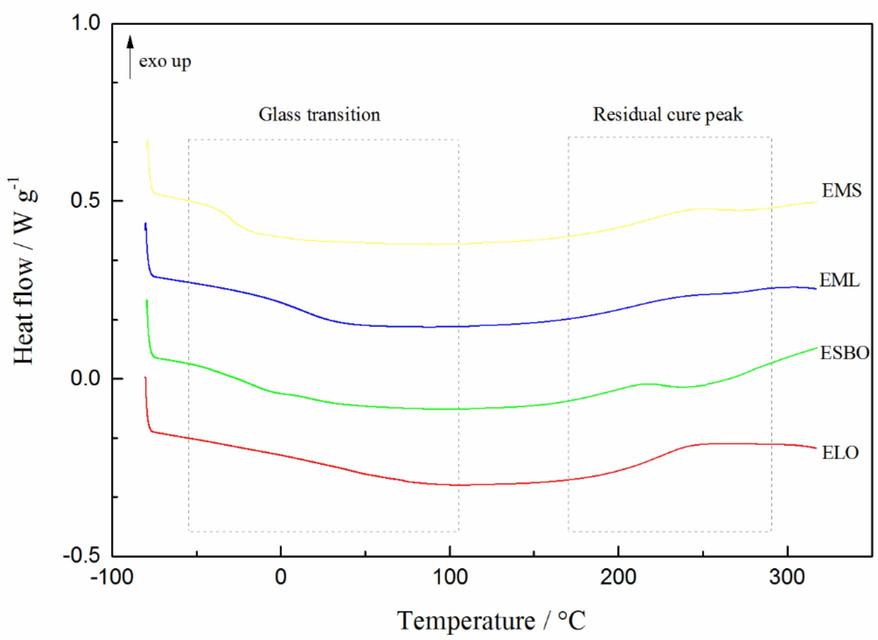

Figure 3.9 Thermograms of cured resins of different epoxy prepolymers cured with glutaric anhydride. (Originally in colour)

All samples are almost fully cured with degree of cure about 98%. As expected, T_g decreases in the order: ELO (41.6 °C) > EML (13.9 °C) > ESBO (-16.9 °C) > EMS (-30.8 °C).

Table 3.5 Thermal properties of different epoxy cured with glutaric anhydride.

Epoxy prepolymer	T_g (°C)	ΔH_R (J.g^{-1})	Degree of cure (%)	T_d (°C)	T_{max1} (°C)	T_{max2} (°C)
ELO	41.6	8.0	98.1	345.6	364.1	450.8
ESBO	-16.9	5.5	98.4	353.8	378.1	431.0
EML	13.9	3.7	97.8	343.5	361.3	443.4
EMS	-30.8	6.9	97.8	342.8	363.8	441.0

3.3.2 FT-IR analysis

Figure 3.10 shows the FT-IR spectra of cured resins of different epoxy prepolymers cured with glutaric anhydride. The characteristic bands include newly formed hydroxyl O-H groups at 3700 cm^{-1} to 3200 cm^{-1}, a shift of ester carbonyl C=O band from 1742 cm^{-1} to 1732 cm^{-1} and disappearance of epoxy groups. Also the carbonyl C=O bands in glutaric anhydride at 1801 cm^{-1} and 1750 cm^{-1} were not observed in the resultant resins. All these findings indicate that epoxy groups were reacted with carbonyl groups in glutaric anhydride to form new ester groups and hydroxyl groups (Appendix Figure A.2).

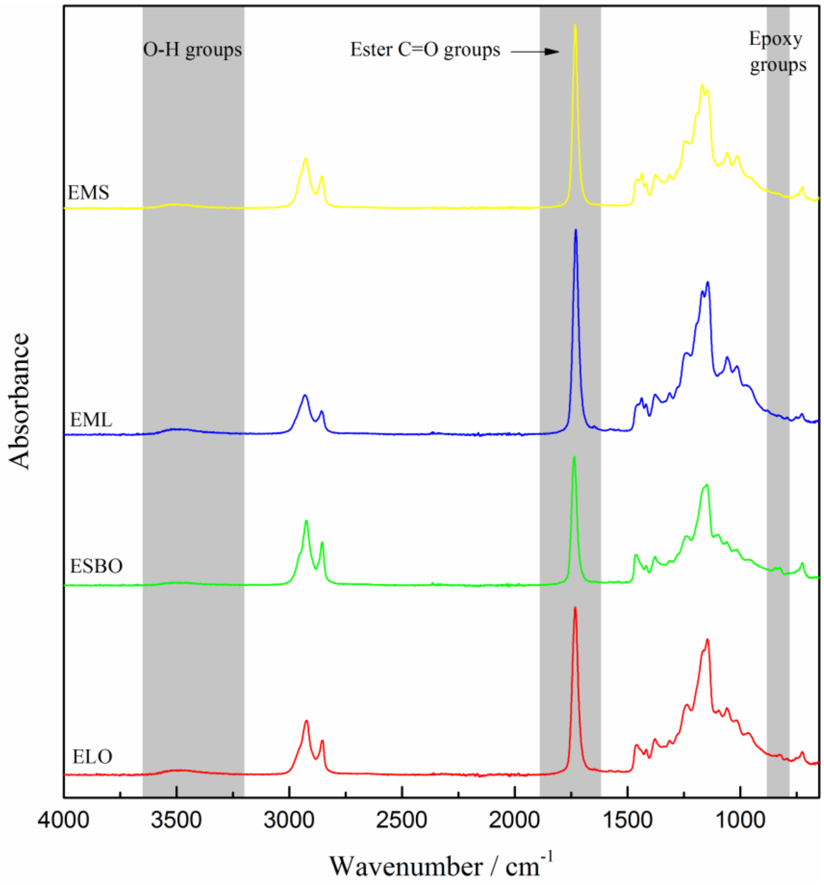

Figure 3.10 FT-IR spectra of cured resins of different epoxy prepolymers cured with glutaric anhydride in the presence of 1 mol% DMAP. (Originally in colour)

3.3.3 Mechanical properties

Figure 3.11 shows the mechanical properties of different epoxy prepolymers cured with glutaric anhydride in the presence of 1 mol% DMAP cured at 180 °C for 2 h. Both ELO and EML samples show brittle and stiff characteristics. The former is more brittle and stiffer than the latter due to the higher cross-link density caused by the higher epoxy functionality with the triglyceride molecules of ELO. The mechanical properties of the ELO and EML samples are: 2.7% and 11.6% (elongation at break), 24.2 and 10.4 MPa (tensile strength) and 1477 and 366 MPa (Young's modulus), respectively.

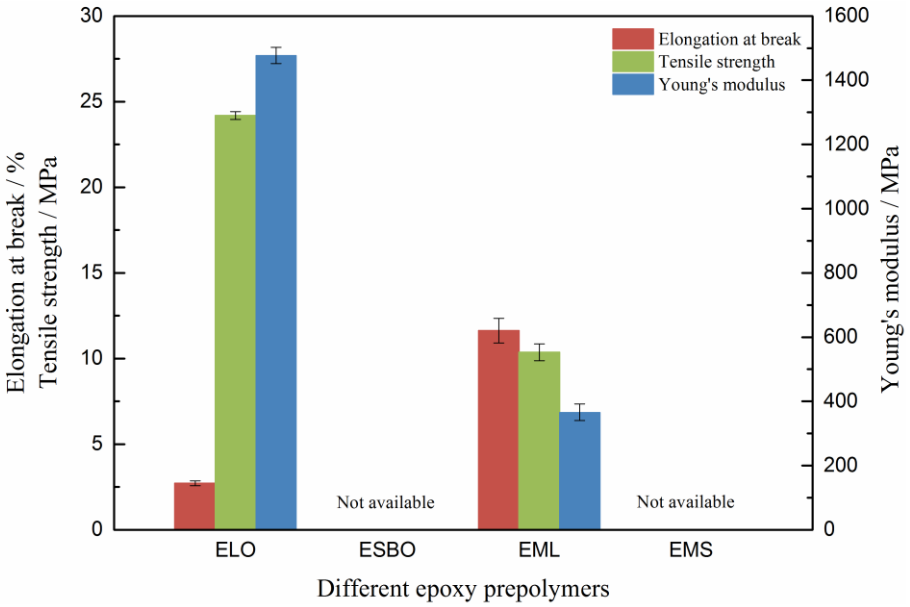

Figure 3.11 Mechanical properties of different epoxy cured with glutaric anhydride. (Originally in colour)

3.3.4 Thermal stability

Figure 3.12 shows the thermal stability of different epoxy prepolymers cured with glutaric anhydride in the presence of 1 mol% DMAP cured at 180 °C for 2 h. All samples show good thermal stability with T_d (onset decomposition temperature) about 350 °C. The residual content for all samples up to 600 °C is about 5 wt%. Figure 3.12 shows that ESBO sample had the highest T_d of 353.8 °C, followed by ELO sample of 345.6 °C and then EML and EMS samples of 343 °C. The triglyceride molecule structure was responsible for the higher thermal stability of ELO and ESBO samples.

The decomposition processes of these samples in N_2 are composed of two stages. The first stage occurring at approximately 350 °C was attributed to the chain session of the ester groups in these epoxidized oils, *i.e.*, triglyceride decomposition. The second stage occurring at approximately 440 °C was attributed to the onset of decomposition of ester groups between the epoxy groups with glutaric anhydride, *i.e.*, breakdown of cross-links associated with polyesterification and polyetherification.

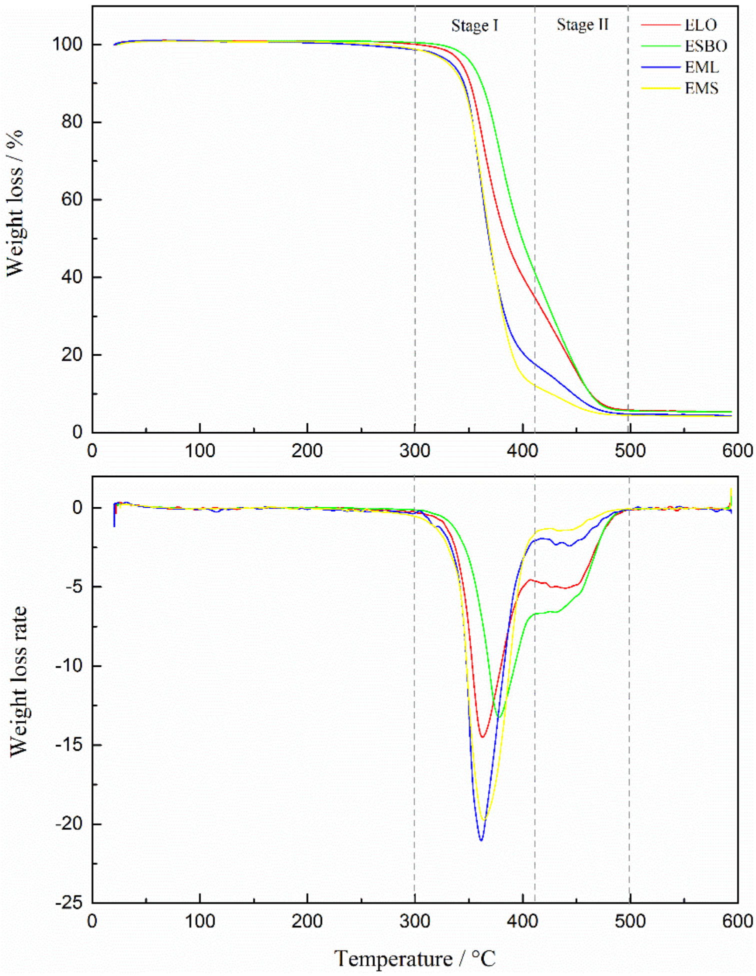

Figure 3.12 Thermal stability of different epoxy cured with glutaric anhydride. (Originally in colour)

3.4 Effect of composition of curing agents (glutaric anhydride and adipic acid)

In this study, in order to study the effects of mixed curing agents on the thermal and mechanical properties of thermoset resins, samples with different compositions of glutaric anhydride (GA) and adipic acid (AA) were prepared ranging from 100% GA to 100% AA (the ratio was actually calculated on anhydride functional groups to acid functional groups). All samples were prepared based on 1:1 stoichiometric ratio of epoxy groups to acid and/or anhydride groups. Figure 3.13 shows samples with different composition of glutaric anhydride and adipic acid.

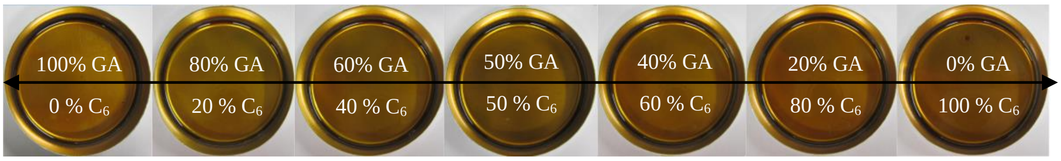

Figure 3.13 Samples of ELO cured with different compositions of glutaric anhydride and adipic acid. (Originally in colour)

3.4.1 DSC analysis

Figure 3.14 shows the thermograms of premixed mixtures of ELO with different compositions of glutaric anhydride and adipic acid and their thermal properties are summarized in Table 3.6.

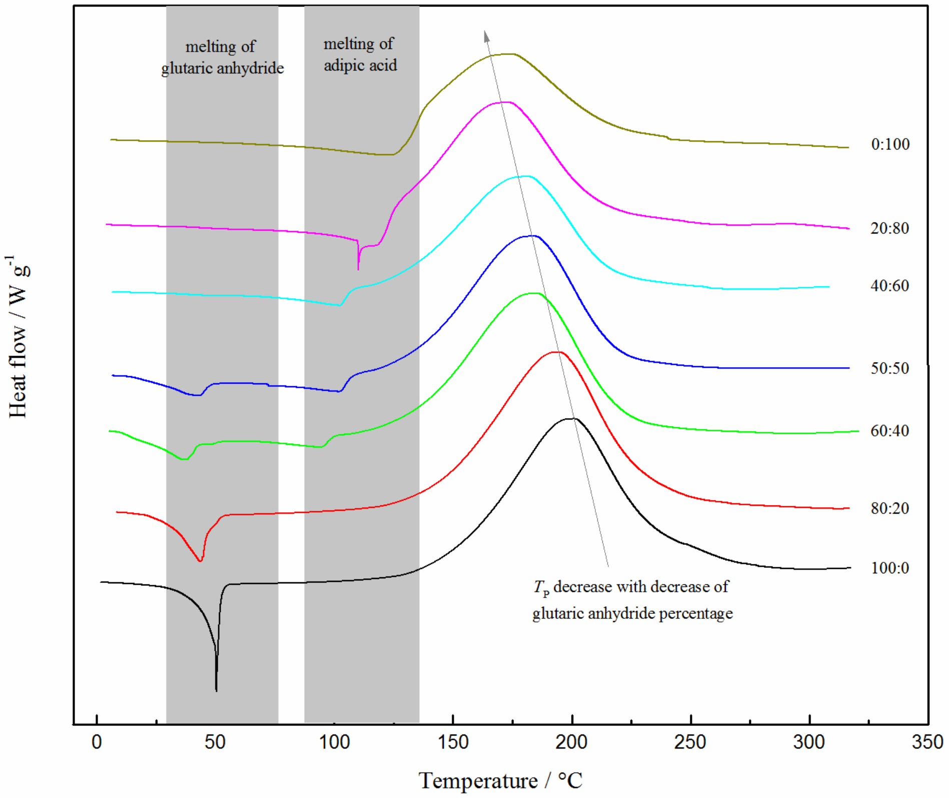

Figure 3.14 Thermograms of premixed mixtures of ELO with different compositions of GA:AA. (Originally in colour)

The first endothermic peak occurring at about 50 °C was attributed to the melting process of glutaric anhydride while the second endothermic peak occurring at about 90 to 120 °C was attributed to the melting process of adipic acid. The major exothermic peak was attributed to the curing reaction. The incorporation of glutaric anhydride lowered the melting point of adipic acid. For 100% and 80% adipic acid compositions, the endothermic and exothermic peaks are not well resolved thus the observed enthalpy of the curing process ΔH_T is probably slightly lower than the real enthalpy. More importantly, with the increase of adipic acid content, T_P was decreased gradually from 200.3 °C of pure glutaric anhydride sample to 174.1 °C of pure adipic acid sample, which was attributed to the higher reactivity of adipic acid compared to glutaric anhydride.

As for the effect of the composition of curing agents on ΔH_T, with the increase of adipic acid content, ΔH_T decreased gradually. ΔH_T of pure glutaric anhydride sample (405.2 J g^{-1}) was 78% higher than that of pure adipic acid sample (228 J g^{-1}).

Table 3.6 Thermal properties of premixed mixtures and cured resins of ELO cured with different compositions of GA and AA.

GA:C_6	ΔH_T (J.g^{-1})	T_P (°C)	T_g (°C)	ΔH_R (J.g^{-1})	Degree of cure / %	T_{on} (°C)	T_{max1} (°C)	T_{max2} (°C)
100:0	405.2	200.3	41.4	6.3	98.4	344.3	362.6	439.7
80:20	392.5	194.0	40.1	6.3	98.4	345.9	365.6	435.4
60:40	351.0	185.3	25.1	9.2	97.4	348.4	370.8	432.5
50:50	330.0	183.5	20.4	8.4	97.5	350.9	372.7	432.7
40:60	285.6	181.5	15.0	8.7	97.0	350.6	373.2	430.4
20:80	302.0	172.8	10.6	6.2	98.0	355.5	377.1	427.7
0:100	228.0	174.1	5.0	7.1	96.9	359.9	385.3	427.6

Figure 3.15 shows the thermograms of cured resins of ELO with different compositions of glutaric anhydride and adipic acid. All samples show only one T_g which may indicate that adipic acid and glutaric anhydride were well mixed and all the samples formed are homogeneous. As expected, pure glutaric anhydride sample show the highest T_g of 41.4 °C and pure adipic acid sample show the lowest T_g of 5 °C, which is attributed to the much higher cross-link density of glutaric anhydride samples. By gradually increasing the content of adipic acid, the cross-link density is gradually decreased and thus T_g is gradually decreased. Samples change from hard plastic (T_g > RT) to soft plastic (T_g near RT), and a soft rubbery polymer (T_g < RT). Therefore, their mechanical properties tested are significantly different from one another as shown below. After curing at 180 °C for 2 h, all samples show high degree of cure over 97%.

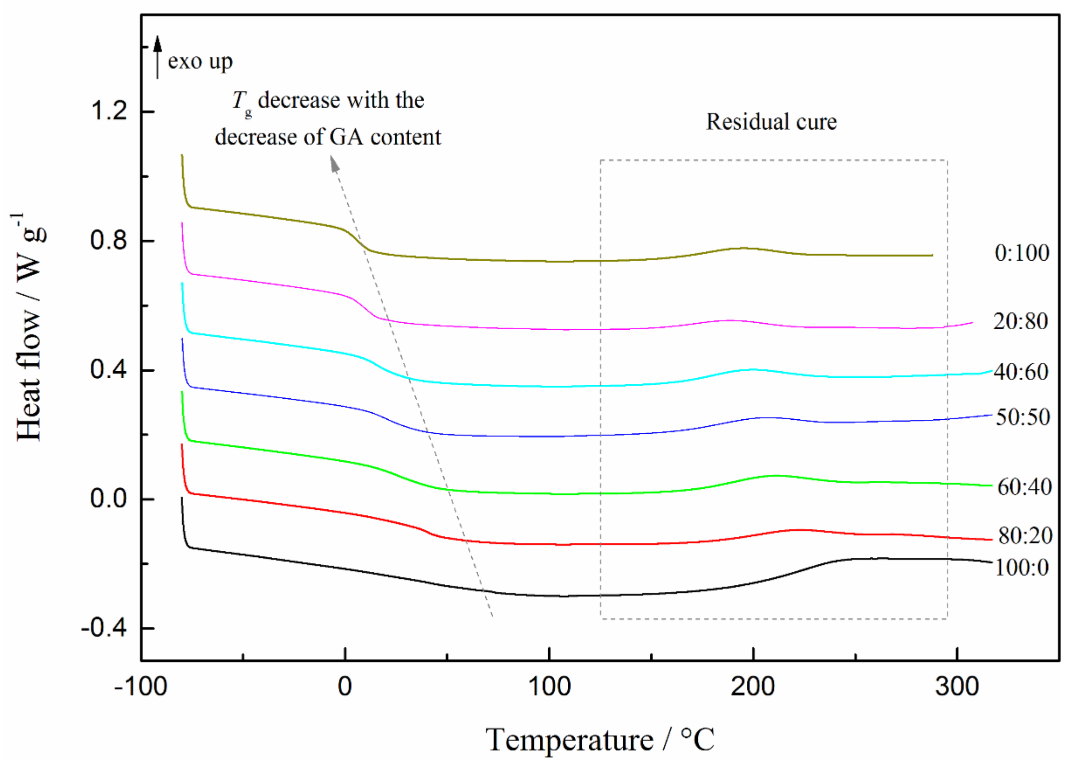

Figure 3.15 Thermograms of cured resins of ELO with different compositions of GA:AA. (Originally in colour)

3.4.2 FT-IR analysis

Figure 3.16 shows the FT-IR spectra of ELO cured with different compositions of glutaric anhydride and adipic acid. As the same with previous studies, all samples show the newly formed O-H groups, ester carbonyl C=O groups and the disappearance of epoxy groups. Interestingly, with the change of the composition of curing agents, the relative intensities of the two ester C-O antisymmetric stretch bands at 1166 and 1143 cm^{-1} are different. For glutaric anhydride rich samples, the intensity at 1143 cm^{-1} is higher than the intensity at 1166 cm^{-1}. When the content of adipic acid is over 50%, the relative intensities of these two bands are reversed. For samples containing 100% and 80% glutaric anhydride, ether antisymmetric stretch band at 1096 cm^{-1} are also observed.

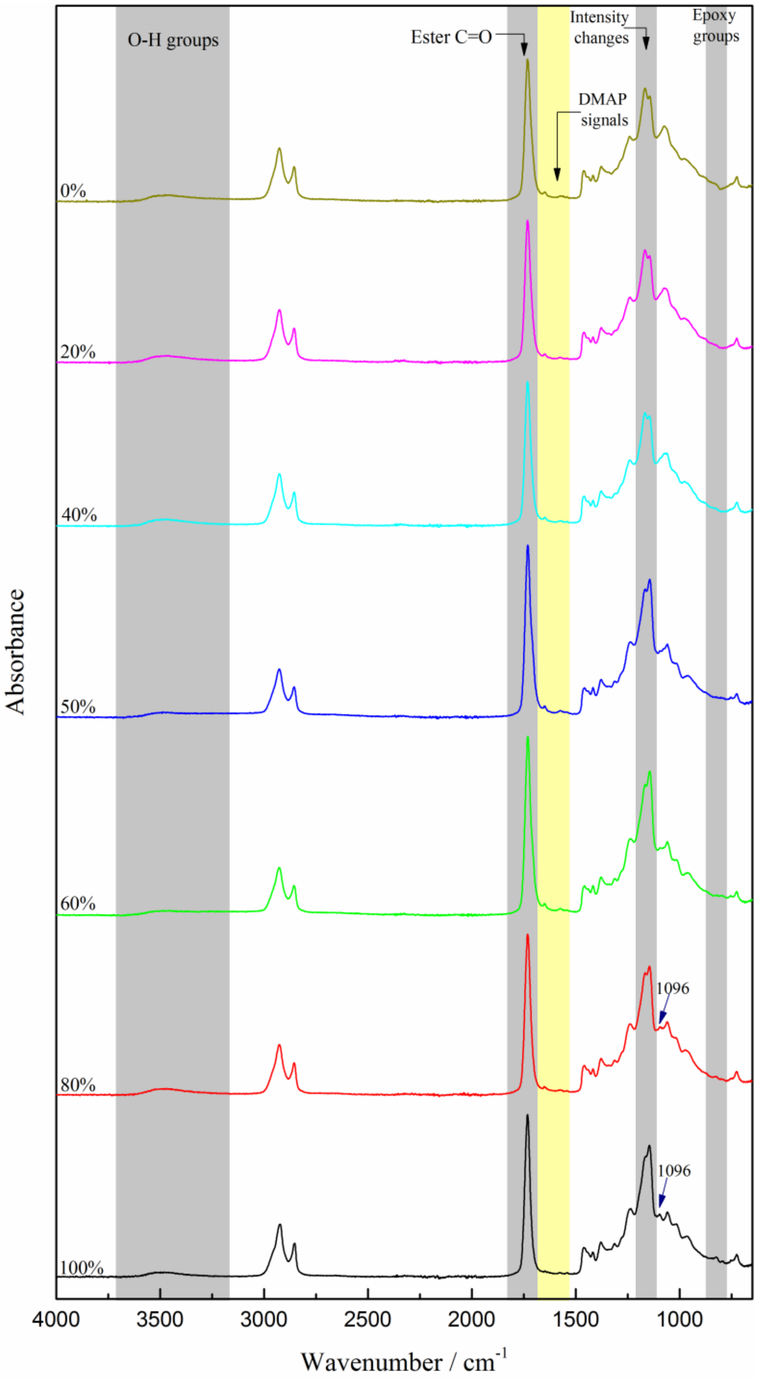

Figure 3.16 FT-IR spectra of ELO cured with different composition of GA and AA. (Originally in colour)

3.4.3 Mechanical properties

Figure 3.17 shows the stress-strain curves of ELO cured resins with different compositions of glutaric anhydride and adipic acid. Resins with various properties are obtained by easily changing the compositions of curing agents, ratio of glutaric anhydride to adipic acid. With the decrease of glutaric anhydride content, resins changed from brittle and stiff to soft and flexible materials, which is well consistent with the change trend of their T_g. The various mechanical properties were also observed by Lu *et al.* in polyurethane films derived from methoxylated soybean oil polyols with different hydroxyl functionalities.[209] With the increase of hydroxyl functionalities, the PU films changed from elastomeric polymers to rigid plastics.

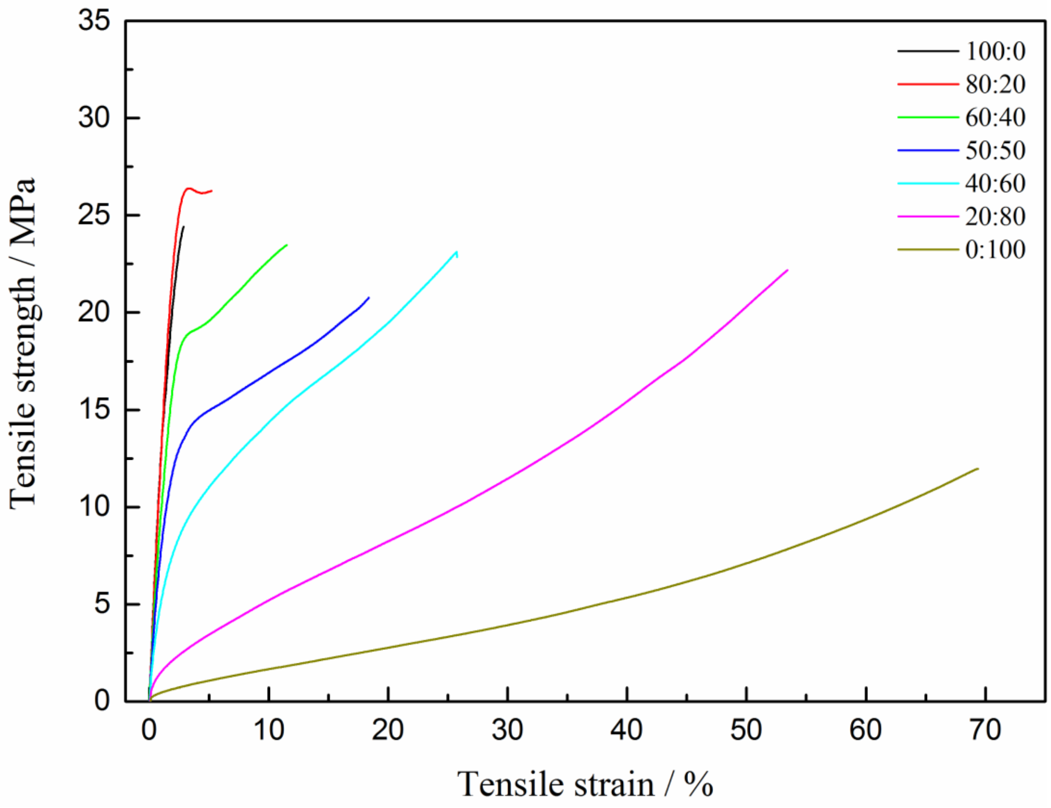

Figure 3.17 Stress-strain curves of ELO cured resins with different compositions of GA:AA. (Originally in colour)

Figure 3.18 shows different mechanical properties including elongation at break, tensile strength, Young's modulus and toughness for ELO cured with different compositions of GA/AA ranging from 100:0 to 0:100. Generally, the higher amount of adipic acid, the higher of elongation at break and toughness but the lower tensile strength and Young's modulus.

100% and 80% Glutaric anhydride samples exhibited behaviour of rigid plastic and break on the verge of its intrinsic yielding point. These two samples had the highest tensile strength and Young's modulus and poorest elongation at break and toughness. The addition of 20% adipic acid had almost no effect on tensile strength and Young's modulus which were 25 MPa and 1400 MPa, respectively. Whilst elongation at break and toughness were improved twice.

Samples containing 60%, 50% and 40% glutaric anhydride exhibited behavior of ductile plastic with a yield point. With the increase of adipic acid content, elongation at break and toughness were improved from 11.6% to 25.3% and from 2.3 MJ m^{-3} to 3.7 MJ m^{-3}, Young's modulus was decreased from 1279 MPa to 511 MPa while tensile strength kept constant about 22 MPa.

Samples containing 80% and 100% adipic acid exhibited behavior of soft rubbery material with quite high elongation at break. Compared to the pure adipic acid sample, the addition of 20% glutaric anhydride doubled tensile strength and Young's modulus without decreasing elongation a lot, which was responsible for its highest toughness of 5 MJ m^{-3}.

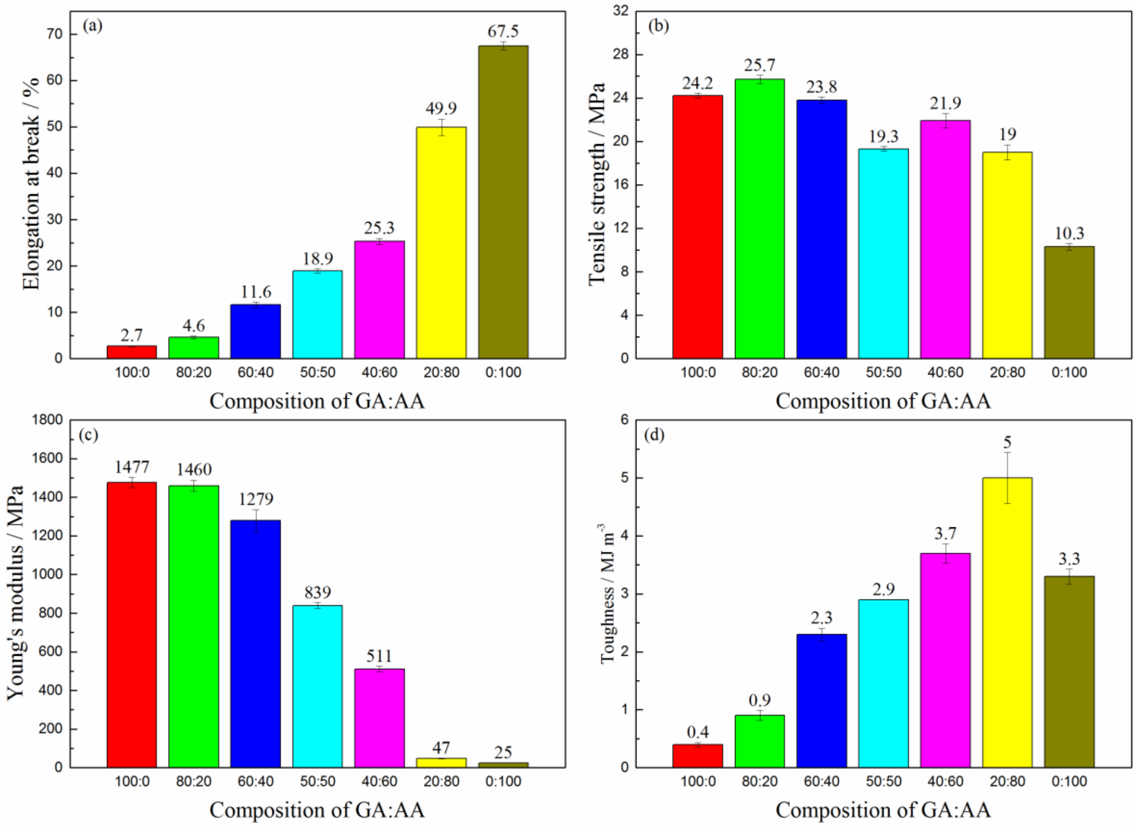

Figure 3.18 Mechanical properties of ELO cured with different compositions of GA: AA. (a) elongation at break, (b) tensile strength, (c) Young's modulus and (d) toughness. (Originally in colour)

3.4.4 Thermal stability

Figure 3.19 shows the thermal stability of cured resins of ELO with different compositions of glutaric anhydride and adipic acid in N_2. Their T_d (onset degradation temperature) and T_{max} (degradation temperature with maximum degradation rate) are summarized in Table 3.6.

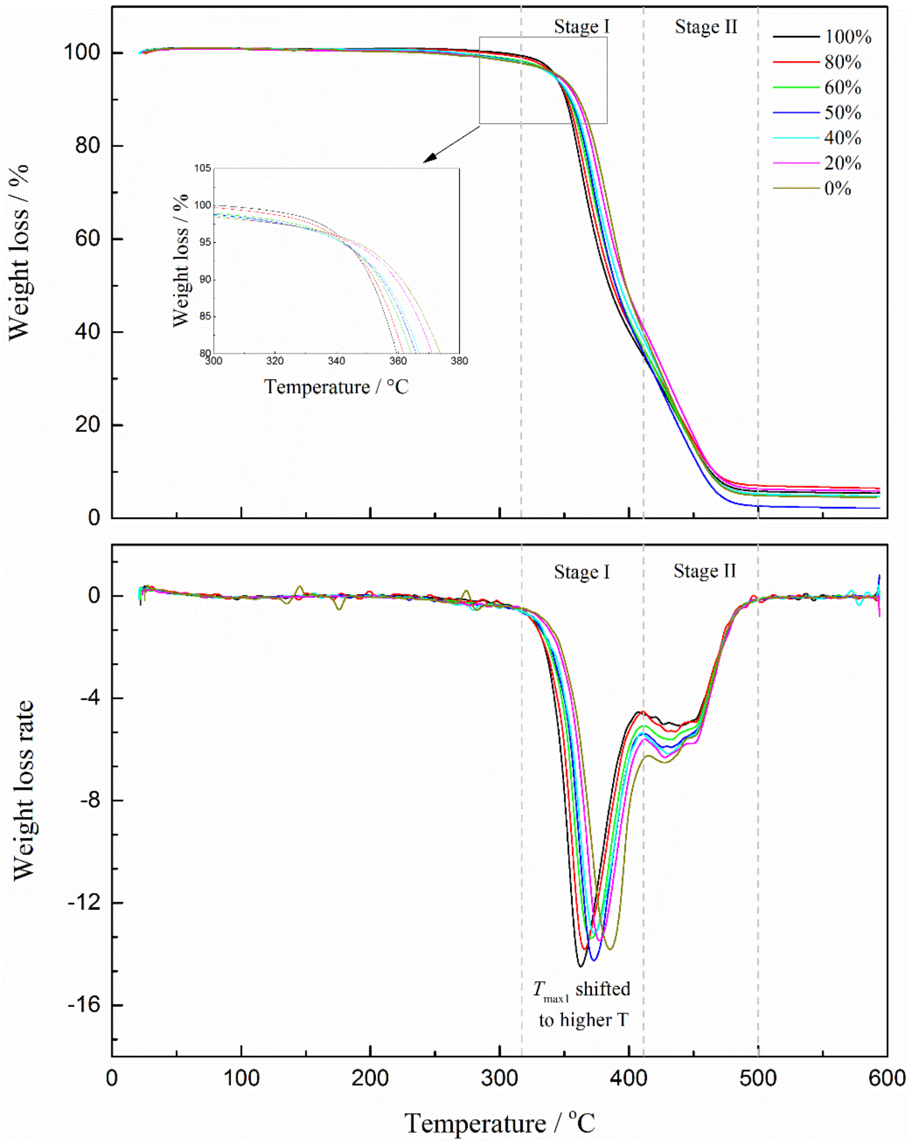

Figure 3.19 Thermal stability of ELO cured with different compositions of GA and AA. (Originally in colour)

All films show good thermal stability with T_d about 350 °C. The increase of adipic acid content gradually increases T_d from 344.3 °C for pure glutaric anhydride sample to 360.0 °C for pure adipic acid sample possibly due to the lower cross-link density for samples containing adipic acid. The lower the cross-link density, the higher the molecular weight between cross-link points (M_c) thus better thermal stability is obtained.

For all samples, two decomposition processes are observed with T_{max} occurring at about 370 °C and 430 °C, respectively. With the increase of adipic acid content, T_{max1} gradually shifts to higher temperatures from 363 °C for pure glutaric anhydride samples to 385 °C for pure adipic acid sample. Also the second decomposition process becomes more apparently while T_{max2} gradually shifts to lower temperatures from 440 °C for pure glutaric anhydride samples to 427 °C for pure adipic acid sample.

3.4.5 SEM analysis

Figure 3.20 shows the fracture surfaces of cured resins of ELO cured with different compositions of glutaric anhydride and adipic acid.

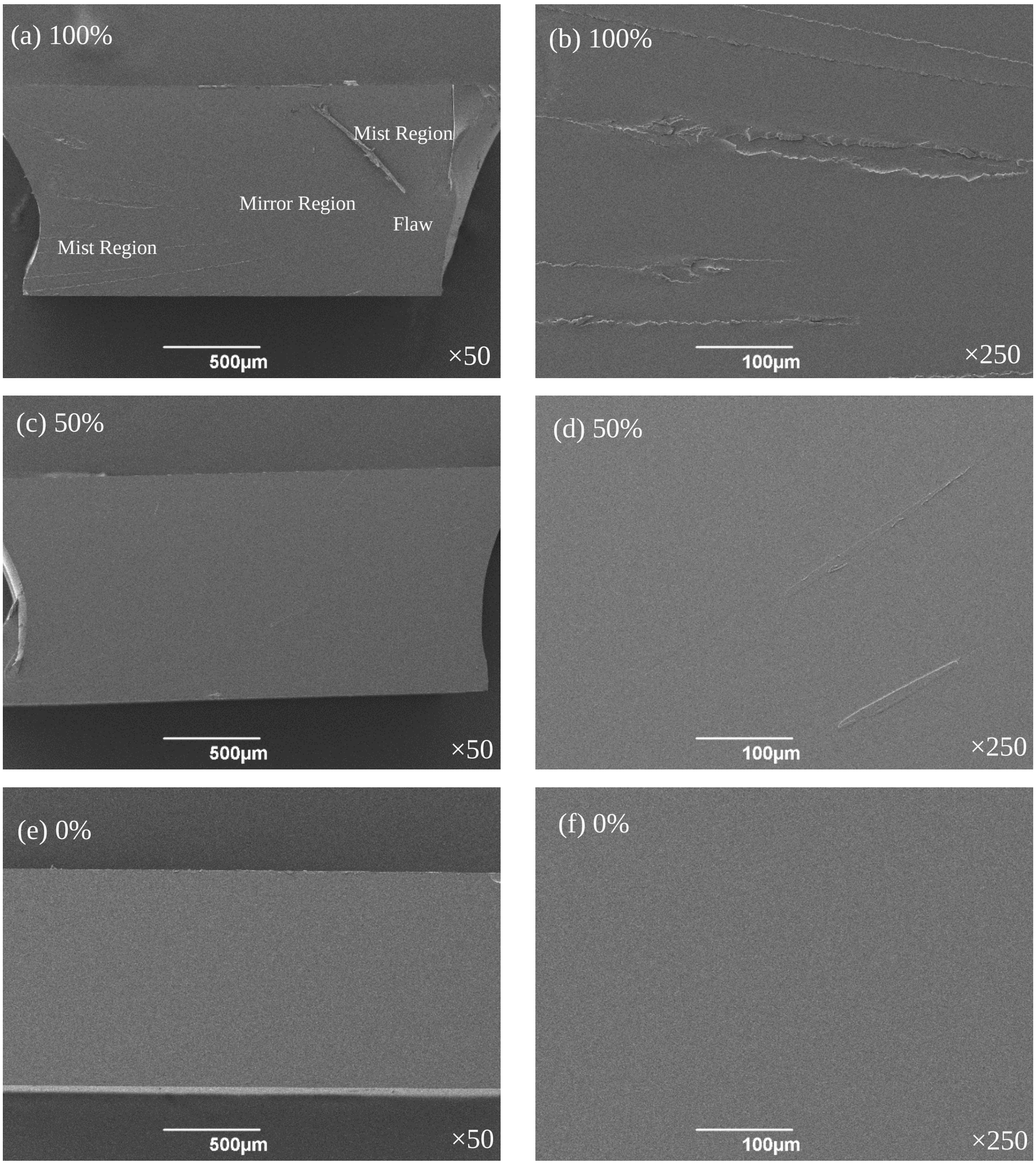
(a) 100%
Mist Region
Mirror Region
Flaw
Mist Region
500μm
×50
(b) 100%
100μm
×250
(c) 50%
500μm
×50
(d) 50%
100μm
×250
(e) 0%
500μm
×50
(f) 0%
100μm
×250

Figure 3.20 SEM of fracture surface after tensile tests of ELO cured with different composition of GA and AA. (a, b) 100%GA, (c, d) 50%GA and (e, f) 0%GA.

Figure 3.20 (a) and (b) show the tensile fracture surface of the rigid plastic containing 100% glutaric anhydride. The fracture surface is typical for rigid epoxy resins containing a flaw region or initiation region, mirror region and mist region.[210] The flaw region is where the cracks generate; the mirror region is an area with a smooth, glossy appearance with relatively slow crack velocity and the mist region is rougher with higher crack velocity compared to the mirror region. Figure 3.20 (c) and (d) show the fracture surface of a ductile plastic containing 50% glutaric anhydride. Compared to the rigid sample, the fracture surface is smoother with fewer ridges and furrows. Figure 3.20 (e) and (f) show the fracture surface of a rubbery material containing 0% glutaric anhydride. The fracture surface of the rubbery materials appeared to be featureless due to immediate disappearance caused by their elastic nature.

All these findings are well in accordance with soybean oil-styrene-divinylbenzene thermosets synthesized by Li *et al.*.[197] Rigid samples gave the roughest fracture surface while rubbery samples showed no fracture features.

3.5 Conclusions

Epoxy resins from plant oil-derived epoxy prepolymers cured with glutaric anhydride in the presence of DMAP as accelerator were successfully made. The effects of the structure and functionality of epoxy prepolymers, the curing conditions and also the compositions of curing agents were studied in detail.

All the four epoxy prepolymers ELO, ESBO, EML and EMS were able to form cured resins and their T_g decreased by the same trend of their oxirane content, thus ELO > EML > ESBO > EMS.

In general, with the increase of curing temperature and curing time, elongation at break was decreased while tensile strength, Young's modulus and T_g increased. The effect of curing temperature and curing time had a slight effect on their thermal stability.

By changing the ratio of glutaric anhydride to adipic acid, different materials including rigid plastic, ductile plastic and rubbery material were obtained. These samples possessed T_g ranging from 5 to 41 °C, elongation at break ranging from 2.5 to 67.5%, tensile strength ranging from 10 to 25 MPa, Young's modulus ranging from 25 MPa to 1477 MPa and toughness ranging from 0.4 to 5.0 MJ m^{-3}.

Chapter 4

Biobased epoxy resin and starch composites

4.1 Summary

In this chapter, starch composites based on ELO-adipic acid epoxy systems were prepared. The effects of curing temperature, the starch type and concentration on the thermal and mechanical properties of the composites were studied initially. In order to improve the compatibility of starch and the resin matrix, starch was expanded and reacted with glutaric anhydride to introduce reactive acid groups onto starch molecules. The obtained starch esters with different degree of substitution (DS) were added into the epoxy systems and their thermal and mechanical properties were studied.

4.2 Introduction

4.2.1 Starch composition and structure

Starch, an important class of bioresource, is widely used in many food and non-food applications because of its ready availability, renewability, and relatively low cost. Starch is mainly composed of linear amylose and a highly branched amylopectin chains (their structures are shown in Figure 4.1 and Figure 4.2)[211] and residual amounts of lipids, proteins, and minerals.[212, 213] The amount of amylose and amylopectin varies according to the botanical origin of the starch.

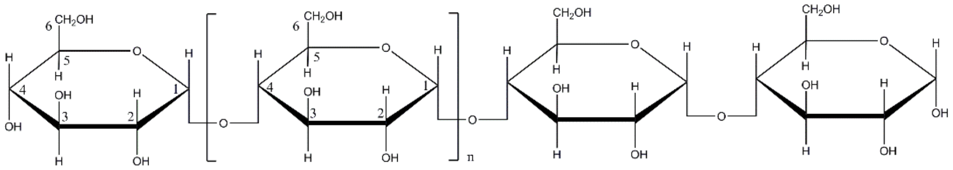

Amylose: α-(1→4)-glucan; average n = ca. 1000. The linear molecule may cary a few occasional moderately long chains linked α-(1→6).

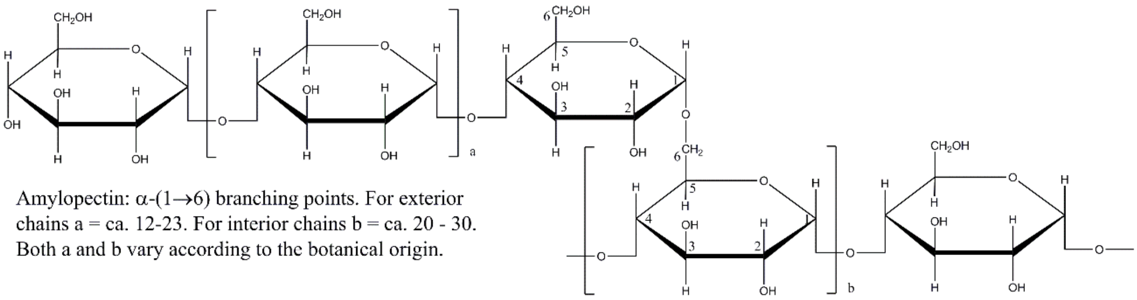

Amylopectin: α-(1→6) branching points. For exterior chains a = ca. 12-23. For interior chains b = ca. 20 - 30. Both a and b vary according to the botanical origin.

Figure 4.1 Structure of amylose and amylopectin.

Starch possesses a semi-crystalline structure containing about 15% to 45% of crystalline materials.[214] When observed through a polarized light microscope, starch granules show characteristic birefringence pattern, known as the Maltese cross, as a consequence of radial arrangement of the macromolecules.[215] These granules comprise concentric amorphous and semi-crystalline growth rings and the latter are made of alternating crystalline and amorphous lamellae. The crystalline lamellae are the result of intertwining of amylopectin side chains to form double helixes and the amorphous lamellae corresponds to the branching points.[216] Both the amorphous and semicrystalline growth rings are organized into blocklets initially proposed by Hanson and Katz in the 1930's.[217]

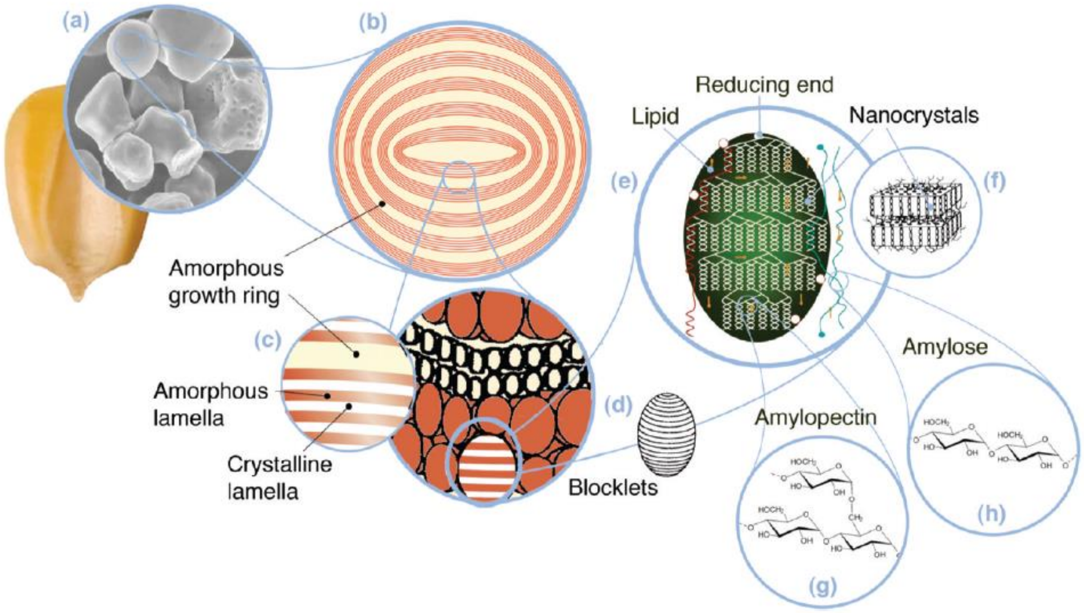

Figure 4.2 Starch multiscale structure. (a) starch granules from normal maize (30 μm), (b) amorphous and semicrystalline growth rings (120-500 nm), (c) amorphous and crystalline lamellae (9 nm), magnified details of the semicrystalline growth ring, (d) blocklets (20-50 nm) constituting a unit of the growth rings, (e) amylopectin double helixes forming the crystalline lamellae of the blocklets, (f) nanocrystals: other representation of the crystalline lamellae called starch nanocrystals when separated by acid hydrolysis, (g) amylopectin's molecular structure, and (h) amylose's molecular structure (0.1-1 nm).[212, 213]

4.2.2 Starch in composites

Starch has been used in manufacturing of composites extensively. In the early days, starch was used directly in its granular state rather than in its thermoplastic state as a filler in polymer blended systems. Griffin blended starch with low density polyethylene (LDPE) even during critical film extrusion process.[218] Better compatibility between the starch particles and the polymer matrix can be obtained with the use of a compatibilizer, chemically modified starches or thermal plasticized starch (TPS).[10] Saint-Pierre *et al.*[219] studied the properties of glycerol plasticized wheat starch and LDPE or linear low density polyethylene (LLDPE) composites and observed very high elongation at break at high loadings of TPS. The addition of plasticisers and/or compatibilizers such as citric acid[220] and maleic anhydride[221] was reported to improve the miscibility of TPS with synthetic polymers. Rivero *et al.* reported dispersed phase and improved mechanical properties by modification of starch with octenyl succinic anhydride.[222]

In addition to non-biodegradable synthetic polymers, starch blending with biodegradable synthetic polymers such as polyvinyl alcohol (PVOH), polylactic acid (PLA), polycaprolactone (PCL), polyhydroxyalkanoate (PHAs) and poly(butylenes succinate-co-butylene adipate) (PBSA) have been reported.[223] However, the studies on composites based on starch and epoxy resin are quite limited. We previously synthesized starch composites based on ELO-Pripol 1009 epoxy resin systems and showed improved tensile strength and Young's modulus.[176]

4.2.3 Starch modification

Esterification has been studied widely to modify starch resulting in improved mechanical properties of the resultant starch composites.[224, 225] Due to the existence of three hydroxyl groups containing in the anhydroglucose unit at C_2, C_3 and C_6 positions, in theory the maximum degree of substitution (DS) that can be attained is three. However, the reactivity of these three hydroxyl groups is different: the primary hydroxyl at C_6 is more reactive than the other two O-H groups due to the lower steric hindrance.[226] The properties of starch esters are quite different to those of native starch and are affected by the DS and the substituent group introduced. The DS of starch esters are affected by a number of factors including type of raw material, reactant concentration, reaction temperature and time, reaction media *etc.*

By reacting starch with cyclic anhydride, acid groups will be introduced onto starch molecules which may further improve the reaction between starch and polymer matrix through the reaction between acid groups with epoxy groups. Starch or dextrin reactive esters have been reported from maleic anhydride, octenyl succinic anhydride, succinic anhydride and trimellitic anhydride.[168, 227-229] In this study, glutaric anhydride was reacted with expanded starch to afford reactive starch esters. The mechanism of the esterification reaction between starch, glutaric anhydride and DMAP is illustrated in Figure 4.3.

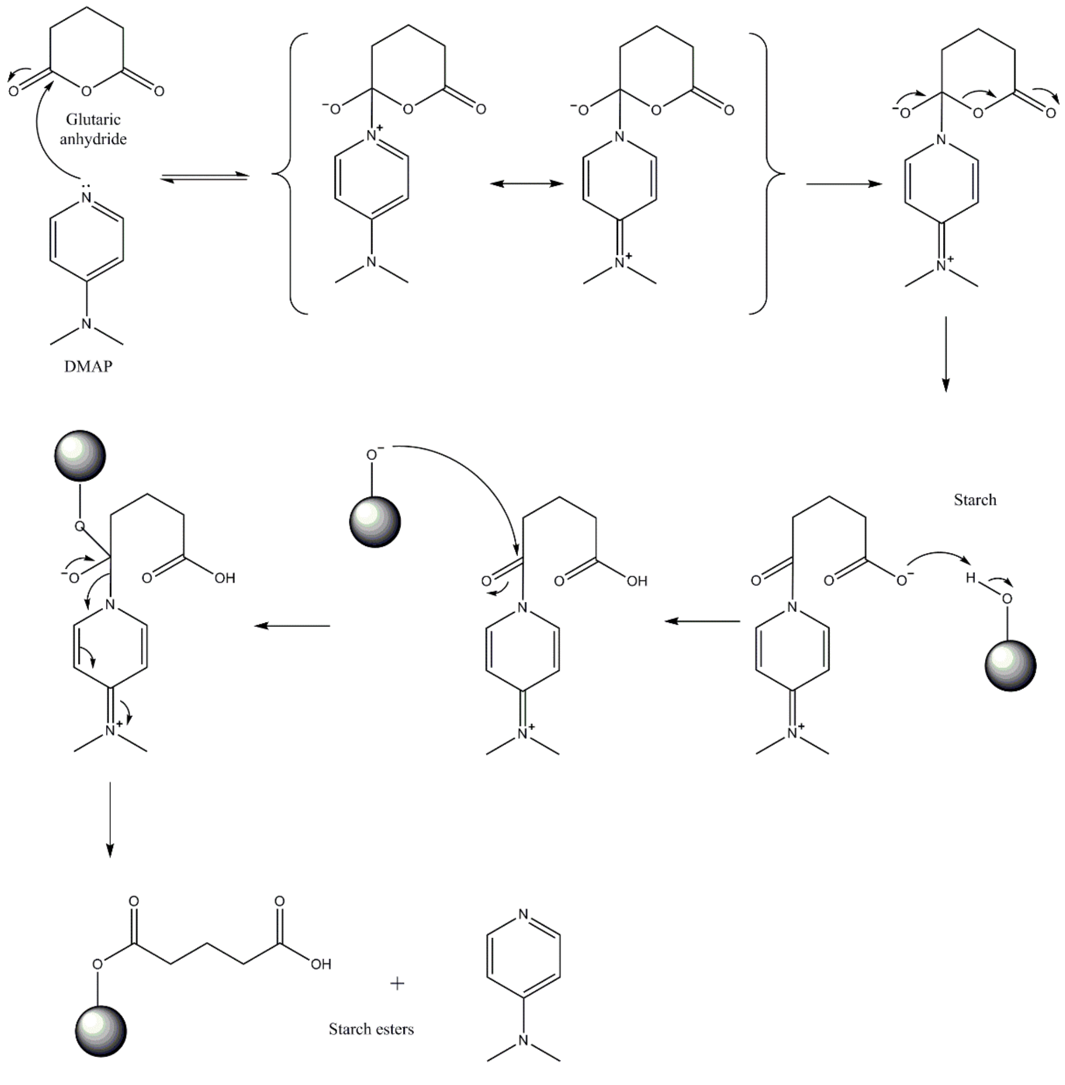

Figure 4.3 Mechanism of esterification of starch using glutaric anhydride and DMAP.

4.3 Effect of curing temperature

In this study, the effects of temperature on the mechanical properties of epoxy resin-starch composites were studied. Curing time of 8 h was chosen because as shown in Chapter 2 Section 2.6, best mechanical properties were obtained for this time period.

Figure 4.4 shows ELO-C_6 sample with and without 10 wt% Hylon VII (the most commonly used starch to prepare expanded starch for further studies in Section 4.6) cured at 140, 160, and 180 °C for 8h. The addition of starch deepened the color of the samples and some starch particles could be seen in the composites.

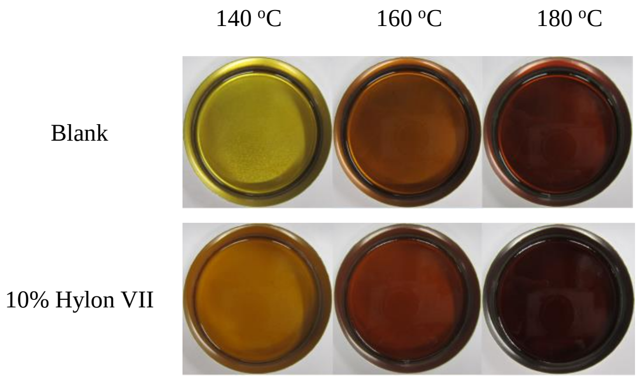

Figure 4.4 Samples (blank and with 10 wt% Hylon VII) cured at different temperatures for 8h. (Originally in colour)

4.3.1 Mechanical properties

Figure 4.5 shows the mechanical properties of blank samples and samples containing 10 wt% Hylon VII cured at 140, 160 and 180 °C for 8 h, respectively.

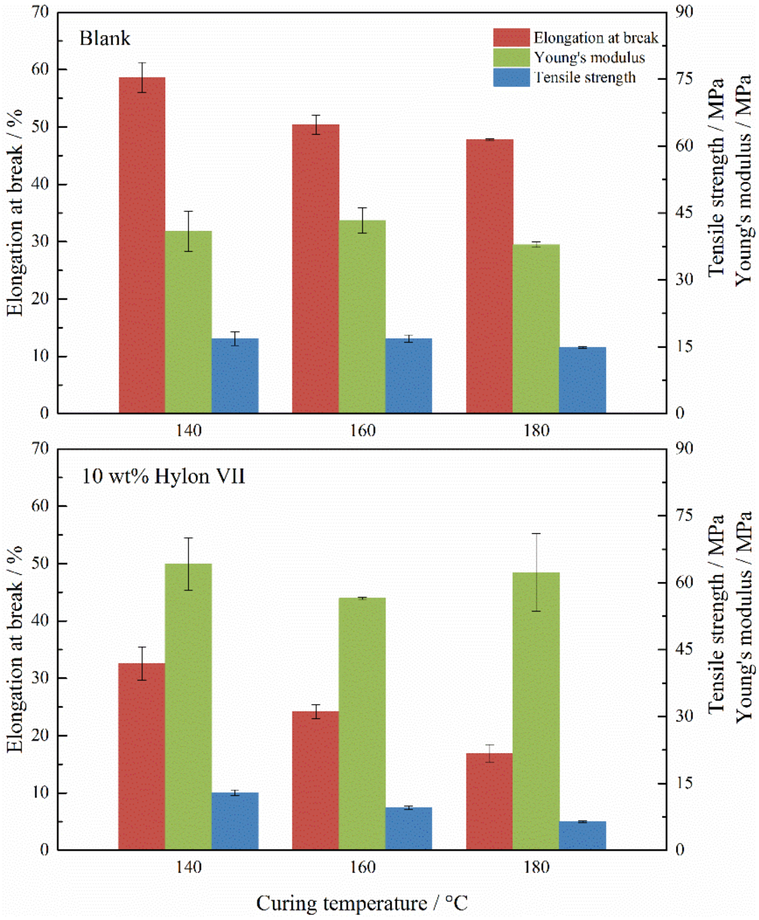

Figure 4.5 Mechanical properties of samples (blank and with 10 wt% Hylon VII) cured at different temperatures for 8h. (Originally in colour)

For the blank samples, with the increase of curing temperature, elongation at break decreased while tensile strength and Young’s modulus kept constant. For the composite samples, the addition of starch decreased the elongation at break by 45%, 52% and 65% for samples cured at 140, 160 and 180 °C, respectively. Whilst, the Young’s modulus improved from 40 MPa to 60 MPa for all samples. For composites cured at 140 and 160 °C, the tensile strength decreased from 17 MPa to 10 MPa; while for composites cured at 180 °C, tensile strength decreased from 15 MPa to 6 MPa. In general, increasing temperature results in films with poorer mechanical properties. Therefore, 140 °C was chosen as the optimal curing temperature and was used in the following studies.

4.4 Effect of starch composition

Due to the large differences of the molecule size between amylose and amylopectin, the effect of starch compositions (from pure amylose to pure amylopectin) on the thermal and mechanical properties were studied.

In this study, pure amylose, Hylon VII (comprising about 70% amylose), corn starch (containing about 30% amylose) and pure amylopectin were used. As shown in Figure 4.6, sample containing amylose showed suspended particles of amylose. The tight packing of molecules within amylose results in strong intramolecular hydrogen bonds and reduces the accessibility by solvent molecule thus leading to precipitation.

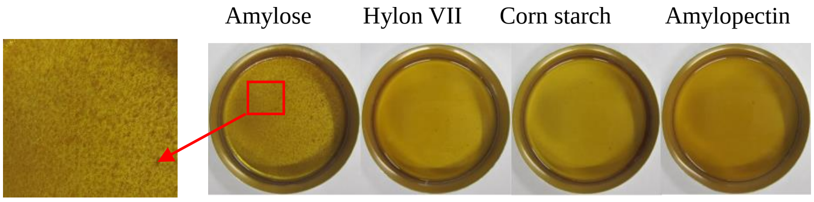

Figure 4.6 Samples containing 10 wt% different starches cured at 140 °C for 8 h. (Originally in colour)

4.4.1 Mechanical properties

Figure 4.7 shows the mechanical properties of epoxy resin composites containing 10 wt% of different starches. Amylose sample (10 wt%) showed the poorest mechanical properties with elongation at break of 28%, tensile strength of 7 MPa and Young’s modulus of 47 MPa, respectively. All the other samples showed almost the same mechanical properties with elongation at break of 30%, tensile strength of 12 MPa and Young's modulus of 68 MPa, respectively. The reason for the poorer mechanical properties of amylose sample was due to poorer mixing as discussed above (see Figure 4.6).

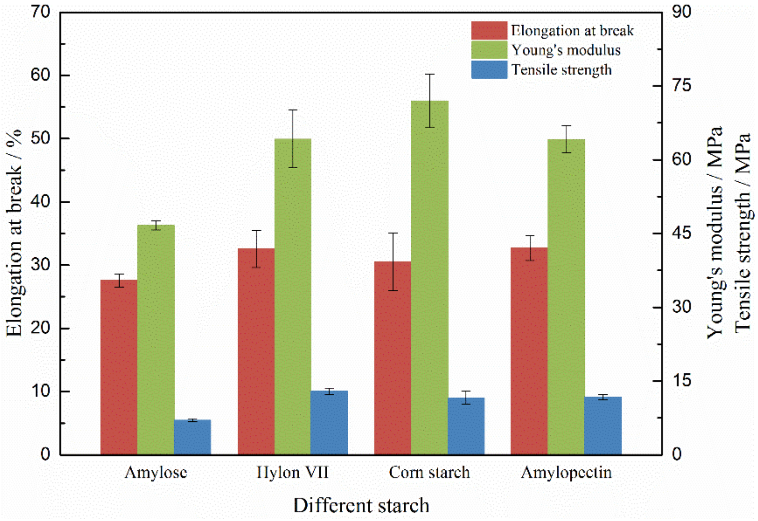

Figure 4.7 Mechanical properties of samples containing 10 wt% of different starches. (Originally in colour)

4.4.2 Thermal stability

Figure 4.8 shows the thermal stability of different starches and are summarized in Table 4.1. All starches contain about 10 wt% of water which can be seen from the first weight loss around 100 °C. The second weight loss was due to the decomposition of starches due to inter- or intramolecular dehydration reactions of the starch molecules with water as the main product.[226] Among these four starches, pure amylose showed the lowest T_5 and T_{max} which were 261 and 270 °C, respectively. The other samples showed similar T_5 and T_{max} with slight differences which were about 290 and 310 °C, respectively. The lower thermal stability of high amylose samples is a result of much easier scission of α-1, 4 linkages than that of α-1, 6 linkages.[230]

Table 4.1 Thermal stability of different starches/their composites.

Sample	T_5 (°C)	T_{max1} (°C)	T_{max2} (°C)	T_{max3} (°C)
Amylose	261/295	270/278	-/385	-/435
Hylon VII	291/321	311/319	-/387	-/431
Corn starch	294/317	313/322	-/386	-/428
Amylopectin	292/318	312/321	-/386	-/428

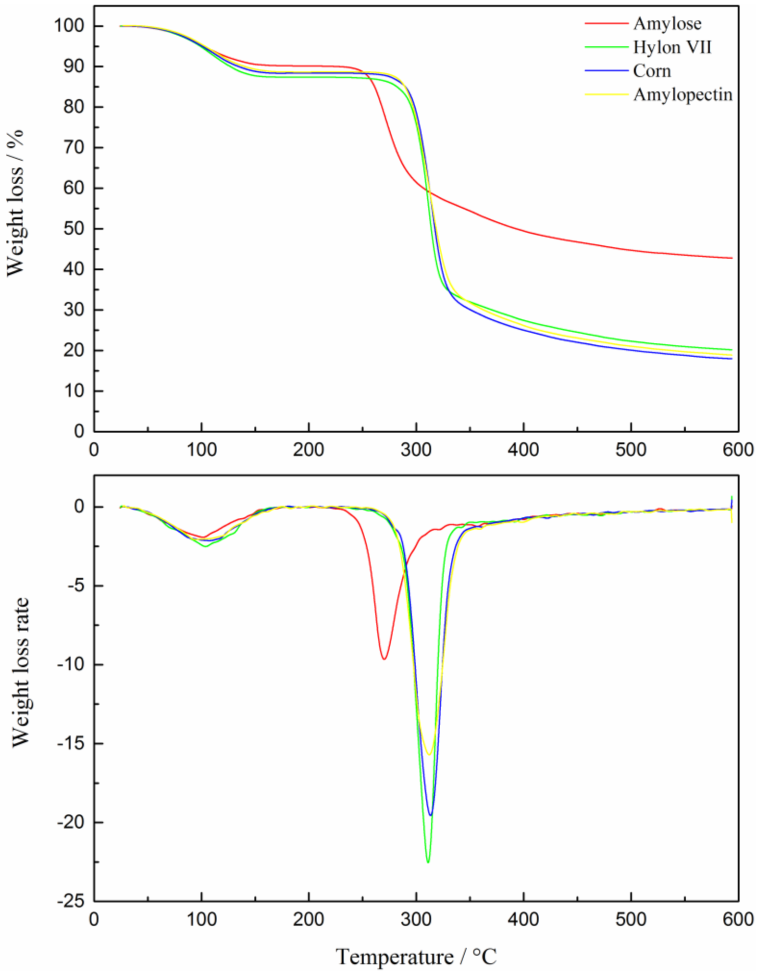

Figure 4.8 Thermal stability of different starches. (Originally in colour)

Figure 4.9 shows the thermal stability of composites containing different types of starches. As expected, the addition of starch decreased the thermal stability of samples by 25 ºC to 50 ºC. In addition, the composite with amylose showed the poorest thermal stability with T_5 of 295 ºC due to the poor thermal stability of amylose as shown in Figure 4.8. The other samples showed similar thermal stability with T_5 of 320 ºC.

All samples showed similar thermal decomposition processes with three decomposition stages. The first decomposition process occurred before 330 ºC was attributed to the decomposition of these starches. The other two decomposition processes were the decomposition of the epoxy resin itself.

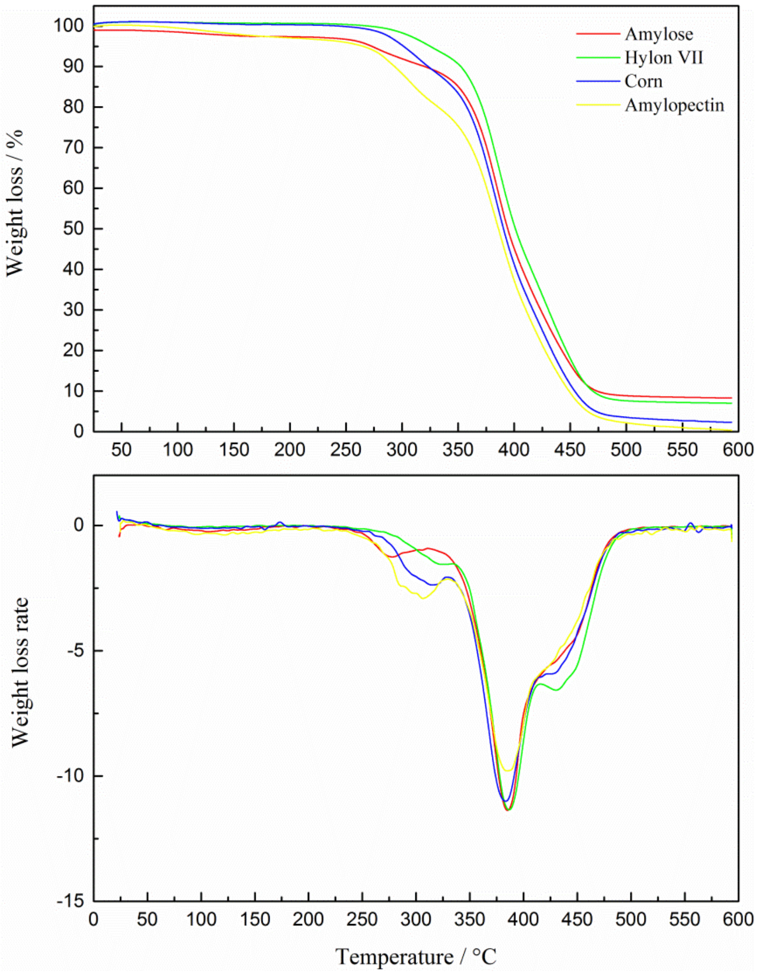

Figure 4.9 Thermal stability of cured composites containing 10 wt% of different starches. (Originally in colour)

4.4.3 SEM analysis

Figure 4.10 shows the fracture surfaces imaged by SEM after tensile tests of composites containing different types of starches. All samples showed phase separation with epoxy resin on the top layer of the composite. Starch particles were physically dispersed in the epoxy resin matrix. The cracks generated in the bottom starch-rich layer and then extended to the pure epoxy resin layer. Starch particle aggregates and voids and holes were also clearly observed in these samples. For the sample containing pure amylose, more and larger voids were generated due to the poor mixing properties of amylose, which accounted for its poorer mechanical properties especially tensile strength and Young's modulus.

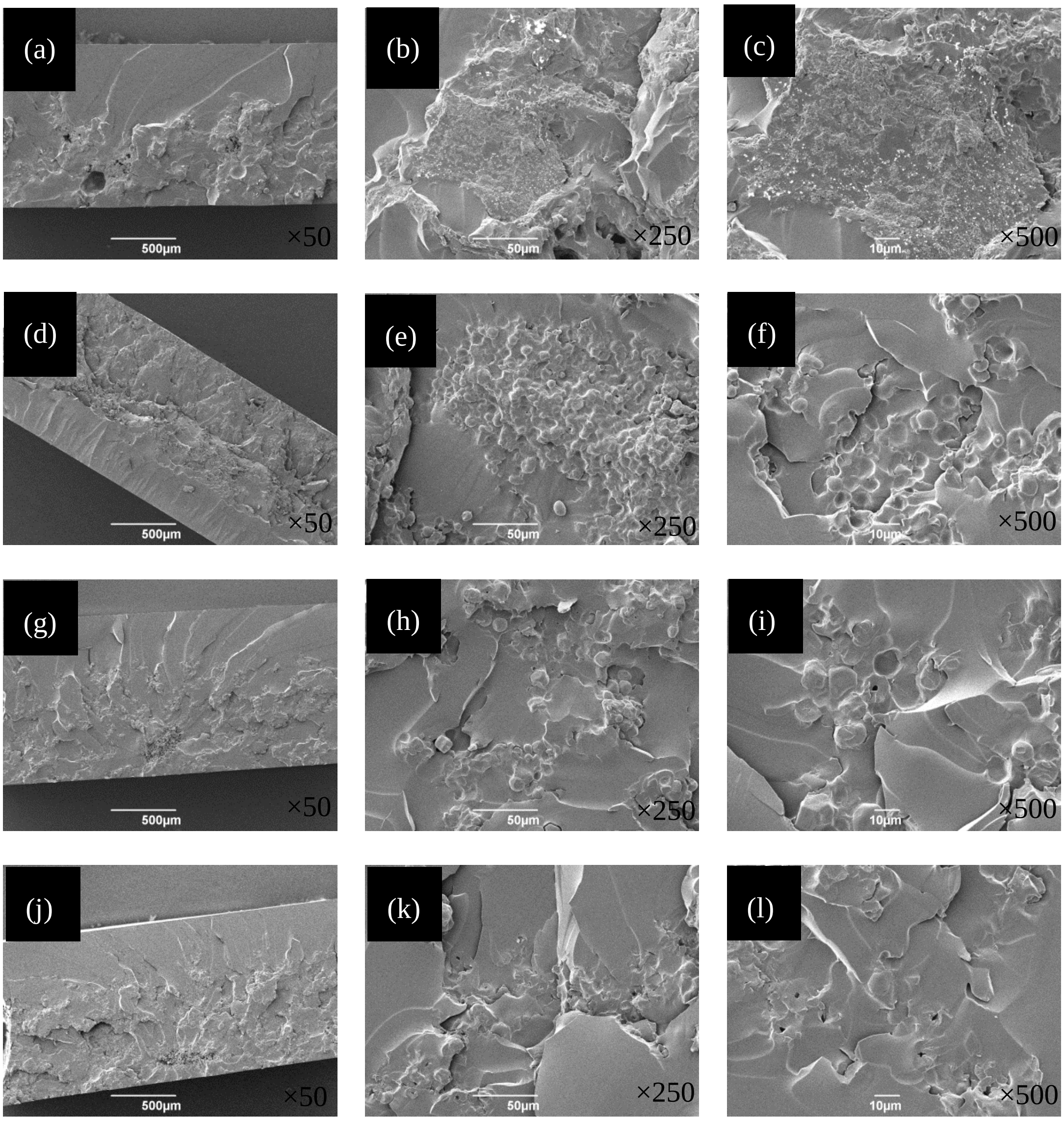
(a)
×50
500μm
(b)
×250
50μm
(c)
×500
10μm
(d)
×50
500μm
(e)
×250
50μm
(f)
×500
10μm
(g)
×50
500μm
(h)
×250
50μm
(i)
×500
10μm
(j)
×50
500μm
(k)
×250
50μm
(l)
×500
10μm

Figure 4.10 Fracture surface of samples containing 10 wt% different kinds of starch. (a, b, c) amylose; (d, e, f) corn starch; (g, h, i) Hylon VII; (j, k, l) amylopectin.

4.5 Effect of starch concentration

In this study, the effects of the amount of starch (Hylon VII) on the thermal and mechanical properties of the composites were studied (Figure 4.11). For the addition of more than 30% of starch films were not made because the mixture was too viscous to pour.

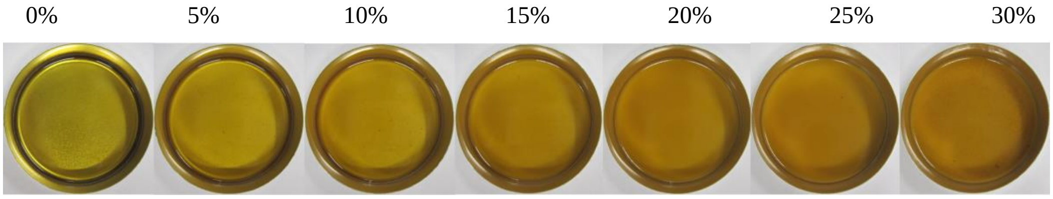
0%
5%
10%
15%
20%
25%
30%

Figure 4.11 Samples containing different amount of Hylon VII cured at 140 ^oC for 8h. (Originally in colour)

4.5.1 Mechanical properties

Figure 4.12 shows the effects of concentration of starch (Hylon VII, ranging from 0% to 30%) on the mechanical properties of the composites. Compared to the blank sample, the addition of starch decreased elongation at break and tensile strength but improved Young's modulus. The variation of starch concentrations had slight effects on Young's modulus and all the composite samples gave a Young's modulus at about 65 MPa. The addition of less than 20 wt% of starch decreased elongation at break by 40% and tensile strength by 17%, respectively. Whilst the addition of more than 20 wt% of starch decreased elongation at break by 66% and tensile strength by 44%, respectively.

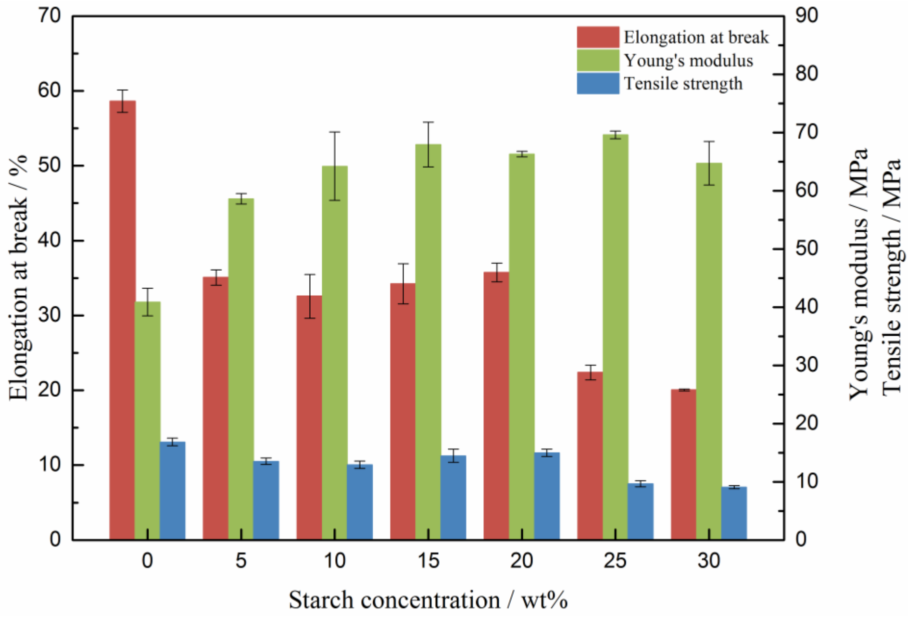

Figure 4.12 Mechanical properties of samples containing different amount of starch. (Originally in colour)

4.5.2 Thermal stability

Figure 4.13 shows the thermal stability of composites containing different amount of starch (0%, 10%, 20% and 30%) and are summarized in Table 4.2. For samples containing 20 wt% and 30 wt% starch, about 2 wt% of water loss was observed at around 100 °C due to the hydrophilic nature of starch. As expected, with the increasing amount of starch, the thermal stability of these composites decreased from 346 °C of the blank sample to 285 °C of the 30 wt% starch sample. All samples show three decomposition stages and starches decomposed firstly and then the epoxy resin.

Table 4.2 Thermal stability of composites containing different amount of starch.

Sample	T_5	T_{max1}	T_{max2}	T_{max3}
Blank	346	-	383	426
10 wt%	321	319	387	431
20 wt%	300	314	383	429
30 wt%	285	306	385	434

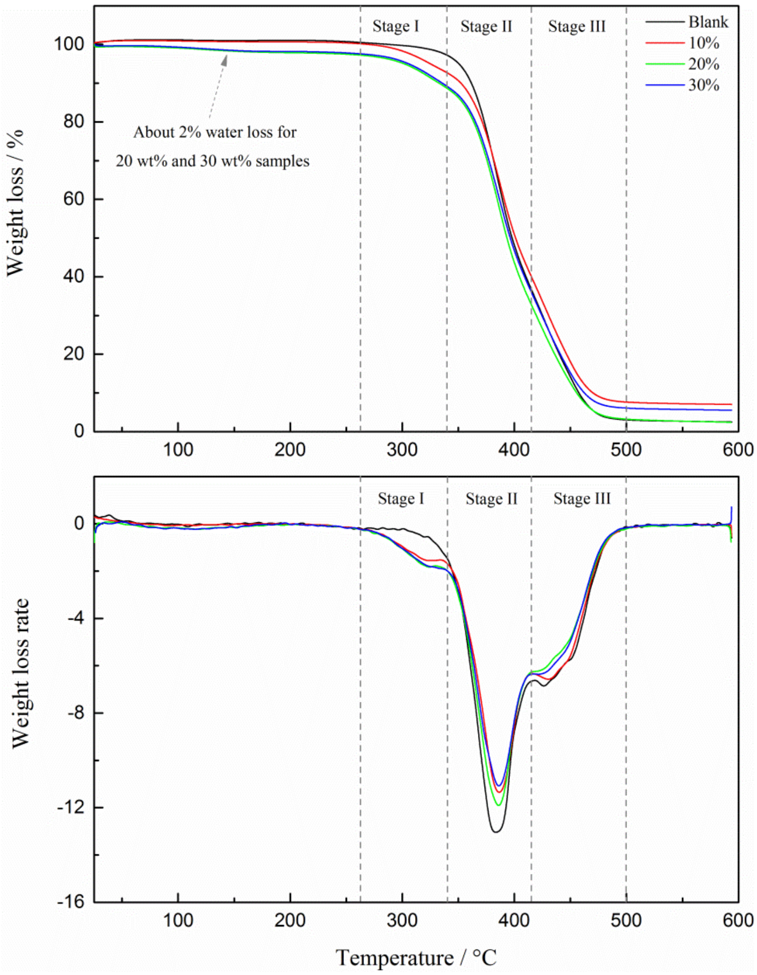

Figure 4.13 Thermal stability of composites containing different amount of starch. (Originally in colour)

4.5.3 SEM analysis

Figure 4.14 shows the fracture surface imaged by SEM after tensile test of the epoxy resin and its composites containing different amount of starch. As discussed before, all composites showed heterogeneity with starch dispersed unevenly within the sample. When starch addition was increased to 30 wt% up, big voids and holes were observed in the sample which was responsible for their decreased mechanical properties.

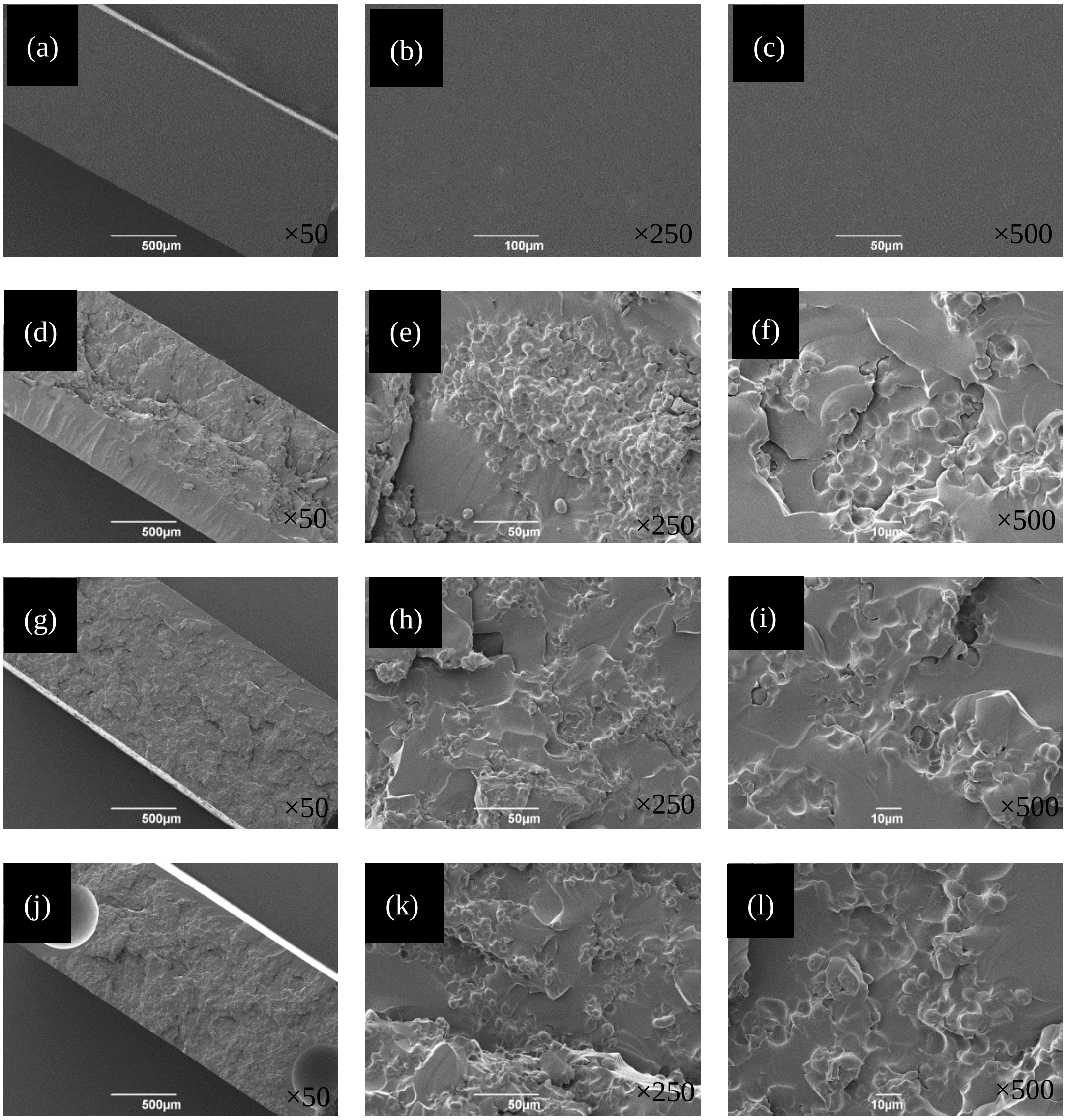
(a)
500μm
×50
(b)
100μm
×250
(c)
50μm
×500
(d)
500μm
×50
(e)
50μm
×250
(f)
10μm
×500
(g)
500μm
×50
(h)
50μm
×250
(i)
10μm
×500
(j)
500μm
×50
(k)
50μm
×250
(l)
10μm
×500

Figure 4.14 Fracture surface of samples containing different amount of Hylon VII. (a, b, c) 0%; (d, e, f) 10 wt%; (g, h, i) 20 wt%; (j, k, l) 30 wt%.

4.6 Effect of starch modification

In this study, expanded starch (ES) was esterified with different amounts of glutaric anhydride in order to introduce reactive acid groups onto starch molecules in order to improve the reactivity of starch and eliminate the phase separation.

Esterified starch with different degree of substitution (DS) was prepared by the method developed by Shuttleworth *et al.* with slight modifications (glutaric anhydride was used instead of acetic anhydride).[231] Expanded starch was reacted with different amounts of glutaric anhydride in the presence of DMAP as catalyst, in toluene at 90 ^{o}C for 12 h. After the reaction, the products were washed and dried and the degree of substitution was determined by the direct titrimetric method as described by Hu *et al.* (Chapter 5 Section 5.4).[229] The determined DS for different amount of glutaric anhydride is shown in Figure 4.15. Increasing the amount of glutaric anhydride increases the actual DS from 0.22 to 0.86. Higher DS means more acid groups were introduced onto starch molecules, which was supposed to further increase the reactivity of starch.

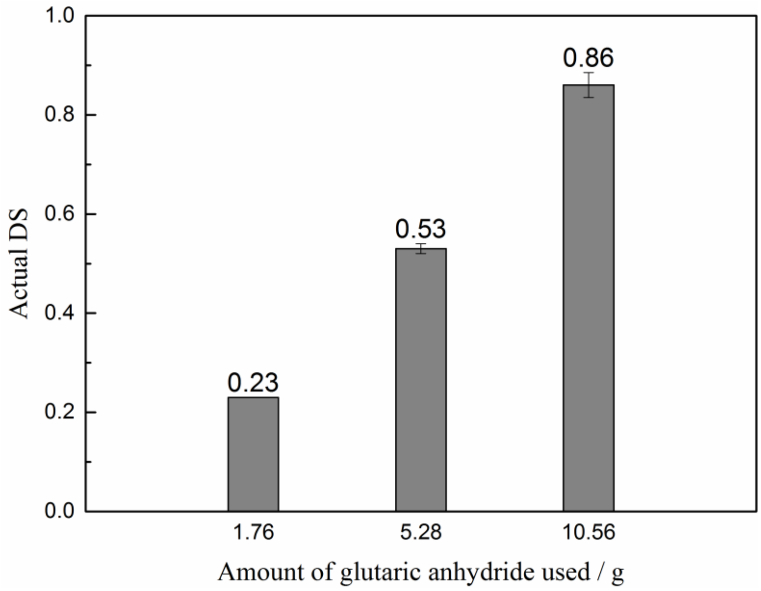

Figure 4.15 Relationship between DS and amount of glutaric anhydride used.

Then starch with different DS was directly mixed with ELO, adipic acid and DMAP at 150 °C and cured at 140 °C for 8 h to make epoxy resin-starch composites. Figure 4.16 shows samples containing 10 wt% esterified starch with different DS and the samples are named as following: NONE, ES, DS0.2, DS0.5 and DS0.8, respectively. Samples containing esterified starch show deeper color.

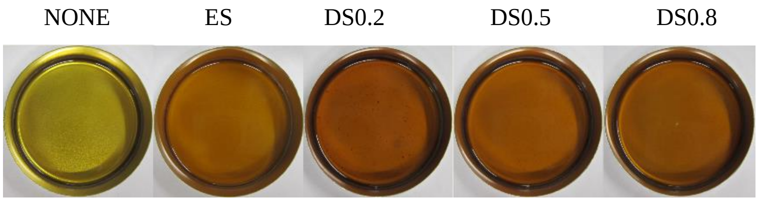

Figure 4.16 Blank sample and its composites containing 10 wt% starches with different DS. (Originally in colour)

4.6.1 Characterization of starch esters

4.6.1.1 FT-IR analysis

Figure 4.17 illustrates the FT-IR spectra of expanded Hylon VII starch and its esters with different DS by reacting with different amount of glutaric anhydride. Compared to the spectrum of expanded Hylon VII starch, new bands appeared at 1720 and 1565 cm^{-1} were observed in starch esters. The bands at 1720 cm^{-1} were assigned as the carbonyl groups in carboxylic acids and esters and the bands at 1565 cm^{-1} were assigned as the antisymmetric stretching of carboxylic anions, which confirmed the esterification reaction and carboxylic acid groups were remained in these esters.[229] Bands in the region of 3600 to 3000 cm^{-1} were assigned as the O-H stretching vibration of the hydroxyl groups. Bands at 2932 cm^{-1} were assigned as C-H vibrations. Bands at 1648 cm^{-1} were assigned as H-O-H bending of tightly bound water. Other bands assignments included 1146, 1074 and 1009 cm^{-1} (C-O vibration of anhydroglucose ring), 940, 863, and 765 cm^{-1} (the entire anhydroglucose ring stretching vibrations).[232-234]

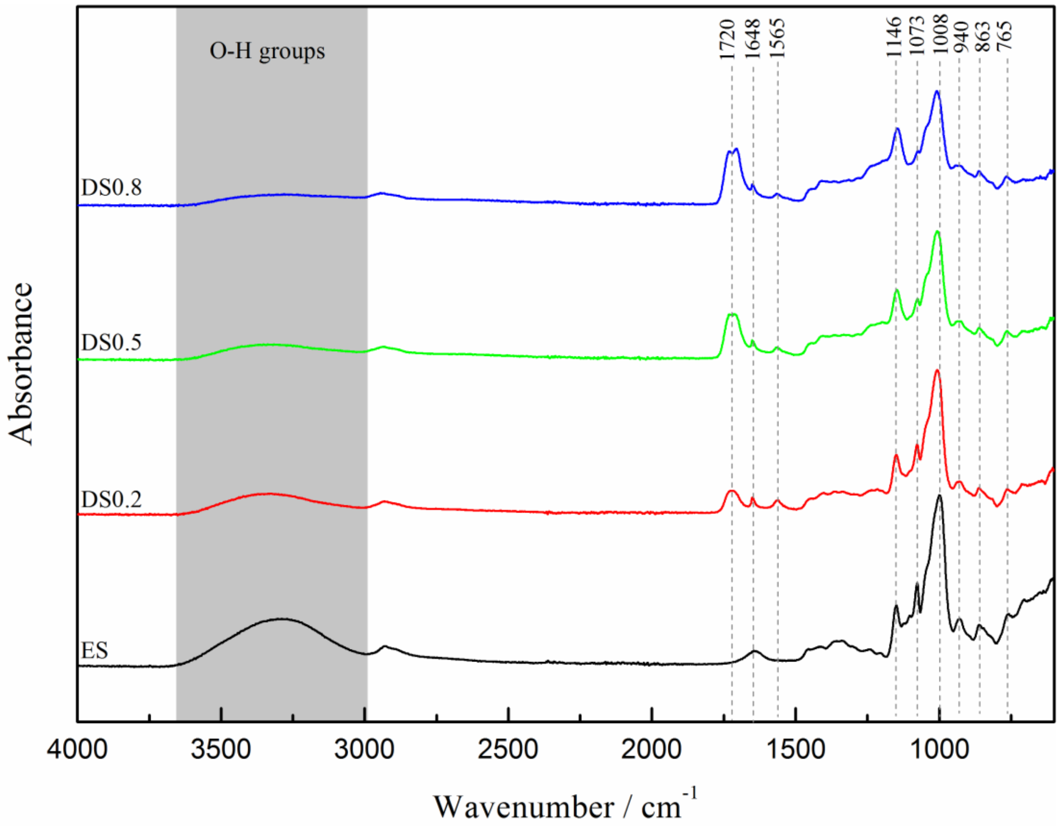

Figure 4.17 FT-IR spectra of starches with different DS. (Originally in colour)

In addition, with an increase in the DS, the intensity of O-H stretching band gradually decreased while the intensity of the ester carbonyl C=O bands at 1720 cm^{-1} gradually increased, indicating the conversion of hydroxyl groups to ester groups.

4.6.1.2 Solid ^{13}C NMR analysis

Both expanded starch and its esters with glutaric anhydride were characterized by solid state ^{13}C CPMAS NMR to further confirm the esterification reaction (Figure 4.18). Due to the higher content of acid groups, only starch esters with DS0.8 were studied.

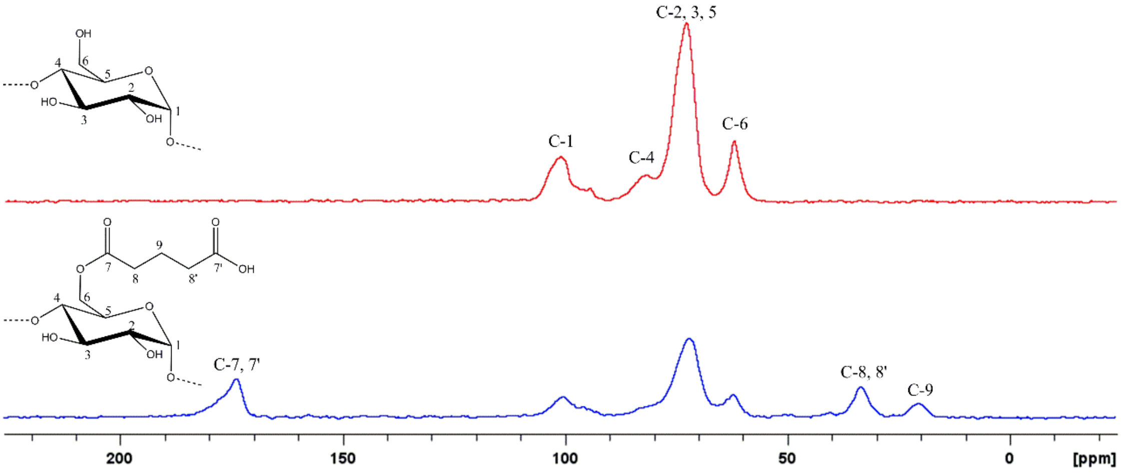

Figure 4.18 Solid state ^{13}C CPMAS NMR of (a) expanded starch; (b) starch esters with DS0.8.

The spectrum of expanded starch shown in Figure 4.18 (a) was consistent with the findings reported in the literature.[235, 236] All noticeable signals were present: δ=100 ppm (C-1); 82 ppm (C-4); 72 ppm (C-2, 3, 5), and; 62 ppm (C-6). As can be seen from Figure 4.18 (b), new signals at δ=175 ppm, 35 ppm and 22 ppm were observed corresponding to carbonyl carbons; the α, and; β CH_2 to the carbonyl group, respectively. These results further indicated the esterification reaction was successful.

4.6.1.3 Thermal stability and TG-IR analysis

Figure 4.19 shows the thermal stability of expanded starch and its esters with different DS and the data are summarized in Table 4.3. Expanded starch shows two decomposition processes while starch esters show three decomposition processes. The first process was attributed to the evaporation of water.

Table 4.3 Thermal stability of expanded starch and its esters with different DS.

Sample	T_5	T_{max1}	T_{max2}	Mass loss 1	Mass loss 2
ES	291	311	-	-	-
DS0.2	251	289	379	51.0	14.9
DS0.5	252	286	365	46.9	21.7
DS0.8	256	287	363	48.0	24. 2

Compared to the decomposition temperature of expanded starch of 291 °C, the thermal stabilities of starch esters were 40 °C lower, which was also found in maleic anhydride esterified corn starch.[227]

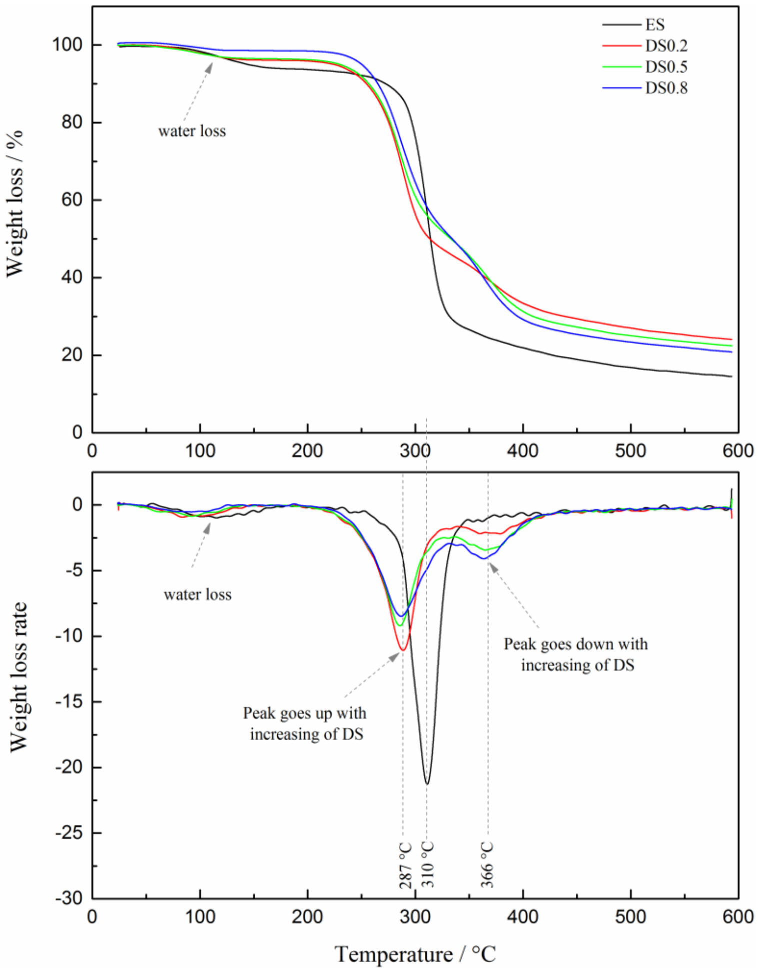

Figure 4.19 Thermal stability of starches with different DS. (Originally in colour)

However, the situation was contrary for starch acetate (modified with acetic anhydride) which showed improved thermal stability compared to native starch.[233] As discussed earlier, the decomposition process of starch was due to the inter- and/or intramolecular dehydration reactions, acid groups instead of ethyl ester groups possibly made the dehydration reactions happened more easily, which explained their decreased thermal stability compared to starch acetate.

In addition, starch esters showed two decomposition processes while expanded starch showed only one decomposition process. With the increase of DS, the thermal stability of starch esters changed slightly. Also, with the increase of DS, weight loss in the first decomposition step decreased slightly from 51% (DS0.2) to 48% (DS0.8), whilst weight loss in the second decomposition step increased from 15% (DS0.2) to 24% (DS0.8).

In order to further understand the differences of these two decomposition stages TG-IR was used to analyze the decomposition process of starch ester with DS0.8 due to its higher content of acid groups. The IR spectra of the gases evolved at the maximum two rates of decomposition are shown in Figure 4.20.

In general, both spectra showed almost the same characteristic bands for starch decomposition: bands at 4000-3500 cm^{-1} (water), bands at 2400–2280 cm^{-1} (CO_2) and 2260–2070 cm^{-1} (CO), band at 1731 cm^{-1} (C=O groups), band at 1486 cm^{-1} (aliphatic structure formed by the cleavage of the main chain of starch), band at 1030 cm^{-1} (CH_2O_2).[237] The band at 1810 cm^{-1} observed at the first decomposition stage 287 ºC was assigned as the carbonyl group in glutaric anhydride, which indicated that the first decomposition stage was a combination of the side glutaric anhydride chain and starch backbone while the second stage was mainly the decomposition of starch.

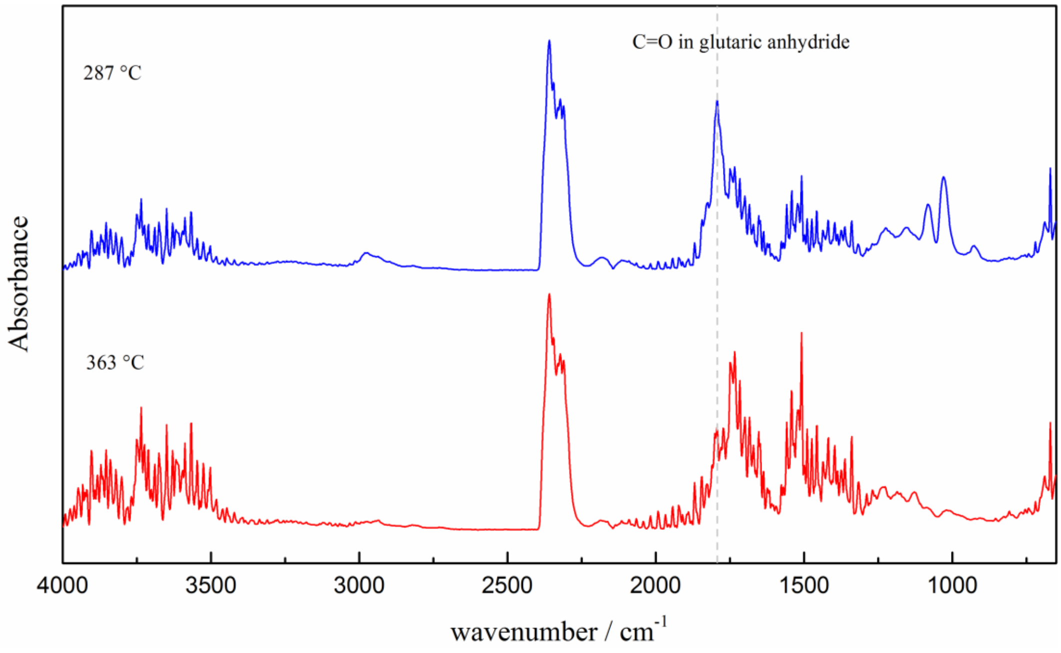

Figure 4.20 IR spectra of evolved gases from TG-IR analysis taken at the maximum rate of decomposition. (Originally in colour)

4.6.2 Characterization of composites

4.6.2.1 DSC analysis

Figure 4.21 shows the effects of the addition of starch on the thermograms of the premixed mixtures and their thermal properties are summarized in Table 4.4.

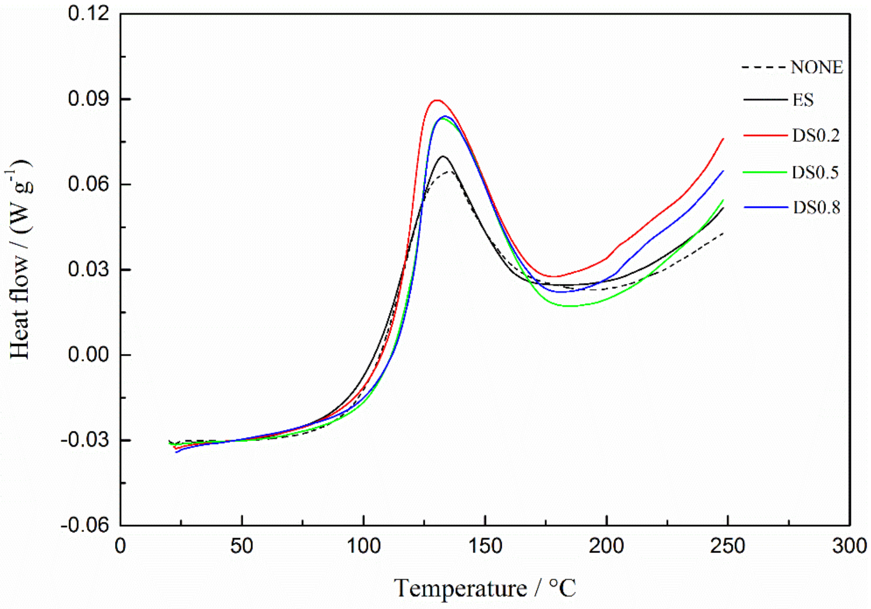

Figure 4.21 DSC thermograms of premixed mixtures of epoxy resin and its composites with different DS. (Originally in colour)

The addition of ES decreased Δ*H* slightly from 188.2 to 179.8 J g^{-1}, which was contrary to our previous findings with the ELO-Pripol 1009 system where Δ*H* increased moderately in the presence of starch.[176] A possible explanation may be due to much higher reactivity of adipic acid than that of Pripol 1009 and thus reduced the chance of reaction between epoxy and the hydroxyl groups of starch.

Table 4.4 Thermal properties of composites (mixtures and cured films) with different DS.

Sample	Δ*H* (J g^{-1})	T_{on} (°C)	T_P (°C)	T_g (°C)	T_5 (°C)	T_{max1} (°C)	T_{max2} (°C)	T_{max3} (°C)
None	188.2	102.5	131.3	10.4	346	-	383	426
ES	179.8	102.7	132.5	12.4	323	320	387	429
DS0.2	201.2	114.2	129.2	14.0	308	291	384	427
DS0.5	203.5	117.6	130.5	12.7	315	295	385	425
DS0.8	194.2	117.9	133.1	14.7	319	295	383	423

While the addition of starch esters showed slightly higher ΔH which was possibly due to the reaction of the introduced reactive acid groups with epoxy groups. In addition, the presence of starch and its esters shifted T_{on} to higher temperatures which may be due to poorer diffusion of the molecules with the incorporation of starch.[176] The incorporation of ES increased T_{on} from 102.5 to 102.7 °C, whilst those for starch esters with DS0.2, 0.5 and 0.8 were increased to 114.2, 117.6 and 117.9 °C, respectively.

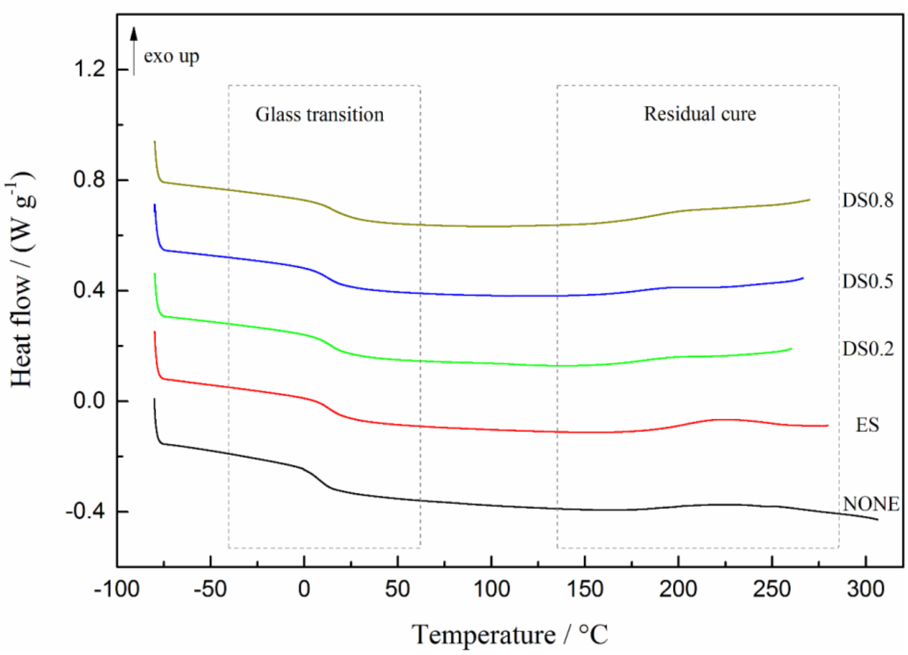

Figure 4.22 DSC thermograms of cured composites containing starches with different DS. (Originally in colour)

The T_g and residual cure detected by DSC analysis of the cured epoxy resin and its composites with heating rate of 10 °C min^{-1} are shown in Figure 4.22. With the addition of starch, T_g was improved slightly by 2 to 4 °C possibly due to enhanced hydrogen bonding between starch particles and the amorphous polymer matrix.[238-240]

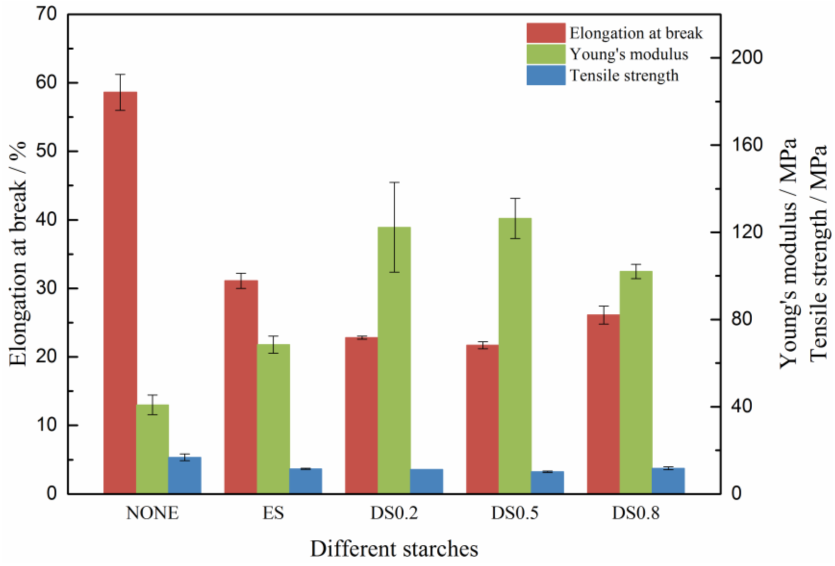

Figure 4.23 Mechanical properties of epoxy resin and their composites with starches (different DS). (Originally in colour)

4.6.2.2 Mechanical properties

Figure 4.23 shows the mechanical properties of epoxy resin and its composites containing 10 wt% starches (ranging from DS0.0 to DS0.8). The addition of starch increased Young's modulus whilst decreasing tensile strength and elongation at break. Compared to the sample containing native Hylon VII, the addition of expanded starch had negligible effect on the mechanical properties (Figure 4.5 and Figure 4.23). Whereas, with the addition of esterified starch, elongation at break was further decreased from 33% to 23% while Young's modulus was further improved from 64 MPa to 120 MPa. However, the mechanical properties of samples containing different DS starch esters showed slight differences.

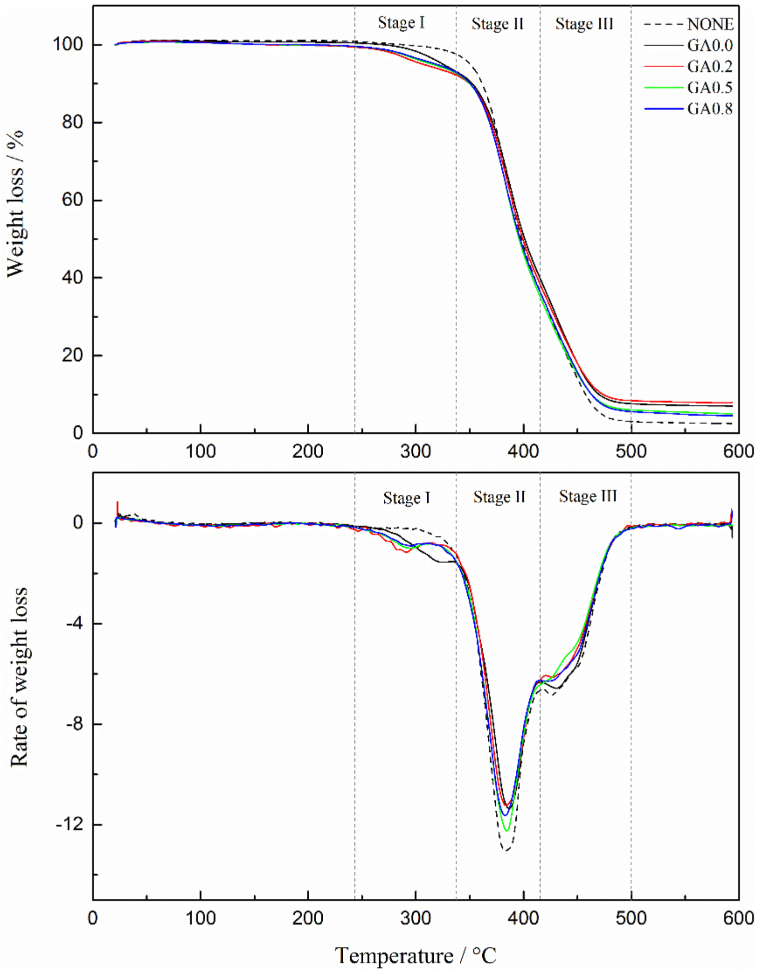

Figure 4.24 Thermal stability of epoxy resin and its composites with starches (different DS). (Originally in colour)

4.6.2.3 Thermal stability

The thermal stability of cured epoxy resin and its composites containing 10 wt% ES and starch esters with different DS is presented in Figure 4.24. Their thermal stabilities are summarized in Table 4.4. Compared to the decrease of thermal stability of 25 °C by addition of ES, the addition of starch esters further decreased the thermal stability of these samples by 4 to 15 °C due to the lower thermal stability of starch esters. Also all samples showed three decomposition stages with starches decomposed firstly followed by the epoxy resins.

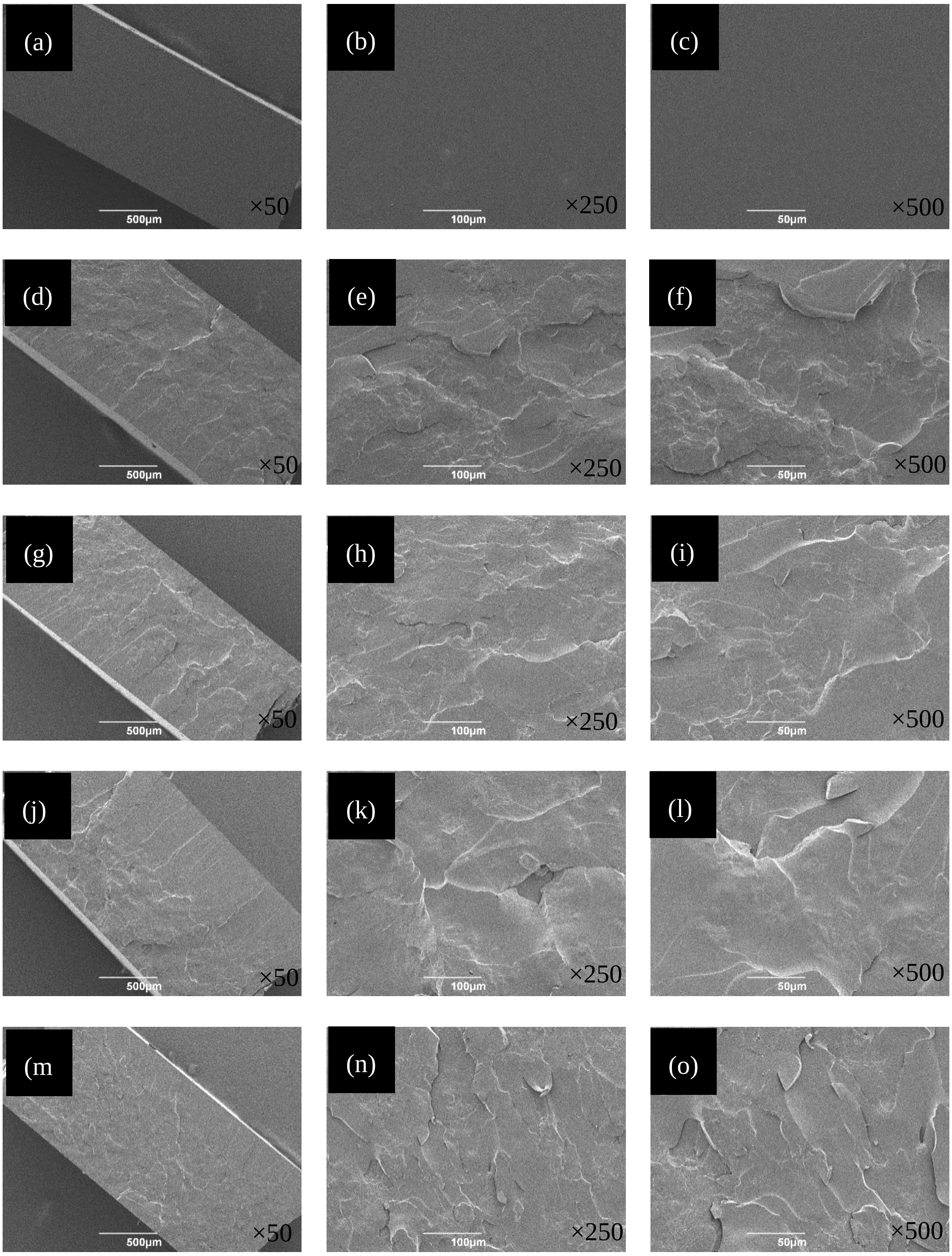
(a)
500µm
×50
(b)
100µm
×250
(c)
50µm
×500
(d)
500µm
×50
(e)
100µm
×250
(f)
50µm
×500
(g)
500µm
×50
(h)
100µm
×250
(i)
50µm
×500
(j)
500µm
×50
(k)
100µm
×250
(l)
50µm
×500
(m
500µm
×50
(n)
100µm
×250
(o)
50µm
×500

Figure 4.25 Fracture surface of composites containing 10 wt% starches with different DS. (a, b, c) blank; (d, e, f) ES; (g, h, i) DS0.2; (j, k, l) DS0.5; (m, n, o) DS0.8.

4.6.2.4 SEM analysis

Figure 4.25 shows the fracture surfaces imaged by SEM of epoxy resin and its composites with 10 wt% ES and starch esters with different DS.

Similar to the samples above, phase separations were observed in all composite samples.

However, compared to the composite containing native Hylon VII, the starch aggregates in composite containing ES were much less and smaller indicating that the compatibility of the epoxy resin and starch was improved. Expanded starch was dispersed better than native Hylon VII into the epoxy resin matrix. While for composites containing starch esters, almost no starch aggregates were observed in the sample and the compatibility between these two components were further improved, *i.e.*, no apparent phase separation as seen in Figure 4.14, which indicated that starch may be chemically connected with the epoxy resin and could explain the large improvement in Young’s modulus.

4.7 Conclusions

Biobased thermosets based on ELO-C_6 epoxy resins with starch were successfully made. Composites cured at 140 ^{o}C gave the best mechanical properties and the increase of curing temperature decreased all the mechanical properties. The addition of starch increased Young’s modulus while decreased tensile strength and elongation at break.

Amongst the various starch types all samples showed similar mechanical properties, except for pure amylose which gave significantly poorer performance.

The variation of concentration of Hylon VII added had slight effect on the Young’s modulus and all samples containing different amount of Hylon VII gave Young’s modulus of 65 MPa. However, when the amount of Hylon VII was over 20% the tensile strength and elongation at break were further decreased.

Reactive acid groups were successfully introduced onto starch molecules by reacting expanded starch with glutaric anhydride. The resultant starch esters showed poorer thermal stability compared to expanded starch which resulted poorer thermal stability of the obtained composites. The addition of starch esters further improved Young’s modulus by almost 100% compared to unmodified starch.

However, all samples showed heterogeneity with starch settling to the bottom of the samples. For the future work, better mixing methods such as high speed mixing would be beneficial. Due to the nanoscale structure of starch crystals, it will be worthwhile to incorporate starch nanocrystals (original and modified) in to composite formulations in order to improve properties.[241]

Chapter 5

Materials and Experimental

5.1 Materials and chemicals

ELO (Lankroflex® L, oxirane content = 9.0%), ESBO (Lankroflex® E2307, oxirane content = 6.5%), EML (Lankroflex® E2568, oxirane content = 8.6%), and EMS (Lankroflex® E2480, oxirane content = 6.2%) were obtained from Akcros Chemicals, Eccles, England.

The C_6-C_{16} diacids and glutaric anhydride were purchased from Sigma Aldrich: C_6 adipic acid (99.5%), C_8 suberic acid (98%), C_{10} sebacic acid (99%), C_{12} dodecanedioic acid (99%), C_{14} tetradecanedioic acid (98%), C_{16} hexadecanedioic acid (96%), glutaric anhydride (95%). C_{18} Octadecanedioic acid (95%) was purchased from Fluorochem and bio-derived C_{36} diacid (Pripol 1009F, acid value 194 mg KOH/g) was kindly supplied by Croda. Oxalic acid (C_2) and succinic acid (C_4) were not used due to their high melting point, .i.e., 189.5 °C and 185 °C, respectively.

4-*N*,*N*-Dimethylaminopyridine (DMAP), 1-methylimidazole (1-MI), 2-methyl imidazole (2-MI), vinylimidazole (VI) and trimethylamine (TEA) were purchased from Sigma Aldrich.

High amylose corn starch HYLON VII® and corn starch were purchased from Ingredion™. Amylose from potato and amylopectin from maize were purchased from Sigma Aldrich. Expanded starch and starch esters were prepared in-house as described later.

All chemicals were used as received without further purification.

5.2 Experimental details and instrumentation for Chapter 2

5.2.1 Film preparation

All DCAs samples were prepared with a stoichiometric relationship, R, of 0.7 (R = acid groups/epoxy groups).[84] For each formulation, the amount of initiator (DMAP, 1-MI, 2-MI, VI and TEA) added was calculated based on 1 mol% of epoxy functional groups.

The mixture was stirred at 150 °C for 5 min, poured in to a hot aluminum plate (internal diameter of 70 mm) and cured in a fan-assisted oven at different temperatures (140 °C, 160 °C, 180 °C, 200 °C and 220 °C for different time (1 h, 2 h, 4 h, 6 h, 8 h, 12 h, 16 h, 20 h and 24 h). The detailed compositions and curing conditions are shown in Table 5.1.

Table 5.1 Sample compositions and curing conditions

Epoxy prepolymer	Curing agents	Accelerators	Curing Temperature	Curing time
ELO	adipic acid	1 mol% DMAP	160 °C	1 h
ESBO				1 h
EML				24 h
EMS				24 h
ELO	DCAs	1 mol% DMAP	160 °C	1 h
ELO	adipic acid	None 1 mol% DMAP/1-MI/2-MI/VI/TEA 2, 3, 4, 5% DMAP	160 °C	1 h
ELO	adipic acid	1 mol% DMAP	140, 160, 180 °C	1, 2, 4, 6, 8, 12, 16, 20, 24 h
			200, 220 °C	1 h

5.2.2 DSC analysis

The DSC analyses were performed with a TA Instruments Q2000 DSC. Premixed samples (7-10 mg), obtained after stirring at 120 °C /150 °C for 5 min, were hermetically-sealed in Tzero aluminum DSC pans. Thermal runs were performed under a constant flow of dry nitrogen (50 mL/min). Dynamic runs were performed under four different heating rates, 5, 10, 15 and 20 °C/min, over a temperature range of 25 °C to 320 °C. The results reported are the averages of the three measurements. Glass transition temperature T_g was obtained by heat-cool cycling (10 °C/min) of the cured resins (7-10 mg) sealed in Tzero aluminum hermetic DSC pans.

MDSC analyses were performed with a TA Instruments Q2000 DSC to separate the melting process of adipic acid with the curing reaction. Dynamic runs were performed at 1 °C/min with modulation period of 60 s and amplitude of ±0.5 °C over a temperature range of 20 °C to 250 °C.

5.2.3 Polymer extraction study

Approximately 2 g *cured* sample was subjected to extract in dichloromethane (DCM, 20 mL) at room temperature for 7 days. Thereafter, the soluble was concentrated *in vacuo* and both the soluble and residue were dried overnight at room temperature under vacuum. The soluble was analysed by GPC, FT-IR and NMR whereas residues were characterized by FT-IR and solid state ^{13}C NMR only. The sol content (%) was determined as the average of two measurements using the equation below

$$\%\ \text{sol content}=100\times\frac{w_{sol}}{w_t}$$

where w_t is the total weight of thermoset sample and w_{sol} is the weight of loss during extraction, which refers to the sol fraction.

5.2.4 ATR-FTIR analysis

ATR-IR (attenuated total reflection infrared) spectra were recorded on a Bruker Vertex 70 Spectrometer equipped with a diamond golden gate ATR cell over a scanning range of 650-4000 cm^{-1} for 32 scans at a spectral resolution of 2 cm^{-1}.

5.2.5 NMR analysis

^{1}H and ^{13}C NMR spectra for starting materials and extracted soluble materials were recorded on a JEOL JNM-ECS 400 MHz spectrometer.

Solid state ^{13}C NMR (CPMAS) spectra for insoluble parts acquired using a 400 MHz Bruker Avance III HD spectrometer equipped with a Bruker 4mm H(F)/X/Y triple- resonance probe and 9.4T Ascend® superconducting magnet. Films after extraction were analyzed by Solid 13C NMR analysis. Solid-state 13C spectra were recorded at 100.56 MHz using a Varian VNMRS spectrometer and a 6 mm (rotor o.d.) magic-angle spinning probe. They were obtained using cross-polarisation (CP) with a 2 s recycle delay, 1 ms contact time, at ambient probe temperature (~25 °C) and at a sample spin-rate of 68 kHz. Another group spectra were obtained using direct excitation (DE) with a 1 s recycle delay, 4.4 us pulse duration, at ambient probe temperature (~25 °C) and at a sample spin-rate of 68 kHz. 1496 and 48 repetitions were accumulated respectively. Spectral referencing was with respect to an external sample of neat tetramethylsilane (carried out by setting the high-frequency signal from adamantane to 38.5 ppm).

5.2.6 GPC analysis

GPC was performed (externally by TARRC, UK) at 40°C in THF stabilised with 0.025% BHT with eluent pumped at the constant flow rate of 1.0 mL/min. The samples were analysed using a

PL-GPC 50 system equipped with PLGel column guard and 3x PLGel 5µm mixed bed-C columns (300X7.5mm). Before injecting the samples, the system was calibrated by performing Universal Calibration with single PL-polystyrene standard and a set of PL-EasyVial PS-H polystyrene standards of molecular known molecular weights. Viscometry (PL-BV 400RT viscometer) and refractometry (PL-RI differential refractometer) were used as detectors and the resultant data was processed by Varian 'Cirrus Multi detector' software.

5.2.7 DMA analysis

DMA analysis was performed at CSIC in Spain supervised by Dr. Peter Shuttleworth. Thermal relaxations of the cross-linked bioplastics were carried out on a dynamic mechanical analyser (DMA Q800, TA Instruments) using a 3-point bending mode accessory at 1, 3, 7, 10 and 20 Hz. Samples with dimensions of 20×10 mm with a film thickness ranging from 1–1.5 mm (thinner than recommended due to sample preparation constraints) were heated from -120 to 50 °C at a heating rate of 1 °C min^{-1}.

5.2.8 Mechanical properties

The resulting films were cut into standard dumb-bell shapes (60 mm × 10 mm). Film thickness was in the region of 1–1.5 mm. Tensile studies were conducted in triplicate using an Instron 3367 universal testing machine fitted with 1000 N capacity load cell. The initial grip separation was set at 35 mm and the crosshead speed was 20 mm/min. The results reported were the average of the three measurements.

5.2.9 CHN analysis

Elemental analysis of nitrogen ratios in the soluble substances of samples with different amounts of DMAP were performed using Exeter Analytical (Warwick, UK) CE-440 Elemental Analyser (calibrated against acetanilide with *S*-benzylthioronium chloride internal standard). The results reported were the average of two measurements.

5.2.10 Thermal stability

The thermal stability of the cured DCAs resins was analyzed using Stanton Redcroft STA 625.

Approximately 10 mg of the sample was heated from room temperature to 600 °C at a heating rate of 10 °C/min under nitrogen gas and air atmosphere, respectively.

5.2.11 SEM analysis

Scanning electron micrographs (SEM) analysis of the fracture surfaces of these samples after tensile tests were taken on a JEOL JSM-6490LV (JEOL, Tokyo, Japan). Prior to analysis, samples were mounted on alumina sample holders and coated in a thin film of gold using a high-resolution sputter SC-7640 coating device at a sputtering rate of 1500 V min^{-1}. The size of the nodules were measure by ruler manually.

5.3 Experimental details and instrumentation for Chapter 3

5.3.1 Film preparation

All anhydride samples were prepared with a stoichiometric relationship, R, of 1.0 (R = ahydride groups/epoxy groups). For each formulation, the amount of DMAP added was calculated based on 1 mol% of epoxy functional groups. The mixture was stirred at 120 °C (above the melting point of DMAP) for 5 min, poured in to a hot aluminum plate (internal diameter of 70 mm) and cured in a fan-assisted oven at different temperatures (140 °C, 160 °C, 180 °C, 200 °C and 220 °C) for different time (1 h, 2 h, 4 h, 6 h, 8 h, 12 h, 16 h, 20 h and 24 h). The detailed compositions and curing conditions are shown in Table 5.2.

Table 5.2 Sample compositions and curing conditions

Epoxy prepolymer	Curing agents	Accelerators	Curing Temperature	Curing time
ELO ESBO EML EMS	glutaric anhydride	1 mol% DMAP	180 °C	2 h
ELO	glutaric anhydride	1 mol% DMAP	140, 160, 180 °C	1, 2, 4, 6, 8, 12, 16, 20, 24 h
			200, 220 °C	1 h

For samples cured with adipic acid and glutaric anhydride samples, the stoichiometric relationship, R, of 1.0 (R= (acid groups + anhydride groups)/epoxy groups) was used. Six samples with different amounts of adipic acid and glutaric anhydride, the ratio of acid groups to anhydride groups ranging from 100/0, 80/20, 60/40, 40/60, 20/80 and 100/0 were made. For each formulation, the amount of DMAP added was calculated based on 1 mol% of epoxy functional groups. The mixture was stirred at 150 °C for 5 min, poured in to a hot aluminum plate (internal diameter of 70 mm) and cured in a fan-assisted oven at 180 °C for 2h.

5.3.2 Thermal stability

The thermal stability of the cured anhydride with/without adipic acid resins were analysed using Netzsch STA 409. Approximately 20 to 30 mg of the sample was heated from room temperature to 600 °C at a heating rate of 10 °C/min under nitrogen gas atmosphere.

All the other analyses used were the same as stated in Chapter 5 Section 5.2.

5.4 Experimental details and instrumentation for Chapter 4

5.4.1 Preparation of expanded starch

Hylon VII starch (200 g, 1.23 mol) was added to of distilled water (4 L) in an adapted All American pressure cooker 915 (~14.7 dm^3). The mixture was stirred and agitated at 140 °C for 2 h. After cooling to room temperature (RT), the mixture was placed in a fridge at 5 °C for 3 days. Then the water within the mixture was solvent exchanged (3×2 L ethanol and 3×2 L toluene) and dried in a vacuum oven at 80 °C for 24 h. A fine white powdered, expanded starch was obtained (180 g, 90%) with a BET surface area of 236 $m^2\ g^{-1}$.

5.4.2 Preparation of starch esters

A mixture of expanded Hylon VII (5 g, 30.86 mmol), toluene (70 cm^3) and the appropriate amount of glutaric anhydride (1.76 g, 15.42 mmol; 5.28 g, 46.28 mmol; and 10.56 g, 92.56 mmol) was added to a 100 cm^3 round bottom flask heated to to 90 °C and stirred for 5 min. After which DMAP (0.11 g, 0.9 mmol) was added and the reaction was maintained at 90 °C with stirring for a further 12 h. The mixture was cooled to 50 °C, ethanol (50 cm^3) was added and the resultant precipitate was filtered, washed with ethanol (3×50 cm^3) and acetone (3×50 cm^3) and dried for 24 h at RT under vaccum. Degree of substitution was determined by titration as described in Section 5.4.4 .

5.4.3 BET surface area measurement

Nitrogen-adsorption analysis was carried out using an ASAP 2020 volumetric adsorption analyser from Micromeritics. Measurements were performed at 77 K. Samples were degased at 65 ^{o}C for 6 h prior to analysis. The Brunauer-Emmett-Teller (BET) theory was used to determine the surface area.

5.4.4 Determination of degree of substitution by titration

The degree of substitution of esterified starches was determined using the direct titration method described by Hu *et al.*[229] About 0.5 g of starch esters was dissolved in distilled water (50 mL) and the solution was titrated with aqueous 0.05 M NaOH solution using phenolphthalein as indicator. The DS was calculated by using the following equation:

$$\mathrm{DS} = \frac{162 \times (V_{\mathrm{NaOH}} \times C_{\mathrm{NaOH}})}{m - 113 \times (V_{\mathrm{NaOH}} \times C_{\mathrm{NaOH}})}$$

Where 162 g/mol is the molar mass of an AGU unit, 113 g/mol is the net increase in the mass of an AGU unit for each glutaric chain, m is the weight of the sample analyzed, V_{NaOH} is the volume of standard NaOH solution, and C_{NaOH} is the concentration of the standard NaOH solution.

5.4.5 Preparation of composites

All samples were prepared by directly mixing starch (native and modified) with ELO, adipic acid and DMAP. The R ratio of acid groups to epoxy groups was 0.7 (the acid groups on starch molecules were not considered) and the amount of DMAP used was 1 mol% calculated based on the total moles of epoxy groups. The mixture was stirred at 150 ^{o}C for 5 min, poured in to a hot aluminum plate (internal diameter of 70 mm) and cured in a fan-assisted oven at 140 ^{o}C for 8 h.

5.4.6 Solid state NMR analysis

^{13}C CPMAS spectra were acquired using a 400 MHz Bruker Avance III HD spectrometer equipped with a Bruker 4mm H(F)/X/Y triple-resonance probe and 9.4T Ascend® superconducting magnet. The CP experiments employed a 1.5ms linearly-ramped contact pulse, spinning rates of 12500 ± 2 Hz, optimized recycle delays of 3-5 seconds, spinal-64 heteronuclear decoupling (at νrf=85 kHz) and are a sum of 600 co-added transients. Chemical shifts are reported with respect to TMS, and were referenced using adamantane (29.5 ppm) as an external secondary reference.

5.4.7 Thermal stability

The thermal stability of raw materials including Hylon VII, amylose, amylopectin, corn starch, starch esters, and the epoxy resin-starch composites were analyzed using Netzsch STA 409. Approximately 20 to 30 mg of the sample was heated from room temperature to 600 °C at a heating rate of 10 °C/min under nitrogen gas atmosphere.

5.4.8 Thermogravimetric-Fourier transform infrared spectroscopy (TG-FTIR)

Starch ester with DS0.8 was analysed using TG-FTIR. About 100 mg of starch ester was heated from 25 °C to 600 °C at 10 °C/min using a Netzsch STA 409 under N_2 with flow rate of 100 mL/min. FT-IR spectra of the volatiles were recorded using a Bruker EQUINOX-55 FT instrument equipped with a liquid N_2 cooled MCT detector with a resolution of 4 cm^{-1} and 32 scans.

The crude results were obtained in units of time (seconds) and were converted into temperature using the following equation:

$$Temperature\ (^\circ\mathrm{C}) = \left\{\left[\frac{Time(sec)}{60}\right] \times 10\right\} + initial\ temperature$$

All the other analyses used were the same as stated in Chapter 5 Section 5.2.

Chapter 6

Concluding remarks and future insight

With the rapid depletion of fossil fuels and increasing concerns about environmental and health issues, the utilization of renewable materials to produce biobased products is of great interests. The development of biobased or bio-derived polymers is regarded as a great opportunity due to their market share of less than 1%. Compared to the rapid development of biobased thermoplastics, studies on biobased thermosets are received less attention.

The structure and functionality of epoxy prepolymers, the structure of curing agents and curing conditions (accelerators and curing temperature and time) are of great importance on determining the final properties of the obtained epoxy resins. The larger the size and the higher the functionality of the epoxy prepolymer, it's more easily to form cured products and products with better thermal and mechanical properties. Among these plant oil-derived epoxy prepolymers ELO, ESBO, EML and EMS, ELO and ESBO formed cured resins while EML and EMS only were able to form viscous oligomers Curing with DCAs gave soft and flexible materials. In order to systematically investigate the effect of chain length of DCAs on the properties of the obtained resins, different chain length of DCAs (C_6, C_8, C_{10}, C_{12}, C_{14}, C_{16}, C_{18} linear α, ω-DCAs and cyclic DCA C_{36}) were used. The increase of chain length decreased T_g and all the mechanical properties including tensile strength, Young's modulus, elongation at break and toughness decreased while increased the thermal stability. Strain hardening effect was only observed in adipic samples which accounted for its best mechanical properties. The utilization of accelerators significantly increased the rate of the curing reaction. Amongst the various accelerators, DMAP gave the fastest curing rate while TEA performed poorest. By either increasing curing temperature or increasing curing time, improved properties may be obtained. Properties obtained at lower temperatures for longer times can be obtained by increasing curing temperature and decreasing curing time. At lower curing temperatures (140 and 160 ^{o}C), with the increase of time, T_g and mechanical properties increased and kept constant. Whilst at high curing temperature (180 ^{o}C), T_g and mechanical properties increased and then started decrease after curing for 8 h.

By curing with glutaric anhydride, hard and tough materials were obtained. For anhydride systems, ELO, ESBO, EML and EMS were all able to form cured resins. Different curing agents resulted in different effects of curing temperature and time on the properties. The increase of temperature and time decreased elongation at break but improved tensile strength and Young's modulus. The study showed in Chapter 3 provides a promising way to change the properties of epoxy resins by easily changing the compositions of the curing agents. By gradually changing the compositions of the curing agents (the ratio of glutaric anhydride to adipic acid), resins were gradually changed from hard tough materials to soft flexible materials.

In furthering the work on biobased epoxy resins, plant oil-derived terminal epoxy fatty acid derivatives are interesting epoxy prepolymers to be investigated. These terminal epoxy fatty acid derivatives were obtained either by reacting fatty acids containing terminal unsaturation such as 10-undecenoic acid (**13**) with glycerol followed by epoxidation[242] or by reacting fatty acid with ECH.[34, 243] They are thought to be more reactive than EPOs. Also other curing agents obtained from renewable materials include plant oil-derived, phenols, rosin and terpene-derived, lignin-derived are worth to be exploited. Reports on the use of mixtures of curing agents are quite limited and utilization of mixtures of other types of curing agents will be possible to make resins with various materials.

Starch is a promising additives for epoxy thermosets due to its renewability, low price and its reinforcing effects. Based on the ELO-adipic acid-DMAP systems, composites with starch (original and modified) were prepared. The addition of 10 wt% Hylon VII decreased elongation at break by 45%, tensile strength by 41% but increased Young’s modulus by 50%. The compatibility between starch particles and the polymer matrix was improved by chemically modification of starch, *i.e.*, esterification with glutaric anhydride. Acid groups were successfully introduced onto starch molecules by reacting expanded starch with glutaric anhydride. By changing the amounts of glutaric anhydride used, starch esters with different DS were made. The addition of these starch esters further increased Young’s modulus from 64 MPa to 120 MPa.

However, all samples showed inhomogeneity with starch settled on the bottom layer of the composites and unevenly dispersed within the matrix. Therefore, for the future work, it is necessary to further improve the compatibility. Better mixing methods such as using high speed mixing machine is needed to improve the mixing process. As mentioned in Chapter 4 Section 4.2, the other two methods to improve compatibility are adding compatibilizer and using TPS such as glycerol plasticized starch. Due to the large amount of hydroxyl groups within glycerol, the compatibility can be improved by chemically reacting epoxy groups with hydroxyl groups. Due to the nanoscale structure of starch nanocrystals, it is worth to incorporate starch nanocrystals (original and modified) in the composite formulations. Starch nanocrystals (as shown in Figure 4.2 (f)), crystalline square-like platelet about 10 nm thick and 50-100 nm equivalent diameters,[244] are easily obtained by H_2SO_4 hydrolysis for 5 days at 40 ^oC.[244] As reviewed by Dufresne, starch nanocrystals have successfully reinforced many natural and synthetic polymers such as starch, chitosan, natural rubber, PLA, PCL and polyurethane.[213] Except for starch nanocrystals, other polysaccharide nanocrystals include cellulose whisker and chitin whisker, which were also reported to be used to make biocomposites with various materials.[241] Lin *et al.* synthesized poly(butylene succinate) (PBS) based biocomposites with cellulose whiskers and starch nanocrystals.[246] They demonstrated that with the loading of 2 wt% cellulose whiskers or 5 wt% starch nanocrystals both strength and elongation were improved. More importantly, based on the study of life cycle analysis (LCA) of the preparation and processing of starch nanocrystals and organically modified nanoclays (OMMT), starch nanocrystals required less energy but showed higher global warming and acidification indicators than the preparation of OMMT.[247] Lignocellulosic fibers, another important class of renewable fillers, are of great interests to be exploited for the development of biocomposites due to their economic production, low specific weight and safer health and environment issues.[248] Improved mechanical properties including tensile strength, tensile modulus and flexural strength were obtained by incorporation of natural fibres into epoxy resin matrix.[249-251]

It has to be pointed out that the color of the sample has no direct relationship with its properties. Although the color itself may cause some customers' concerns, the formulation used at this stage is not the final formulation and white fillers will be added in the future.

In conclusion, the biobased materials reported in thesis provides an interesting addition to the knowledge base that will be needed for the development of a future biobased economy. Such materials contribute to legislative drivers such as Lead Market Initiative[8] and the BioPreferred[9] that advocate the need for more biobased materials. The materials reported also target one of the largest growth areas in biobased polymers, *i.e.* epoxy thermosets, which may be viable alternatives for current PVC-based, phthalate-containing products such as PVC flooring, liners and gaskets. The future will see an increase in biobased materials at the expense of PVC but more research and open innovation will be needed. The supply chain from renewable feedstock to biobased product and beyond (cradle to cradle and/or circular economy) within the context of life cycle analysis along with biobased standards will play an important role.

Appendix A

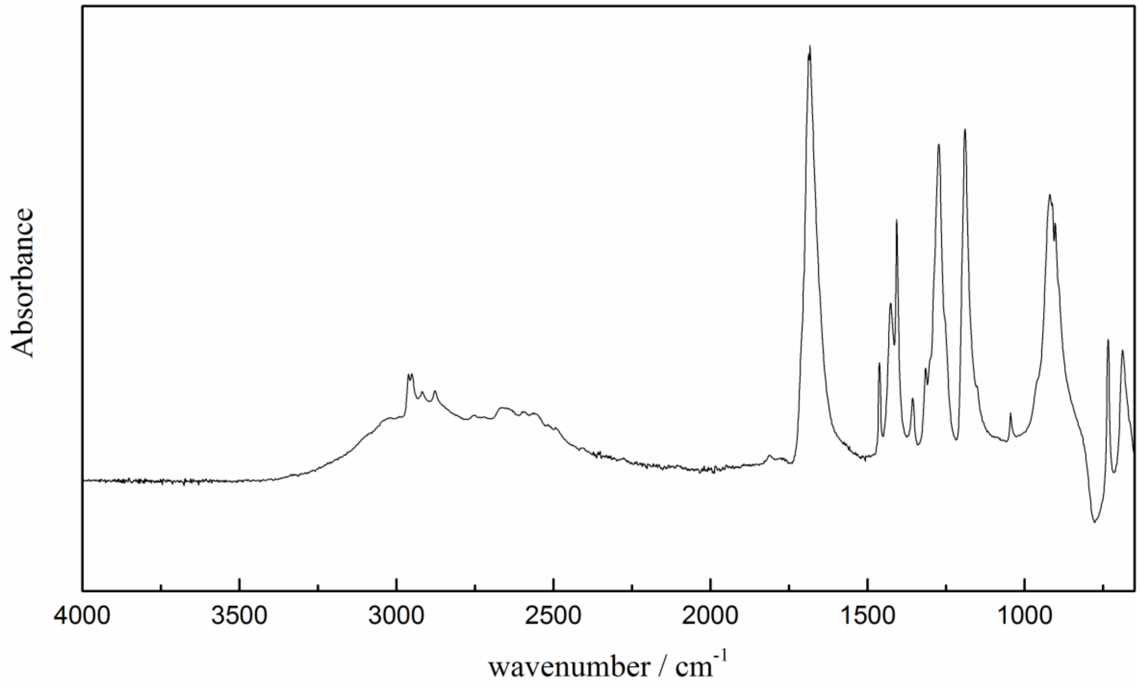

Figure A.1 FT-IR spectrum of adipic acid.

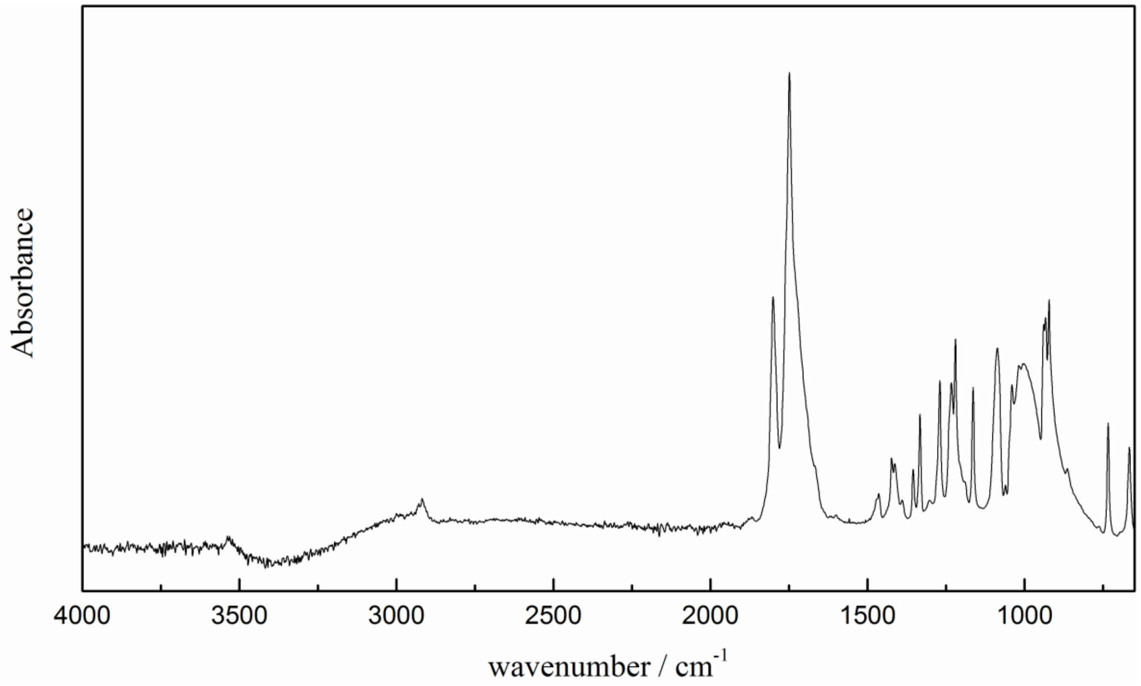

Figure A.2 FT-IR spectrum of glutaric anhydride.

Glossary

AA	adipic acid
AESO	acrylated epoxidized soybean oil;
AGSO	polyamine grapeseed oil
AMPA	vinyl ester of MPA
APA	acryloabietic acid
ASP	aspartic acid
BMI	1,1'-(methylenedi-4,1- phenylene)bismaleimide
BPA	Bisphenol A
BPH	*N*-benzylpyrazinium hexafluoroantimonate
BTCA	1,2,4-benzenetricarboxylic anhydride
CAHC	cysteamine hydrochloride
CHDB	1,2-cyclohexanedicarboxylic anhydride
CNSL	cashew nut shell liquid
CPMI	carboxyphenylmaleimide
DAK	diabietyl ketone
DBU	1,8-diazabicyclo[5.4.0]undec-7- ene
DCAs	dicarboxylic acids
1, 3-DCH	1,3-dichlorohydrin
DDA	decamethylene diamines
DDM	diaminodiphenyl- methane
DDS	dodecenylsuccinic anhydride
DEG	diethylene glycol
DETA	diethylenetri- amine
DGEBA	diglycidyl ether of bisphenol A
DGE-DHBP	diglycidyl ether of 4, 4'-di- hydroxybiphenol
DMA	dynamic mechanical analysis
DMAP	4-dimethylaminoyridine
DOE	Department of Energy
D-RMID	di-RMID
DS	degree of substitution
DSO	dihydroxyl soybean oil

ECO	epoxidized castor oil
EGDE	ethylene glycol diglycidyl ether
ELO	epoxidized linseed oil
EML	epoxidized methyl esters of linseed oil
EMO	epoxidized methyl oleate
EMS	epoxidized methyl esters of soybean oil
ENR	epoxidized natural rubber
EPOs	epoxidized plant oils
ESBO	epoxidized soybean oil
GA	glutaric anhydride
GO	grapheme oxide
GPE	glycerol polyglycidyl ether
G-POSS	3-glycidylpropylheptaisobutyl-T8-polyhedral oligomeric silsesquioxane
HHPA	hexahydrophthalic anhydride
HMD	hexamethylenediamine
IPDA	isophoronediamine
LC	liquid crystalline
LCEs	liquid crystalline elastomers
LDPE	low density polyethylene
LLDPE	linear low density polyethylene
MA	maleic anhydride
MDA	methylenedianiline
MEG	monoethylene glycol
MFC	microfibrillated cellulose
MG	coniferyl alcohol
MH	p-coumaryl alcohol
MHHPA	methylhexahydrophthalic anhydride
1-MI	1-methylimidazole
2-MI	2-methylimidazole
MLO	maleated linseed oil

MMP	methyl maleopimarate
MMS	maleated methyl soyate
mMT	million metric tons
MNA	methyl Nadic anhydride
MPA	maleopimaric acid
MPALA	lactic ester of MPA
MPA-PCL	MPA terminated polycaprolactones
MPO	maleated plant oil
MS	sinapyl alcohol
MSO	maleated soybean oil
MTHPA	methyl tetrahydrophthalic anhydride
OA	oleic acid
oleo-GO	oleo-functionalized reduced GO
PA	phthalic anhydride
p-ABA	p-aminobenzoic acid
PBSA	poly(butylenes succinate-co-butylene adipate)
PCL	polycaprolactone
PCO	phosphorylated castor oil
PEGDE	poly(ethylene glycol) diglycidyl ether
PEHA	pentaethylene hexamine
PESD	poly(epoxidized soybean oil-co-decamethylene diamine)
PG	pyrogallol
PGPE	polyglycidyl ether of polyglycerol
PGVNC	pyrogallol–vanillin calixarene
PHA	polyhydroxyalkanoates
PL	ε-polylysine
PLA	polylactic acid
PN	petroleum-based phenol novolac
PPh_3	triphenylphosphine
PSA	pressure sensitive adhesive
PTC	phase transfer catalysis

PVOH	polyvinyl alcohol
QC	quercetin
RMIA	rosin-based imidoamine
RMID	rosin maleic anhydride imidodicarboxylic acid
RMPA	rosin-based polyamide
SOMGs	soybean oil monoglycerides
SPE	sorbitol polyglycidyl ether
TBD	triazobicyclodecene
TCPA	tetrachlorophthalic anhydride
TEA	triethylamine
TEPA	tetrathylenepentamine
TETA	triethylenetetramine
$T_{5/10}$	5% or 10% weight losss temperature
T_d	onset decomposition temperature
T_g	glass transition temperature
THPA	tetrahydrophthalic anhydride
TMA	trimellitic anhydride
TOA	tung oil anhydride
T_{on}	onset curing temperature
T_P	peak curing temperature
TPA	terpene-based acid anhydride
TPD	terpene diphenol
TPDB	terpenediphenol- based benzoxazine
TPG	tung oil-pyrogallol resin
TPS	thermal plasticized starch
UDETA	aminoethylimidazolidone
VI	vinylimidazole
VN	vanillin
xLCEs	liquid-crystal elastomers with exchangeable links
$Zn(acac)_2$	zinc acetylacetonate dehydrate
$Zn(OAc)_2$	zinc acetate

References

1. WCED, *Our Common Future*, Oxford University Press, USA, 1987.
2. C. McGlade and P. Ekins, *Nature*, 2015, **517**, 187-190.
3. P. Anastas and J. Warner, *Green Chemistry: Theory and Practice*, OUP Oxford, New York, 2000.
4. J. Bozell Joseph, in *Chemicals and Materials from Renewable Resources*, American Chemical Society, 2001, vol. 784, ch. 1, pp. 1-9.
5. J. Bozell Joseph, in *Feedstocks for the Future*, American Chemical Society, 2006, vol. 921, ch. 1, pp. 1-12.
6. A. Gandini and M. N. Belgacem, in *Monomers, Polymers and Composites from Renewable Resources*, eds. M. N. Belgacem and A. Gandini, Elsevier, Amsterdam, 2008, pp. 1-16.
7. Bioplastics: technologies and global markets, BBC research reports PLS050C, 2014.
8. Final evaluation of the lead market initiative, Centre for strategy & evaluation services, 2011.
9. http://www.biopreferred.gov/BioPreferred/faces/pages/AboutBioPreferred.xhtml., Accessed 240715.
10. M. M. Reddy, S. Vivekanandhan, M. Misra, S. K. Bhatia and A. K. Mohanty, *Prog. Polym. Sci.*, 2013, **38**, 1653-1689.
11. L. Yu, K. Dean and L. Li, *Prog. Polym. Sci.*, 2006, **31**, 576-602.
12. M. Flieger, M. Kantorová, A. Prell, T. Řezanka and J. Votruba, *Folia Microbiol.*, 2003, **48**, 27-44.
13. L. Shen, J. Haufe and M. K. Patel, Product overview and market projection of emerging bio-based plastics PRO-BIP 2009, Utrecht University, 2009.
14. PERP program - epoxy resins, http://thinking.nexant.com/sites/default/files/report/field_attachment_abstract/200512/0405S11_abs.pdf, Accessed 240715.
15. W. R. Ashcroft, in *Chemistry and Technology of Epoxy Resins*, ed. B. Ellis, Springer Netherlands, Glasgow, first edn., 1993, ch. Curing agents for epoxy resins, pp. 37-71.
16. L. Sun, PhD Thesis, Louisiana State University, 2001.
17. T. F. Mika and R. S. Bauer, in *Epoxy Resins Chemistry and Technology*, ed. C. May, CRC Press, New York, second edn., 1988, ch. Curing Agents and Modifiers, pp. 465-550.
18. Y. Li, F. Xiao and C. P. Wong, *J. Polym. Sci., Part A: Polym. Chem.*, 2007, **45**, 181-190.
19. Epoxy resins and curing agents: toxicology, health, safety and environmental aspects. Plastics Europe Epoxy Resins Committee, 2006, pp. 1-28.
20. Cyclic acid anhydrides: health-based recommended occupational exposure limit., The Health Council of the Netherlands, 2010.
21. B. M. Bell, J. R. Briggs, R. M. Campbell, S. M. Chambers, P. D. Gaarenstroom, J. G. Hippler, B. D. Hook, K. Kearns, J. M. Kenney, W. J. Kruper, D. J. Schreck, C. N. Theriault and C. P. Wolfe, *CLEAN – Soil, Air, Water*, 2008, **36**, 657-661.
22. WO2005021476 A1, 2005.
23. J. J. Bozell and G. R. Petersen, *Green. Chem.*, 2010, **12**, 539-554.
24. Y. Q. Huang, C. K. C. Wong, J. S. Zheng, H. Bouwman, R. Barra, B. Wahlström, L. Neretin and M. H. Wong, *Environ. Int.*, 2012, **42**, 91-99.
25. R. Auvergne, S. Caillol, G. David, B. Boutevin and J.-P. Pascault, *Chem. Rev.*, 2013, **114**, 1082-1115.
26. A. Mahendran, G. Wuzella, A. Kandelbauer and N. Aust, *J. Therm. Anal. Calorim.*,

2012, **107**, 989-998.

27. J. O. Metzger, *Eur. J. Lipid Sci. Technol.*, 2009, **111**, 865-876.
28. Y. Xia and R. C. Larock, *Green. Chem.*, 2010, **12**, 1893-1909.
29. A. Gerbase, C. Petzhold and A. Costa, *J. Am. Oil Chem. Soc.*, 2002, **79**, 797-802.
30. G. L. I. Puig, PhD Thesis, Rovira i Virgili University, 2006.
31. N. Mann, S. Mendon, J. Rawlins and S. Thames, *J. Am. Oil Chem. Soc.*, 2008, **85**, 791-796.
32. S. G. Tan and W. S. Chow, *Polymer-Plastics Technology and Engineering*, 2010, **49**, 1581-1590.
33. C. Bueno-Ferrer, M. C. Garrigós and A. Jiménez, *Polym. Degrad. Stab.*, 2010, **95**, 2207-2212.
34. R. Wang and T. P. Schuman, *eXPRESS Polym. Lett.*, 2013, **7**, 272-292.
35. S.-J. Park, F.-L. Jin and J.-R. Lee, *Macromol. Rapid Commun.*, 2004, **25**, 724-727.
36. N. Boquillon and C. Fringant, *Polymer*, 2000, **41**, 8603-8613.
37. A. Gerbase, C. Petzhold and A. Costa, *J. Am. Oil Chem. Soc.*, 2002, **79**, 797-802.
38. J. D. Espinoza-Perez, B. A. Nerenz, D. M. Haagenson, Z. Chen, C. A. Ulven and D. P. Wiesenborn, *Polym. Compos.*, 2011, **32**, 1806-1816.
39. S.-J. Park, F.-L. Jin and J.-R. Lee, *Macromol. Chem. Phys.*, 2004, **205**, 2048-2054.
40. F.-L. Jin and S.-J. Park, *Polym. Int.*, 2008, **57**, 577-583.
41. F.-L. Jin and S.-J. Park, *Mater. Sci. Eng. A*, 2008, **478**, 402-405.
42. Z. Liu, S. Z. Erhan, D. E. Akin and F. E. Barton, *J. Agric. Food. Chem.*, 2006, **54**, 2134-2137.
43. G. Lligadas, J. C. Ronda, M. Galià and V. Cádiz, *Biomacromolecules*, 2006, **7**, 3521-3526.
44. H. Uyama, M. Kuwabara, T. Tsujimoto, M. Nakano, A. Usuki and S. Kobayashi, *Chem. Mater.*, 2003, **15**, 2492-2494.
45. H. Warth, R. Mülhaupt, B. Hoffmann and S. Lawson, *Angew. Makromol. Chem.*, 1997, **249**, 79-92.
46. US2374381, 1945.
47. P. Tran, K. Seybold, D. Graiver and R. Narayan, *J. Am. Oil Chem. Soc.*, 2005, **82**, 189-194.
48. P. Tran, D. Graiver and R. Narayan, *J. Appl. Polym. Sci.*, 2006, **102**, 69-75.
49. A. R. Mahendran, N. Aust, G. Wuzella and A. Kandelbauer, *Macromol.. Symp.*, 2012, **311**, 18-27.
50. J. Lu, S. Khot and R. P. Wool, *Polymer*, 2005, **46**, 71-80.
51. E. Can, S. Küsefoğlu and R. P. Wool, *J. Appl. Polym. Sci.*, 2001, **81**, 69-77.
52. U. Biermann, W. Butte, T. Eren, D. Haase and J. O. Metzger, *Eur. J. Org. Chem.*, 2007, **2007**, 3859-3862.
53. T. P. Hilditch and A. Mendelowitz, *J. Sci. Food Agric.*, 1951, **2**, 548-556.
54. W. B. Xu, S. P. Bao and P. S. He, *J. Appl. Polym. Sci.*, 2002, **84**, 842-849.
55. A. B. Lowe, *Polym. Chem.*, 2010, **1**, 17-36.
56. G. Lligadas, J. C. Ronda, M. Galià and V. Cádiz, *J. Polym. Sci., Part A: Polym. Chem.*, 2013, **51**, 2111-2124.
57. F. Jaillet, M. Desroches, R. Auvergne, B. Boutevin and S. Caillol, *Eur. J. Lipid Sci. Technol.*, 2013, **115**, 698-708.
58. M. Desroches, S. Caillol, V. Lapinte, R. m. Auvergne and B. Boutevin, *Macromolecules*,

2011, **44**, 2489-2500.

59. M. Stemmelen, F. Pessel, V. Lapinte, S. Caillol, J. P. Habas and J. J. Robin, *J. Polym. Sci., Part A: Polym. Chem.*, 2011, **49**, 2434-2444.
60. M. Shibata, N. Teramoto, S. Yoshihara and Y. Itakura, *J. Appl. Polym. Sci.*, 2013, **129**, 282-288.
61. M. Desroches, R. Auvergne, B. Boutevin and S. Caillol, *Oléagineux, Corps Gras, Lipides*, 2013, **20**, 16-22.
62. H.-P. Zhao, J.-F. Zhang, X. Susan Sun and D. H. Hua, *J. Appl. Polym. Sci.*, 2008, **110**, 647-656.
63. G. Lligadas, J. C. Ronda, M. Galià and V. Cádiz, *Biomacromolecules*, 2010, **11**, 2825-2835.
64. M. Desroches, M. Escouvois, R. Auvergne, S. Caillol and B. Boutevin, *Polym. Rev.*, 2012, **52**, 38-79.
65. P. Czub, *Polym. Adv. Technol.*, 2009, **20**, 194-208.
66. B. K. Ahn, S. Kraft, D. Wang and X. S. Sun, *Biomacromolecules*, 2011, **12**, 1839-1843.
67. Z. Liu, Y. Xu, L. Cao, C. Bao, H. Sun, L. Wang, K. Dai and L. Zhu, *Soft Matter*, 2012, **8**, 5888-5895.
68. Top value added chemicals from biomass volume I - results of screening for potential candidates from sugars and synthesis gas. U.S. Department of Energy, vol. 2013.
69. Y. Xu, M. A. Hanna and L. Isom, *The Open Agricultural Journal*, 2008, **2**, 54-61.
70. A. Corma, S. Iborra and A. Velty, *Chem. Rev.*, 2007, **107**, 2411-2502.
71. E. d. Jong, A. Higson, P. Walsh and M. Wellisch, *Bio-based chemicals: value added products from biorefineries*, IEA Bioenergy, 2012.
72. F. W. Lichtenthaler, in *Ullmann's Encyclopedia of Industrial Chemistry*, Wiley-VCH Verlag GmbH & Co. KGaA, 2000.
73. A. K. Vasishtha, R. K. Trivedi and G. Das, *J. Am. Oil Chem. Soc.*, 1990, **67**, 333-337.
74. U. Schörken and P. Kempers, *Eur. J. Lipid Sci. Technol.*, 2009, **111**, 627-645.
75. K. Kroha, *Informatics*, 2004, **15**, 568-571.
76. B.-J. K. Ahn, S. Kraft and X. S. Sun, *J. Agric. Food. Chem.*, 2012, **60**, 2179-2189.
77. R. Shogren, Z. Petrovic, Z. Liu and S. Erhan, *J. Polym. Environ.*, 2004, **12**, 173-178.
78. L. Shechter and J. Wynstra, *J. Ind. Eng. Chem.*, 1956, **48**, 86-93.
79. R. L. Shogren, *J. Appl. Polym. Sci.*, 1999, **73**, 2159-2167.
80. C. S. Lee and S. C. Lee, *Chin. J. Chem* . 2011, **29**, 840-846.
81. S. Caillol, M. Desroches, G. Boutevin, C. Loubat, R. Auvergne and B. Boutevin, *Eur. J. Lipid Sci. Technol.*, 2012, **114**, 1447-1459.
82. M. Pire, S. Norvez, I. Iliopoulos, B. Le Rossignol and L. Leibler, *Polymer*, 2010, **51**, 5903-5909.
83. V. Ambrogi, M. Giamberini, P. Cerruti, P. Pucci, N. Menna, R. Mascolo and C. Carfagna, *Polymer*, 2005, **46**, 2105-2121.
84. N. Supanchaiyamat, P. S. Shuttleworth, A. J. Hunt, J. H. Clark and A. S. Matharu, *Green. Chem.*, 2012, **14**, 1759-1765.
85. D. Montarnal, F. Tournilhac, M. Hidalgo and L. Leibler, *J. Polym. Sci., Part A: Polym. Chem.*, 2010, **48**, 1133-1141.
86. D. Montarnal, M. Capelot, F. Tournilhac and L. Leibler, *Science*, 2011, **334**, 965-968.
87. M. Capelot, D. Montarnal, F. Tournilhac and L. Leibler, *J. Am. Chem. Soc.*, 2012, **134**, 7664-7667.

88. M. Capelot, M. M. Unterlass, F. Tournilhac and L. Leibler, *ACS Macro Lett.*, 2012, **1**, 789-792.
89. Z. Q. Pei, Y. Yang, Q. Chen, E. M. Terentjev, Y. Wei and Y. Ji, *Nat. Mater.*, 2014, **13**, 36-41.
90. D. T. Carter, N. Stansfield, R. J. Mantle, C. M. France and P. A. Smith, *Ind. Crop. Prod.*, 2008, **28**, 309-319.
91. Y. L. Hu, X. G. Zhao and M. Lu, *B. Chem. Soc. Ethiopia*, 2011, **25**, 255-262.
92. S. K. Yedur, J. Dulebohn, T. Werpy and K. A. Berglund, *Ind. Eng. Chem. Res.*, 1996, **35**, 663-671.
93. N. Alonso-Fagúndez, M. L. Granados, R. Mariscal and M. Ojeda, *ChemSusChem*, 2012, **5**, 1984-1990.
94. Z. T. Du, J. P. Ma, F. Wang, J. X. Liu and J. Xu, *Green. Chem.*, 2011, **13**, 554-557.
95. US20120015411A1, 2012.
96. E. Mahmoud, D. A. Watson and R. F. Lobo, *Green. Chem.*, 2014, **16**, 167-175.
97. W. Leuchtenberger, K. Huthmacher and K. Drauz, *Appl. Microbiol. Biotechnol.*, 2005, **69**, 1-8.
98. Y. Li, F. Xiao, K.-S. Moon and C. P. Wong, *J. Polym. Sci., Part A: Polym. Chem.*, 2006, **44**, 1020-1027.
99. P. Kahar, T. Iwata, J. U. N. Hiraki, E. Y. Park and M. Okabe, *J. Biosci. Bioeng.*, 2001, **91**, 190-194.
100. P. Kahar, K. Kobayashi, T. Iwata, J. Hiraki, M. Kojima and M. Okabe, *J. Biosci. Bioeng.*, 2002, **93**, 274-280.
101. M. Scholl, T. Q. Nguyen, B. Bruchmann and H.-A. Klok, *J. Polym. Sci., Part A: Polym. Chem.*, 2007, **45**, 5494-5508.
102. M. Scholl, T. Q. Nguyen, B. Bruchmann and H.-A. Klok, *Macromolecules*, 2007, **40**, 5726-5734.
103. Y. Takada, K. Shinbo, Y. Someya and M. Shibata, *J. Appl. Polym. Sci.*, 2009, **113**, 479-484.
104. S. Kind and C. Wittmann, *Appl. Microbiol. Biotechnol.*, 2011, **91**, 1287-1296.
105. D. S. Van Es, *J. Renew. Mater.*, 2013, **1**, 61-72.
106. S. Thiyagarajan, L. Gootjes, W. Vogelzang, J. v. Haveren, M. Lutz and D. S. v. Es, *ChemSusChem*, 2011, **4**, 1823-1829.
107. US6608167 B1, 2003.
108. WO 2008145921 A3, 2008.
109. CN101088983, 2007.
110. Z. Wang, X. Zhang, R. Wang, H. Kang, B. Qiao, J. Ma, L. Zhang and H. Wang, *Macromolecules*, 2012, **45**, 9010-9019.
111. M. T. Harvey and S. Caplan, *Ind. Eng. Chem.*, 1940, **32**, 1306-1310.
112. D. Wasserman and C. R. Dawson, *Ind. Eng. Chem.*, 1945, **37**, 396-399.
113. J. H. P. Tyman, *Chem. Soc. Rev.*, 1979, **8**, 499-537.
114. M. C. Lubi and E. T. Thachil, *Des. Monomers. Polym.*, 2000, **3**, 123-153.
115. P. L. Nayak, *J. Macromol. Sci. Part C*, 2000, **40**, 1-21.
116. Z. S. Dai, A. Constantinescu, A. Dalal and C. Ford, *Phenalkamine multipurpose epoxy resin curing agents*, Cardolite Corporation, New Jersey, 1994.
117. Phenalkamine curing agents, http://www.cardolite.com/?q=phenalkamine, Accessed 240715.

118. US20100286345 A1, 2009.
119. US6262148 B1, 2001.
120. P. Vijayalakshmi, T. C. Rao, V. Kale, R. S. Balakrishna and R. Subbarao, *Polymer*, 1992, **33**, 3252-3256.
121. F. Fenouillot, A. Rousseau, G. Colomines, R. Saint-Loup and J. P. Pascault, *Prog. Polym. Sci.*, 2010, **35**, 578-622.
122. E. V. Fomina, *Polym. Sci. Ser. D*, 2010, **3**, 87-91.
123. Phenalkamide curing agents, http://www.cardolite.com/?q=phenalkamide, Accessed 240715.
124. P. Campaner, D. D'Amico, L. Longo, C. Stifani and A. Tarzia, *J. Appl. Polym. Sci.*, 2009, **114**, 3585-3591.
125. S. Quideau, D. Deffieux, C. Douat-Casassus and L. Pouységu, *Angew. Chem. Int. Ed.*, 2011, **50**, 586-621.
126. A. Schieber, F. C. Stintzing and R. Carle, *Trends Food Sci. Technol.*, 2001, **12**, 401-413.
127. A. Pizzi, in *Monomers, Polymers and Composites from Renewable Resources*, eds. M. N. Belgacem and A. Gandini, Elsevier, Amsterdam, 2008, pp. 179-199.
128. M. Shibata and K. Nakai, *J. Polym. Sci., Part B: Polym. Phys.*, 2010, **48**, 425-433.
129. M. Shibata, N. Teramoto and K. Makino, *J. Appl. Polym. Sci.*, 2011, **120**, 273-278.
130. T. Shimasaki, S. Yoshihara and M. Shibata, *Polym. Compos.*, 2012, **33**, 1840-1847.
131. M. Shibata, S. Yoshihara, M. Yashiro and Y. Ohno, *J. Appl. Polym. Sci.*, 2013, **128**, 2753-2758.
132. A. Gandini, *Macromolecules*, 2008, **41**, 9491-9504.
133. A. J. D. Silvestre and A. Gandini, in *Monomers, Polymers and Composites from Renewable Resources*, eds. M. N. Belgacem and A. Gandini, Elsevier, Amsterdam, 2008, pp. 67-88.
134. S. Maiti, S. S. Ray and A. K. Kundu, *Prog. Polym. Sci.*, 1989, **14**, 297-338.
135. H. Wang, B. Liu, X. Liu, J. Zhang and M. Xian, *Green. Chem.*, 2008, **10**, 1190-1196.
136. X. Liu, W. Xin and J. Zhang, *Green. Chem.*, 2009, **11**, 1018-1025.
137. X. Liu and J. Zhang, *Polym. Int.*, 2010, **59**, 607-609.
138. H. Wang, X. Liu, B. Liu, J. Zhang and M. Xian, *Polym. Int.*, 2009, **58**, 1435-1441.
139. X. Liu, W. Xin and J. Zhang, *Bioresour Technol*, 2010, **101**, 2520-2524.
140. F. R. Mustata and N. Tudorachi. *Ind. Eng. Chem. Res.*, 2010, **49**, 12414-12422.
141. Z. Mi, X. A. Nie, Y. G. Wang, X. Chang and G. F. Liu, *J. For. Prod. Ind.*, 2013, **2**, 5-11.
142. H. Wang, H. Wang and G. Zhou, *Polym. Int.*, 2011, **60**, 557-563.
143. A. J. D. Silvestre and A. Gandini, in *Monomers, Polymers and Composites from Renewable Resources*, eds. M. N. Belgacem and A. Gandini, Elsevier, Amsterdam, 2008, pp. 17-38.
144. J. E. Milks and J. E. Lancaster, *J. Org. Chem*, 1965, **30**, 888-891.
145. T. Tsutomu, H. Ken-ichi, T. Naozumi and S. Mitsuhiro, *J Appl Polym Sci*, 2008, **108**, 1596-1602.
146. R. Chang, J. Qin and J. Gao, *J. Polym. Res.*, 2014, **21**, 1-7.
147. US5066461, 1991.
148. US2955138 A, 1960.
149. US2811564 A, 1957.
150. US5416138 A, 1995.
151. H. Kimura, Y. Murata, A. Matsumoto, K. Hasegawa, K. Ohtsuka and A. Fukuda, *J. Appl.*

Polym. Sci., 1999, **74**, 2266-2273.

1512. G. Gellerstedt and G. Henriksson, in *Monomers, Polymers and Composites from Renewable Resources*, eds. M. N. Belgacem and A. Gandini, Elsevier, Amsterdam, 2008, pp. 201-224.
153. H. Chung and N. R. Washburn, *Green. Mater*, 2012, **1**, 137-160.
154. T. Koike, *Polym. Eng. Sci.*, 2012, **52**, 701-717.
155. B. Tomita, K. Kurozumi, A. Takemura and S. Hosoya, in *Lignin*, American Chemical Society, 1989, vol. 397, ch. 39, pp. 496-505.
156. H. J. Lee, B. Tomita and S. Hosoya, *Mokuzai Kogyo*, 1991, **46**, 412-417.
157. Y. Nonaka, B. Tomita and Y. Hatano, *Holzforschung*, 1997, **51**, 183-187.
158. J. Qin, M. Woloctt and J. Zhang, *ACS Sustainable Chem. Eng.*, 2013, **2**, 188-193.
159. S. Hirose, T. Hatakeyama and H. Hatakeyama, *Macromol.. Symp.*, 2003, **197**, 157-170.
160. S. Hirose, T. Hatakeyama and H. Hatakeyama, *Thermochim. Acta*, 2005, **431**, 76-80.
161. T. N. M. T. Ismail, H. A. Hassan, S. Hirose, Y. Taguchi, T. Hatakeyama and H. Hatakeyama, *Polym. Int.*, 2010, **59**, 181-186.
162. S. Hirose, *J. Oil. Palm. Res.*, 2011, **23**, 1110-1114.
163. US20110024168 A1, 2011.
164. H. Kiuchi, W. Kai and Y. Inoue, *J. Appl. Polym. Sci.*, 2008, **107**, 3823-3830.
165. M.-C. Chen, H.-W. Tsai, Y. Chang, W.-Y. Lai, F.-L. Mi, C.-T. Liu, H.-S. Wong and H.-W. Sung, *Biomacromolecules*, 2007, **8**, 2774-2780.
166. A. R. Cestari, E. F. S. Vieira, F. J. Alves, E. C. S. Silva and M. A. S. Andrade Jr, *J. Hazard. Mater.*, 2012, **213–214**, 109-116.
167. N. Illy, S. Benyahya, N. Durand, R. Auvergne, S. Caillol, G. David and B. Boutevin, *Polym. Int.*, 2013, **63**, 420-426.
168. X. Liu, Y. Wang, Y. Cao, V. Yadama, M. Xian and J. Zhang, *Carbohydr. Polym.*, 2011, **83**, 1180-1184.
169. B. K. Ahn, J. Sung, Y. Li, N. Kim, M. Ikenberry, K. Hohn, N. Mohanty, P. Nguyen, T. S. Sreeprasad, S. Kraft, V. Berry and X. S. Sun, *Adv. Mater.*, 2012, **24**, 2123-2129.
170. J. Puig, C. E. Hoppe, L. A. Fasce, C. J. Pérez, Y. Piñeiro-Redondo, M. Bañobre-López, M. A. López-Quintela, J. Rivas and R. J. J. Williams, *J. Phys. Chem. C*, 2012, **116**, 13421-13428.
171. *Adipic Acid Market Analysis And Segment Forecasts to 2020*, Grand View Research, 2014.
172. S. Van de Vyver and Y. Roman-Leshkov, *Catal. Sci. Technol.*, 2013, **3**, 1465-1479.
173. T. Polen, M. Spelberg and M. Bott, *J. Biotechnol.*, 2013, **167**, 75-84.
174. J.-L. Yu, X.-X. Xia, J.-J. Zhong and Z.-G. Qian, *Biotechnol. Bioeng.*, 2014, **111**, 2580-2586.
175. L. Matějka, S. Pokomý and K. Dušek, *Polym. Bull.*, 1982, **7**, 123-128.
176. N. Supanchaiyamat, A. J. Hunt, P. S. Shuttleworth, C. Ding, J. H. Clark and A. S. Matharu, *RSC Advances*, 2014, **4**, 23304-23313.
177. P.-J. Madec and E. Maréchal, in *Analysis/Reactions/Morphology*, Springer Berlin Heidelberg, 1985, vol. 71, ch. 4, pp. 153-228.
178. C. E. Hoppe, M. J. Galante, P. A. Oyanguren and R. J. J. Williams, *Macromol. Mater. Eng.*, 2005, **290**, 456-462.
179. I. E. Dell'Erba and R. J. J. Williams, *Polym. Eng. Sci.*, 2006, **46**, 351-359.
180. Q. B. Reiznautt, I. T. S. Garcia and D. Samios, *Mater. Sci. Eng., C*, 2009, **29**,

2302-2311.

181. W. H. Park and J. K. Lee, *J. Appl. Polym. Sci.*, 1998, **67**, 1101-1108.
182. F. Liu, Z. Wang, D. Liu and J. Li, *Polym. Int.*, 2009, **58**, 912-918.
183. L. H. Sinh, N. N. Trung, B. T. Son, S. Shin, D. T. Thanh and J.-Y. Bae, *Polym. Eng. Sci.*, 2014, **54**, 695-703.
184. J. S. Hwang, M. J. Yim and K. W. Paik, *J. Electron. Mater.*, 2006, **35**, 1722-1727.
185. J. Zhu, K. Chandrashekhara, V. Flanigan and S. Kapila, *J. Appl. Polym. Sci.*, 2004, **91**, 3513-3518.
186. P. G. Laye, in *Principles of Thermal Analysis and Calorimetry*, The Royal Society of Chemistry, 2002, pp. 55-93.
187. Y.-C. Chiu, C.-C. Huang, H.-C. Tsai, A. Prasannan and I. Toyoko, *Polym. Bull.*, 2013, **70**, 1367-1382.
188. G. Mashouf Roudsari, A. K. Mohanty and M. Misra, *ACS Sustainable Chem. Eng.*, 2014, **2**, 2111-2116.
189. M. Shimbo, M. Ochi and Y. Shigeta, *J. Appl. Polym. Sci.*, 1981, **26**, 2265-2277.
190. M. Shimbo, M. Ochi and Y. Konishi, *Zairyo*, 1979, **28**, 319-325.
191. X. Pan, P. Sengupta and D. C. Webster, *Biomacromolecules*, 2011, **12**, 2416-2428.
192. A. Adhvaryu and S. Z. Erhan, *Ind. Crop. Prod.*, 2002, **15**, 247-254.
193. Z. Liu and S. Erhan, *J. Am. Oil Chem. Soc.*, 2010, **87**, 437-444.
194. P. S. Lathi and B. Mattiasson, *Appl. Catal., B*, 2007, **69**, 207-212.
195. O. Zovi, L. Lecamp, C. Loutelier-Bourhis, C. M. Lange and C. Bunel, *Green. Chem.*, 2011, **13**, 1014-1022.
196. E. Honcoop and E. Appelman, *Eur. Coat. J.*, 2002, **9**, 1-6.
197. F. Li and R. C. Larock, *J. Polym. Sci., Part B: Polym. Phys.*, 2001, **39**, 60-77.
198. J. Hong, Q. Luo, X. Wan, Z. S. Petrović and B. K. Shah, *Biomacromolecules*, 2011, **13**, 261-266.
199. G. Yang, S.-Y. Fu and J.-P. Yang, *Polymer*, 2007, **48**, 302-310.
200. L. Barral, J. Cano, A. López, P. Nogueira and C. Ramírez, *J. Therm. Anal.*, 1994, **41**, 1463-1467.
201. Z. S. Petrović, W. Zhang and I. Javni, *Biomacromolecules*, 2005, **6**, 713-719.
202. C. Vilela, A. J. D. Silvestre and M. A. R. Meier, *Macromol. Chem. Phys.*, 2012, **213**, 2220-2227.
203. J.-M. Pin, N. Sbirrazzuoli and A. Mija, *ChemSusChem*, 2015, **8**, 1232-1243.
204. C. Zhang, Y. Li, R. Chen and M. R. Kessler, *ACS Sustainable Chem. Eng.*, 2014, **2**, 2465-2476.
205. B. Yu, Y. Shi, B. Yuan, S. Qiu, W. Xing, W. Hu, L. Song, S. Lo and Y. Hu, *J. Mater. Chem. A*, 2015, **3**, 8034-8044.
206. J.-P. Pascault, H. Sautereau, J. Verdu and R. J. J. Williams, *Thermosetting polymers*, Marcel Dekker Inc, New York, 2002.
207. C. I. Vallo, P. M. Frontini and R. J. J. Williams, *J. Polym. Sci., Part B: Polym. Phys.*, 1991, **29**, 1503-1511.
208. J. Cheng, J. Li and J. Y. Zhang, *eXPRESS Polym. Lett.*, 2009, **3**, 501-509.
209. Y. Lu and R. C. Larock, *Biomacromolecules*, 2008, **9**, 3332-3340.
210. L. Plangsangmas, J. J. Mecholsky and A. B. Brennan, *J. Appl. Polym. Sci.*, 1999, **72**, 257-268.
211. R. F. Tester, J. Karkalas and X. Qi, *J. Cereal Sci.*, 2004, **39**, 151-165.

212. D. Le Corre, J. Bras and A. Dufresne, *Biomacromolecules*, 2010, **11**, 1139-1153.
213. A. Dufresne, *Curr. Opin. Colloid Interface Sci.*, 2014, **19**, 397-408.
214. H. F. Zobel, *Starch - Stärke*, 1988, **40**, 1-7.
215. A. Buléon, P. Colonna, V. Planchot and S. Ball, *Int. J. Biol. Macromol.*, 1998, **23**, 85-112.
216. C. G. Oates, *Trends Food Sci. Technol.*, 1997, **8**, 375-382.
217. D. J. Gallant, B. Bouchet and P. M. Baldwin, *Carbohydr. Polym.*, 1997, **32**, 177-191.
218. G. Gerald J. L, in *Fillers and Reinforcements for Plastics*, eds. R. D. Deannin and N. R. Schott, American Chemical Society, 1974, vol. 134, ch. 16, pp. 159-170.
219. N. St-Pierre, B. D. Favis, B. A. Ramsay, J. A. Ramsay and H. Verhoogt, *Polymer*, 1997, **38**, 647-655.
220. W. Ning, Y. Jiugao, M. Xiaofei and W. Ying, *Carbohydr. Polym.*, 2007, **67**, 446-453.
221. W. Shujun, Y. Jiugao and Y. Jinglin, *Polym. Degrad. Stab.*, 2005, **87**, 395-401.
222. I. E. Rivero, V. Balsamo and A. J. Müller, *Carbohydr. Polym.*, 2009, **75**, 343-350.
223. X.-L. Wang, K.-K. Yang and Y.-Z. Wang, *J. Macromol. Sci., C*, 2003, **43**, 385-409.
224. Z.-F. Wang, Z. Peng, S.-D. Li, H. Lin, K.-X. Zhang, X.-D. She and X. Fu, *Compos. Sci. Technol.*, 2009, **69**, 1797-1803.
225. R. Santayanon and J. Wootthikanokkhan, *Carbohydr. Polym.*, 2003, **51**, 17-24.
226. Y. Xu, V. Miladinov and M. A. Hanna, *Cereal Chem.*, 2004, **81**, 735-740.
227. Y. Zuo, J. Gu, L. Yang, Z. Qiao, H. Tan and Y. Zhang, *Int. J. Biol. Macromol.*, 2013, **62**, 241-247.
228. M. C. Sweedman, M. J. Tizzotti, C. Schäfer and R. G. Gilbert, *Carbohydr. Polym.*, 2013, **92**, 905-920.
229. X. Hu, B. Wei, B. Zhang, X. Xu, Z. Jin and Y. Tian, *Carbohydr. Polym.*, 2013, **97**, 111-115.
230. X. Liu, L. Yu, F. Xie, M. Li, L. Chen and X. Li, *Starch - Stärke*, 2010, **62**, 139-146.
231. P. S. Shuttleworth, J. H. Clark, R. Mantle and N. Stansfield, *Green. Chem.*, 2010, **12**, 798-803.
232. H. Chi, K. Xu, X. Wu, Q. Chen, D. Xue, C. Song, W. Zhang and P. Wang, *Food Chem.*, 2008, **106**, 923-928.
233. Z. Zhang, D. J. Macquarrie, J. H. Clark and A. S. Matharu, *RSC Advances*, 2014, **4**, 41947-41955.
234. S. M. Goheen and R. P. Wool, *J. Appl. Polym. Sci.*, 1991, **42**, 2691-2701.
235. M.-Y. Baik, L. C. Dickinson and P. Chinachoti, *J. Agric. Food. Chem.*, 2003, **51**, 1242-1248.
236. K. R. Morgan, R. H. Furneaux and N. G. Larsen, *Carbohydr. Res.*, 1995, **276**, 387-399.
237. X. Liu, H. Ma, L. Yu, L. Chen, Z. Tong and P. Chen, *J. Therm. Anal. Calorim.*, 2014, **115**, 659-665.
238. X. C. Ge, X. H. Li, Q. Zhu, L. Li and Y. Z. Meng, *Polym. Eng. Sci.*, 2004, **44**, 2134-2140.
239. S. Peng, X. Wang and L. Dong, *Polym. Compos.*, 2005, **26**, 37-41.
240. E. Kristo and C. G. Biliaderis, *Carbohydr. Polym.*, 2007, **68**, 146-158.
241. G. Chen, M. Wei, J. Chen, J. Huang, A. Dufresne and P. R. Chang, *Polymer*, 2008, **49**, 1860-1870.
242. G. Lligadas, J. C. Ronda, M. Galià and V. Cádiz, *J. Polym. Sci., Part A: Polym. Chem.*, 2006, **44**, 6717-6727.

243. V. Thulasiraman, S. Rakesh and M. Sarojadevi, *Polym. Compos.*, 2009, **30**, 49-58.
244. D. LeCorre, J. Bras and A. Dufresne, *Carbohydr. Polym.*, 2012, **87**, 658-666.
245. H. Angellier, L. Choisnard, S. Molina-Boisseau, P. Ozil and A. Dufresne, *Biomacromolecules*, 2004, **5**, 1545-1551.
246. N. Lin, J. Yu, P. R. Chang, J. Li and J. Huang, *Polym. Compos.*, 2011, **32**, 472-482.
247. D. LeCorre, C. Hohenthal, A. Dufresne and J. Bras, *J. Polym. Environ.*, 2013, **21**, 71-80.
248. M. J. John and S. Thomas, *Carbohydr. Polym.*, 2008, **71**, 343-364.
249. L. Yan, N. Chouw and X. Yuan, *J. Reinf. Plast. Compos.*, 2012.
250. B. F. Yousif, A. Shalwan, C. W. Chin and K. C. Ming, *Mater. Des.*, 2012, **40**, 378-385.
251. M. Jawaid, H. P. S. Abdul Khalil, A. Hassan, R. Dungani and A. Hadiyane, *Composites Part B: Engineering*, 2013, **45**, 619-624.